

**Contracted and Expanded Porphyrin analogues:
Syntheses, Conformation, Aromaticity and
Coordination Chemistry**

By

MAINAK DAS

CHEM 11201404006

**National Institute of Science Education and Research,
Bhubaneswar, Odisha**

*A thesis submitted to the
Board of Studies in Chemical Sciences
In partial fulfillment of requirements
for the Degree of*

DOCTOR OF PHILOSOPHY

Of

HOMI BHABHA NATIONAL INSTITUTE


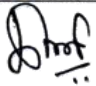

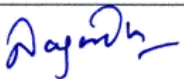




December, 2019

Homi Bhabha National Institute

Recommendations of the Viva Voce Committee

As members of the Viva Voce Committee, we certify that we have read the dissertation prepared by **Mainak Das** entitled “**Contracted and Expanded Porphyrin analogues: Syntheses, Conformation, Aromaticity and Coordination Chemistry**” and recommend that it may be accepted as fulfilling the thesis requirement for the award of Degree of Doctor of Philosophy.

Chairman – Dr. Moloy Sarkar		Date: 28.11.19
Guide / Convener – Prof. A. Srinivasan		Date: 28.11.19
Examiner – Prof. Pradeepta K. Panda		Date: 28/11/19
Member 1- Dr. Nagendra K. Sharma		Date: 28/11/19
Member 2- Dr. V. Krishnan		Date: 28/11/19
Member 3- Dr. Pankaj V. Alone		Date: 28/11/19

Final approval and acceptance of this thesis is contingent upon the candidate's submission of the final copies of the thesis to HBNI.

I/We hereby certify that I/we have read this thesis prepared under my/our direction and recommend that it may be accepted as fulfilling the thesis requirement.

Date: 28.11.19

Place: Bhubaneswar



Signature

Guide

STATEMENT BY AUTHOR

This dissertation has been submitted in partial fulfillment of requirements for an advanced degree at Homi Bhabha National Institute (HBNI) and is deposited in the Library to be made available to borrowers under rules of the HBNI.

Brief quotations from this dissertation are allowable without special permission, provided that accurate acknowledgement of source is made. Requests for permission for extended quotation from or reproduction of this manuscript in whole or in part may be granted by the Competent Authority of HBNI when in his or her judgment the proposed use of the material is in the interests of scholarship. In all other instances, however, permission must be obtained from the author.

Mainak Das

Mainak Das

DECLARATION

I, hereby declare that the investigation presented in the thesis has been carried out by me. The work is original and has not been submitted earlier as a whole or in part for a degree / diploma at this or any other Institution / University.

Mainak Das

Mainak Das

LIST OF PUBLICATIONS

Published

- #1. K. S. Anju[†], **Mainak Das**[†], B. Adinarayana, C. H. Suresh* and A. Srinivasan*, “*meso*-Aryl [20] π Homoporphyrin: The Simplest Expanded Porphyrin with the Smallest Möbius Topology”, *Angew. Chem. Int. Ed.* **2017**, *56*, 15667 –15671. (†equally contributed).
- #2. B. Adinarayana[†], Muthuchamy Murugavel[†], **Mainak Das**, Narasinga Rao Palepu and A. Srinivasan*, “Rhodium(III) and Iridium(III) Bipyricorrole Complexes: Syntheses, Structures, and Properties”, *Inorg. Chem.* **2018**, *57*, 1840–1845. (†equally contributed).
- #3. **Mainak Das**, B. Adinarayana, M. Murugavel, Subhashree Nayak and A. Srinivasan*, “Di-(*m-m-m*)terphenyl-Embedded Decaphyrin and Its Bis-Rh(I) Complex”, *Org. Lett.* **2019**, *21*, 2867–2871.
4. B. Adinarayana, **Mainak Das**, C. H. Suresh and A. Srinivasan*, “Homocarbaporphyrinoids: The *m-o-m* and *p-o-p* Terphenyl Embedded Expanded Porphyrin Analogues and Their Rh^I Complexes”, *Chem. Eur. J.* **2019**, *25*, 4683 – 4687.
5. S. Chitranshi[†], B. Adinarayana[†], **Mainak Das**, W.-Y. Cha, D. Kim and A. Srinivasan*, “Bis-4,4'-biphenyl Ring Embedded Octaphyrin with Three Distinct Conformational Structures”, *Chem. Eur. J.* **2019**, *25*, 12911 – 12915. (Hot Paper). (†equally contributed).

Communicated

#1. **Mainak Das**, S. Chitranshi, M. Murugavel, B. Adinarayana, A. Srinivasan*, “2,6-Di-*m*-phenylpyridine embedded Isosmaragdyrin: A stable analogue with N₃C₂ core to stabilize Rh(I) and Organo-Pt(II) complexes”, (Manuscript Communicated).

#2. **Mainak Das**, D. Singh, S. Chitranshi, B. Adinarayana and A. Srinivasan*, “Carbatriphyrin[3.3.1] – A New Class of Triphyrin and its Calixphyrin Analogue”, (Manuscript Communicated).

pertaining to this thesis

Mainak Das
Mainak Das

Conferences

1. “ 20π Homoporphyrin: The Smallest Expanded Porphyrin with Möbius Topology”, **Mainak Das**, B. Adinarayana, Ch. Sangya and A. Srinivasan* in 5th Symposium on Advanced Biological Inorganic Chemistry (SABIC-2017), January 7-11th, 2017. Organized by the Tata Institute of Fundamental Research (TIFR) and Indian Association for the Cultivation of Science (IACS) at Kolkata. **(Poster Presentation)**.
2. “Carbahomoporphyrins: Allowed and restricted conjugation in homoporphyrinoids by incorporation of *o*-terphenyl system”, **Mainak Das**, B. Adinarayana and A. Srinivasan* in International Symposium on Modern Trends in Inorganic Chemistry-XVII (MTIC-XVII), December 11-14th, 2017. Organized by Department of Chemistry, IISER Pune and NCL Pune at Pune. **(Poster Presentation)**.
3. “Core-modified Isosmaragdyrin[1.1.1.0.0] and Its Rh(I), organo Pt(II) Complexes”, **Mainak Das** in National Bioorganic Chemistry Conference (NBCC-2018), 22nd-24th December 2018, Organized by NISER Bhubaneswar at Bhubaneswar. **(Oral Presentation)**.

Mainak Das
Mainak Das

Dedicated to....

My Family

&

My Alma mater

ACKNOWLEDGEMENTS

The prolonged voyage of five years and one month has come to an end. This is the time to reminisce and express my debt of gratitude to everyone who travels with me throughout the journey and supported me to reach my destination.

I am tremendously grateful to the **Almighty** for immense blessings and giving strength at the twists and turns of my life.

Candidly, I must acknowledge the struggles of my **parents** for helping me to grow to this level. Their unconditional love, blessings and inspiration have strengthened me to face all the hurdles in my journey of life. I am in debt to my mother for all the love and care showered on me to see my progress. I salute my father's entire endeavor and endless sacrifice for my success.

I would like to express my gratitude and respect to my supervisor, **Prof. A. Srinivasan**, NISER, for continuous support, encouragement and kind-heartedness. He gave full freedom for free thinking and work out the problems, which helped me a lot in my research career. His humble behavior throughout the entire phase of my PhD will be remembered life-long.

I am thankful to, Director, **Prof. S. Panda**, NISER, **Prof. T. K. Chandrashekar**, founder-Director, NISER and also previous-Director, **Prof. V. Chandrasekhar**, NISER, for providing the laboratory facilities, which help me to complete my research work.

I thank my Doctoral committee members, Chairman **Dr. M. Sarkar**, **Dr. V. Krishnan**, **Dr. N. K. Sharma**, **Dr. P. Alone** and all other faculties in SCS NISER, especially **Dr. S. Peruncheralathan**, **Dr. C. Gunanathan**, **Dr. S. Nembenna**, **Dr. H. Biswal** for their useful suggestions and scientific officer **Dr. Arun Kumar** for his support on numerous occasions.

I owe my sincere thanks to my collaborator, **Dr. C. H. Suresh**, NIIST-Trivandrum, for his valuable assistance regarding theoretical studies described in the thesis.

I sincerely thank **Mr. Deepak**, **Mr. Sanjaya**, **Mr. Amit**, **Mr. Prakash**, **Dr. Mriganka** and **Mr. Raj Kumar**, NISER for performing characterization of my samples.

I am immensely obliged to **all my teachers** of school, graduation and post-graduation (**Dr. S. K. Baitalik**, **Prof. S. Bhattacharya**, Jadavpur University) who inculcated knowledge, discipline and inspiration for Chemistry.

It gives me enormous pleasure to thank all those seniors, friends and juniors who made my life at NISER certainly gratifying and memorable. Special mention must be made of my labmates, **Subhashree, Syamasrit, Prerna, Garima, Kavya, Khushboo, Deepak, Mahaprasad, Dr. Narasingha Rao, Dr. Antara, Dr. Woormi, Dr. Yogesh, Dr. Subbu, Dr. Jitendra, Dr. Ranjay**, and special thanks to my seniors **Dr. B. Adinarayana, Dr. A. Ghosh, Dr. M. Murugavel, Dr. Sumit Roy** (Jadavpur University) for their help and guidance and my best friends **Dipanjan** (Kolkata), **Debanjan** (Jadavpur University), **Pankaj** (NISER) for their colossal support in various stages of my research work. Also I thank my Ph.D batchmates **Bratati, Dipak** and **Pankaj** for their help. No words are enough for my pillar of strength during my Ph.D tenure, my bosom friend **Sangya Chitranshi**. Thanks a million **Sangya!** My sincere thanks to all my hostelmates, in particular **Siva Subramani, Murali, Milan, Prakash, Shreenibasa** for their friendship and support in all deeds. My special thanks to **Subhayan** who helped me in most of the NMR related problems. Also, I would like to acknowledge my special friend **Purba** for her support to record the variable temperature NMR data in IISc Bengaluru. Her company will be remembered forever. I am greatly thankful to all of my relatives, particularly my maternal uncle **Prof. K. Sengupta** and maternal aunt **Mrs. Asita Sengupta** for their support, suggestions and care.

I am privileged to stay strongly bonded to my beloved sister **Pallabi Das**, who cared and stood with me whenever I got stuck in any kind of snags.

Finally, I would like to express my earnest gratitude to everyone who contributed for the accomplishment of my course and I express my apology for those whom I could not mention here.

Mainak Das
Mainak Das

CONTENTS

	Page No.
Summary	xi
List of Tables	xiii
List of Schemes	xiv
List of Figures	xvi
List of Abbreviations	xxii
Chapter 1	1
Chapter 2	27
Chapter 3	56
Chapter 4	83
Chapter 5	118
Chapter 6	154

SUMMARY

Porphyrins are tetrapyrrolic macrocycles that contain 16 atoms in the inner core with 18π electrons in their conjugated pathway and follow Hückel aromatic character. By reducing or augmenting an atom in the inner core leads to formation of contracted or expanded porphyrinoids. Usually, the contracted derivatives are utilized for stabilizing higher oxidation state of metal ions, whereas the expanded analogues are exploited for aromatic – antiaromatic switching, structural diversity and stabilizing multi-metal ions in the macrocyclic core. By substituting one or more pyrrole units by polycyclic aromatic units such as arene / pyridine unit led to carba / pyriporphyrinoids, which are mainly exploited to study weak metal-arene interactions and stabilization of organometallic complexes. This thesis is mainly focuses on such analogs. It highlights syntheses, conformation, aromaticity and coordination chemistry of various contracted and expanded porphyrin analogues with thorough spectral studies and confirmed by crystal analyses. The first chapter describes the comprehensive literature survey of arene / pyridyl unit incorporated contracted, normal and expanded porphyrinoids. The second chapter deals with coordination chemistry of monoanionic bipyridyl corrole; especially Rh^{III} and Ir^{III} metal ions. The synthesis of [3.3.1]carbatriphyrin and structural characterization of respective calix analog as discussed in third chapter. The fourth chapter outlines synthesis of the simplest expanded porphyrin such as Homoporphyrin, where the macrocycle adopts Möbius aromatic character in (a) freebase; (b) protonated and (c) metal ion insertion. The fifth chapter reports on synthesis of innovative isosmaragdyrin(1.1.1.0.0) with a N_3C_2 core and further exploits the coordination chemistry of Rh^I and organo- Pt^{II} complexes. The Pt^{II} complex forms an unsymmetrical pincer type complex inside the macrocyclic core. The sixth chapter demonstrates the

synthesis of (*m-m-m*)terphenyl embedded carbadecaphyrin with open framework and stabilizes bis-Rh^I metal ions in the core.

List of Tables

1	Table 2.1	Bond length (Å) and bond angle around the metal ion (°) in 9 and 10b	43
2	Table 2.2	Saddling dihedral angle (°) in 9 and 10b	44
3	Table 2.3	Crystal data for 9 and 10b	45
4	Table 2.4	Electronic absorption spectral data of 5 , 9 and 10a recorded in CH ₂ Cl ₂	46
5	Table 3.1	Electronic absorption spectral data of 25 , 25.2H⁺ and 26 & emission spectral data of 25 and 26	74
6	Table 3.2	Crystal data for 26	79
7	Table 4.1	Torsion angles (°) at the twisted position of 17 and 19	105
8	Table 4.2	Crystal data for 17 and 19	107
9	Table 4.3	NICS (0) (ppm), HOMA and BLA (Å) values of 16 , 17 , 16.H⁺ , 17.H⁺ , 18 and 19	109
10	Table 4.4	Torsion angles at the twisted position of 16-19 obtained from optimized structure	111
11	Table 5.1	Crystal data for 38 , 38.2H⁺ , 39 and 40	143
12	Table 5.2	Electronic absorption spectral data of 38 , 38.2H⁺ , 39 and 40 & emission spectral data of 38 and 40	144
13	Table 5.3	Electrochemical data of 38 , 39 and 40	147
14	Table 6.1	Crystal data for 14 and 15	170

List of Schemes

1	Scheme 1.1	One-pot synthesis of porphyrin (1)	7
2	Scheme 1.2	One-pot synthesis of <i>meso</i> -aryl corrole (2)	11
3	Scheme 1.3	Coordination modes in metallocorroles	13
4	Scheme 1.4	Synthesis of tribenzosubporphine (3)	14
5	Scheme 1.5	Synthesis of 4 , 5 , 6	15
6	Scheme 1.6	Synthesis of 7 , 8 , 9 , 10 and 11	16
7	Scheme 1.7	Synthesis of benzocarbasapphyrin (23)	19
8	Scheme 1.8	Syntheses of dibenziamethyrin (25) and its Rh(I) (26), Ni (27) and Pd(28) complexes	20
9	Scheme 2.1	Synthesis of 9 and 10	33
10	Scheme 3.1	Synthesis of 25 and 26	65
11	Scheme 4.1	Synthesis of azahomoporphyrin 2 and its decomposition to corresponding metallated porphyrin derivatives	86
12	Scheme 4.2	Synthesis of Ni ^{II} homoporphyrins	87
13	Scheme 4.3	Synthesis of free base homoporphyrins	88
14	Scheme 4.4	Metallation of homoporphyrins	88
15	Scheme 4.5	Synthesis of core-modified homoporphyrin	89
16	Scheme 4.6	Synthesis of 16 and 17 and their Rh ^I complexes 18 and 19	92
17	Scheme 5.1	Synthesis of 4	121
18	Scheme 5.2	Redox reaction between 7b and 7a	122
19	Scheme 5.3	Synthesis of 8	122
20	Scheme 5.4	Synthesis of 11	123

21	Scheme 5.5	Synthesis of 14	124
22	Scheme 5.6	Synthesis of carbasapphyrin 18	124
23	Scheme 5.7	Synthesis of carbasapphyrin 21	125
24	Scheme 5.8	Synthesis of 22	125
25	Scheme 5.9	Synthesis of 25	126
26	Scheme 5.10	Synthesis of 28 and 29	126
27	Scheme 5.11	Synthesis of 30 , 34 and 37	127
28	Scheme 5.12	Synthesis of 38 , 39 and 40	128
29	Scheme 6.1	Synthesis of turcasarin (3)	156
30	Scheme 6.2	Synthesis of dioxo-turcasarin (4)	157
31	Scheme 6.3	Synthesis of planar decaphyrin (8)	157
32	Scheme 6.4	Template synthesis of decaphyrin (9)	158
33	Scheme 6.5	Synthesis of decaphyrin (11)	159
34	Scheme 6.6	Synthesis of 14 and 15	160

List of Figures

1	Figure 1.1	Typical UV-visible absorption spectrum of porphyrins	4
2	Figure 1.2	Frontier molecular orbital of porphyrin molecule	5
3	Figure 1.3	Nomenclature of porphyrin molecule	6
4	Figure 1.4	Modification of porphyrinoids	8
5	Figure 1.5	Contracted porphyrinoids	9
6	Figure 1.6	Periodic table indicates the elements form metallocorroles	12
7	Figure 2.1	Structures of phenanthroline (1) and carbazole-pyridine (2) embedded porphyrins	30
8	Figure 2.2	Structures of subporphyrin (3) and pyricorrole (4)	31
9	Figure 2.3	Structures of bipyricorrole (5) and Zinc ^{II} complex (6)	31
10	Figure 2.4	Structures of Rhodium ^{III} (7) and Iridium ^{III} (8) corrole complexes	32
11	Figure 2.5	Structures of Rhodium ^{III} (9) and Iridium ^{III} (10) bipyricorrole complexes	33
12	Figure 2.6	ESI-MS spectrum of 9	34
13	Figure 2.7	ESI-MS spectrum of 10a	34
14	Figure 2.8	¹ H-NMR spectra of 9 (a), 10a (b) in CDCl ₃ at 298K	35
15	Figure 2.9	Single crystal X-ray structures of 9 and 10b	37
16	Figure 2.10	Self-assembled dimers of 9	38
17	Figure 2.11	1-D arrays of 9	38

18	Figure 2.12	Single crystal X-ray structure of 10b	39
19	Figure 2.13	self-assembled dimers of 10b	39
20	Figure 2.14	2-D array of 10b	40
21	Figure 2.15	1-D array of 10b	41
22	Figure 2.16	1-D array of 10b	42
23	Figure 2.17	2-D arrays of 10b	42
24	Figure 2.18	Bond lengths in (Å)	43
25	Figure 2.19	Saddling dihedral angles of 9 and 10b	44
26	Figure 2.20	Steady state electronic absorption of 9 and 10a in CH ₂ Cl ₂	47
27	Figure 2.21	(a) Fluorescence emission spectra and (b) lifetime measurements of 9 and 5a in CH ₂ Cl ₂ .	47
28	Figure 2.22	Differential pulse voltammograms of 5a , 9 and 10a in CH ₂ Cl ₂ (scan rate = 0.1 Vs ⁻¹)	48
29	Figure 3.1	Structures of Subporphyrin (1) and subpyriporphyrin (2)	58
30	Figure 3.2	Structures of triphyrin(2.1.1) derivatives	59
31	Figure 3.3	Structures of core-modified triphyrin(2.1.1) derivatives	59
32	Figure 3.4	Structures of triphyrin(n.1.1) analogues	60
33	Figure 3.5	Structures of porphyrin (A), calixpyrrole (17) and calixphyrin (18)	61
34	Figure 3.6	Carbatriphyrin(3.1.1) (19) and their B ^{III} complexes (20,21)	62
35	Figure 3.7	Structures of carbacalixphyrins (22-24)	63
36	Figure 3.8	Carbatriphyrin (25) and its calixphyrin analogue	64

		(26)	
37	Figure 3.9	ESI-HR mass spectrometric analysis of a) 25 and b) 26	66
38	Figure 3.10	^1H NMR spectra of 25 (a) and 26 (b) in CD_2Cl_2	67
39	Figure 3.11	Variable temperature ^1H -NMR spectrum of 25 in CD_2Cl_2	68
40	Figure 3.12	^1H -NMR spectra of 25.2H⁺ with various equivalents of TFA in CD_2Cl_2	68
41	Figure 3.13	Single crystal X-ray structure of 26 .	69
42	Figure 3.14	Self-assembled dimers of 26	70
43	Figure 3.15	2-D array of 26	71
44	Figure 3.16	Selected Bond lengths in 26 (Å)	71
45	Figure 3.17	Electronic absorption spectra of 25 , 25.2H⁺ and 26	73
46	Figure 3.18	The electronic absorption spectrum of 25 with various equivalents of TFA in CH_2Cl_2	73
47	Figure 3.19	Emission spectra of 25 and 26 in CH_2Cl_2	74
48	Figure 4.1	Structures of homoporphyrins A-D	86
49	Figure 4.2	Structures of carba-homoporphyrins	89
50	Figure 4.3	Selective examples of Möbius aromatic expanded porphyrins	91
51	Figure 4.4	ESI-MS spectrum of 16	93
52	Figure 4.5	ESI-MS spectrum of 17	94
53	Figure 4.6	ESI-MS spectrum of 18	94
54	Figure 4.7	ESI-MS spectrum of 19	95
55	Figure 4.8	^1H NMR spectra of 16 and 18 in CD_2Cl_2	97

56	Figure 4.9	Variable temperature ^1H NMR spectrum of 16 in CD_2Cl_2	97
57	Figure 4.10	$^1\text{H} - ^1\text{H}$ COSY spectrum of 16 in CD_2Cl_2	98
58	Figure 4.11	^1H NMR spectrum of 16.H⁺ in CD_2Cl_2	98
59	Figure 4.12	$^1\text{H} - ^1\text{H}$ COSY spectra of 18 in CD_2Cl_2	99
60	Figure 4.13	Variable temperature ^1H NMR spectroscopy of 18 in CD_2Cl_2	99
61	Figure 4.14	Single crystal X-ray structure of 17 and 19	101
62	Figure 4.15	Self-assembled dimers of 17	102
63	Figure 4.16	1-D arrays of 17	103
64	Figure 4.17	1-D arrays of 17	103
65	Figure 4.18	self-assembled dimers of 19	104
66	Figure 4.19	Self-assembled dimers of 19	104
67	Figure 4.20	2-D array of 19	105
68	Figure 4.21	Torsion angles at the twisted position (in deg.) in 17 (a) and 19 (b)	106
69	Figure 4.22	Bond lengths in 17 (a) and 19 (b) (\AA)	106
70	Figure 4.23	Electronic absorption spectra of 16 , 16.H⁺ and 18 in CH_2Cl_2	108
71	Figure 4.24	Optimized geometry (B3LYP/DGDZVP level) of a) 16 and b) 18 with NICS(0) and HOMA values (in parentheses)	110
72	Figure 4.25	a), b) and c) are AICD Plots of 16 (a), 16.H⁺ (b) and 18 (c) at isosurface value 0.015 calculated at B3LYP/DGDZVP level of DFT	110
73	Figure 4.26	Bond length data in \AA for 16 , 16.H⁺ and 18 at B3LYP/DGDZVP level	111

74	Figure 5.1	Chemical structures of 1) pentaphyrin, 2) sapphyrin and 3) smaragdyrin	120
75	Figure 5.2	ESI-MS spectrum of 38	129
76	Figure 5.3	ESI-MS spectrum of 39	130
77	Figure 5.4	ESI-MS spectrum of 40	130
78	Figure 5.5	¹ H-NMR spectra of 38 , 39 and 40 in CD ₂ Cl ₂	132
79	Figure 5.6	Variable temperature ¹ H-NMR spectrum of 38 CD ₂ Cl ₂	133
80	Figure 5.7	¹ H NMR of 38 with various equiv. of TFA in CD ₂ Cl ₂	133
81	Figure 5.8	The solid state structures of 38 , 39 and 40	136
82	Figure 5.9	Single crystal X-ray structure of 38.2H⁺ with trifluoroacetate anion	136
83	Figure 5.10	Self-assembled dimers 38	137
84	Figure 5.11	2-D array of 38	137
85	Figure 5.12	Self-assembled dimers 39	138
86	Figure 5.13	1-D array of 39	138
87	Figure 5.14	2-D array of 39	139
88	Figure 5.15	Self-assembled dimers 40	139
89	Figure 5.16	2-D array of 40	140
90	Figure 5.17	Bond lengths of 38 in (Å)	140
91	Figure 5.18	Bond lengths of 38.2H⁺ in (Å)	141
92	Figure 5.19	Bond lengths of 39 in (Å)	141
93	Figure 5.20	Bond lengths of 40 in (Å)	142

94	Figure 5.21	The electronic absorption spectra of 38 , 38.2H⁺ , 39 and 40 in CH ₂ Cl ₂	145
95	Figure 5.22	The emission spectra of 38 and 40 in CH ₂ Cl ₂	145
96	Figure 5.23	Cyclic (□) and differential pulse (...) voltammograms of 38 , 39 and 40	147
97	Figure 6.1	HR-MS spectrum of 14	161
98	Figure 6.2	HR-MS spectrum of 15	161
99	Figure 6.3	¹ H NMR spectra of 14 (a) and 15 (b) in CDCl ₃	162
100	Figure 6.4	Single crystal X-ray structures of 14 and 15	164
101	Figure 6.5	1-D arrays of 14	165
102	Figure 6.6	3-D arrays of 14	166
103	Figure 6.7	Self-assembled dimers of 15	167
104	Figure 6.8	1-D arrays of 15	168
105	Figure 6.9	Bond lengths in (Å) 14 as present in the unit cell	168
106	Figure 6.10	Bond lengths in (Å) 15 as present in the unit cell	169
107	Figure 6.11	The electronic absorption spectra of 14 and 15 in CH ₂ Cl ₂	171

List of Abbreviations

^1H NMR	Proton Nuclear Magnetic Resonance
^{13}C NMR	Carbon-13 Nuclear Magnetic Resonance
^{11}B NMR	Boron-11 Nuclear Magnetic Resonance
^{19}F NMR	Fluorine-19 Nuclear Magnetic Resonance
^{31}P NMR	Phosphorus-31 Nuclear Magnetic Resonance
EPR	Electron Paramagnetic Resonance
UV-Vis	Ultraviolet–Visible
ESI	Electrospray Ionization
GOF	Goodness of Fit
CCDC	Cambridge Crystallographic Data Centre
DFT	Density Functional Theory
DDQ	2,3-Dichloro-5,6-dicyano-1,4-benzoquinone
CH_2Cl_2	Dichloromethane
CHCl_3	Chloroform
EtOAc	Ethyl acetate
CH_3CN	Acetonitrile
CH_3OH	Methanol
THF	Tetrahydrofuran
$\text{ClCH}_2\text{CH}_2\text{Cl}$	1,2-Dichloroethane
DMF	Dimethylformamide
$\text{C}_6\text{F}_5\text{COCl}$	Benzoyl chloride
$\text{CH}_3\text{SO}_2\text{Cl}$	Methanesulfonyl chloride
NaBH_4	Sodium borohydride
$\text{C}_6\text{F}_5\text{CHO}$	Pentafluorobenzaldehyde
POCl_3	Phosphorus oxychloride
PhMgBr	Phenylmagnesium bromide
PhBCl_2	Dichlorophenyl borane
TEA	Triethylamine
DMAP	4-Dimethylaminopyridine
TMP	Tetramethylpiperidine
NCP	N-confused porphyrin

CO	Carbon monooxide
HCl	Hydrogen chloride
TFA	Trifluoroacetic acid
BF ₃ .Et ₂ O	Boron trifluoride diethyl etherate
<i>p</i> -TSA	<i>para</i> -toluenesulphonic acid
TMS	Tetramethylsilane
CDCl ₃	Deuterated chloroform
CD ₂ Cl ₂	Dideuteromethylenechloride
CD ₃ CN	Deuterated acetonitrile
CD ₃ OD	Deuterated methanol
Toluene-d ₈	Deuterated toluene
DMSO- <i>d</i> ₆	Hexadeuterodimethyl sulfoxide
FB	Free-Base
TLC	Thin Layer Chromatography
Na ₂ SO ₄	Sodium sulphate
Zn(OAc) ₂	Zinc acetate
Cu(OAc) ₂	Copper acetate
Pd(OAc) ₂	Palladium acetate
Zn(ClO ₄) ₂	zinc perchlorate
Ag(PF ₆)	silver hexafluorophosphate
Ag(OTf)	silver triflate
[Rh(CO) ₂ Cl] ₂	Di- μ -chloro-tetracarbonyldirhodium(I)

CHAPTER 1

Evolution of Porphyrins and its derivatives

1.1	Porphyrin	3
1.2	Nomenclature	5
1.3	Synthesis	7
1.4	Modifications of porphyrins	7
1.4.1	Contracted porphyrins	9
1.4.2.1	Corroles	9
1.4.2.1.1	Characteristic properties of corrole	10
1.4.2.1.2	Synthetic Protocols	11
1.4.2.1.3	Metallocorroles	12
1.4.2.2.1	Subporphyrins	14
1.4.2.2.2	Triphyrins	15
1.4.3.1	Expanded porphyrins	17
1.4.3.2	Expanded carbaporphyrinoids	18
1.4.3.2.1	Expanded benziporphyrins	19
1.5	Conclusion	20
1.6	References	21

1.1 Porphyrins

Porphyrins (**1**) are tetrapyrrolic macrocycles and connected by four methine carbons.¹ These are found most of the biological systems such as hemoglobin, chlorophyll etc and due to this ubiquity, it termed as "pigments of life".² The derivatives of porphyrins play a pivotal role in numerous biological functions such as; i) oxygen transport and storage by hemoglobin and myoglobin; ii) electron transport processes mediated by cytochromes and iii) the light energy harvesting for photosynthetic process, a) in green plants as chlorophylls and b) in bacteria as bacteriochlorophyll.³ In addition, it has also been validated that porphyrin can act as efficient photosensitizers for photodynamic therapy^{4,5} and found applications in many research fields outspreading from biology, material sciences, electronics, catalysis to medicine.¹

Porphyrins are highly conjugated 22π electronic systems in the comprehensive conjugation pathway, while the shortest conjugation pathway comprises with 18π electrons.¹ Therefore, the macrocycle adapts $[4n+2]\pi$ Hückel rule and emerges as aromatic molecule. The general molecular formula of porphyrin is $C_{20}H_{14}N_4$ and the inner core of the macrocyclic framework contains 16 (C/N) atoms.¹ The name "porphyrin" stem from the Greek word "*porphura*" which means purple color. Utmost of the naturally obtain porphyrin dyes are purple in color. Porphyrin is a dianionic tetradentate square planar ligand with D_{2h} symmetry. The macrocycle contains two imine and two amine nitrogens and the cavity size is ideal to bind almost all metal ions. The versatility of porphyrin chemistry has encouraged researchers to synthesize and study the innovative porphyrin analogues in last three decades.^{1, 6-7}

The electronic absorption spectra were decisively used to characterize porphyrin macrocycle. Around 400 nm, a strong and sharp band is observed along with high value of molar extinction coefficients ($\sim 10^5 \text{ M}^{-1}\text{cm}^{-1}$). This band is known as Soret or B band. The other four weak bands are appeared in the range of 450-700 nm and called as Q bands (Figure 1.1). The metal ion insertion leads to change in symmetry from D_{2h} to D_{4h} , thus the decrease the number of Q bands from four to two. Such significant change in optical spectra aids to distinguish free base porphyrin and its coordinated complex.

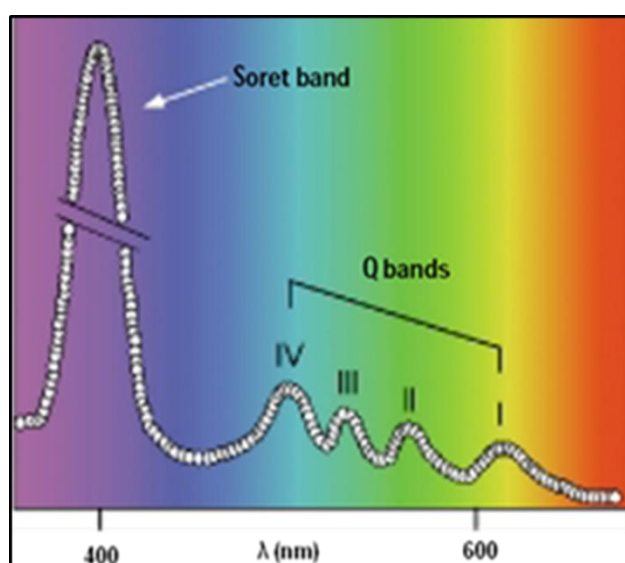


Figure 1.1: Typical UV-visible absorption spectrum of porphyrins

The electronic absorption spectral pattern of porphyrin follows a renowned Gouterman four orbital model (Figure 1.2) about the electronic transitions from $S_0 \rightarrow S_n$.⁸ As per the model, there are two sets of degenerate orbitals, one is the highest occupied molecular orbitals (HOMO) and another is the lowest unoccupied molecular orbital (LUMO). The HOMO are labeled as a_{2u} , a_{1u} and the LUMO are e_{gx} , e_{gy} respectively. Electronic transitions among $a_{2u} \rightarrow e_{gx}$ and $a_{1u} \rightarrow e_{gy}$ are optically allowed transitions, which generates Soret band with high molar extinction coefficient. Whereas, the cross

transitions between $a_{2u} \rightarrow e_{gy}$ and $a_{1u} \rightarrow e_{gx}$ are optically forbidden transitions, produces Q-bands with less molar extinction coefficient.

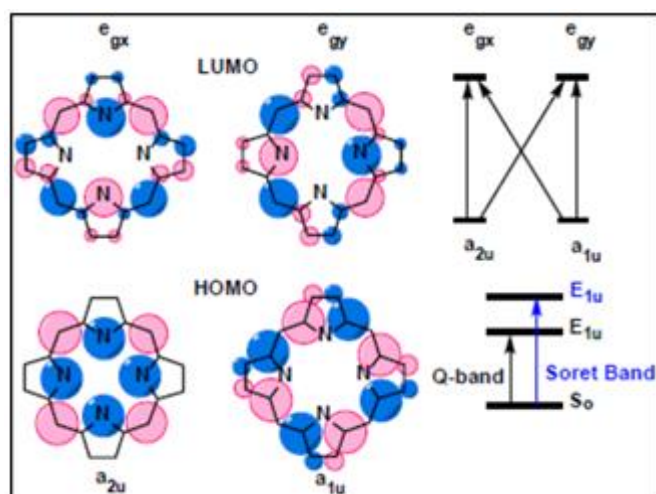


Figure 1.2: Frontier molecular orbital of porphyrin molecule

1.2 Nomenclature:

As per the convention, the 2- and 5-positions of five-membered heterocycles (pyrrole, furan and thiophene etc) denoted as the alpha (α) positions, whereas the 3- and 4-positions are commonly mentioned as the beta (β) positions. The same nomenclature are used when these heterocycles are incorporated into the porphyrin structure. Therefore, the 1-, 4-, 6-, 9-, 11-, 14-, 16-, 19-positions of a porphyrin system are referred as α positions while 2-, 3-, 7-, 8-, 12-, 13-, 17- and 18- are termed as β positions. The bridging atoms which connect the heterocyclic units are entitled as “*meso*”. Hence, the 5-, 10-, 15- and 20-positions of a porphyrin ring are termed as the *meso*-positions (Figure 1.3).

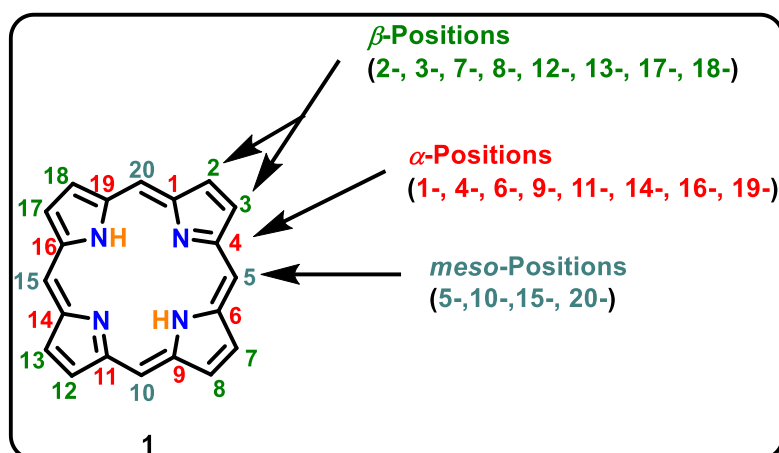
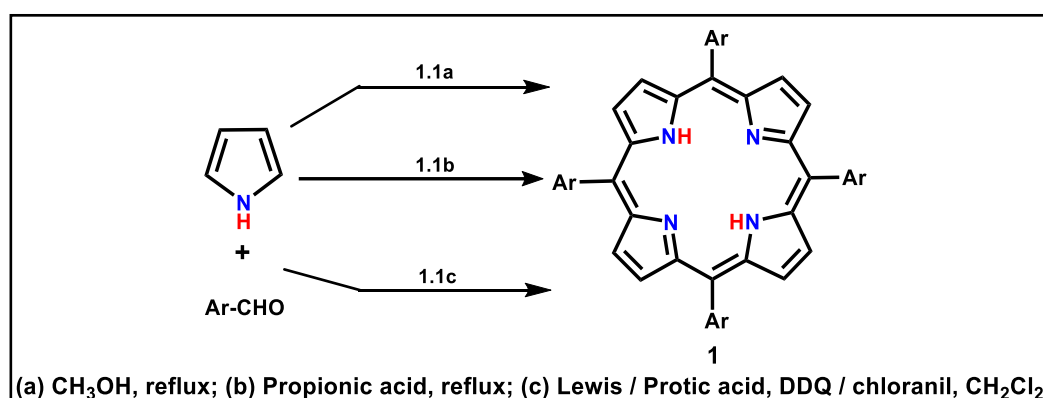


Figure 1.3: Nomenclature of porphyrin molecule

With the progress in porphyrin chemistry, several complexities arose while doing nomenclature of the porphyrin molecule according to IUPAC norms, thus to overcome trivial names were allotted by their discoverers. These names are created based on the colour or other characteristics of the macrocycle, followed by the suffix “phyrin” or “rin” taken from the parent porphyrin macrocycle. Woodward and co-workers initiated this trend by assigning the name “sapphyrin” to a pentapyrrolic macrocycle, as the molecule crystallizes as dark blue solid.⁹ Correspondingly, many molecules were named akin to prior fashion, e.g. rubyrin (red-coloured). Later on, the nomenclature were adopted based on the following three essential parts: (1) the total number of π electrons in the shortest conjugation pathway denoted in square brackets (2) a core name representing the number of pyrroles or other heterocycles in the complete systems [e.g., pentaphyrin (with five pyrroles), hexaphyrin (with six pyrroles), heptaphyrin (with seven pyrroles) etc.] and (3) numbers in round brackets separated by dots subsequent to the main name, instruct the number of *meso* carbon atoms present between each pyrrole / heterocyclic ring and always it commences with the largest *meso* carbon bridge. For example, as per this nomenclature procedure, porphyrin **1** would be named as [18]tetraphyrin(1.1.1.1).

1.3 Synthesis

In 1935, porphyrin **1** (Scheme 1.1a) was first synthesized by Rothmund,¹⁰ by condensation of pyrrole and aldehydes in methanol at different temperatures. Subsequently, various improved synthetic methodologies have been established, i) Adler and Longo developed a synthetic process by the condensation of pyrrole and benzaldehyde in propionic acid in the presence of air under reflux condition (Scheme 1.1b);¹¹ and ii) Lindsey and co-workers reported the synthesis of porphyrin in good yields by the protic or Lewis acid-catalyzed condensation of pyrrole and aryl aldehydes followed by oxidation with chloranil or 2,3-dichloro-5,6-dicyano-1,4-benzoquinone (DDQ) (Scheme 1.1c),¹²



Scheme 1.1: One-pot synthesis of porphyrin (**1**).

1.4 Modifications of porphyrins

The intrinsic properties of porphyrin prompted to explore different porphyrinoids with distinct type of modifications in the core as well as periphery for various applications. Such porphyrinoids are listed below (Figure 1.4): (a) *Peripheral modification*: Substituents are introduced at the peripheral β -carbon atom and / or meso-carbon bridges;¹³⁻¹⁵ (b) *Contracted porphyrinoids*: decreasing the number of pyrrole and / or

meso-carbon in the porphyrin skeleton, which forms contracted porphyrin;¹⁶⁻¹⁸ (c) *N-confused porphyrinoids*: instead of α connection, β position of one or more pyrrole units are connected to the *meso*-carbon bridges;¹⁹⁻²⁰ (d) *Core-modified porphyrinoids*: one or more pyrrole nitrogen atoms are replaced by chalcogen atoms, generates core-modified porphyrinoids;²¹⁻²² (e) *Expanded porphyrinoids*: Increment of the π electronic conjugation in the porphyrin framework by augmenting one or more pyrrolic/heterocyclic rings or number of *meso* carbon units leads to formation of expanded porphyrinoids.²³⁻²⁴

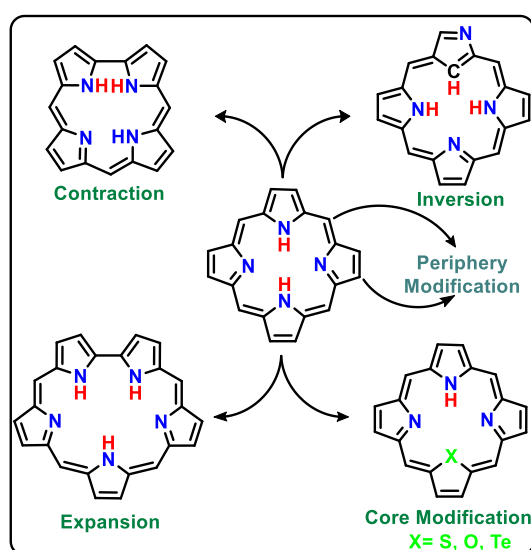


Figure 1.4: Modifications of Porphyrinoids.

As this thesis is mainly focused on the syntheses, spectral, structural characterization and coordination chemistry of arene / pyridine unit incorporated contracted as well as expanded porphyrinoids and all aza homoporphyrinoids, the brief introduction about these porphyrinoids and its analogues are highlighted in the respective chapters. Hence, this chapter describes the brief literature survey on contracted and expanded porphyrinoids.

1.4.1 Contracted porphyrins

The contracted porphyrin has smaller internal cavity compared to normal porphyrin frame work with one *meso*-carbon / pyrrole rings less in their macrocyclic core. Among the contracted porphyrinoids, corroles (2) and subporphyrins (3) (Figure 1.5) are well known and further discussed below.

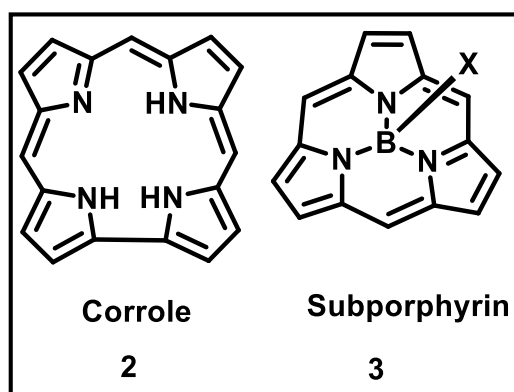


Figure 1.5: Contracted porphyrinoids.

1.4.2.1 Corroles

The research on contracted porphyrins was initiated after the structural characterization of vitamin B₁₂, which exposed the presence of a naturally occurring macrocycle, corrin. The structure of corrin ring is similar to porphyrin framework, however, one *meso* carbon less in its core.²⁵ After successful structural elucidation of Vitamin B₁₂, remarkable efforts were devoted to develop efficient synthetic methodologies for such molecule.²⁶ Subsequently, in the year 1960, a series of metallic derivatives of pentahydrocorrins was prepared by Johnson & Price and coined such derivatives as corroles.²⁷ Later, same group has also demonstrated the synthesis of corrole in its freebase form, which is an oxidized form of corrin system and can act as an intermediate between porphyrins and corrins.²⁸ The most notable structural difference between

porphyrin and corrole is that one *meso*-carbon less with direct pyrrole-pyrrole linkage between two pyrrole rings. Thus, corroles contribute as contracted porphyrinoids in porphyrin chemistry.

1.4.2.1.1 Characteristic properties of corrole

Corroles (**2**) are highly stable 18π aromatic systems. The presence of three protons in the inner core and behave as trianionic chelating ligands which is contrary to the monoanionic corrin and dianionic porphyrin **1**. This specific property is exploited effectively to stabilize metal ions in higher oxidation state.

The electronic absorption spectra of corroles exhibit an intense band at around 400 nm and weaker bands in the region of 500-600 nm.²⁸ This spectral characteristic resembles the B and Q bands of porphyrins. Corroles are fluorescent molecules and the luminescence is observed in the region of 600-700 nm with a fluorescence lifetime in nanosecond range.²⁹

Corroles are more acidic in nature than porphyrins. In presence of dilute bases, freebase corrole releases a protons and produce monoanionic species to ease out from trianionic steric crowding.²⁸ On the other hand, in presence of dilute acids, it forms monoprotonated specie.^{28,30} Both the monoanionic and monocationic forms of corroles sustain the aromaticity.

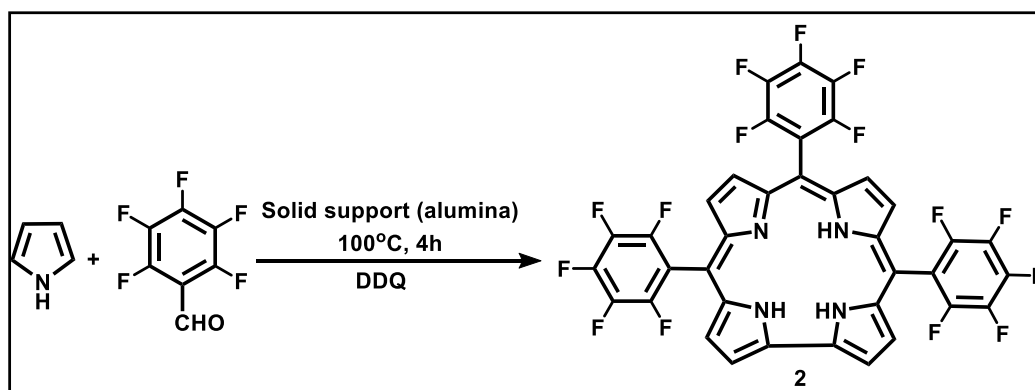
¹H NMR spectral analysis of corroles exhibit diatropic ring current. The pyrrolic β -protons and the *meso*-protons appear in the strongly deshielded region, whereas, inner imino protons resonate in the shielded region between -2.00 and -3.00 ppm, as a broad singlet. The broadness of peak signifies two reasons: a) presence of non-identical

tautomers and b) highly acidic nature of the corrole molecule.³¹ However, in some cases the three different types of NH protons are observed at ~226 K.

The crystal analyses revealed that the macrocycle is slightly deviated from the planarity in order to curtail the steric crowding inside the macrocyclic core.³² Further, one of the inner core protons is in the macrocyclic mean plane whereas the other two are above and below the plane respectively, which instigate saddling of the pyrrole rings.

1.4.2.1.2 Synthetic Protocols

In the year 1965, corrole was first synthesized by Johnson and Kay.²⁸ Since then, several synthetic methodologies have been reported to increase the corrole yields. The corrole chemistry (2) research received much attention after introducing the proficient synthetic methods by different groups, such as Gross *et al.*, Paolesse *et al.*, and Gryko *et al.*³³⁻³⁵ One pot synthetic methodology of Gross *et al.* is shown in scheme 1.2, where pyrrole and aryl aldehyde are condensed to obtain freebase corrole without column purification in 11% yield.³³



Scheme 1.2: One-pot synthesis of *meso*-aryl corrole (2).

1.4.2.1.3 Metalloporroles

Tri-anionic core of porroles encouraged researchers to explore the chemistry of metalloporroles shortly after the discovery of the freebase porroles. Due to the lack of facile synthetic procedures for the freebase ligands, formation of the metalloporroles remained as the herculean task. Fundamentally, there are two methodologies for the synthesis of metalloporroles: a) as a metal template for macrocyclization and b) usual metal ion inclusion into the porrole cavity, however, choice of the metal ion plays a remarkable role in both the cases.

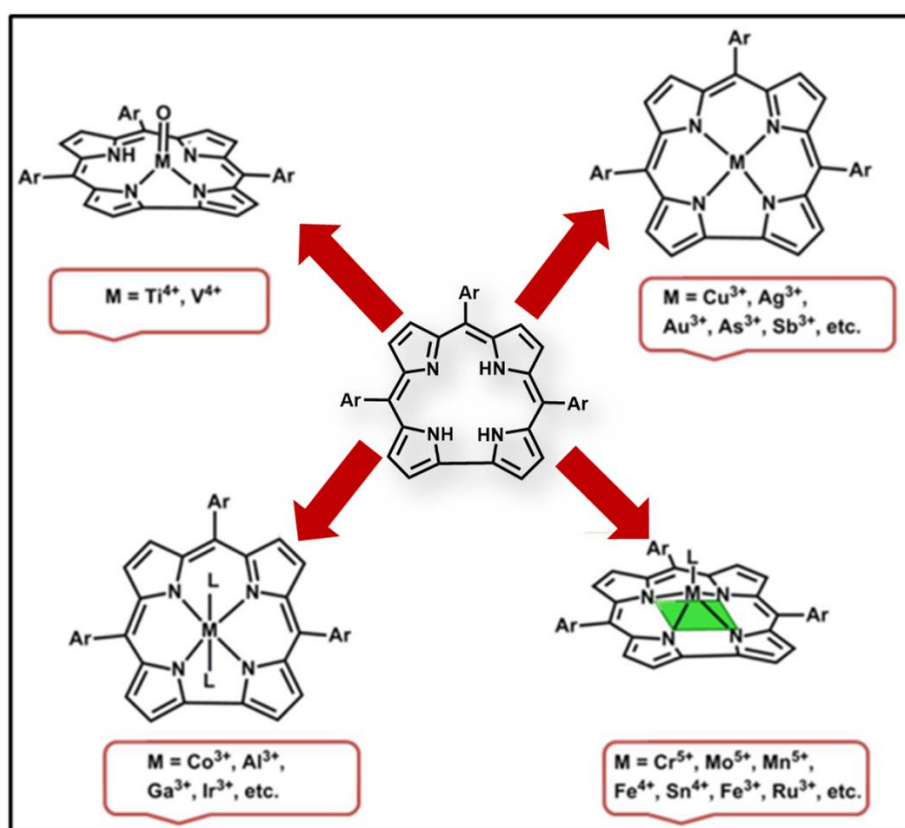
Metalloporrole chemistry has not yet been enriched like metalloporphyrins, however, ample amount of research has been devoted to insert cations in the macrocyclic core. Such elements are highlighted in the periodic table (Figure 1.6).

The periodic table shows elements highlighted in red, indicating their suitability for metalloporroles. The highlighted elements are: Li, Be, B, C, N, O, F, Ne, Na, Mg, Al, Si, P, S, Cl, Ar, K, Ca, Sc, Ti, V, Cr, Mn, Fe, Co, Ni, Cu, Zn, Ga, Ge, As, Se, Br, Kr, Rb, Sr, Y, Zr, Nb, Mo, Tc, Ru, Rh, Pd, Ag, Cd, In, Sn, Sb, Te, I, Xe, Cs, Ba, La, Lu, Hf, Ta, W, Re, Os, Ir, Pt, Au, Hg, Tl, Pb, Bi, Po, At, Rn, Fr, Ra, Ac, Th, Pa, U, Np, Pu, Am, Cm, Bk, Cf, Es, Fm, Md, No.

Figure 1.6: Periodic table indicates the elements form metalloporroles.

Based on metal ion stabilization, the complexes are placed in four different categories and shown in Scheme 1.3. Square-pyramidal geometry around the central metal ion is the most usual coordination mode of binding by porroles.³⁶ This construct domed type

of configuration due to the axial displacement of the central metal atom from the N4 plane of macrocyclic core. In case of complexes with Cr, Mo, Mn, Fe, Co, Rh, Ge, Sn or P have anionic axial ligands such as triphenylphosphine, pyridine or halides (F^- , Cl^- , Br^- , I^-), phenyl, methyl, oxo, nitride and nitrosyl, thus form domed configuration.^{37, 38}



Scheme 1.3: Coordination modes in metallocorroles.

Another coordination approach is to form hexa-coordinated complex (Scheme 1.3). Such octahedral geometry is observed for cobalt(III), aluminium(III), gallium(III) and iridium(III) metal complexes with pyridine as axially ligands.³⁹⁻⁴²

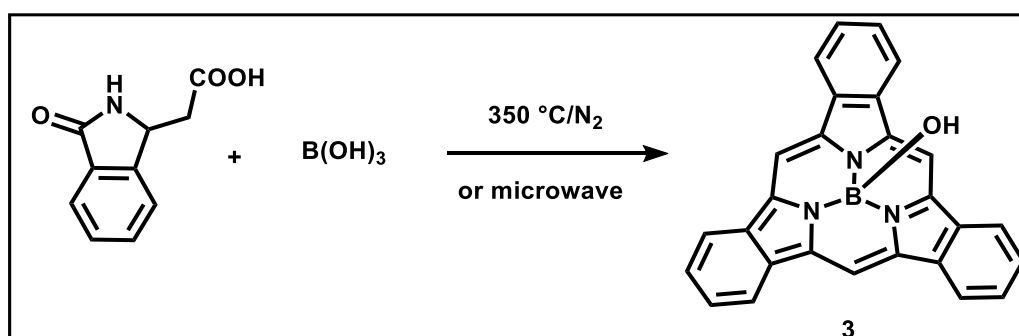
Certain transition metals and main group metals such as Cu(III), Ag(III), Au(III), In(III), As(III), Sb(III), Bi(III) etc form four-coordinated complexes of corroles and attain square planar geometry (Scheme 1.3).⁴³⁻⁴⁶ Also, Co(III), Mn(III) and Ru(III) complexes maintain geometry in absence of any coordinating solvents.^{28, 47-48}

Henceforth, corroles were recorded as trianionic and tetradentate ligands. However, sporadically behave as oxovanadium(IV) and oxotitanium(IV) corrole complexes.⁴⁹

The corrole complexes with alkali metals (merely lithium corrole has structurally characterized),⁵⁰ early transition metals (from Group 4 to Group 11, heavier elements), main group corroles (Group 13-15, late main group elements), lanthanides (namely lanthanum, gadolinium and terbium corroles) and actinide series (namely thorium and uranium corroles) were hardly stated.⁵¹ Recent advances overcome the obscure synthetic processes and make the availability of these air-sensitive complexes.

1.4.2.2.1 Subporphyrins

Subporphyrins (**3**) are the simplest ring contracted porphyrinoids, where three pyrrole rings are connected through three meso carbon bridges. As per the nomenclature, these can be represented as triphyrin(1.1.1). In 2006, the first subporphyrin, tribenzosubporphine **3** was synthesized by the group of Osuka as the B(III) complex (Scheme 1.4), under harsh reaction conditions in ~1.4% yield.⁵² Since then, several subporphyrin derivatives were synthesized and studied their unusual properties in various fields.⁵³

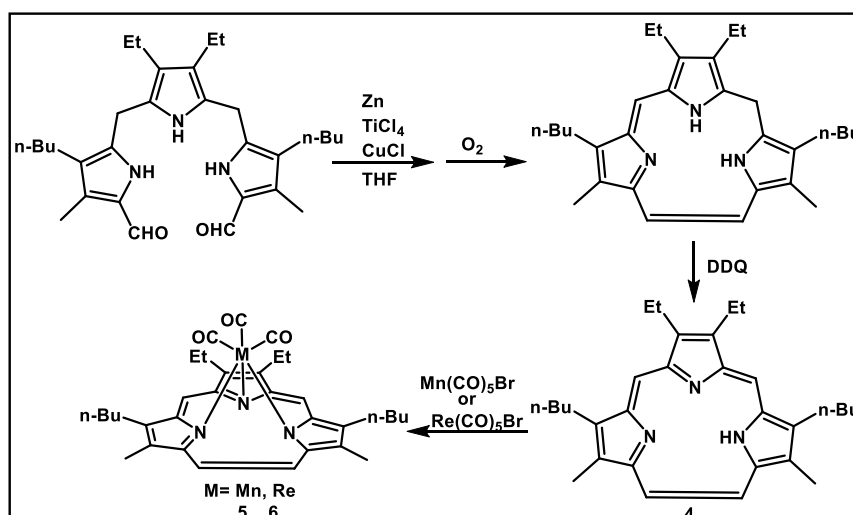


Scheme 1.4: Synthesis of tribenzosubporphine (**3**).

1.4.2.2 Triphyrins

Subporphyrins with three *meso* carbons are mostly stabilized as B(III) complex. The freebase analogue was reported by introducing additional *meso*-carbon in the macrocyclic core. Thus, the synthesized triphyrin(2.1.1) is relatively stable as compared to **3** and its rich coordination chemistry is further exploited.

The *meso*-free[14]triphyrin(2.1.1) (**4**) was synthesized by Yamada and co-workers through McMurry coupling reaction. The core was utilized to stabilize Mn(I) (**5**) and Re(I) (**6**) complexes (Scheme 1.5) and the yield were 80% and 71% respectively.⁵⁴

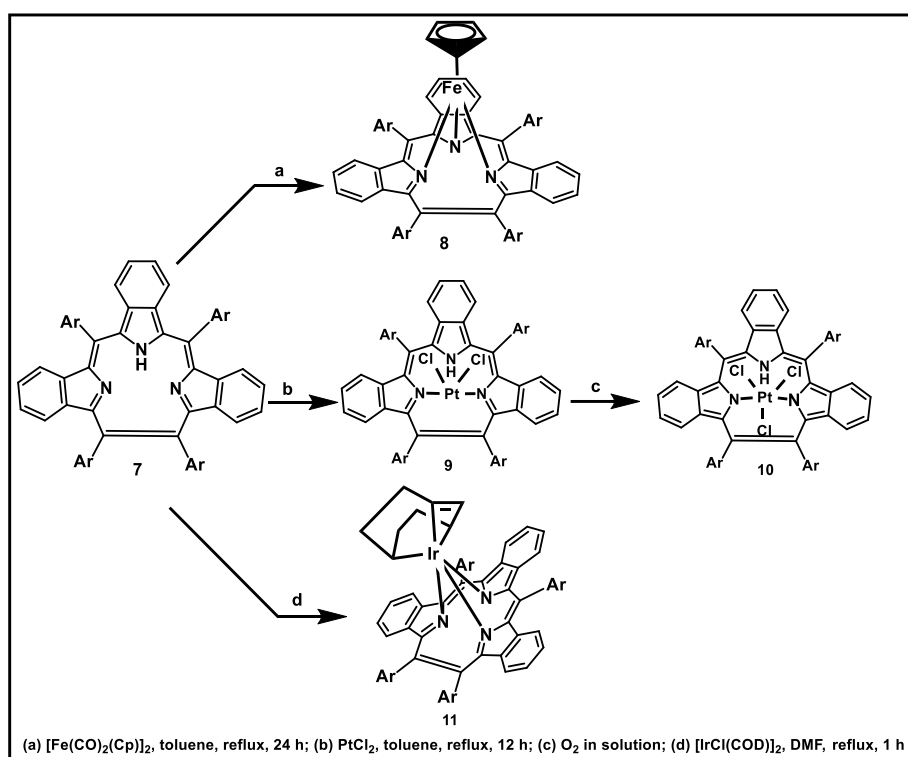


Scheme 1.5: Synthesis of **4**, **5**, **6**.

The same group was also reported η^5 -cyclopentadienyliron(II)-[14]triphyrin(2.1.1) sandwich complex (**8**).⁵⁵ Dry toluene solution of *meso*-aryl freebase (**7**) was treated with 5 equiv of [Fe(CO)₂(Cp)]₂ and refluxed for 24 h under argon to obtain **8** in 40-45% yield (Scheme 1.6a).

The Pt(II) (**9**) and Pt(IV) (**10**) complexes were further reported by same group. The metalation of [14]triphyrin(2.1.1) (**7**) with PtCl₂ under toluene reflux condition afforded

platinum(II) complex (**9**) in 47% yield (Scheme 1.6b). The crystal analysis confirmed the complex with a saddle-shaped square-planar coordination structure with two pyrrolic nitrogen atoms and two chloride ions. The complex **9** was simply oxidized by air to a platinum(IV) complex (**10**) in 11% yield, where Pt(IV) was coordinated by three pyrrolic nitrogen atoms as a tridentate monoanionic cyclic ligand and three chloride ions (Scheme 1.6c).⁵⁶



Scheme 1.6: Synthesis of **7**, **8**, **9**, **10** and **11**.

The same group has also demonstrated the synthesis of Ir(III) triphyrin complex (**11**).⁶⁶ A sandwich complex of iridium(III) benzotriphyrin (**11**) was synthesized by refluxing DMF solution of **7** with $[\text{IrCl}(\text{cod})]_2$ (COD = 1,5- cyclooctadiene) to obtain in 46% yield. The crystal analysis revealed that the COD ring was converted from 1,5-COD to an η^1, η^3 - C_8H_{12} unit as a π -allyl ligand to stabilize Iridium ion in +3 oxidation state (Scheme 1.6d).⁵⁷

1.4.3.1 Expanded porphyrins

Expanded porphyrins are higher analogues of porphyrin with more than 18π electrons in their shortest conjugated pathway. These are achieved by increasing either the number of heterocyclic rings or *meso*-carbon atoms or both in a fashion that the internal ring pathway contains minimum of 17 atoms in the core.²⁴ Research on expanded porphyrins gained momentum due to larger internal cavity as compared to porphyrin, thus leads to; (i) stabilize multi-metallic complexes; (ii) bind with different anionic and neutral substrate and (iii) structural diversity as well as switching of aromaticity.

In 1966, serendipitous discovery of sapphyrin by Woodward and co-workers embarked the chemistry of expanded porphyrin.⁹ Sapphyrin is a cyclic pentapyrrolic macromolecule, where the five units are connected via four *meso* linkages and one direct linkage. Initially (1966–1990), sapphyrins were mainly investigated by Johnson and co-workers. Afterward, Vogel and co-workers reported a series of octaphyrin derivatives.⁵⁸ Simultaneously, several expanded porphyrins were mainly reported by Sessler & co-workers and Osuka & co-workers during last three decades. These analogues received ample attention due to its potential applications in various fields such as; (i) MRI contrasting agents; (ii) non-linear optical materials (NLO); (iii) photodynamic therapeutic agents (PDT) etc.²⁴ Till now, numerous expanded porphyrins are reported in the literature, such as homoporphyrin **12**, sapphyrins **13**,⁹ smaragdyrins,⁵⁹ pentaphyrins,⁶⁰ amethyrins **14**,⁶¹ rubyrins **15**,⁶² hexaphyrins **16**,⁶³ heptaphyrins **17**,⁶⁴ octaphyrins **18**,⁶⁵ nonaphyrins **19**,⁶⁶ turcasarins / decaphyrins **20**,⁶⁷ dodecaphyrins, hexadecaphyrins, icosapphyrins, tetracosapphyrin and the expanded derivative with 96π electrons in the macrocyclic framework. Some of the examples of expanded porphyrinoids are shown in Figure 1.7.

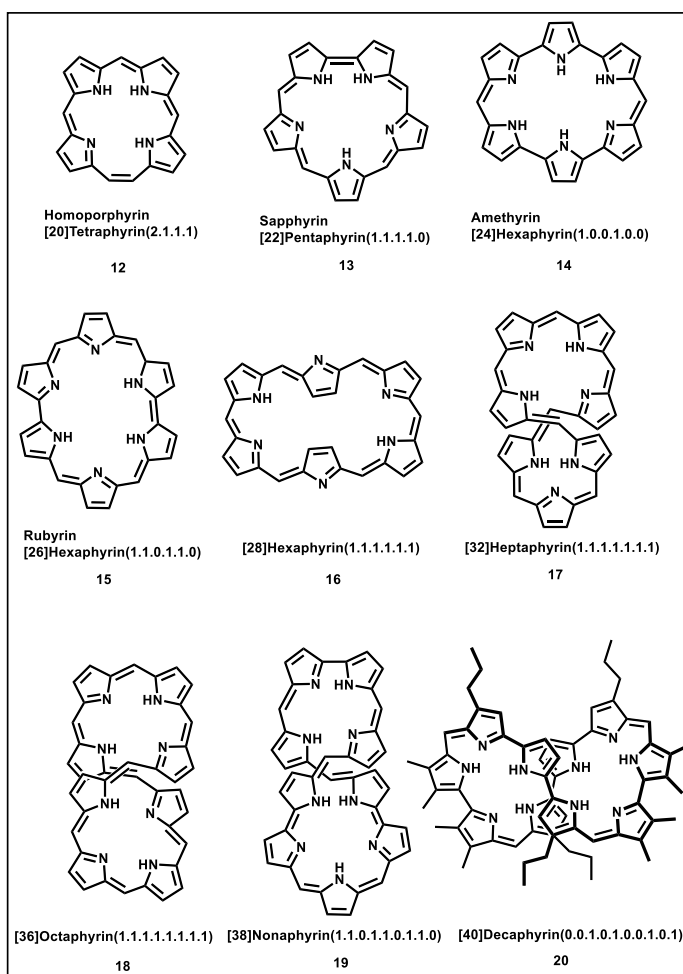
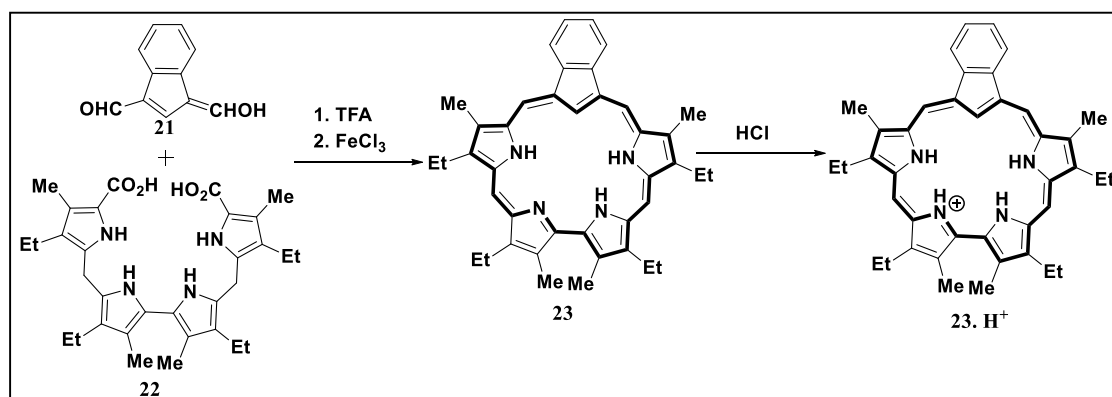


Figure 1.7: Structures of expanded porphyrinoids.

1.4.3.2 Expanded carbaporphyrinoids

The first expanded carbaporphyrin, benzocarbasapphyrin **23** was reported by T. D. Lash.⁶⁸ Indene dialdehyde **21** was reacted with tetrapyrrole **22** in the presence of trifluoroacetic acid followed by oxidation with DDQ to form benzocarbasapphyrin **23** in 36% yield (Scheme 1.7). The yield was increased to 38% by changing the oxidizing agent from DDQ to aqueous ferric chloride under similar reaction condition. The compound **23** in freebase form was unstable and gradually decomposed in solution state. However, the respective monocationic specie (**23.H⁺**) was found to be stable in the presence of HCl. The spectral analyses revealed the diatropic ring current, where

the inner CH and NH protons were observed at -7.9 ppm (-CH) and -5.1 & -4.4 ppm (-NH). In addition, the Soret band at 476 nm and Q-bands between 550 and 800 nm further supported the aromatic characteristics.

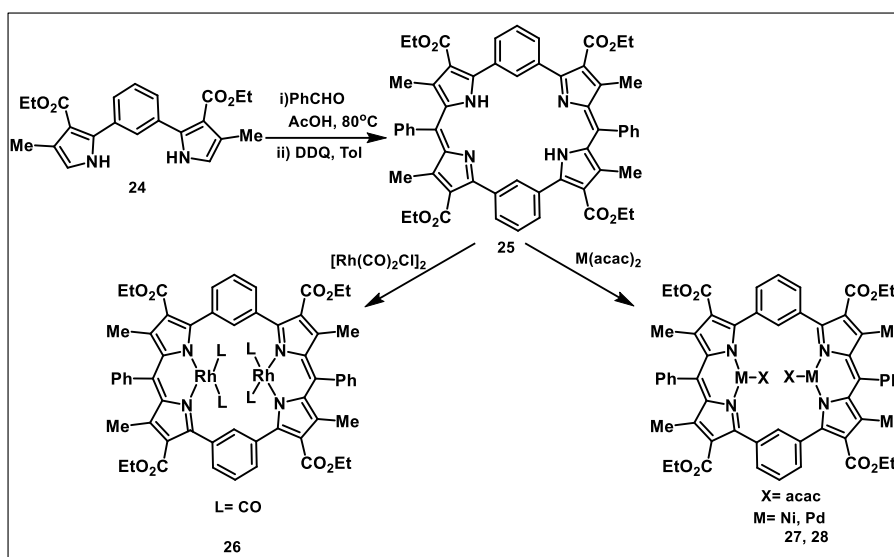


Scheme 1.7: Synthesis of benzocarbasapphyrin (**23**).

1.4.3.2.1 Expanded benziporphyrins

The first example of an expanded benziporphyrin, dibenzihexaphyrin (1.0.0.1.0.0) (**25**) was reported by Corriu and coworkers.⁶⁹ The *cis*- and *trans*-isomers were synthesized by reaction between *m*-dipyrrolylbenzene (**24**) and benzaldehyde in refluxing acetic acid (Scheme 1.8). To accomplish fully conjugated dibenziamethyrin (**25**), the oxidation with DDQ in toluene was further performed.⁶⁹⁻⁷⁰ The presence of *m*-arene unit in the macrocyclic core restricts the macrocyclic conjugation, thus revealed nonaromatic characteristics, where ¹H NMR showed the *meso*-protons at 7.90 ppm and NH at 14.10 ppm and the absorption spectral analysis displayed two bands at 454 and 487 nm. The core of **25** was effectively utilized for coordination chemistry. Bis-Rh(I) complex of dibenziamethyrin (**26**) was formed by reaction of **36** with [Rh(CO)₂Cl]₂ in benzene in 91% yield. Bimetallic Ni(II) (**27**) and Pd(II) (**28**) derivatives of **25** were also obtained by treating dibenziamethyrin (**25**) with nickel(II) or palladium(II)

acetylacetonate in 61% and 99% yield respectively. The spectral studies of metal complexes (**26-28**) suggested the typical nonaromatic characteristics as observed in **25**.



Scheme 1.8: Synthesis of dibenziamethyrin (**25**) and its Rh(I) (**26**), Ni(II) (**27**) and Pd(II) (**28**) complexes.

Since then, several expanded benziporphyrins were reported in the literature, such as A,C-di-*p*-benzi[24]pentaphyrin,⁷¹ N-fusedA-*p*-benzi[24]pentaphyrin,⁷² A,D-di-*p*-benzi[28]hexaphyrin,⁷¹ A,C-di-*p*-benzi[28]hexaphyrin,⁷¹ di-*m*-benzi-decaphyrin⁷³ etc. Some of these expanded porphyrinoids were further discussed in the individual chapters.

1.5 Conclusion

In light of the widespread literature discussions covering the chemistry of different types of corrole, triphyrin and expanded porphyrin derivatives, it is clear that the coordination chemistry, aromaticity switching and structural diversity of such derivatives have been a growing area of research. Among these, incorporation of pyridine and benzene into the macrocyclic core received much attention. Albeit, in

particular the chemistry of contracted and expanded porphyrinoids of respective moieties are relatively rare till date. Hence, the progress on pyridine and as well as benzene moiety introduced porphyrinoids offer an astute platform to explore various applications. In the present thesis, an attempt has been made to develop new synthetic methodologies to incorporate pyridine and benzene in the porphyrin skeleton from a simple novel precursor and exploring the intriguing coordination chemistry of these analogues. In addition, another objective of this thesis is to develop new methodology to synthesize hitherto unknown *meso*-aryl substituted aza homoporphyrin from 5,6 diaryldipyrroethane. Further, there is a broad scope of work with trianionic freebase homoporphyrin and also to explore its coordination chemistry in order to understand their aromatic characteristics.

1.6 References

1. K. M. Kadish, K. Smith, R. Guilard, *The Porphyrin Handbook, Volume 1: Synthesis and Organic Chemistry*. Academic Press–San Diego, CA and London, UK: **2000**.
2. A. R. Battersby, C. J. Fookes, G. W. Matcham, E. McDonald, *Nature* **1980**, 285, 17-21.
3. S. J. Lippard, J. M. Berg, *Principles of bioinorganic chemistry*. University Science Books: **1994**.
4. T. J. Dougherty, S. L. Marcus, *Eur. J. Cancer* **1992**, 28, 1734-1742.
5. J. Moan, K. Berg, *Photochem. Photobiol.* **1992**, 55, 931-948.
6. J. L. Sessler, S. J. Weghorn, *Expanded, contracted & isomeric porphyrins*. Elsevier: **1997**; Vol. 15.
7. A. Jasat, D. Dolphin, *Chem. Rev.* **1997**, 97, 2267-2340.

-
8. M. Gouterman, G. H. Wagnière, L. C. Snyder, *J. Mol. Spectrosc.* **1963**, *11*, 108-127.
 9. V. J. Bauer, D. L. J. Clive, D. Dolphin, J. B. Paine, F. L. Harris, M. M. King, J. Loder, S. W. C. Wang, R. B. Woodward, *J. Am. Chem. Soc.* **1983**, *105*, 6429-6436.
 10. P. Rothmund, *J. Am. Chem. Soc.* **1935**, *57*, 2010-2011.
 11. A. D. Adler, F. R. Longo, J. D. Finarelli, J. Goldmacher, J. Assour, L. Korsakoff, *J. Org. Chem.* **1967**, *32*, 476.
 12. J. S. Lindsey, I. C. Schreiman, H. C. Hsu, P. C. Kearney, A. M. Marguerettaz, *J. Org. Chem.* **1987**, *52*, 827-836.
 13. X.-D. Xu, J. Zhang, L.-J. Chen, R. Guo, D.-X. Wang, H.-B. Yang, *Chem. Commun.* **2012**, *48*, 11223-11225.
 14. H. Yorimitsu, A. Osuka, *Asian J. Org. Chem.* **2013**, *2*, 356-373.
 15. K. A. D. de Freitas Castro, F. Wypych, A. Antonangelo, K. M. Mantovani, A. Bail, G. M. Ucoski, K. J. Ciuffi, T. E. Cintra, S. Nakagaki, *J. Colloid. Interf. Sci.* **2016**, *478*, 374-383.
 16. A. W. Johnson, A. Todd, *Vitamins & Hormones* **1957**, *15*, 1-30.
 17. A. W. Johnson, R. Price, *J. Chem. Soc.* **1960**, 1649-1653.
 18. Z. Gross, N. Galili, I. Saltsman, *Angew. Chem. Int. Ed.* **1999**, *38*, 1427-1429.
 19. H. Furuta, T. Asano, T. Ogawa, *J. Am. Chem. Soc.* **1994**, *116*, 767-768.
 20. P. J. Chmielewski, L. Latos-Grażyński, K. Rachlewicz, T. Glowiak, *Angew. Chem. Int. Ed. Engl.* **1994**, *33*, 779-781.
 21. R. Kumar, R. Misra, T. K. Chandrashekar, *Org. Lett.* **2006**, *8*, 4847-4850.
-

-
22. E. Pacholska-Dudziak, M. Szczepaniak, A. Książek, L. Latos-Grażyński, *Angew. Chem. Int. Ed.* **2013**, *52*, 8898-8903.
23. J. L. Sessler, D. Seidel, *Angew. Chem. Int. Ed.* **2003**, *42*, 5134-5175.
24. S. Saito, A. Osuka, *Angew. Chem. Int. Ed.* **2011**, *50*, 4342-4373.
25. A. Johnson, A. Todd, *Vitamins & Hormones* **1957**, *15*, 1-30.
26. D. C. Hodgkin, J. Kamper, J. Lindsey, M. MacKay, J. Pickworth, J. Robertson, C. B. Shoemaker, J. White, R. Prosen, K. Trueblood, *In The Structure of Vitamin B12. An Outline of the Crystallographic Investigation of Vitamin B12*, Proceedings of the Royal Society of London A: Mathematical, Physical and Engineering Sciences, The Royal Society: **1957**; pp 228-263.
27. A. Johnson, R. Price, *J. Chem. Soc.* **1960**, 1649-1653.
28. A. Johnson, I. Kay, *J. Chem. Soc.* **1965**, 1620-1629.
29. R. Paolesse, F. Sagone, A. Macagnano, T. Boschi, L. Prodi, M. Montalti, N. Zaccheroni, F. Bolletta, K. M. Smith, *J. Porphyrins Phthalocyanines*, **1999**, *3*, 364-370.
30. M. J. Broadhurst, R. Grigg, G. Shelton, A. W. Johnson, *J. Chem. Soc., Perkin Trans. 1*, **1972**, 143-151.
31. Y. S. Balazs, I. Saltsman, A. Mahammed, E. Tkachenko, G. Golubkov, J. Levine, Z. Gross, *Magn. Reson. Chem.* **2004**, *42*, 624-635.
32. H. R. Harrison, O. J. R. Hodder, D. C. Hodgkin, *J. Chem. Soc. B* **1971**, 640.
33. Z. Gross, N. Galili, I. Saltsman, *Angew. Chem. Int. Ed.* **1999**, *38*, 1427-1429.
34. R. Paolesse, S. Mini, F. Sagone, T. Boschi, L. Jaquinod, D. J. Nurco, K. M. Smith, *Chem. Commun.* **1999**, 1307-1308.
35. D. T. Gryko, K. Jadach, *J. Org. chem.* **2001**, *66*, 4267-4275.
36. I. Aviv-Harel, Z. Gross, *Chem. Eur. J.* **2009**, *15*, 8382-8394.
-

37. Z. Gross, *J. Biol. Inorg. Chem.* **2001**, *6*, 733-738.
38. L. Simkhovich, A. Mahammed, I. Goldberg, Z. Gross, *Chem. Eur. J.* **2001**, *7*, 1041-1055.
39. J. H. Palmer, M. W. Day, A. D. Wilson, L. M. Henling, Z. Gross, H. B. Gray, *J. Am. Chem. Soc.* **2008**, *130*, 7786-7787.
40. A. Mahammed, I. Giladi, I. Goldberg, Z. Gross, *Chem. Eur. J.* **2001**, *7*, 4259-4265.
41. J. Bendix, I. J. Dmochowski, H. B. Gray, A. Mahammed, L. Simkhovich, Z. Gross, *Angew. Chem. Int. Ed.* **2000**, *39*, 4048-4051.
42. A. Mahammed, Z. Gross, *J. Inorg. Biochem.* **2002**, *88*, 305-309.
43. S. Will, J. Lex, E. Vogel, H. Schmickler, J. -P. Gisselbrecht, C. Hauptmann, M. Bernard, M. Gorss, *Angew. Chem. Int. Ed. Engl.* **1997**, *36*, 357-361.
44. K. M. Kadish, C. Erben, Z. Ou, V. A. Adamian, S. Will, E. Vogel, *Inorg. Chem.* **2000**, *39*, 3312-3319.
45. K. E. Thomas, A. B. Alemayehu, J. Conradie, C. Beavers, A. Ghosh, *Inorg. Chem.* **2011**, *50*, 12844-12851.
46. C. Brückner, C. A. Barta, R. P. Brinas, J. A. K. Bauer, *Inorg. Chem.* **2003**, *42*, 1673-1680.
47. Z. Ou, C. Erben, M. Autret, S. Will, D. Rosen, J. Lex, E. Vogel, K. M. Kadish, *J. Porphyrins Phthalocyanines*, **2005**, *9*, 398-412.
48. F. Jérôme, B. Billier, J. M. Barbe, E. Espinosa, S. Dahaoui, C. Lecomte, R. Guillard, *Angew. Chem. Int. Ed.* **2000**, *39*, 4051-4053.
49. S. Licoccia, R. Paolesse, E. Tassoni, F. Polizio, T. Boschi, *Dalton Trans.* **1995**, 3617-3621.

-
50. H. L. Buckley, W. A. Chomitz, B. Koszarna, M. Tasior, D. T. Gryko, P. J. Brothers, J. Arnold, *Chem. Commun.* **2012**, 48, 10766-10768.
51. I. Aviv-Harel, Z. Gross, *Coord. Chem. Rev.* **2011**, 255, 717-736.
52. Y. Inokuma, J. H. Kwon, T. K. Ahn, M. C. Yoo, D. Kim, A. Osuka, *Angew. Chem. Int. Ed.* **2006**, 45, 961-964.
53. Y. Inokuma, A. Osuka, *Dalton Trans.* **2008**, 2517-2526.
54. D. Kuzuhara, H. Yamada, Z. L. Xue, T. Okujima, S. Mori, Z. Shenc, H. Unoa, *Chem. Commun.* **2011**, 47, 722-724.
55. Z. Xue, D. Kuzuhara, S. Ikeda, Y. Sakakibara, K. Ohkubo, N. Aratani, T. Okujima, H. Uno, S. Fukuzumi, H. Yamada, *Angew. Chem. Int. Ed.* **2013**, 52, 7306-7309.
56. Z. Xue, D. Kuzuhara, S. Ikeda, T. Okujima, S. Mori, H. Uno, H. Yamada, *Inorg. Chem.* **2013**, 52, 1688-1690.
57. S. Xue, D. Kuzuhara, N. Aratani, H. Yamada, *Inorg. Chem.* **2016**, 55, 10106-10109.
58. E. Vogel, M. Bröring, J. Fink, D. Rosen, H. Schmickler, J. Lex, K. W. K. Chan, Y.-D. Wu, D. A. Plattner, M. Nendel, K. N. Houk, *Angew. Chem. Int. Ed. Engl.* **1995**, 34, 2511-2514.
59. M. J. Broadhurst, R. Grigg, A. W. Johnson, *J. Chem. Soc., Perkin Trans. 1*, **1972**, 1124-1135.
60. H. Rexhausen, A. Gossauer, *J. Chem. Soc., Chem. Commun.* **1983**, 275.
61. J. L. Sessler, S. J. Weghorn, Y. Hisaeda, V. Lynch, *Chem. Eur. J.* **1995**, 1, 56-67.
62. J. L. Sessler, T. Morishim, V. Lynch, *Angew. Chem. Int. Ed. Engl.* **1991**, 30, 977-980.
-

63. A. Gossauer, *Bull. Soc. Chim. Belg.* **1983**, *92*, 793-795.
64. J. L. Sessler, D. Seidel, V. Lynch, *J. Am. Chem. Soc.* **1999**, *121*, 11257-11258.
65. E. Vogel, M. Bröring, J. Fink, D. Rosen, H. Schmickler, J. Lex, K. W. K. Chan, Y.-D. Wu, D. A. Plattner, M. Nendel, K. N. Houk, *Angew. Chem. Int. Ed. Engl.* **1995**, *34*, 2511-2514.
66. Y. Kamimura, S. Shimizu, A. Osuka, *Chem. Eur. J.* **2007**, *13*, 1620-1628.
67. J. L. Sessler, S. J. Weghorn, V. Lynch, M. R. Johnson, *Angew. Chem. Int. Ed. Engl.* **1994**, *33*, 1509-1512.
68. T. D. Lash, D. T. Richter, *J. Am. Chem. Soc.* **1998**, *120*, 9965- 9966.
69. R. J. P. Corriu, G. Bolin, J. J. E. Moreau, C. Vernhet, *J. Chem. Soc., Chem. Commun.* **1991**, *27*, 211-213.
70. F. H. Carré, R. J. P. Corriu, G. Bolin, J. J. E. Moreau, C. Vernhet, *Organometallics.* **1993**, *12*, 2478-2486.
71. B. Szyszko, N. Sprutta, P. Chwalisz, M. Stępień, L. Latos-Grażyński, *Chem. Eur. J.* **2014**, *20*, 1985-1997.
72. M. Stępień, B. Szyszko, L. Latos-Grażyński, *Org. Lett.* **2009**, *11*, 3930-3933.
73. S. Kumar, K. G. Thorat, M. Ravikanth, *J. Org. Chem.* **2018**, *83*, 14277-14285.

CHAPTER 2

Rhodium(III) and Iridium(III) Bipyricorrole Complexes: Syntheses, Structures, and Properties

2.1	Introduction	29
	2.1.1 Corrole analogues	29
	2.1.2 Pyridine based porphyrinoids	29
2.2	Objective of our work	32
2.3	Results and Discussion	33
	2.3.1 Synthesis	33
	2.3.2 Spectral characterisation	34
	2.3.2.1 Mass spectrometric analysis	34
	2.3.2.2 NMR Analysis	35
	2.3.2.3 Single crystal X-ray analysis	36
	2.3.2.4 Electronic spectral analysis	45
2.4	Conclusions	49
2.5	Experimental Section	49
	2.5.1 General Information	49
	2.5.2 Synthetic procedure and spectral characterization of 5a-10b	50
2.6	References	52

2.1 Introduction

2.1.1 Corrole analogues

Corrole is a contracted porphyrin analogue and recently received much attention for its intriguing structural and spectroscopic characteristics.¹ The name “corrole” was coined by Johnson and Price as it has structural resemblance with the naturally occurring corrin ring such as vitamin B₁₂.² Like porphyrin, corrole is also 18 π -electronic aromatic macrocycle. In terms of structural feature, corroles can be considered as intermediates between corrins and porphyrins. Corrole is a trianionic ligand and its core is exploited to stabilize higher oxidation state metal complexes. It has wide application in catalysis field, can act as sensors and most importantly dye-sensitized solar cells.³ The structural modification in the macrocyclic framework can alter the electronic structure, which radically influence the optical, photophysical and coordination properties of the parent corrole system.⁴ In order to achieve such properties, several core-modified corroles were synthesized by different research groups. The modified corrole analogues are *iso*-carbacorrole,⁵ N-confused derivative,⁶ norrole,⁷ benzonorrole,⁸ oxacorrole,⁹ dioxacorrole,¹⁰ and thiacorrole.¹¹ Recently we have also contributed *meso*-aryl biphenyl corrole system. The bipyrrrole moiety in the corrole framework was replaced by biphenyl unit and the core was effectively utilized to stabilize organo-Cu(III) complex.¹²

2.1.2 Pyridine based porphyrinoids

The first pyridine based porphyrinoids, pyriporphyrinone was synthesized by Berlin and Breitmaier. Since then, series of pyridyl derivatives has been reported which includes, true pyriporphyrin, confused pyriporphyrin, oxypyriporphyrin, dipyrityl ring substituted porphyrin and their coordination complexes were explored.¹³⁻²⁰

Naruta and co-workers described the synthesis of 1,10-phenanthroline embedded porphyrin (**1**) by [2+2] acid catalyzed condensation of 1,10-phenanthroline vinyl derivative with *meso*-phenyldipyrromethane followed by oxidation with DDQ. The sensing experiment of **1** was performed with various metal ions under biological pH condition, where the macrocycle exhibited emission enhancement selectively with Mg^{II} salts (Figure 2.1).²¹

Klaus Mullen and co-workers demonstrated the synthesis of novel porphyrin related macrocycle (**2**) by inserting carbazole and pyridine moiety in the macrocyclic framework. The macrocycle was achieved; (i) by introducing a similar cavity as that of porphyrin molecule and (ii) an ability to stabilize the metal ions to afford neutral metal complexes (Figure 2.1). The core was effectively stabilized Co(II) ion.²² Same group also reported the synthesis of new class of ligands with phenanthroline and indole moieties in the macrocyclic framework and explored its coordination chemistry by stabilizing Co(II) and the complex acted as electrochemical catalyst for oxygen reduction.²³

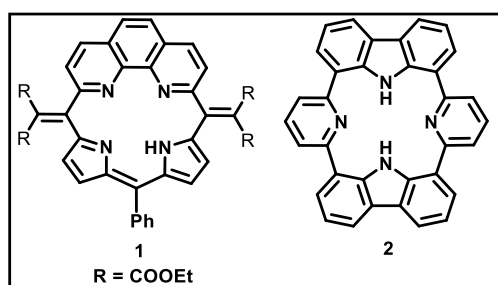


Figure 2.1: Structures of phenanthroline (**1**) and carbazole-pyridine (**2**) embedded porphyrins.

The pyridine based simplest contracted porphyrin, subpyriporphyrin (**3**) was first synthesized by Latos-Grazynski and co-workers²⁴ by acid-catalyzed condensation of pyridine based tripyrromethene with arylaldehyde. Upon coordination with boron in +1

oxidation state, the complex switches its macrocyclic aromaticity from nonaromatic to [14] π aromatic characteristics.

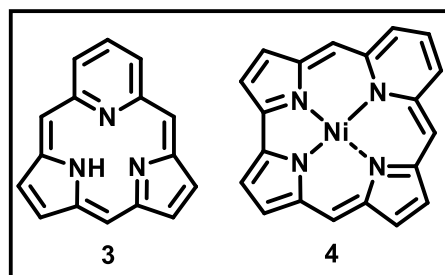


Figure 2.2: Structures of subpyrriporphyrin (**3**) and pyricorrole (**4**).

The next higher analogue of subpyrriporphyrin, pyricorrole (**4**) was reported by Neya and co-workers (Figure 2.2), where the macrocycle was achieved by acid-catalyzed condensation of tripyrromethene with pyridine dicarboxaldehyde and the Ni^{II} was inserted in the macrocyclic core.²⁵ The structural and spectral property wise, the macrocycle **4** behaves as a hybrid molecule of porphyrin and corrole. The structure is similar to corrole as it has one meso-carbon less as compared to normal porphyrin. On the other hand, it is a divalent ligand like porphyrin which is contrast to trivalent corrole ligand.

Later on, the bipyridyl unit was introduced in the corrole macrocycle by our group, where the trianionic core turned into monoanionic ligand (**5**) and the core further exploited as a fluorescence Zn^{II} sensor (**6**). The stabilization of higher oxidation state in the monoanionic core could be an ideal platform to coordinate various metal ions in different oxidation states (Figure 2.5).²⁶

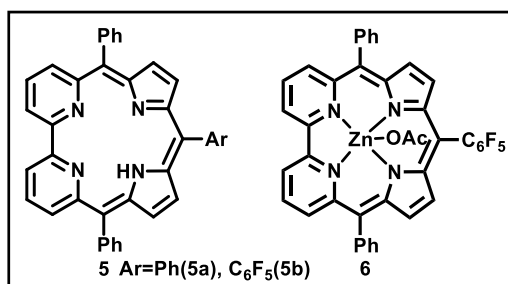


Figure 2.3: Structures of bipyricorrole (**5**) and zinc^{II} complex (**6**).

2.2 Objective of our work

The chemistry of rhodium and iridium corroles are well known. The rhodium^{III} corrole (**7**), [(tpfc)Rh^{III}P-(C₆H₁₁)₃], where tpfc = tris(pentafluorophenyl)corrole, was obtained by the aerial oxidation of the intermediate rhodium^I complex in the presence of excess P(C₆H₁₁)₃ **7** (Figure 2.4).²⁷ On the other hand, the first example of iridium^{III} corrole complex (**8**), [(tpfc)Ir^{III}(tma)₂], where tma = trimethylamine, was made by excess [Ir(cod)Cl]₂ (cod = cyclooctadiene) and K₂CO₃ in hot THF under Ar to form (tpfc)Ir^I(cod), which was converted to an axially tma-ligated Ir^{III} complex upon addition of tma N-oxide and exposure to the atmosphere (Figure 2.4).²⁸

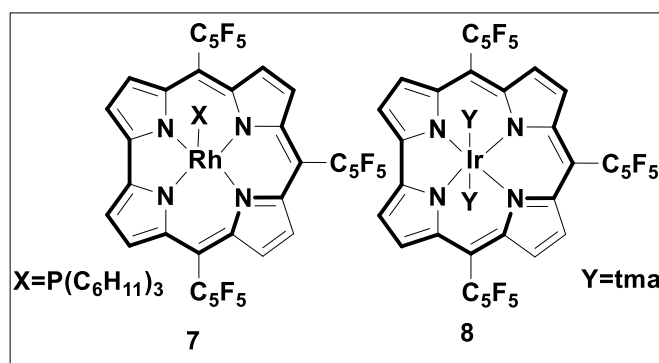


Figure 2.4: Structures of Rhodium^{III} (**7**) and Iridium^{III} (**8**) corrole complexes.

The Ir^{III} complex (**8**) has excellent photophysical properties such as, high phosphorescence quantum yield, long phosphorescence lifetime etc.²⁹

Overall, the Rh^{III} and Ir^{III} complexes were synthesized from *trianionic* or *dianionic* corrole ligand system while formation of such complexes by using the *monoanionic* corrole is unknown in the literature. It is noteworthy to mention that the basic framework of biologically important Cobalamin is constituted by ‘corrin’ unit which is in *monoanionic* state and stabilize Co^{III} ion.³⁰

Herein, we wish to report the syntheses, structures and properties of rhodium^{III} **9** and iridium^{III} **10** bipyricorrole complexes (Figure 2.5), where the monoanionic core is

successfully stabilized Rh and Ir metal ion in the higher oxidation state for the first time.

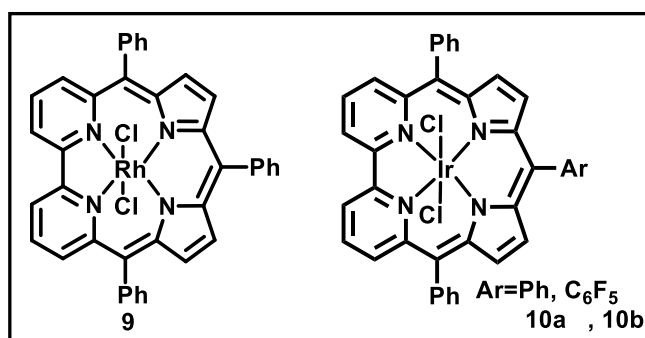
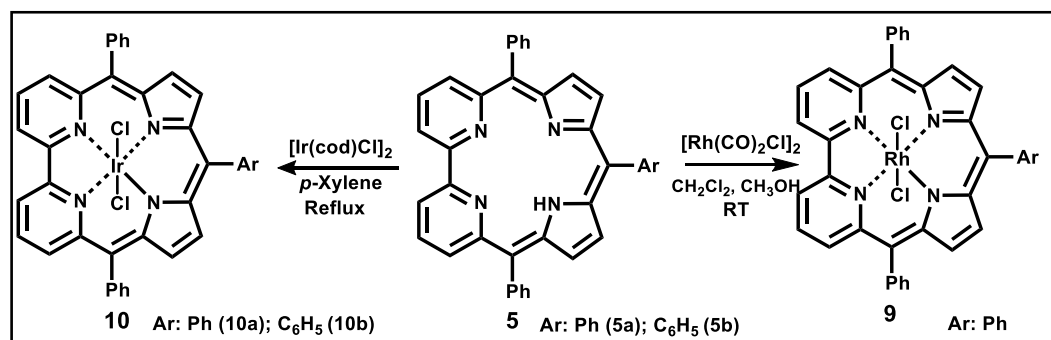


Figure 2.5: Structures of Rhodium^{III} (**9**) and Iridium^{III} (**10**) bipyricorrole complexes.

2.3 Results and discussions

2.3.1 Synthesis

The coordination chemistry of *monoanionic* bipyricorrole was performed by treating a CH₂Cl₂ solution of **5a** with [Rh(CO)₂Cl]₂ in methanol and afforded **9** in 45% yield. The insertion of iridium^{III} was achieved by refluxing a *p*-xylene solution of **5a** and **5b** with bis(1,5-cyclooctadiene)diiridium dichloride ([Ir-(cod)Cl]₂); (Scheme 2.1), and **10a** and **10b** were obtained in 68% and 56% yield, respectively. In both cases, the color of the solution turns into dark green from blue.



Scheme 2.1: Synthesis of **9** and **10**.

2.3.2 Spectral Characterization

2.3.2.1 Mass spectrometric analysis

Rhodium^{III} bipyricorrole (**9**) shows a prevalent mass peak at 687.0830, which corresponds to the chemical formula $C_{39}H_{25}Cl_2N_4Rh$ (Figure 2.6), whereas iridium^{III} bipyricorrole (**10a**) was identified as adduct of two chlorine atoms and a sodium ion that matches with the mass peak at 835.0798 ($C_{39}H_{25}Cl_2IrN_4Na$; Figure 2.7). It was envisioned from the mass spectral pattern that compound **10a** might have an octahedral geometry with two axially coordinated chloride ligands.

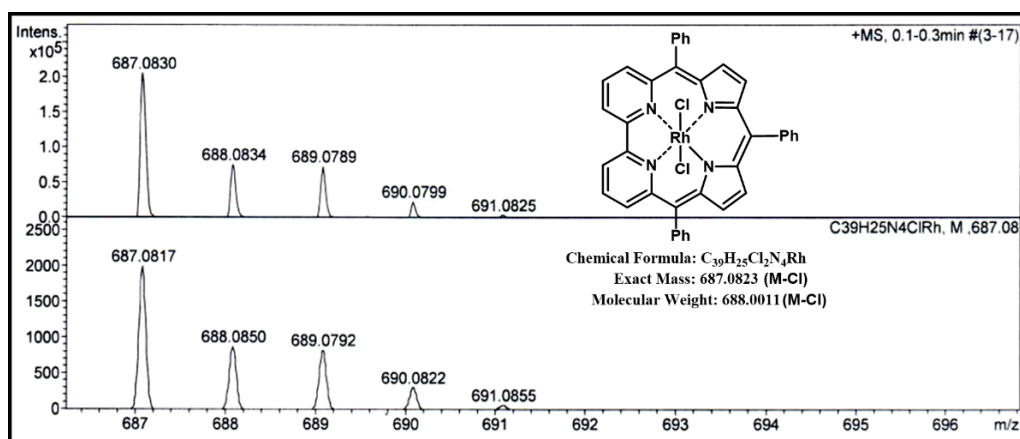


Figure 2.6: ESI-MS spectrum of **9**.

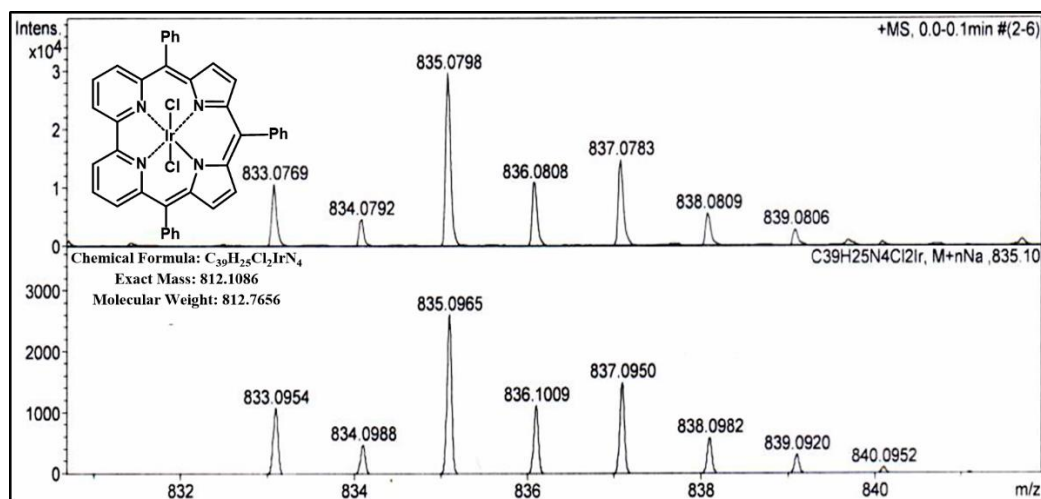


Figure 2.7: ESI-MS spectrum of **10a**.

2.3.2.2 NMR analysis

The solution-state structures of **9** and **10a** were deduced from ^1H NMR spectra recorded at 298 K in CDCl_3 (Figure 2.8). The disappearance of the NH signal in **9** and **10a** confirms the insertion of metal ions in bipyrriocorrole **5a**. The bipyrriidyl protons in **9** are resonated as a triplet at 9.12 ppm (H3 and H19) and as a multiplet at 8.50 ppm (H2, H20, H4, and H18; Figure 2.8a). The pyrrolic β -CH protons appear as a set of doublets at 7.46 ppm (H8 and H14) and 7.32 ppm (H9 and H13), and *meso*-phenyl protons are in the range of 7.81–7.52 ppm. In contrast to **9**, the bipyrriidyl protons in **10a** resonate as doublets at 9.10 ppm (H2 and H20) and 8.58 ppm (H4 and H18) and a triplet at 8.19 ppm (H3 and H19; Figure 2.8). The pyrrolic β -CH protons are observed as a set of doublets at 7.58 ppm (H8 and H14) and 7.22 ppm (H9 and H13), and *meso* phenyl protons are between 7.83 and 7.53 ppm. In comparison, the ^1H NMR signals of **9** and **10a** are more shielded than those of **5a**.

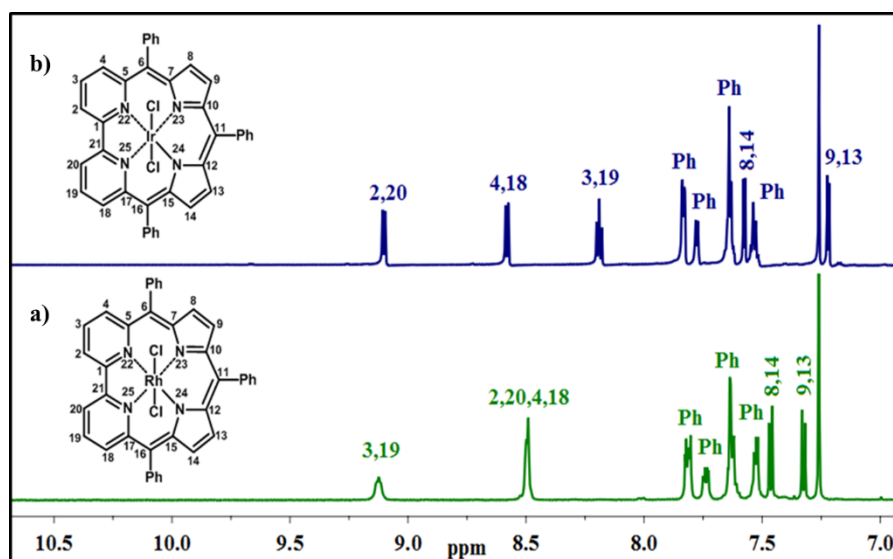


Figure 2.8: ^1H -NMR spectra of **9** (a), **10a** (b) in CDCl_3 at 298 K.

2.3.2.3 Single crystal X-ray structure and analysis of **9** and **10b**

The molecular structures of complexes **9** and **10b** were unambiguously confirmed by single-crystal X-ray diffraction studies, and the structures are shown in Figure 2.9. Suitable crystals of **9** were grown by the slow evaporation of a CH₂Cl₂ solution in the presence of *n*-hexane. As reflected from NMR and mass analyses, rhodium^{III} ion insertion and axial coordination are confirmed from the single-crystal X-ray structure (Figure 2.9a), where the rhodium^{III} ion is placed exactly at the center of the ligand. The geometry around the metal ion is octahedral with a basal plane containing four nitrogen atoms, and the axial positions are occupied by two chloride ligands. The bond lengths of Rh–N1 and Rh–N4 are 2.008(3) and 2.009(3) Å, respectively, which are moderately longer than the Rh–N2 and Rh–N3 distances, viz., 1.978(3) and 1.977(2) Å (Figure 2.9 a & b and Table 2.1). The saddling dihedral angle values of **9** are between 0.64(7)° and 9.67(9)°, which are comparable with the earlier reported bipyricorrole complexes (Figure 2.19 and Table 2.2).^{26, 31} The presence of axial chloride ligands in the complex generates an intermolecular hydrogen-bonding interaction to form self-assembled dimers with bond distances and angles of C2–H2...Cl2 2.665(1) Å and 151.15(2)° and C19–H19...Cl1 2.828(1) Å and 153.18(2)°, respectively (Figure 2.10). These dimers are combined together to generate a 1D array in the solid state (Figure 2.11).

On the other hand, the unit cell of the iridium^{III} complex **10b** contains two crystallographically independent molecules (Ir1 and Ir2; Figure 2.12), and one of the structures (Ir1) is shown in Figure 2.9 c&d. As observed in the rhodium^{III} complex **9**, the axial positions are occupied by chloride ligands and the geometry around the metal ion is octahedral. The bond lengths of Ir1–N1 and Ir1–N4 are 2.021(5) and 2.019(5) Å, respectively, which are slightly longer than those of Ir1–N2 and Ir1–N3, viz., 1.992(4)

and 1.997(5) Å (Table 2.1 and Figure 2.18). However, these values are higher than those of their respective iridium^{III} corrole complexes.³² The saddling dihedral angles of **10b** are from 0.82(2) to 5.01(2)° (Figure 2.19 and Table 2.2). The presence of fluorine atoms in the pentafluoro unit and axial chloride ions generates a series of intermolecular hydrogenbonding interactions to form self-assembled dimers (Figure 2.13) and 1D arrays (Figures 2.14-2.16). The dimers and arrays are combined together to generate a 2D supramolecular assembly in the solid state (Figure 2.17). In addition, the bond lengths of the bipyridine unit in **9** (1.355–1.411 Å) and **10b** (1.341–1.415 Å) (Figure 2.18) are in the range of typical sp²–sp² double-bond character and remain isolated from the overall macrocyclic conjugation, thus exhibiting nonaromatic character.

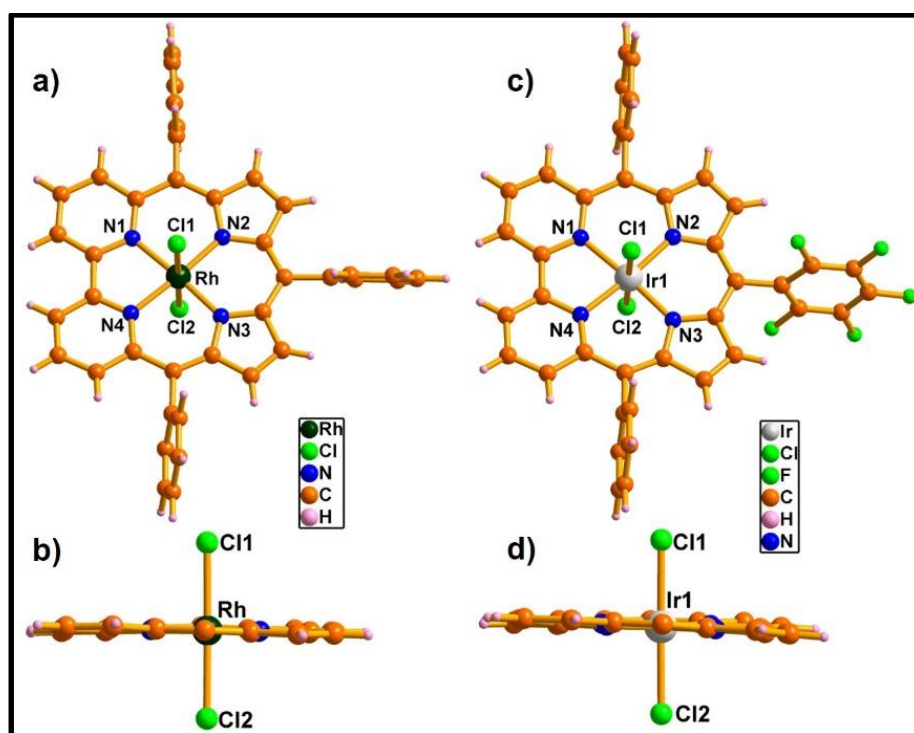


Figure 2.9: Single crystal X-ray structures of **9** and **10b**. a) & c) Top views and b) & d) side views. The *meso*-aryl groups are omitted for clarity in (b) and (d).

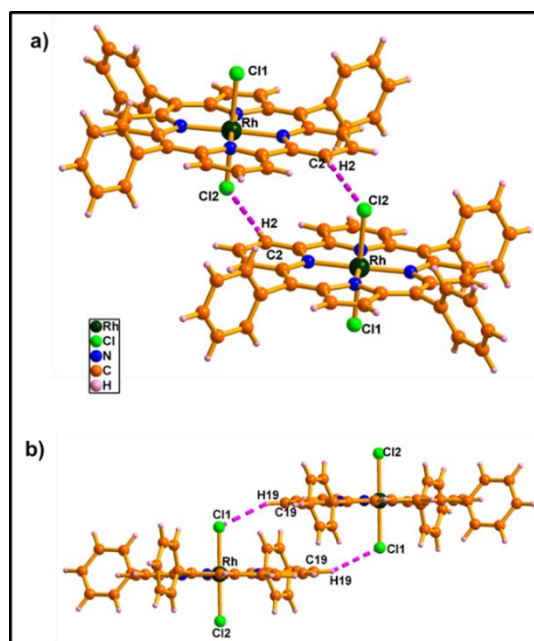


Figure 2.10: self-assembled dimers of **9**. The bond distances and angles are: C2-H2...Cl2: 2.665(1) Å & 151.15(2)° and C19-H19...Cl1: 2.828(1)Å & 153.18(2)° respectively.

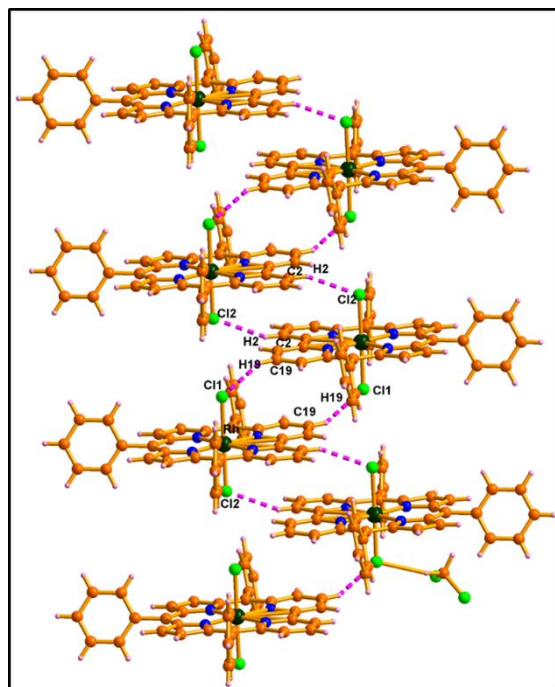


Figure 2.11: 1-D arrays of **9**. The bond distances and angles are: C2-H2...Cl2: 2.665(1) Å & 151.15(2)° and C19-H19...Cl1: 2.828(1) Å & 153.18(2)°.

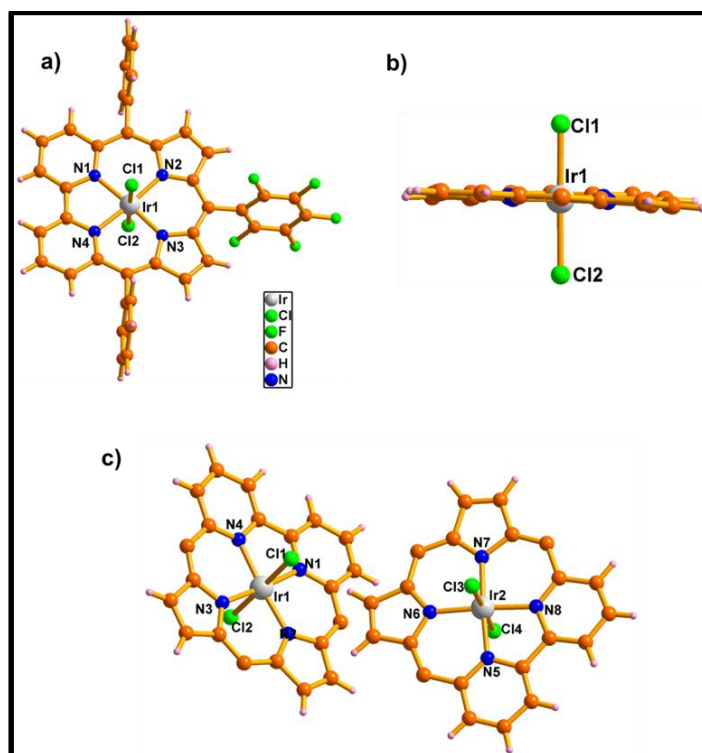


Figure 2.12: Single crystal X-ray structure of **10b**. **a)** Top view, **b)** side view and **c)** molecules present in the unit cell. The *meso*-aryl groups in **b** and **c** are omitted for clarity.

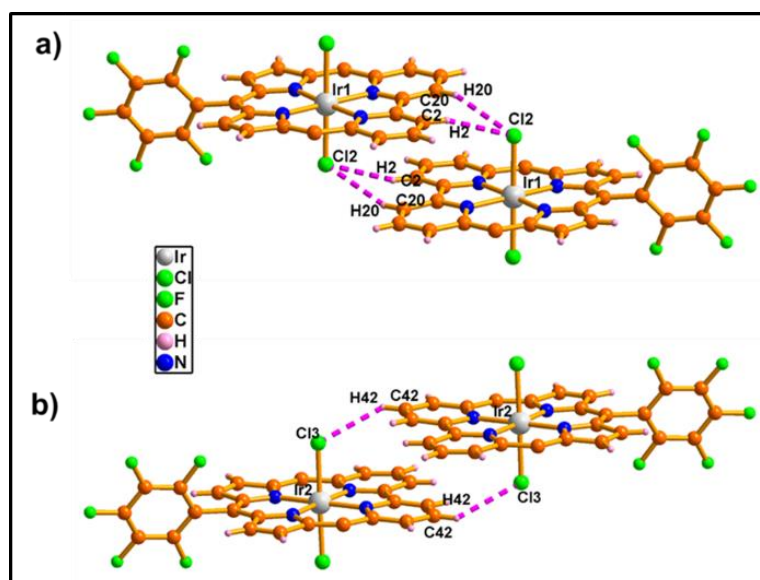


Figure 2.13: self-assembled dimers of **10b**. The bond distances and angles are: C2-H2...Cl2: 2.764(2) Å & 161.37(5)°; C20-H20...Cl2: 2.774(2) Å & 153.04(5)° and

C42-H42...Cl3: 2.873(2) Å & 134.95(5)° respectively. The *meso*-phenyl groups in **a** and **b** are omitted for clarity.

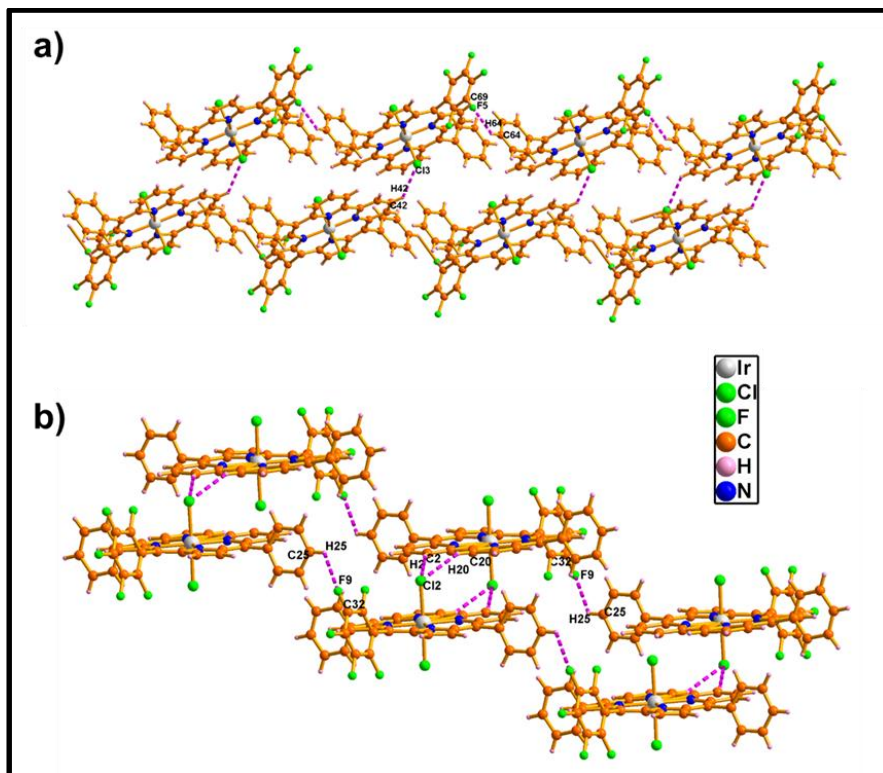


Figure 2.14: 2-D array of **10b**. The bond distances and angles are: C42-H42...Cl3: 2.873(2) Å & 134.95(5)°; C64-H64...F5: 2.677(6) Å & 141.96(6)°; C2-H2...Cl2: 2.764(2) Å & 161.37(5)°; C20-H20...Cl2: 2.774(2) Å & 153.04(5)° and C25-H25...F9: 2.782(5) Å & 125.82(6)° respectively.

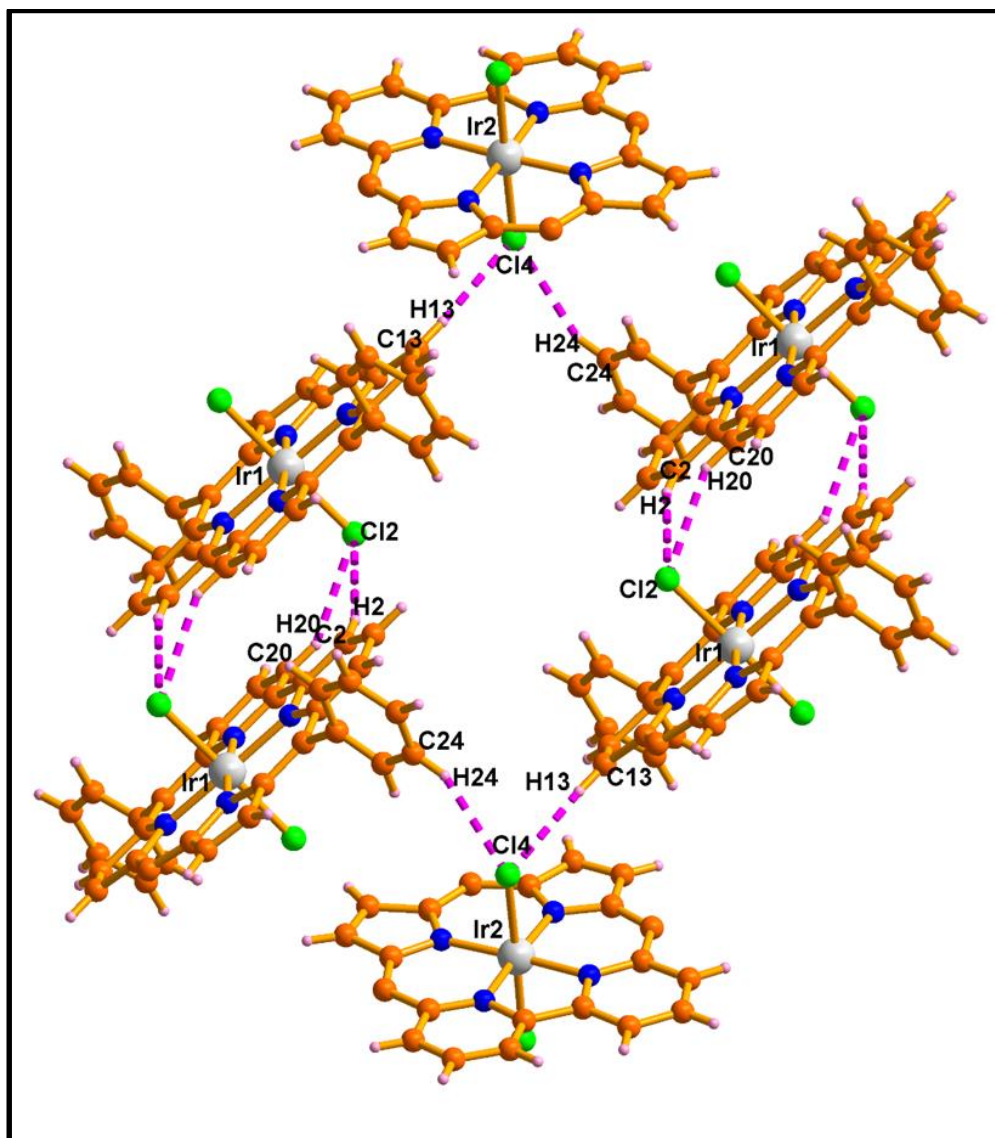


Figure 2.15: 1-D array of **10b** by involving both molecules in unit cell. The bond distances and angles are: C13-H13...Cl4: 2.696(2) Å & 175.24(4)°; C24-H24...Cl4: 2.804(2) Å & 149.80(6)° and C2-H2...Cl2: 2.764(2) Å & 161.37(5)°; C20-H20...Cl2: 2.774(2) Å & 153.04(5)° respectively.

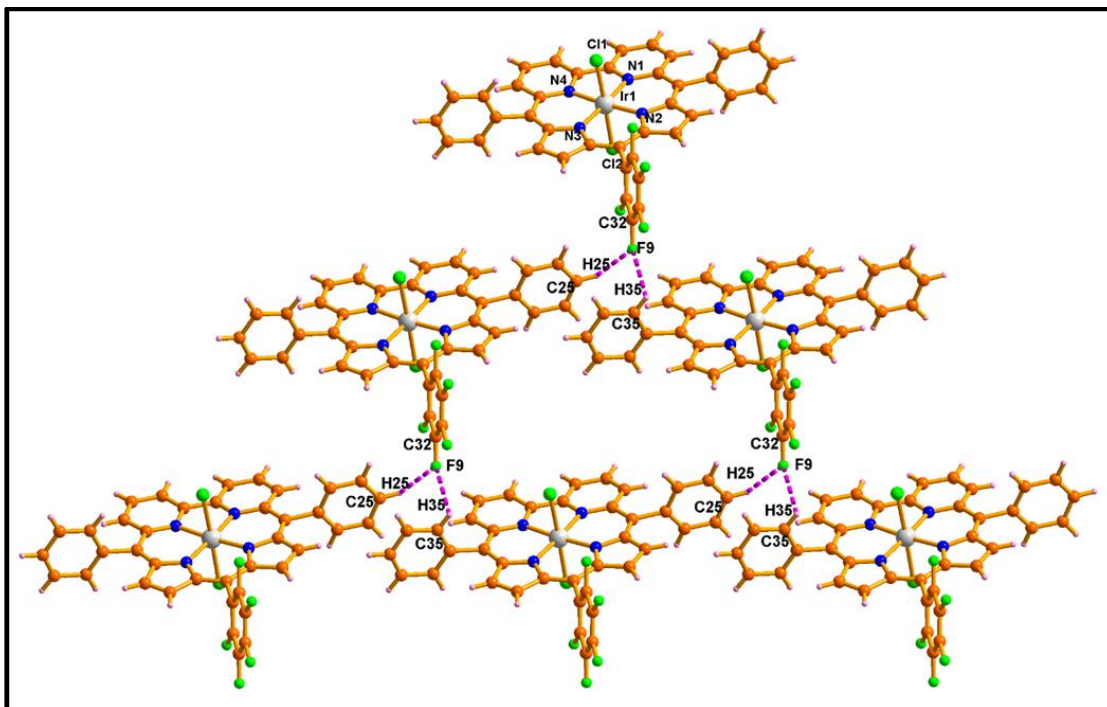


Figure 2.16: 1-D array of **10b**. The bond distances and angles are: C35-H35...F9:

2.851(6) Å & 98.34(6)° and C25-H25...F9: 2.782(5) Å & 125.82(6)°.

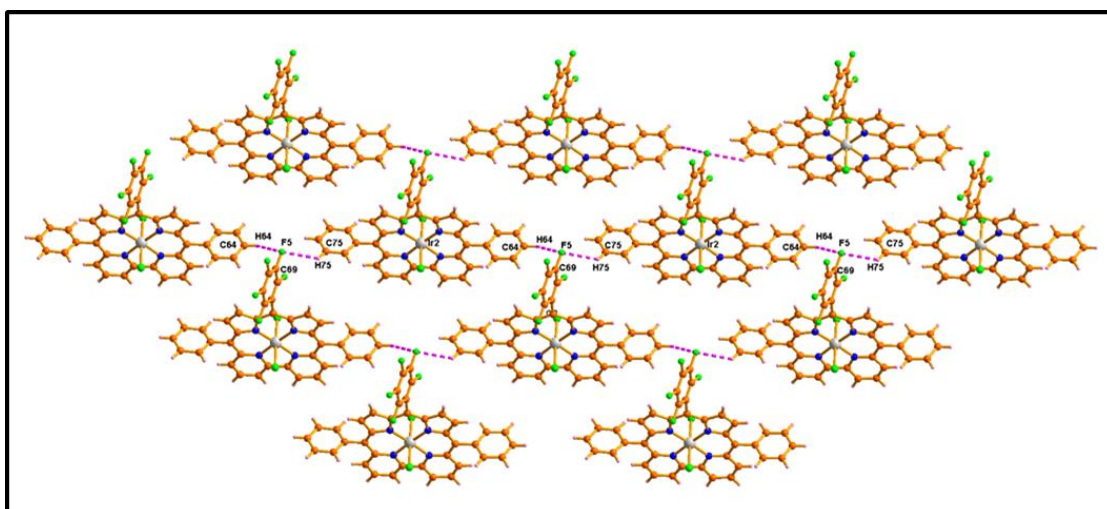


Figure 2.17: 2-D array of **10b**. The bond distances and angles are: C64-H64...F5:

2.677(6) Å & 141.96(6)°, C75-H75...F5: 2.830(6) Å & 128(5)°.

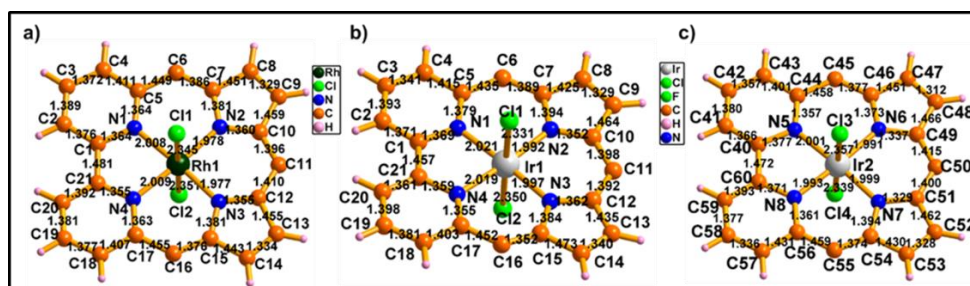


Figure 2.18: Bond lengths in (Å).

Table 2.1 Bond length (Å) and bond angle around the metal ion (°) in **9** and **10b**.

	Rh (Å)		Ir1		Ir2
N1-Rh	2.008(3)	N1-Ir1	2.021(5)	N5-Ir2	2.001(5)
N2-Rh	1.978(3)	N2-Ir1	1.992(4)	N6-Ir2	1.991(6)
N3-Rh	1.977(2)	N3-Ir1	1.997(5)	N7-Ir2	1.999(5)
N4-Rh	2.009(3)	N4-Ir1	2.019(5)	N8-Ir2	1.993(5)
Cl1-Rh	2.345(1)	Cl1-Ir1	2.331(2)	Cl3-Ir2	2.357(2)
Cl2-Rh	2.351(1)	Cl2-Ir1	2.350(2)	Cl4-Ir2	2.340(1)

Bond angle around metal ion (°)	M=Rh	M=Ir1	Bond angle around metal ion (°)	M=Ir2
N1-M-N2	93.47(1)	93.78(2)	N5-M-N6	93.78(2)
N2-M-N3	90.25(1)	90.25(2)	N6-M-N7	89.78(2)
N3-M-N4	93.61(1)	94.04(2)	N7-M-N8	93.80(2)
N4-M-N1	82.68(1)	81.92(2)	N8-M-N5	82.63(2)
N1-M-Cl1	88.66(8)	90.29(2)	N5-M-Cl3	90.35(1)
N2-M-Cl1	90.24(8)	91.08(2)	N6-M-Cl3	90.48(1)
N3-M-Cl1	91.37(8)	89.47(2)	N7-M-Cl3	90.35(1)
N4-M-Cl1	90.16(8)	87.17(2)	N8-M-Cl3	89.64(2)
N1-M-Cl2	90.88(8)	90.94(1)	N5-M-Cl4	88.24(2)
N2-M-Cl2	90.17(8)	89.47(1)	N6-M-Cl4	89.17(1)
N3-M-Cl2	89.07(8)	89.26(1)	N7-M-Cl4	91.09(2)
N4-M-C2	89.41(8)	92.38(1)	N8-M-Cl4	90.63(1)

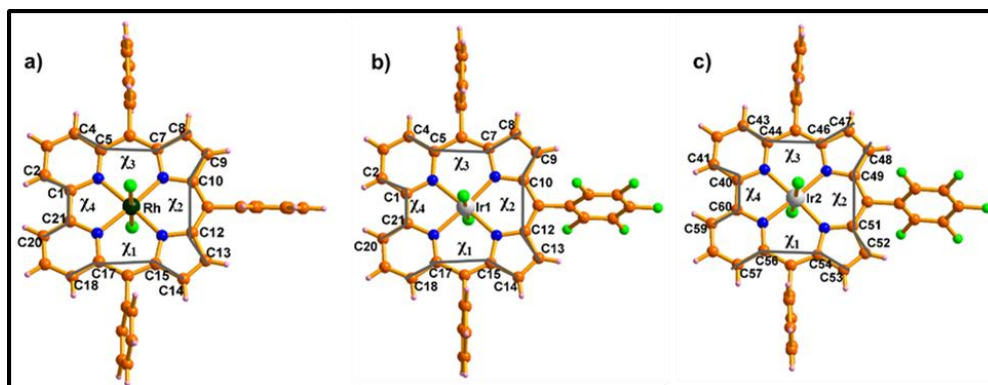


Figure 2.19. Saddling dihedral angles of **9** and **10b**

Table 2.2. Saddling dihedral angle ($^{\circ}$) in **9** and **10b**.

Saddle dihedral angle ($^{\circ}$)	Rh	Ir1	Saddle dihedral angle ($^{\circ}$)	Ir2
C4-C5-C7-C8	0.64(7)	2.67(2)	C43-C44-C46-C47	1.31(2)
C9-C10-C12-C13	9.67(9)	5.01(2)	C48-C49-C51-C52	10.47(2)
C14-C15-C17-C18	4.45(7)	0.82(2)	C53-C54-C56-C57	5.93(2)
C20-C21-C1-C2	1.11(4)	2.54(1)	C59-C60-C40-C41	4.76(1)

Table 2.3: Crystal data for **9** and **10b**:

Crystal parameters	9	10b
Formula	C ₄₁ H ₂₉ Cl ₆ N ₄ Rh	C ₄₀ H ₂₂ Cl ₄ F ₅ Ir N ₄ O
<i>M</i> /g mol ⁻¹	893.29	987.61
<i>T</i> /K	100 K	100 K
Crystal dimensions/mm ³	0.1 × 0.08 × 0.06	0.1 × 0.09 × 0.06
Crystal system	triclinic	triclinic
Space group	<i>P</i> -1	<i>P</i> -1
<i>a</i> /Å	9.318(5)	12.4409(14)
<i>b</i> /Å	13.017(2)	13.2996(17)
<i>c</i> /Å	17.813(5)	25.043(3)
α /°	77.470(5)	93.320(7)
β /°	83.571(5)	90.339(8)
γ /°	81.196(5)	106.903(6)
<i>V</i> /Å ³	2077.3(13)	3956.8(9)
<i>Z</i>	2	4
ρ_{calcd} /mg m ⁻³	1.428	1.658
μ /mm ⁻¹	0.830	3.702
<i>F</i> (000)	900	1920.0
Reflns. collected	30591	56921
Indep.reflns.[<i>R</i> (int)]	10345 [0.0471]	20943 [0.1143]
Max/min transmission	0.745 and 0.671	0.746 and 0.599
Data/restraints/parameters	10345 / 0 / 469	20943/0/973
GOF on <i>F</i> ²	1.105	0.931
Final <i>R</i> indices [<i>I</i> > 2 σ (<i>I</i>)]	<i>R</i> 1 = 0.0471, w <i>R</i> 2 = 0.1241	<i>R</i> 1 = 0.0573, w <i>R</i> 2 = 0.1146
<i>R</i> indices (all data)	<i>R</i> 1 = 0.0657, w <i>R</i> 2 = 0.1331	<i>R</i> 1 = 0.1032, w <i>R</i> 2 = 0.1287
Largest diff peak and hole [e Å ⁻³]	1.989 and -1.733	1.06 and -1.58

2.3.2.4 Electronic absorption and emission spectral analysis:

The steady-state electronic absorption spectra of **9** and **10a** were recorded in CH₂Cl₂ (Figure 2.20) and their molar extinction coefficients are listed in Table 2.4. In comparison to **5a**, the high-energy band of **10a** is hypsochromically shifted by a wavelength of 15 nm and the low-energy band of **10a** is bathochromically shifted by 21 nm, and they appear at 356 and 686 nm, respectively. In contrast, **9** exhibits a split high-energy band at 353 and 407 nm and prominent low-energy bands at 653 and 719

nm. The spectral pattern is comparable and bathochromically shifted with respect to the split Soret and Q bands of rhodium^{III} corrole.³³ The molar extinction coefficients of **9** and **10a** at high-energy bands are less than those of **5a**.

Table 2.4. Electronic absorption spectral data of **5**, **9** and **10a** recorded in CH₂Cl₂

Compound	High energy bands λ_{\max}/nm ($\log \epsilon / \text{M}^{-1}\text{cm}^{-1}$)	Low energy bands λ_{\max}/nm ($\log \epsilon / \text{M}^{-1}\text{cm}^{-1}$)
5a	371 (4.73)	665 (4.40)
9	353 (4.60), 407 (4.55)	653 (4.18), 719 (4.79)
10a	356 (4.58)	686 (4.29)

(concentration $\approx 10^{-5}$ M)

The steady-state and time-resolved fluorescence emissions of metal complexes **9** and **10a** were examined along with those of ligand **5a** (Figure 2.21). In contrast to **7**, surprisingly, the rhodium^{III} complex **9** exhibits fluorescence emission at 740 and 806 nm, where the spectral pattern is the exact mirror image of its low-energy absorption bands. The quantum yield and lifetime of **9** were calculated to be 0.06 and 0.47 ns, respectively. It is worth mentioning that the quantum yield of **9** is 3-fold higher than that of **5a** (0.02).

On the other hand, the iridium^{III} complex **10a** shows neither fluorescence nor phosphorescence emission. In general, the iridium^{III} corrole **8** and iridium^{III} benzonorrole are phosphorescent in nature; however, **10a** reveals contrasting behavior and is similar to iridium^{III} carbaporphyrinoids.

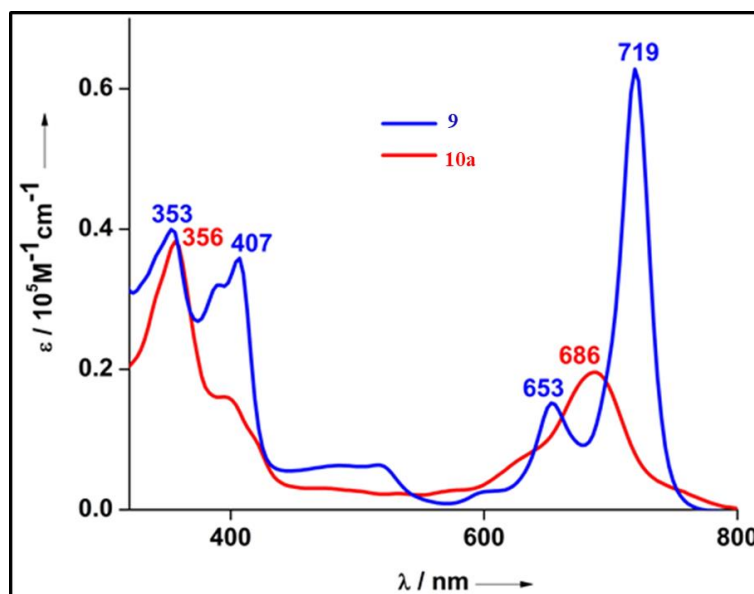


Figure 2.20: Steady state electronic absorption of **9** and **10a** in CH_2Cl_2 .

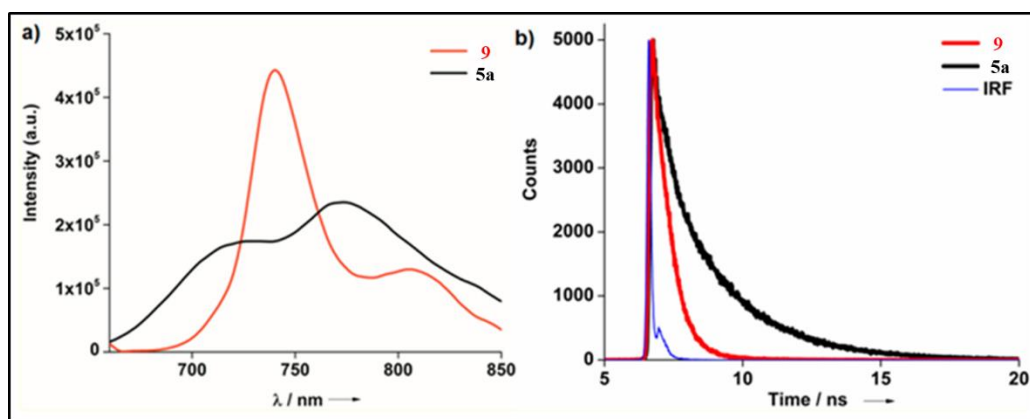


Figure 2.21: (a) Fluorescence emission spectra and (b) lifetime measurements of **9** and **5a** in CH_2Cl_2 .

2.3.2.5 Electrochemical analysis:

The electrochemical properties of **9**, **10a** and **5a** have been investigated by differential pulse voltammetry in a CH_2Cl_2 solution containing 0.1 M tetrabutylammonium hexafluorophosphate (TBAPF_6) as the supporting electrolyte (Figure 2.22). Compound **5a** exhibits five distinct oxidation potentials at -0.46, 0.03, 0.62, 0.90, and 1.08 V and one reduction potential at -1.59 V. The third, fourth, and fifth oxidation potentials of **5a** are reminiscent of the oxidation potentials of free-base

corrole.³⁴ Surprisingly, the first oxidation potentials of **9** and **10a** are very similar and occur at 0.42 and 0.44 V, which might be attributed to ligand-centered rather than metal-centered oxidation.³⁵ The first reduction potentials of **9** and **10a** at -1.35 and -1.42 V are positively shifted by 240 and 170 mV with respect to **5a**. The second oxidation and reduction potentials of **9** appear at 0.80 and -1.73 V, and the second oxidation is perhaps due to the oxidation of rhodium^{III} to rhodium^{IV}. The electrochemical HOMO–LUMO gaps of **9** and **10a** were calculated to be 1.77 and 1.86 V, respectively.

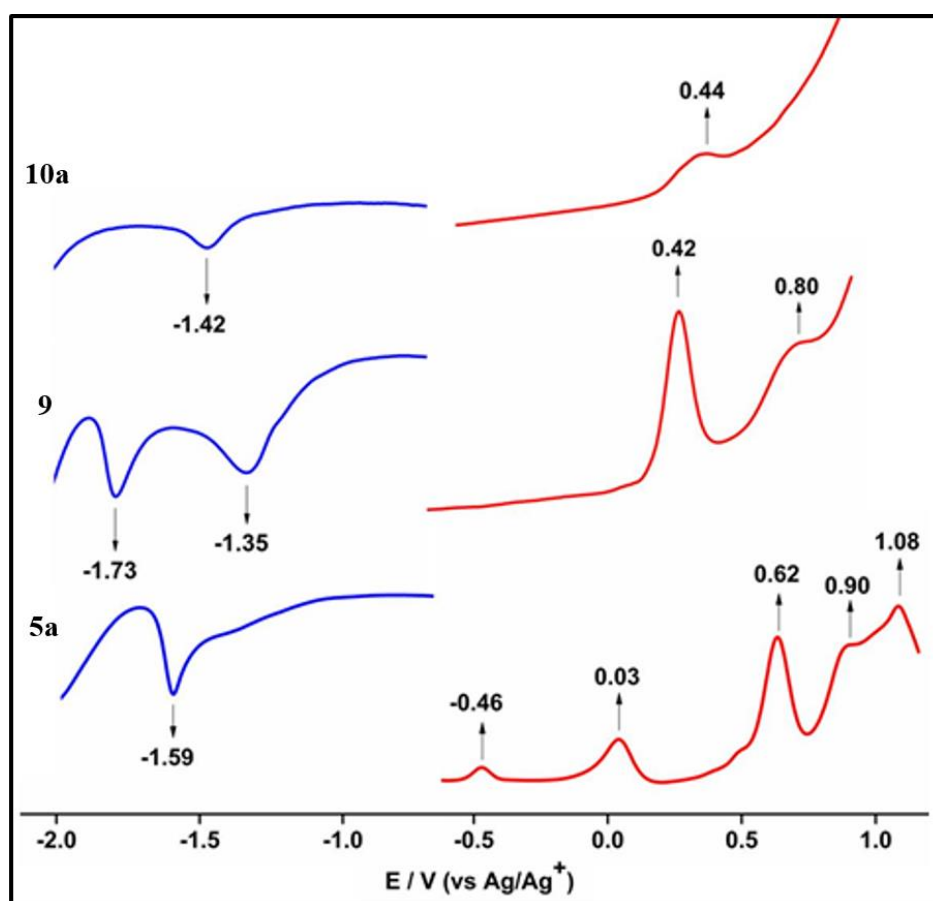


Figure 2.22. Differential pulse voltammograms of **5a**, **9** and **10a** in CH_2Cl_2 (scan rate = 0.1 V s^{-1})

2.4 Conclusion

In conclusion, we have successfully demonstrated the coordination chemistry of a monoanionic bipyridinacorrole with rhodium and iridium salts. The core, which was effectively utilized to stabilize the metal ions in the 2+ oxidation state, is further extended to stabilize rhodium and iridium ions in the 3+ oxidation state. Spectral and structural analyses reveal that the complexes exhibit nonaromatic character. The electronic absorption spectra of these complexes are reminiscent of their corrole analogues.

2.5 Experimental Section

2.5.1 General Information

Reagents and materials for synthesis were used as obtained from Sigma-Aldrich chemical suppliers. All solvents were purified and dried by standard methods prior to use. NMR solvents were used as received. The NMR spectra were recorded with Bruker 400 and 700 MHz spectrometers with tetramethylsilane [Si(CH₃)₄] as an internal standard. High-resolution electrospray ionization mass spectrometry spectra were recorded on a Bruker micro-TOF-QII mass spectrometer. The electronic absorption and steady-state fluorescence spectra were recorded with a PerkinElmer- Lambda 750 UV-vis spectrophotometer and an Edinburgh FS5 fluorescence spectrometer, respectively. Time-resolved fluorescence measurements were recorded on an Edinburgh instrument. X-ray quality crystals of the synthesized complexes were grown by the vapor diffusion of *n*-hexane into a CH₂Cl₂ solution. Single-crystal X-ray diffraction data of **9** and **10b** were collected on a Bruker Kappa APEX-II CCD four-angle rotation system, with Mo K α radiation ($\lambda = 0.71073\text{\AA}$). For collection of the data of the ϕ and ω scans, a diffraction measurement method was used for the experiment. A SQUEEZE routine

was applied using the PLATON program to remove the highly disordered solvent molecules to proceed to the final refinement of the main structure. The crystals have been deposited in the Cambridge Crystallographic Data Centre with reference no. CCDC 1576275, CCDC 1576274. Electrochemical studies were carried out on a CHI 1120A instrument with a three-electrode system, which consisted of a platinum disk as the working electrode, a platinum wire as the counter electrode, and Ag/AgCl as the reference electrode. Fluorescence quantum yields were determined by using *meso*-tetraphenylporphyrin (TPPH₂) in toluene ($\Phi_f = 0.11$) as a reference.

2.5.2 Synthetic procedure and spectral characterization

2.5.2.1 Synthesis of 5a: A mixture of 6,6'-bis(phenyl(1H-pyrrol-2-yl)methyl)-2,2'-bipyridine (0.400 g, 0.86 mol) and benzaldehyde (0.105 mL 0.86 mol) was dissolved in 300 mL of dry CH₂Cl₂ and stirred for 10 min in dark and under an inert atmosphere. Trifluoroacetic acid (0.39 mL, 5.16 mol) was added, stirring was continued for 3 h, and the mixture was oxidized with 2,3-dichloro-5,6-dicyano-1,4-benzoquinone (0.585 g, 2.58 mol). The compound was then purified through basic alumina column chromatography followed by silica gel (100–200 mesh) column chromatography and eluted with 0.5% CH₃OH/CH₂Cl₂. The compound was recrystallized with CH₂Cl₂/*n*-hexane to give **5a** in 15% yield.

¹H NMR (400 MHz, CDCl₃, 298K): δ = 10.62 (s, 1H), 9.46 (d, J = 6.5 Hz, 2H), 8.58 (t, J = 7.4 Hz, 2H), 8.06 (d, J = 7.7 Hz, 2H), 7.70–7.49 (m, 15H), 7.30 (d, J = 5.1 Hz, 2H), 7.00 (d, J = 5.2 Hz, 2H).

¹³C NMR (100 MHz, CD₃OD): δ = 155.19, 154.17, 151.84, 145.56, 138.33, 136.10, 135.06, 132.16, 131.92, 131.26, 130.62, 129.76, 129.20, 128.86, 128.65, 122.76, 108.47.

ESI-MS: m/z calculated for C₃₉H₂₆N₄ = 550.2157; found = 551.2224 (M+1).

UV-Vis (CH₂Cl₂): λ_{\max}/nm [(log ϵ): 371 (4.73), 665 (4.40).

$\lambda_{\max\text{-emission}}/\text{nm}$: 699, 775. **Quantum yield (Φ_f):** 0.02.

2.5.2.2 Synthesis of 9: A solution of [Rh(CO)₂Cl]₂ (2.81 mg, 0.007 mmol) in 2 mL of CH₃OH was added to a solution of **5a** (8 mg, 0.015 mmol) in 15 mL of CH₂Cl₂ and allowed to stir for 4 h. The compound was then extracted with CH₂Cl₂, and the solvent was removed by a rotary evaporator. The crude reaction mixture was subjected to neutral alumina column chromatography and eluted with 50% CH₂Cl₂/*n*-hexane. The compound was recrystallized with CH₂Cl₂/*n*-hexane to give **9** in 45% yield.

¹H NMR (400 MHz, CDCl₃, 298K): δ = 9.12 (t, *J* = 4.1 Hz, 2H), 8.50 (m, 4H), 7.81 (m, 4H), 7.74 (m, 2H), 7.66–7.61 (m, 6H), 7.54–7.52 (m, 3H), 7.46 (d, *J* = 5.3 Hz, 2H), 7.32 (d, *J* = 5.3 Hz, 2H).

¹³C NMR (100 MHz, CDCl₃): δ = 155.67, 154.58, 149.70, 149.26, 139.59, 138.85, 137.29, 134.96, 134.22, 133.44, 133.07, 130.99, 128.65, 128.23, 127.86, 127.82, 126.08, 120.57.

ESI-MS: *m/z* calculated for C₃₉H₂₅Cl₂N₄Rh = 722.0511; found = 687.0830 (M – Cl).

UV-Vis (CH₂Cl₂): λ_{\max}/nm [(log ϵ): 353 (4.60), 407 (4.55), 653 (4.18), 719 (4.79).

$\lambda_{\max\text{-emission}}/\text{nm}$: 740, 806. **Quantum yield (Φ_f):** 0.06.

2.5.2.3 Synthesis of 10a: Compound **5a** was dissolved in 100 mL of dry *p*-xylene and anhydrous sodium acetate (6 mg, 0.01 mmol) was added to the reaction mixture and allowed to stir for 15 min. [Ir(cod)Cl]₂ (30 mg, 0.046 mmol) was then added and refluxed at 140 °C under a nitrogen atmosphere for 16 h. The crude reaction mixture was subjected to neutral alumina column chromatography and eluted with 100% CH₂Cl₂. The compound was recrystallized with CH₂Cl₂/*n*-hexane to give **10a** in 68% yield.

¹H NMR (700 MHz, CDCl₃, 298K): δ = 9.10 (d, J = 7.5 Hz, 2H), 8.58 (d, J = 8.3 Hz, 2H), 8.19 (t, J = 8.0 Hz, 2H), 7.83 (dd, J = 7.2 and 1.7 Hz, 4H), 7.78 (dd, J = 7.5 and 1.4 Hz, 2H), 7.64 (m, 6H), 7.58 (d, J = 5.3 Hz, 2H), 7.53 (m, 3H), 7.22 (d, J = 5.3 Hz, 2H).

¹³C NMR (176 MHz, CDCl₃): δ = 157.32, 149.31, 147.85, 139.49, 139.36, 138.19, 135.44, 133.23, 133.02, 132.11, 129.80, 128.60, 128.21, 128.07, 127.81, 127.76, 119.41, 112.35.

ESI-MS: m/z calculated for C₃₉H₂₅Cl₂N₄Ir = 812.1086; found = 835.0798 (M + Na).

UV-Vis (CH₂Cl₂): λ_{\max}/nm [(log ϵ): 356 (4.58), 686 (4.29).

2.5.2.4 Synthesis of 10b: Anhydrous sodium acetate was added to a solution of **5b** (6 mg, 0.01 mmol) in *p*-xylene (100 mL) and allowed to stir for 15 min. Then [Ir(cod)Cl]₂ (30 mg, 0.05 mmol) was added and refluxed for 16 h under a nitrogen atmosphere. The compound was purified through neutral alumina column chromatography with 100% CH₂Cl₂ and recrystallized with CH₂Cl₂/*n*-hexane to give **10b** in 56% yield.

¹H NMR (700 MHz, CDCl₃, 298K): δ = 9.09 (d, J = 7.5 Hz, 2H), 8.56 (d, J = 8.4 Hz, 2H), 8.20 (t, J = 8.0 Hz, 2H), 7.85–7.80 (m, 4H), 7.80–7.60 (m, 6H), 7.42 (d, J = 5.2 Hz, 2H), 7.29 (d, J = 5.3 Hz, 2H).

¹³C NMR (176 MHz, CDCl₃): δ = 157.68, 156.94, 149.52, 147.42, 139.70, 138.92, 136.02, 133.12, 130.21, 130.13, 129.57, 128.85, 128.33, 119.92.

ESI-MS: m/z calculated for C₃₃H₂₀Cl₂F₅IrN₄ = 902.0614; found = 925.0504 (M + Na).

UV-Vis (CH₂Cl₂): λ_{\max}/nm [(log ϵ): 353 (4.35), 653 (4.00).

2.6 References

1. I. Aviv-Harel, Z. Gross, *Chem. Eur. J.* **2009**, *15*, 8382-8394.

2. A. Johnson, R. Price, *J. Chem. Soc.* **1960**, 1649-1653.
3. L. Flamigni, D. T. Gryko, *Chem. Soc. Rev.* **2009**, *38*, 1635-1646.
4. H. L. Buckley, J. Arnold, *Dalton Trans.* **2015**, *44*, 30-36.
5. J. Skonieczny, L. Latos-Grażyński, L. Szterenberga, *Chem. Eur. J.* **2008**, *14*, 4861-4874.
6. K. Fujino, Y. Hirata, Y. Kawabe, T. Morimoto, A. Srinivasan, M. Toganoh, Y. Miseki, A. Kudo, H. Furuta, *Angew. Chem. Int. Ed.* **2011**, *50*, 6855-6859.
7. M. Toganoh, Y. Kawabe, H. Furuta, *J. Org. Chem.* **2011**, *76*, 7618-7622.
8. M. Toganoh, Y. Kawabe, H. Uno, H. Furuta, *Angew. Chem. Int. Ed.* **2012**, *51*, 8753-8756.
9. C. H. Lee, W. S. Jo, J. W. Ga, H. J. Kim, P. H. Lee, *Bull. Korean Chem. Soc.* **2000**, *21*, 429-433.
10. M. Pawlicki, L. Latos-Grażyński, L. Szterenberga, *J. Org. Chem.* **2002**, *67*, 5644-5653.
11. V. S. Shetti, U. R. Prabhu, M. Ravikanth, *J. Org. Chem.* **2010**, *75*, 4172-4182.
12. B. Adinarayana, A. P. Thomas, C. H. Suresh, A. Srinivasan, *Angew. Chem. Int. Ed.* **2015**, *54*, 10478 - 10482.
13. R. J. P. Corriu, G. Bolin, J. J. E. Moreau, C. Vernhet, *J. Chem. Soc., Chem. Commun.* **1991**, 211-213.
14. T. W. Bell, P. Cragg, M. G. Drew, A. Firestone, A.-I. Kwok, J. Liu, R. Ludwig, A. Papoulis, *Pure Appl. Chem.* **1993**, *65*, 361-366.
15. F. H. Carre, R. J. P. Corriu, G. Bolin, J. J. E. Moreau, C. Vernhet, *Organometallics* **1993**, *12*, 2478-2486.
16. D. T. Richter, T. D. Lash, *J. Org. Chem.* **2004**, *69*, 8842-8850.
17. J.-i. Setsune, M. Kawama, T. Nishinaka, *Tetrahedron Lett.* **2011**, *52*, 1773-1777.

-
18. J.-i. Setsune, Yamato, K. *Chem. Commun.* **2012**, 48, 4447-4449.
 19. Z. Zhang, J. M. Lim, M. Ishida, V. V. Roznyatovskiy, V. M. Lynch, H.-Y. Gong, X. Yang, D. Kim, J. L. Sessler, *J. Am. Chem. Soc.* **2012**, 134, 4076-4079.
 20. Z. Zhang, W.-Y. Cha, N. J. Williams, E. L. Rush, M. Ishida, V. M. Lynch, D. Kim, J. L. Sessler, *J. Am. Chem. Soc.* **2014**, 136, 7591-7594.
 21. M. Ishida, Y. Naruta, F. Tani, *Angew. Chem. Int. Ed.* **2010**, 49, 91-94.
 22. L. Arnold, H. Norouzi-Arasi, M. Wagner, V. Enkelmann, K. Müllen, *Chem. Commun.* **2011**, 47, 970-972.
 23. M. Quernheim, H. Liang, Q. Su, M. Baumgarten, N. Koshino, H. Higashimura, K. Müllen, *Chem. Eur. J.* **2014**, 20, 14178-14183.
 24. R. Myśliborski, L. Latos-Grażyński, L. Szterenber, T. Lis, *Angew. Chem. Int. Ed.* **2006**, 45, 3670-3674.
 25. S. Neya, M. Suzuki, T. Matsugae, T. Hoshino, *Inorg. Chem.* **2012**, 51, 3891-3895.
 26. B. Adinarayana, A. P. Thomas, P. Yadav, A. Kumar, A. Srinivasan, *Angew. Chem. Int. Ed.* **2016**, 55, 969-973.
 27. L. Simkhovich, A. Mahammed, I. Goldberg, Z. Gross, *Chem. Eur. J.* **2001**, 7, 1041-1055.
 28. J. H. Palmer, M. W. Day, A. D. Wilson, L. M. Henling, Z. Gross, H. B. Gray, *J. Am. Chem. Soc.* **2008**, 130, 7786 - 7787.
 29. Y. K. Maurya, T. Ishikawa, Y. Kawabe, M. Ishida, M. Toganoh, S. Mori, Y. Yasutake, S. Fukatsu, H. Furuta, *Inorg. Chem.* **2016**, 55, 6223-6230.
 30. A. S. Rury, T. E. Wiley, R. Sension, *J. Acc. Chem. Res.* **2015**, 48, 860-867.
 31. B. Adinarayana, A. P. Thomas, P. Satha, A. Srinivasan, *Org. Lett.* **2017**, 19, 1986-1989.
-

32. J. H. Palmer, M. W. Day, A. D. Wilson, L. M. Henling, Z. Gross, H. B. Gray, *J. Am. Chem. Soc.* **2008**, *130*, 7786–7787.
33. J. H. Palmer, A. Mahammed, K. M. Lancaster, Z. Gross, H. B. Gray, *Inorg. Chem.* **2009**, *48*, 9308–9315.
34. M. Murugavel, R. V. R. Reddy, D. Dey, J. Sankar, *Chem. Eur. J.* **2015**, *21*, 14280–14286.
35. G. Calogero, G. Giuffrida, S. Serroni, V. Ricevuto, S. Campagna, *Inorg. Chem.* **1995**, *34*, 541–545.

CHAPTER 3

Carbatriphyrin[3.3.1] – A New Class of Triphyrin and its Calixphyrin Analogue

3.1	Introduction	58
	3.1.1 Nomenclature of calixphyrins	61
	3.1.2 Modifications of calixphyrins	61
	3.1.3 Carba triphyrins and calixphyrins	62
3.2	Objective of our work	63
3.3	Results and Discussion	64
	3.3.1 Synthesis	64
	3.3.2 Calixphyrin formation	65
	3.3.3 Spectral characterisation	65
	3.3.3.1 Mass spectrometric analysis	65
	3.3.3.2 NMR Analysis	66
	3.3.3.3 Single crystal X-ray analysis	69
	3.3.3.4 Electronic absorption and emission spectral analyses	72
3.4	Conclusions	74
3.5	General Information	75
3.6	Synthetic procedure and spectral characterization of 25-29	75
3.7	References	79

3.1 Introduction

Triphyrins are considered as a class of contracted porphyrins where three pyrrolic units are connected via *meso*-sp² carbon atoms. Subporphyrin (**1**), a triphyrin analogue contains three *meso*-carbons and designates as triphyrin(1.1.1). In 2006, the first subporphyrin was reported by Osuka and coworkers. It is a 14 π aromatic conjugated system and stable only as boron complex.¹ The complex displays fascinating properties such as; bright-green emission and nonlinear optics (NLO).^[2-4] Subporphyrin in its freebase was first reported by Latos-Grażyński and co-workers, where pyridine was introduced in the macrocyclic core and named as subpyriporphyrin⁵ (**2**) (Figure 3.1). The core was used for B^{III} ion insertion and the nonaromatic nature of the freebase was turned into aromatic.

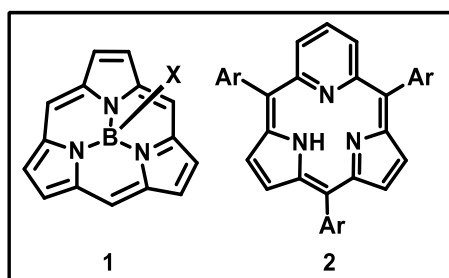


Figure 3.1: Structures of Subporphyrin (**1**) and subpyriporphyrin (**2**).

In terms of number of *meso* carbons, the molecular architecture of free base triphyrin analogues is with [n.1.1] nomenclature, where ‘n’ varies from 2 to 6. The triphyrin homologue [14]triphyrin(2.1.1) was accidentally (**3**, **4**) (Figure 3.2) synthesized by Kobayashi *et al.* but subsequently they developed proper methodologies for the synthesis of [14]benzotriphyrin(2.1.1). The pyrrole derivative and aryl aldehyde were condensed in presence of BF₃.OEt₂.⁶ Later, *meso*-unsubstituted [14]triphyrin(2.1.1) (**5**) was synthesized by using McMurry coupling reaction between diformyl-tripyrane by Yamada and co-workers.⁷ The *meso*-aryl [14]triphyrin(2.1.1)

(6) (Figure 3.2) was reported by our group, by acid-catalyzed reaction of 5,6-diphenyldipyrroethane with pentafluorobenzaldehyde in CH_2Cl_2 and followed by DDQ oxidation, where acidolysis of the dipyrroethane unit resulted the formation of **6**.^{8a} Later, the efficient methodology by Ravikanth and co-workers were discovered, where free base (**6**) was obtained in better yield and the core is used for Re^{I} ion complexation.^{8b} They condensed dipyrroethene-dicarbonyl with pyrrole in the presence of trifluoroacetic acid in CH_2Cl_2 for 30 min under an inert atmosphere followed by oxidation with DDQ in open air for an additional 30 min to obtain **6**.

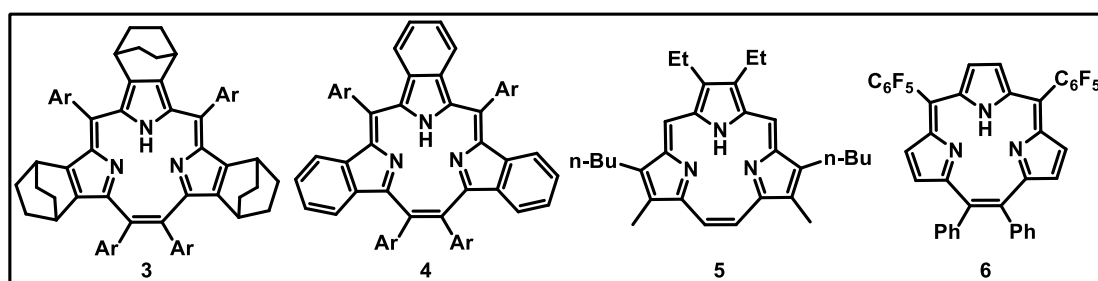


Figure 3.2: Structures of triphyrin(2.1.1) derivatives.

The core-modified triphyrin with (2.1.1) nomenclature, where one or more pyrrole units are replaced by heterocyclic rings, was reported simultaneously and shown in Figure 3.3. The thiatriphyrin(2.1.1) (**7**) was reported by Yamada and co-workers. However, thiophene fused oxatriphyrin(2.1.1) (**8**, **9**) and phenylene fused oxatriphyrin(2.1.1) (**10**) were synthesized by Latos-Grażyński and co-workers, where switching in aromaticity was exploited in **8-10**.⁹⁻¹¹

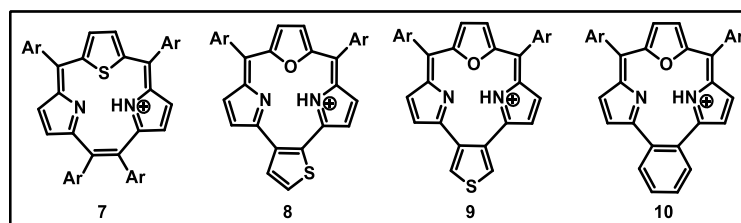


Figure 3.3: Structures of core-modified triphyrin(2.1.1) derivatives.

Apart from triphyrins(2.1.1), numerous higher analogues of triphyrin (**11-16**) (Figure 3.4) were synthesized and characterised by Latos-Grażyński and Anderson group. These includes oxatriphyrin(4.1.1),¹² thia-¹³ and dithia-^{14,15} triphyrin(4.1.1), triphyrin(3.1.1),¹⁶ oxatriphyrin(3.1.1),^{17,18} carbatriphyrin(4.1.1) (**15**)¹⁹ and triphyrin(6.1.1) (**16**).^{20,21}

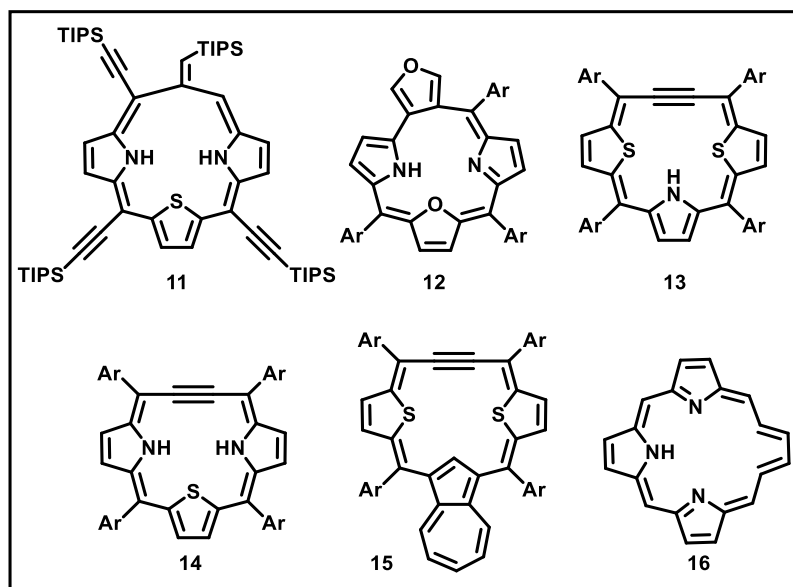


Figure 3.4: Structures of triphyrin(n.1.1) analogues.

On the other hand, calixphyrins are chemical hybrids of porphyrins **18** and calixpyrroles **17** which contain both sp^2 and sp^3 hybridized *meso* carbons (Figure 3.5). Presence of sp^3 *meso* carbon induces reasonable flexibility in the framework whereas, sp^2 *meso* carbon provides partial π -conjugated network. These macrocycles are exploited to sense cations and anions selectively and are better represented as chemosensor.²²⁻²⁵

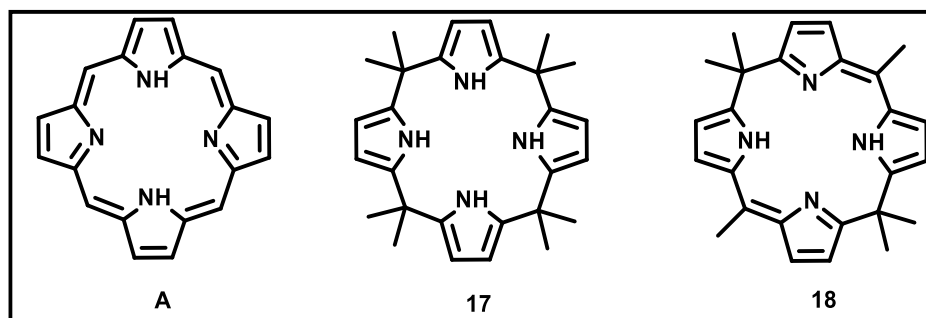


Figure 3.5: Structures of porphyrin (A), calixpyrrole (17) and calixphyrin (18).

3.1.1 Nomenclature of calixphyrins

The nomenclature of **18** was proposed as calix[4]phyrin(***1.1.1.1***). Starting with the highest order sp^2 *meso* center, the molecule is named in the direction in which the nearest sp^2 *meso* center present. The numbers in the square bracket represents the number of pyrrole units in the macrocycle. The bold and italicized number in the circular bracket represents the number of bridging *meso* centers between each pyrrole subunit, where bold numbers signify to sp^2 centers, and italicized numbers refer to sp^3 centers.²⁶

3.1.2 Modifications of calixphyrins:

To improve the coordination property of the calixphyrin system, several modifications of the macrocyclic skeleton were happened. These are: (a) *peripheral-modified*, the modifications are done on the periphery, i.e the β and *meso* positions of the parent tetrapyrrolic macrocycles; (b) *expansion*, by increasing the number of heterocyclic rings or *meso* carbons; (c) *N-confusion*, instead of α connection, where the pyrrole rings are connected through β -carbon with rest of the macrocycle; (d) *three dimensional calixphyrins*, these are cryptand-like system with sp^2 hybridized protruding bridging carbon atom; and

(e) *core-modified* calixphyrins, where one or more pyrrole rings of parent calixphyrin is replaced by other heterocyclic rings.

3.1.3 Carba triphyrins and calixphyrins:

Carbaporphyrinoids are porphyrin analogues where one or more pyrrole units are replaced by cyclopentadiene moieties or aromatic hydrocarbons. The syntheses and coordination chemistry were recently reviewed by T. D. Lash.²⁷ These porphyrin analogues are well known promising candidates for; i) study the nature of aromaticity, ii) weak metal-arene interaction and iii) stabilize higher oxidation state organometallic complexes. However, there are only two example of carbatriphyrins are reported. In the first report, the azulene unit was introduced in the carbatriphyrin(**15**) framework, stabilized by organo-Ru^{II} complex and confirmed by spectral techniques.¹⁹ Recently, our group has also demonstrated the synthesis of arene ring incorporated [3.1.1]carbatriphyrin **19**, where the *o*, *m*-biphenylene units are connected with dipyrromethene unit and also exploited weak B...Arene interaction (**20**) and stabilized organo-B^{III} complex (**21**) (Figure3.6).²⁸

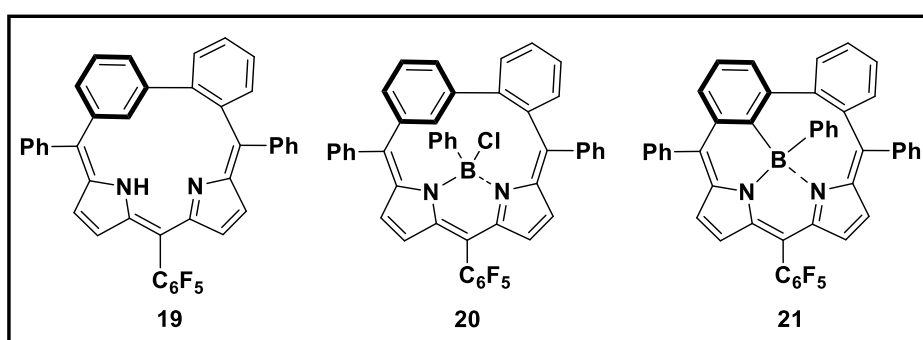


Figure 3.6: Carbatriphyrin(3.1.1) (**19**) and their B^{III} complexes (**20,21**).

The arene unit incorporated normal (**22**)²⁵ and expanded carbaporphyrinoids (**23, 24**) are scarcely known in the literature and the respective analogues are shown in Figure

3.7. These analogues exhibited non-covalent interactions, weak metal-arene interactions and sensing properties with metal ions.²⁹

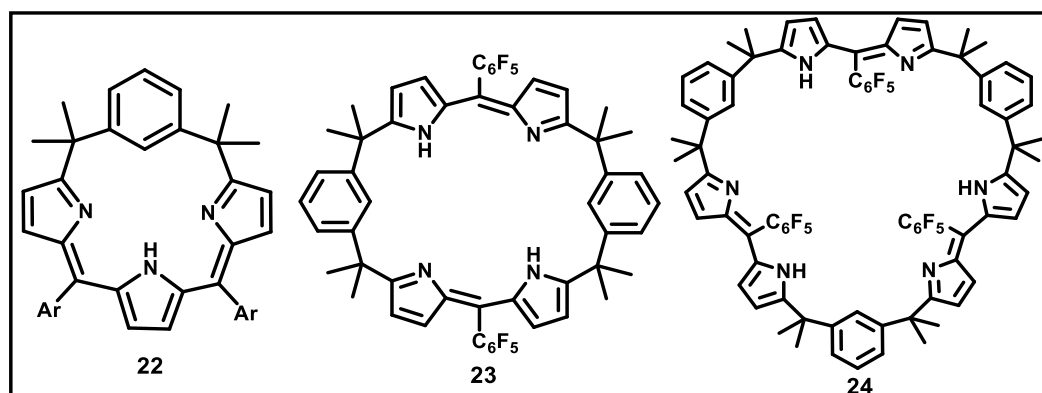


Figure 3.7: Structures of carbacalixpyrins (22-24).

3.2 Objective of our work

From the literature survey it is clear that, (i) the carba analogues of triphyrin and its respective calixpyrin analogues are scarcely reported; (ii) conversion of triphyrin into calixpyrin is hitherto unknown; (iii) the nomenclature for the triphyrin analogues are confined to [n.1.1] category and (iv) the pyritriphyrin is connected with 2,6-position to the respective of the core.

In this chapter, we wish to report the synthesis of arene ring and pyridyl unit incorporated carbaphyrin (**25**) analogue. The 3,5-position of the pyridyl unit is connected with *o*-phenylene unit and generate the triphyrin framework with [3.3.1] nomenclature, where pyridyl N is pointed outside the macrocyclic core to generate additional coordination environment. Further, the carbatriphyrin analogue is converted into respective carbacalixpyrin (**26**) derivative by simple NaBH₄ reduction. Overall, this chapter reports the first example of [3.3.1] carbatriphyrin (**25**) and structurally elucidated its calix[2]pyrin(2.2.1.1.1) (**26**) analogue (Figure 3.8).

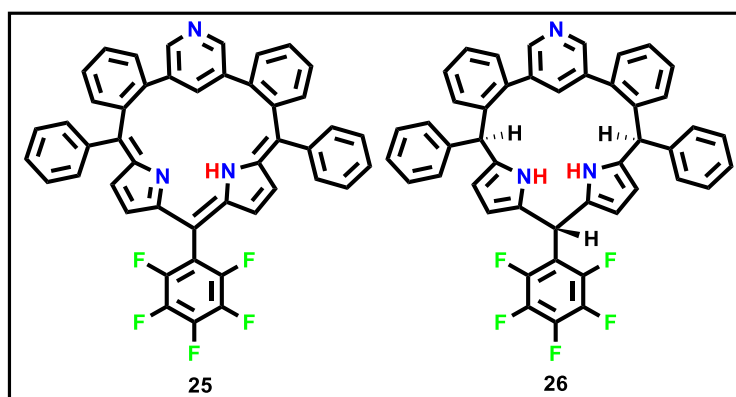
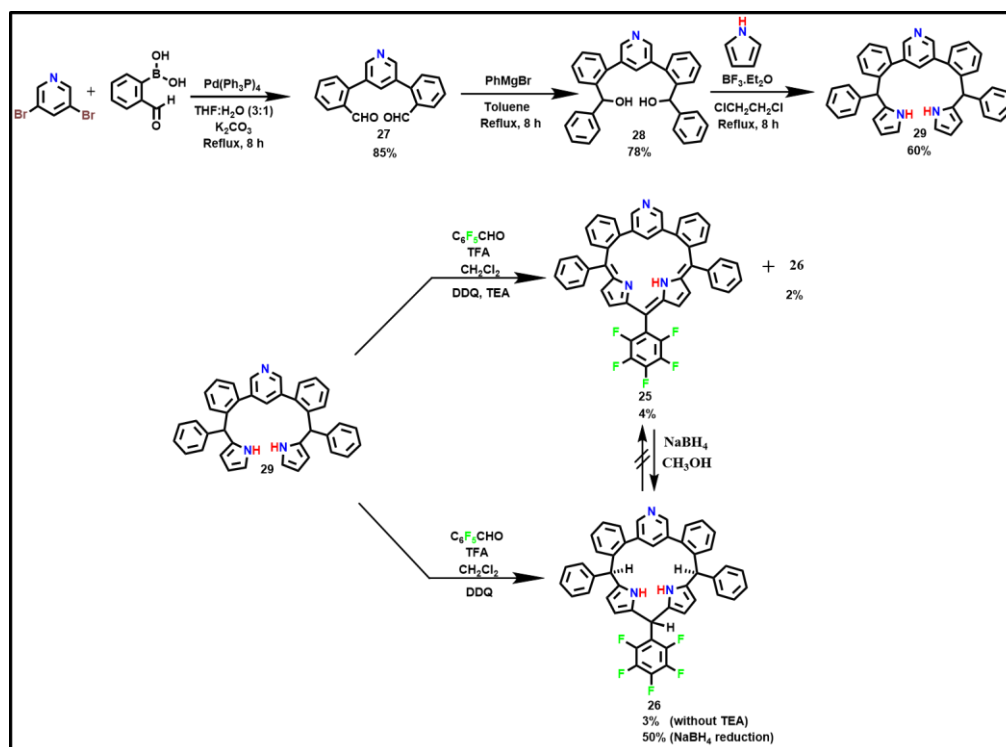


Figure 3.8: Carbatriphyrin (**25**) and its calixphyrin analogue (**26**).

3.3 Results and discussion

3.3.1 Synthesis

The synthesis of required precursors as well as target macrocycle, carbatriphyrin (**25**) are shown in Scheme 3.1. The Suzuki-Miyaura cross-coupling reaction of 3,5-dibromopyridine with 2-formylphenylboronic acid in 1:3 mixture of water and THF gave corresponding dicarbaldheyde **27** in 85% yield. The Grignard reaction of **27** with freshly prepared phenylmagnesium bromide in dry toluene under reflux conditions afforded respective diol **28** in 78% yield. The final precursor, dipyrromethane **29** was obtained in 60% yield by refluxing a 1,2-dichloroethane solution of **28** with excess pyrrole in the presence of $\text{BF}_3 \cdot \text{OEt}_2$. The trifluoroacetic acid (TFA) catalyzed condensation of **29** with 2,3,4,5,6-pentafluorobenzaldehyde followed by oxidation with 2,3-dichloro-5,6-dicyano-1,4-benzoquinone (DDQ) and triethyl amine (TEA) gave the target molecule **25** in 4% yield.



Scheme 3.1: Synthesis of **25** and **26**.

3.3.2 Calixphyrin formation:

In addition to **25**, in the presence of TEA, the compound **26** was isolated in 2% yield. In the absence of TEA, the compound **26** was exclusively separated, however, afforded only 3% yield. Simultaneously, carbatriphyrin (**25**) was easily reduced to its calix[2]phyrin(**2.2.1.1.1**) analogue **26** using NaBH_4 as a reducing agent and obtained 50% yield (Scheme 3.1). The color reaction was accompanied by a color change from greenish blue to orange. However, the conversion of **26** into **25** by using higher equivalents of oxidizing agent, such as DDQ was not successful.

3.3.3 Spectral characterisation

3.3.3.1 Mass spectrometric analysis

The high resolution electron spray ionization (ESI-HR) mass spectrometric analyses of **25** and **26** showed the molecular ion signal at 716.2092[M+1] (**25**) and

720.2433[M+1] (**26**) which confirmed the exact composition of the macrocycles (Figure 3.9).

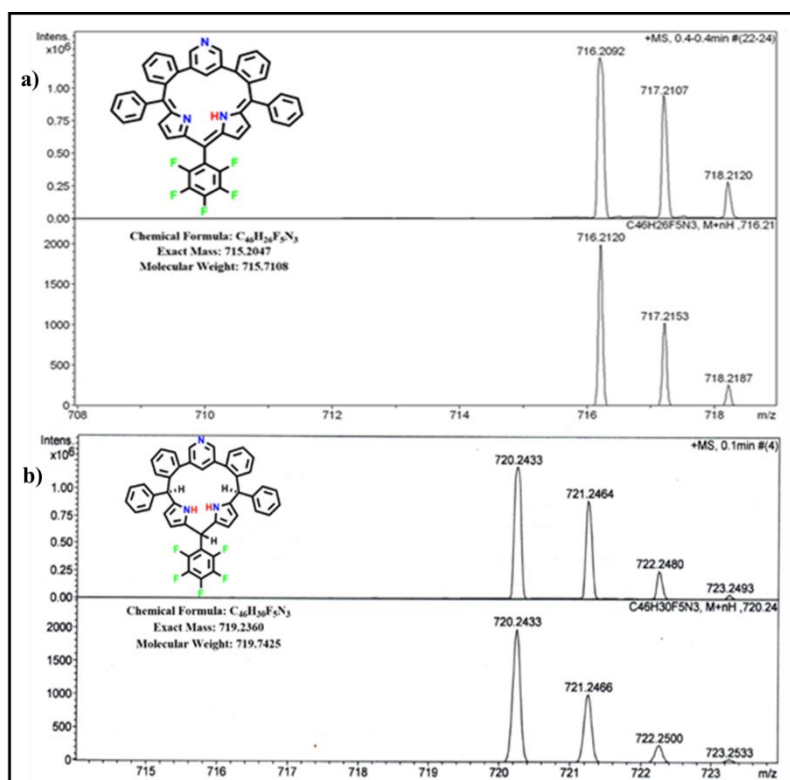


Figure 3.9: ESI-HR mass spectrometric analysis of a) **25** and b) **26**.

3.3.3.2 NMR Analysis

The ¹H NMR spectra of **25** and **26** are shown Figure 3.10. The individual proton signals of macrocycle **25** clearly indicates unsymmetrical nature. The pyrrolic β-CH protons [H(9,10,14,15)] are resonated as a doublet and appeared between 6.72 and 5.86 ppm. One of the *o*-phenylene protons (*o1*), [H(19,22)] are observed at 8.01 ppm as a set of doublet, [H(20)] as a triplet at 7.23 ppm and [H(21)] at 7.45 ppm as a broad signal. The other *o*-phenylene (*o2*) protons are resonated between 7.11 and 6.85 ppm. The [H(5)] are observed at 6.86 ppm as a doublet, whereas [H(3,4) & H(2)] are appeared as a multiplet at 6.95 and 7.11 ppm respectively. The pyridine(*Py*) inner CH proton [H(28)] is resonated at 7.88 ppm, whereas the outer peripheral protons [H(25)] and [H(26)] are observed at 9.05 and 8.35 ppm. At room temperature, the NH signal was

not appeared, hence, variable temperature ^1H NMR (Figure 3.11) was performed. The NH signal was observed as a broad signal at 233 K, however, the signal was sharp at 193 K and appeared at 9.46 ppm. All the other signals are retained its original peak position. Overall, the spectral pattern reveals the typical nonaromatic carbaporphyrinoids.³⁰ The protonation study was performed by CD_2Cl_2 solution of **25** with gradual addition of TFA (Figure 3.12). The pyridyl CH protons are slightly deshielded, whereas, *o*-phenylene protons are upfield shifted. The inner NH and the protonated imine NH are resonated at 10.45 ppm in **25.2H⁺** as a broad signal. Overall, there is a marginal shift in the macrocyclic ring protons, thus retains nonaromatic character upon protonation.

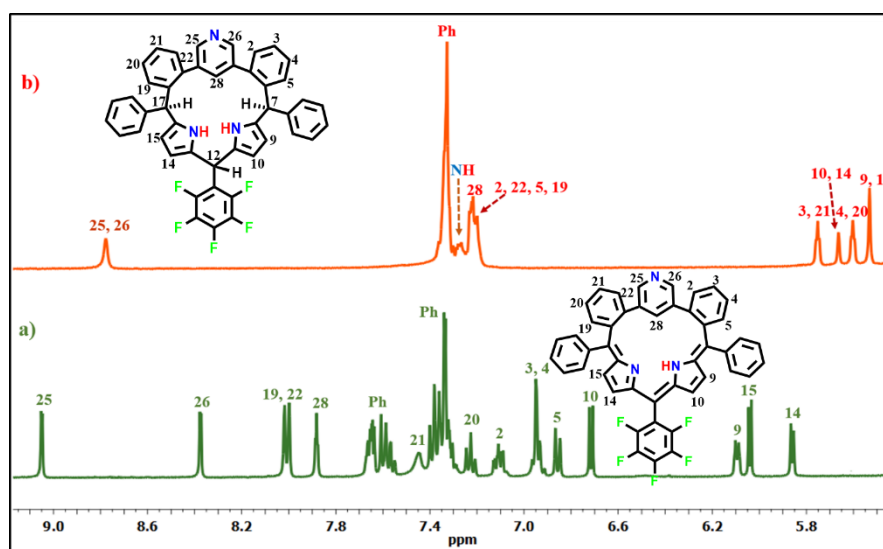


Figure 3.10: ^1H NMR spectra of **25** (a) and **26** (b) in CD_2Cl_2 .

The ^1H NMR spectral analysis of **26** manifests its symmetry as it exhibits the signals exactly for half of the molecule (Figure 3.10b). The *meso* CH protons are appeared as singlets at 1.26 ppm (Figure 3.10). The pyrrolic β -CH protons are upfield shifted with respect to **25** and resonated at 5.66 ppm [H(10,14)] and 5.53 ppm [H(9,15)]. The pyridine (*Py*) CH-protons [H(25,26)] and [H(28)] are resonated as a singlet at 8.78 and 7.23 ppm respectively.

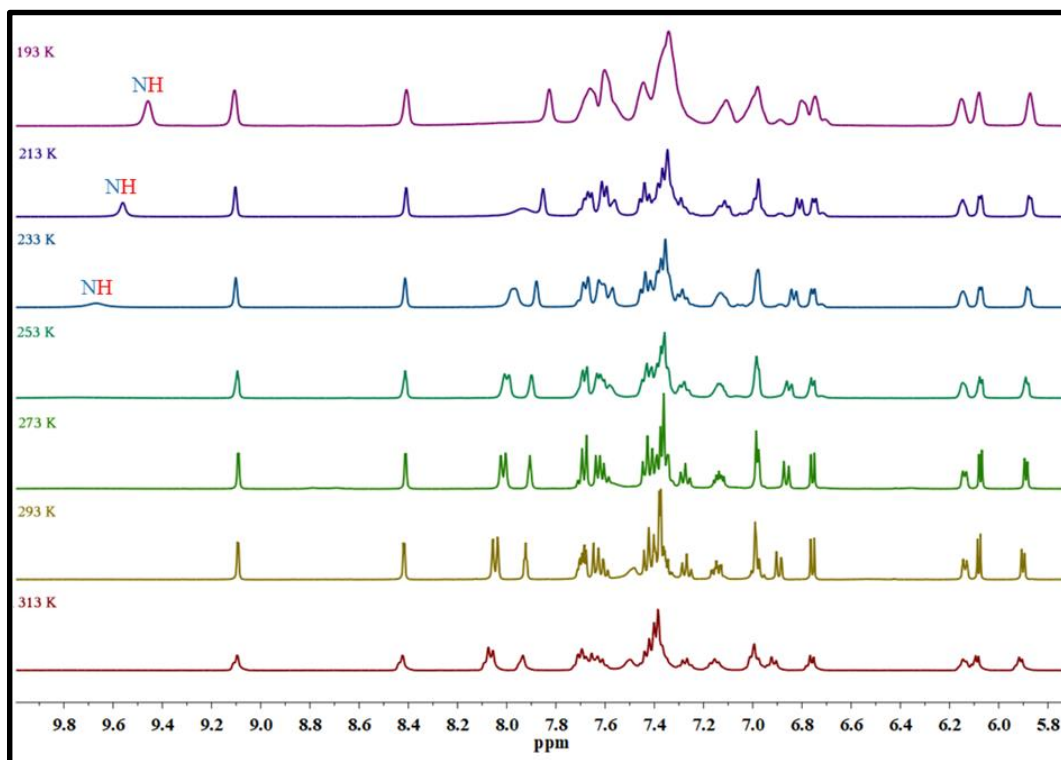


Figure 3.11: Variable temperature $^1\text{H-NMR}$ spectrum of **25** in CD_2Cl_2 .

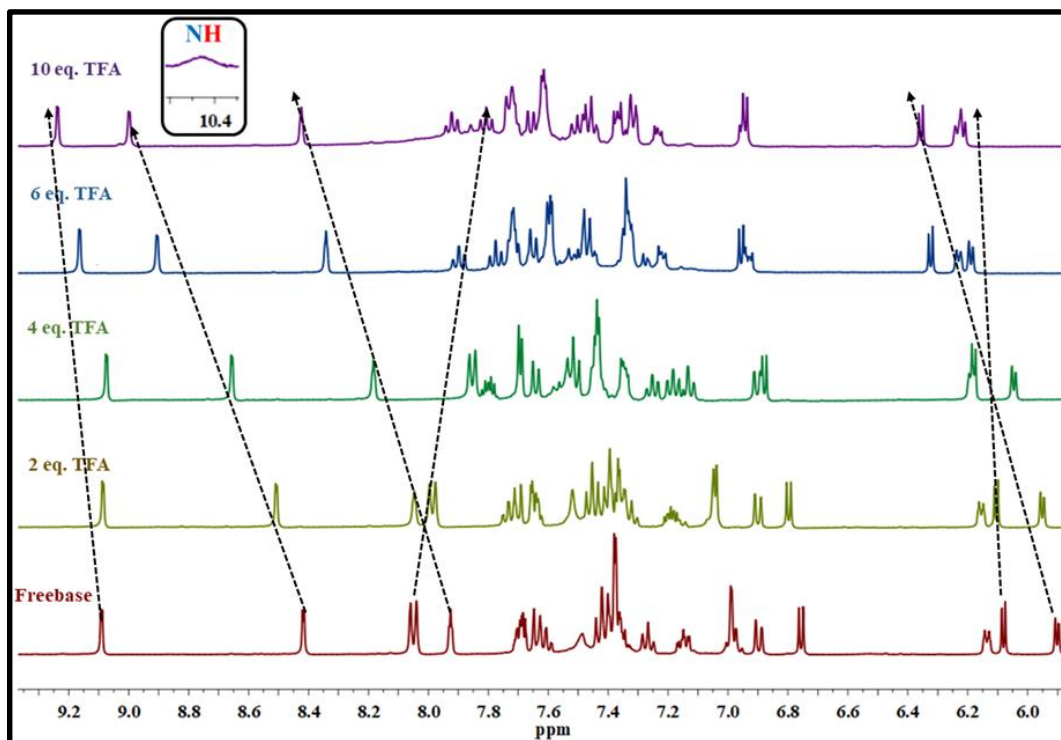


Figure 3.12: $^1\text{H-NMR}$ spectra of 25.2H^+ with various equivalents of TFA in CD_2Cl_2 .

3.3.3.3 Single crystal X-ray analysis:

To obtain a single crystal of **25** was not successful, however, the molecular structure of **26** was unambiguously confirmed by single crystal X-ray analysis (Figure 3.13). The crystal structure reveals that the three sp^2 *meso* carbon atoms and pyrrole imine N as observed in **25** are reduced to sp^3 carbon atom (C7, C12, C17) and pyrrole amine NH. In addition, the presence of four fused sp^2 (where two each from *o1* and *o2* phenylene) carbon atoms combined with three sp^3 *meso*-carbon atoms to generate calixphyrin(2.2.1.1.1) **26**. The crystal analysis reveals the following; (i) both the pyrrole amine hydrogen atoms are pointing towards the inner macrocyclic core; (ii) one of the pyrrole unit (N1) is highly tilted by $68.65(5)^\circ$ as compared to other pyrrole $30.66(4)^\circ$ and pyridine unit (*py*) by $55.81(4)^\circ$ and (iii) overall the macrocycle exhibits partial ruffled confirmation to mitigate the steric repulsion caused by the contracted core. Furthermore, the carbon–carbon bond lengths of pyridine(*Py*) unit are between 1.395(2) Å to 1.336(2) Å and for pyrrole rings (N1)& (N2) are 1.417(2) Å to 1.356(2) Å and 1.426(2) Å to 1.356(2) Å respectively (Figure 3.16) confirms that each heterocyclic rings maintain its individual aromatic character.

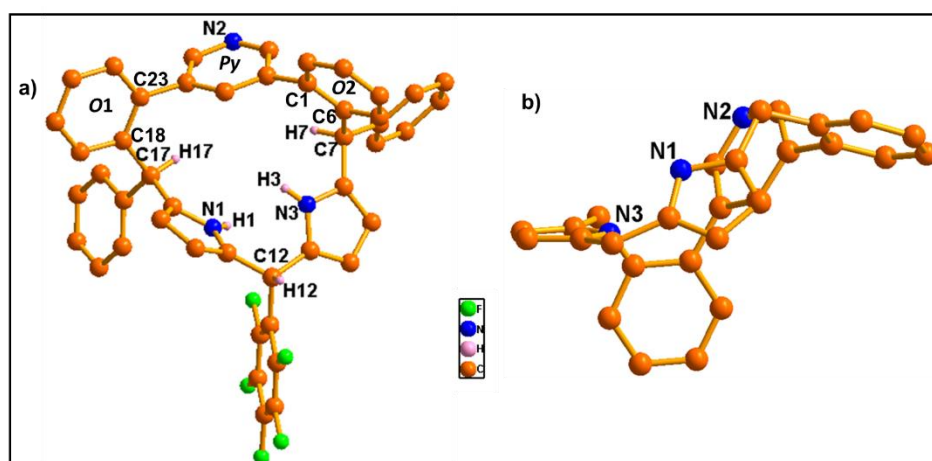


Figure 3.13: Single crystal X-ray structure of **26**. **a)** Top view and **b)** side view. The peripheral hydrogen atoms in **a** & **b** and *meso*-aryl groups in **b** are omitted for clarity in the side view.

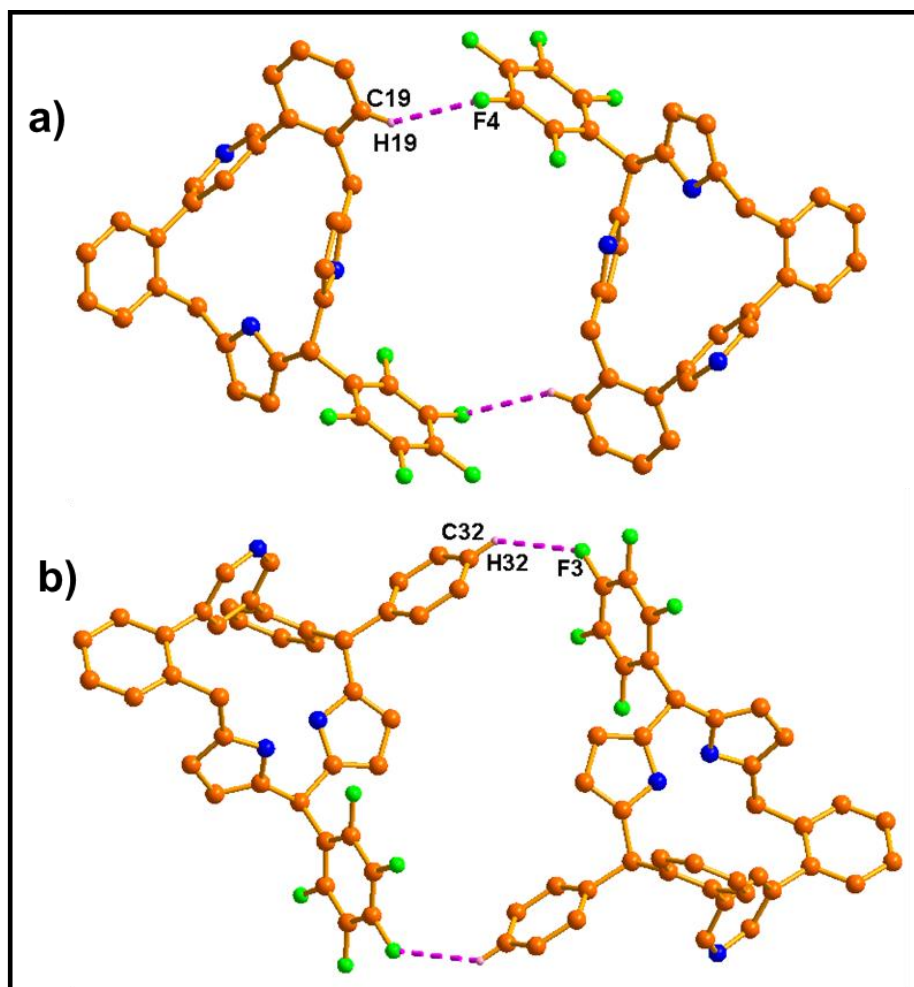


Figure 3.14: Self-assembled dimers of **26**. The bond distances and angles are: a) C19-H19...F4: 2.776(1) Å & 146.22(1)°; b) C32-H32...F3: 2.870(1) Å & 132.57(1)° respectively. The peripheral hydrogen atoms and the *meso*-aryl groups are omitted for clarity.

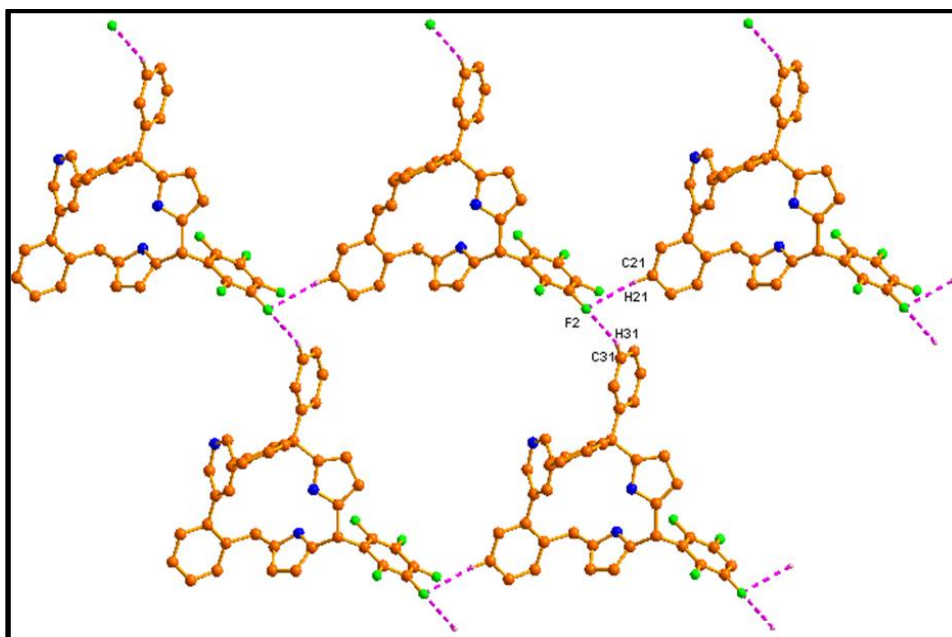


Figure 3.15: 2-D array of **26**. The bond distances and angles are C21-H21...F2: 2.690(1)Å and 170.20(1)°; C31-H31...F2: 2.548(1)Å and 156.42(1)° respectively. The peripheral hydrogen atoms and the *meso*-aryl groups are omitted for clarity.

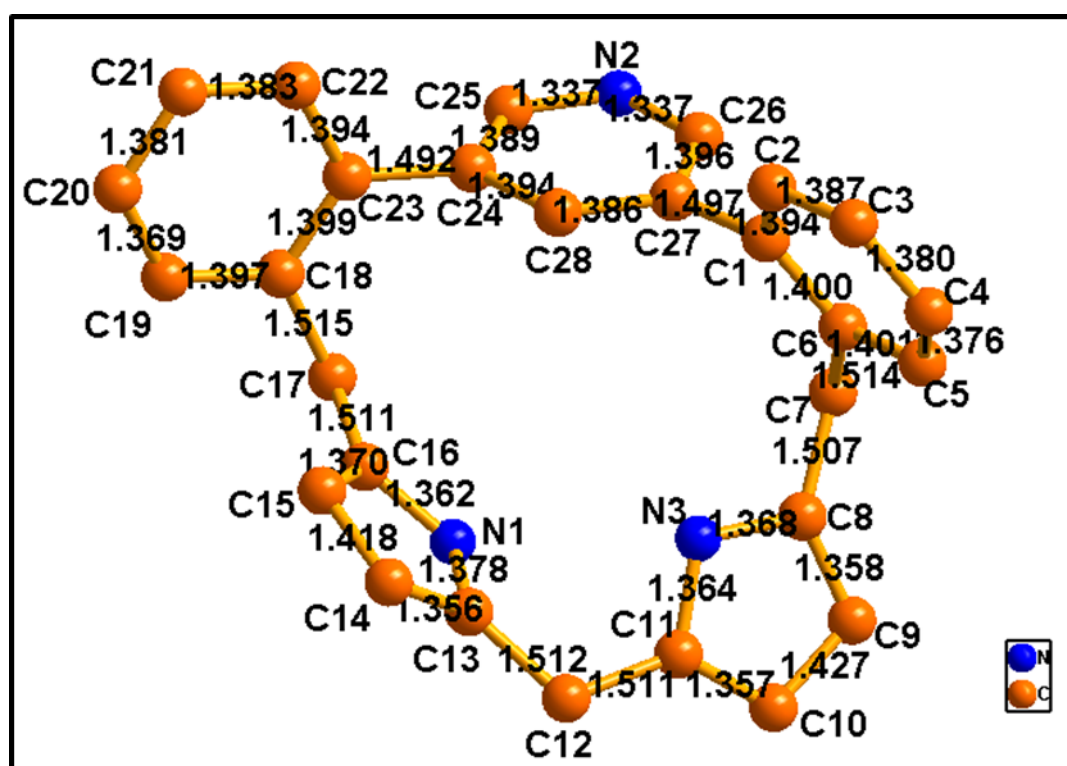


Figure 3.16: Selected Bond lengths in **26** (Å).

3.3.3.4 Electronic absorption and emission spectral analyses

Compound **25** shows a prominent band at 370 nm and a broad band at 620 nm. Upon gradual addition of TFA in **25**, the bands are bathochromically shifted by 5 nm and 100 nm and showed the isosbestic point at 373 nm and 650 nm (Figure 3.18) and appeared at 375 nm and 720 nm in **25.2H⁺** respectively. The molar extinction coefficient values of both **25** and **25.2H⁺** are in the order of 10^4 and the results are comparable with carbaporphyrinoids with nonaromatic characteristics.³¹ In the case of **26**, an intense band is appeared at 469 nm and its molar absorption coefficients are higher as compared to **25** and **25.2H⁺**, however maintains the similar order. The appearance of band in **26** perhaps should be due to π - π^* transitions of the 3,5-diphenylpyridyl moiety.

The emission profile of compounds **25** and **26** are shown in Figure 3.19. The compound **25** exhibits two weak emissive band at 557 nm and 656 nm with fluorescence quantum yield of (Φ_F) is 0.011 (Table 3.1). Interestingly, the calixphyrin analogue shows an intense emissive maximum at 563 nm with almost seven fold increase in emission intensity and three fold increase in (Φ_F) is 0.031 (Table 3.1). It is pertinent to point out that such phenomenal increment in emission intensity via mere structural change from carbatriphyrin to its calixphyrin analogue is hitherto unknown in the literature.

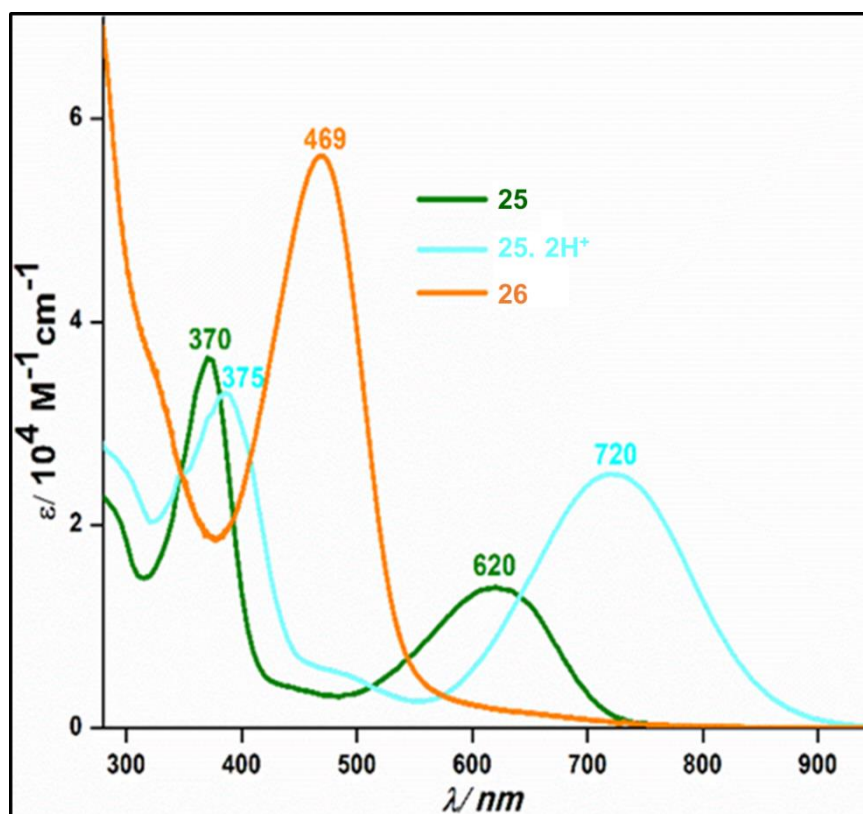


Figure 3.17: Electronic absorption spectra of 25, 25.2H⁺ and 26.

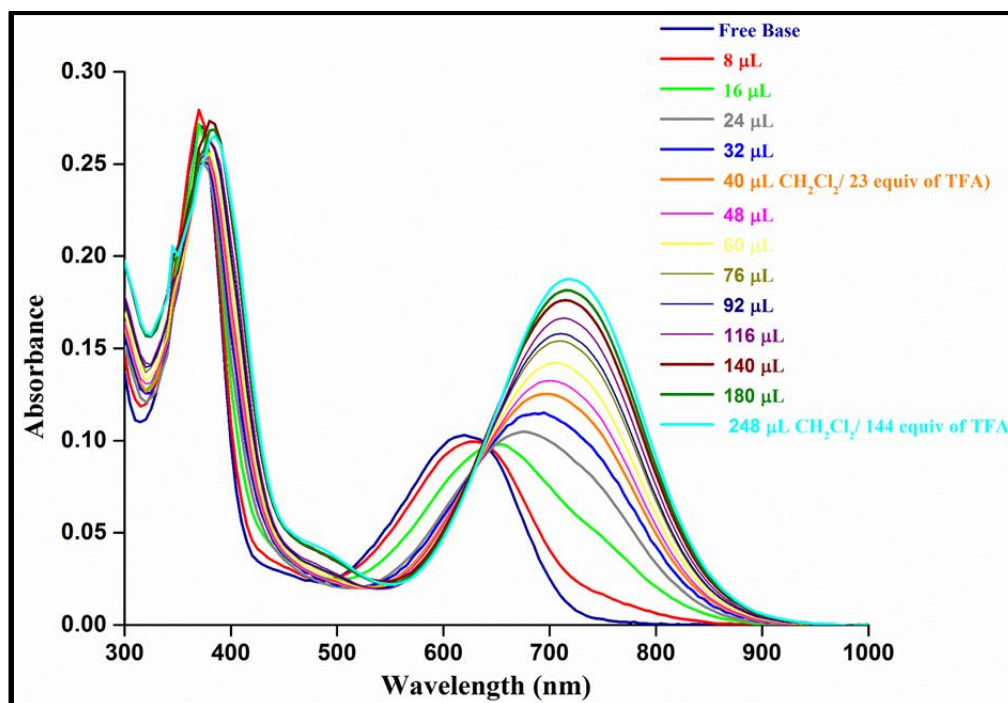


Figure 3.18: The electronic absorption spectrum of 25 with various equivalents of TFA in CH₂Cl₂.

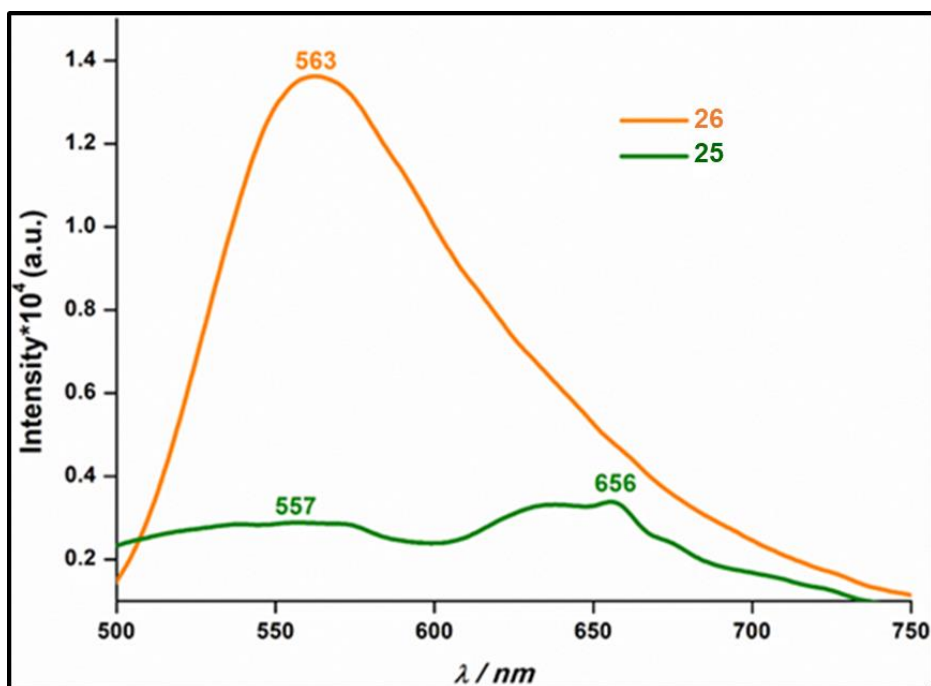


Figure 3.19: Emission spectra of **25** and **26** in CH_2Cl_2 .

Table 3.1: Electronic absorption spectral data of **25**, **25.2H⁺** and **26** & emission spectral data of **25** and **26**

Compd.	$\lambda_{\text{max}}/\text{nm}$ ($\epsilon/\text{M}^{-1}\text{cm}^{-1}$)* 10^4	$\lambda_{\text{max}}/\text{nm}$	ϕ_f
25	370 (3.64), 620 (1.38)	557, 656	0.011
25.2H⁺	375 (3.27), 720 (2.51)
26	469 (5.62)	563	0.031

3.4 Conclusions

In summary, we have successfully synthesized [3.3.1]Carbatriphyrin and its calix[2]phyrin(2.2.1.1.1) analogue. The carbatriphyrin and its protonated derivative adopts nonaromatic characteristics due to the local aromaticity of the individual heterocyclic ring. The crystal analysis of calix[2]phyrin reveals partial ruffled conformation with maximum deviation of one of the pyrrole units. Finally to the best of our knowledge, the calix[2]phyrin reported in this chapter is the simplest contracted calixphyrin till date.

3.5 General Information

The reagents and materials for the synthesis were used as obtained from Sigma Aldrich chemical suppliers. All solvents were purified and dried by standard methods prior to use. The NMR solvents were used as received and the spectra were recorded in Bruker 400 and 700 MHz spectrometer with TMS as internal standard. The ESI (HR-MS) mass spectra were recorded in Bruker, micro-TOF-QII mass spectrometer. The Electronic absorption and emission spectra were recorded in Jasco V-730 UV-Visible spectrophotometer and Edinburgh Fluorescence spectrometer respectively. The X-ray quality crystals for **26** was grown by slow diffusion of methanol over CH₂Cl₂ solution. Single-crystal X-ray diffraction data of **26** was collected in Rigaku Oxford diffractometer. Fluorescence quantum yields were determined by using *meso*-tetraphenylporphyrin (TPPH₂) in toluene ($\phi_f = 0.11$) as a reference.

3.6 Synthetic procedure and spectral characterization of 25-29

3.6.1 Synthesis of 27: 3,5-dibromopyridine (1 gm, 4.2 mmol) and 2-formylphenyl boronic acid (1.58 gm, 10.5 mmol) was added in 3:1 (V/V) THF and water solvents mixture under nitrogen atmosphere. Then K₂CO₃ (2.90 gm, 21 mmol) was added in the reaction mixture. The solution was further purged with nitrogen for about 15 min and then Pd(PPh₃)₄ (0.392 gm, 0.34 mmol) was added under nitrogen atmosphere. The reaction was allowed to stir for 8 h then work up was performed, dried by Na₂SO₄ and purified by column chromatography using silica gel (100-200 mesh) in hexane and ethyl acetate (70:30). The compound was further recrystallized from CH₂Cl₂/n-hexane to afford white solid **27** in 85% (1.02 g, 3.57 mmol) Yield.

¹H NMR (400 MHz, CD₂Cl₂): δ 10.10 (s, 2H), 8.74 (s, 2H), 8.09 (d, $J = 7.8$ Hz, 2H), 7.78 (dd, $J = 13.6, 6.1$ Hz, 3H), 7.65 (t, $J = 7.6$ Hz, 2H), 7.55 (d, $J = 7.6$ Hz, 2H).

^{13}C NMR (101 MHz, CD_2Cl_2): δ 191.15, 149.42, 140.98, 138.12, 133.94, 133.47, 131.28, 128.94.

ESI-HRMS: m/z calculated for $\text{C}_{19}\text{H}_{13}\text{NO}_2 = 287.0946$ and found = 288.1014[M+1]

3.6.2 Synthesis of 28: The freshly prepared phenylmagnesium bromide was added into toluene solution of **27** (1.0 gm, 3.4 mmol) in presence of ice bath. After 10 min, the reaction was allowed to attain room temperature and refluxed overnight. The completion of the reaction was monitored by TLC and the reaction was quenched with 2N HCl and work up was performed, dried by sodium sulphate and purified by column chromatography using silica gel (100-200 mesh) in Hexane and ethyl acetate (70:30) to afford white crystalline solid **28** in 78% (1.17 g, 2.65 mmol) yield.

^1H NMR (400 MHz, CDCl_3): δ 8.17 (d, $J = 1.8$ Hz, 2H), 7.99 (d, $J = 7.7$ Hz, 2H), 7.75 (s, 1H), 7.63 (d, $J = 7.4$ Hz, 2H), 7.44 – 7.39 (m, 6H), 7.38 (s, 2H), 7.33 (t, $J = 7.6$ Hz, 4H), 7.28 – 7.25 (m, 2H), 5.86 (d, $J = 4.9$ Hz, 2H), 3.19 (s, 2H).

^{13}C NMR (101 MHz, CDCl_3): δ 147.62, 144.82, 143.66, 141.58, 138.20, 136.81, 136.43, 130.16, 128.73, 128.29, 127.90, 127.45, 127.24, 126.72, 125.89, 74.04, 72.20, 62.36, 36.24, 29.04.

ESI-HRMS: m/z calculated for $\text{C}_{31}\text{H}_{25}\text{NO}_2 = 443.1885$ and found = 444.1940[M+1]

3.6.3 Synthesis of 29: The compound **28** (0.500 gm, 1.20 mmol) was dissolved in dry DCE solvent under nitrogen atmosphere covered with aluminum foil. Pyrrole (7.75 ml, 112 mmol) was added and allowed to stir for about 15 minutes. Then, $\text{BF}_3 \cdot \text{OEt}_2$ (0.820 ml, 6.76 mmol) was slowly added and reaction mixture was allowed to reflux for 6 hours. Further workup was performed using CH_2Cl_2 and water, dried by Na_2SO_4 and

purified by column chromatography using silica gel (100-200 mesh) in Hexane and ethyl acetate (90:10) to afford white solid **29** in 60% (389 mg, 0.72 mmol) yield.

¹H NMR (400 MHz, CD₂Cl₂): δ 8.25 (s, 2H), 7.81 (s, 2H), 7.24 (t, *J* = 7.3 Hz, 4H), 7.14 – 7.04 (m, 11H), 6.85 (d, *J* = 7.0 Hz, 4H), 6.51 (d, *J* = 5Hz, 2H), 5.95 (d, *J* = 4.6Hz, 2H), 5.56 (d, *J*=4.5Hz, 2H), 5.34 (s, 2H).

¹³C NMR (101 MHz, CD₂Cl₂): δ 148.14, 143.22, 141.07, 137.09, 136.17, 133.05, 130.43, 129.32, 128.72, 128.39, 126.62, 117.29, 108.10.

ESI-HRMS: *m/z* calculated for C₃₉H₃₁N₃ = 541.2518 and found = 542.2576[M+1].

3.6.4 Synthesis of 25: Solution of **29** (0.100 gm, 0.184 mmol) was mixed in 100 ml CH₂Cl₂ solvent under nitrogen atmosphere covered with aluminum foil. Pentafluorobenzaldehyde (0.043 gm, 0.221 mmol) was added in the reaction mixture. After 15 min TFA (0.105 gm, 0.923 mmol) was added under same condition and allowed to stir for about 3 hours. Then DDQ (0.125 gm, 0.553 mmol) was added and reaction was continued for another 1 hour in absence of nitrogen atmosphere. Further, 1 ml of TEA was added in reaction crude and allowed to stir for another 1 hr. The crude product was then passed through basic alumina and purified using neutral alumina column chromatography. At first the orange coloured **26** was separated with 10:90 CH₂Cl₂: hexane in 3% (3 mg, 0.005 mmol) yield and the greenish-blue colour band was eluted with 80:20 CH₂Cl₂: hexane and identified as **25** as a greenish blue crystalline solid in 4% (5 mg, 0.007 mmol) yield.

¹H NMR (400 MHz, CD₂Cl₂): δ 9.05 (s, 1H), 8.38 (d, *J* = 2.1 Hz, 1H), 8.01 (d, *J* = 7.6 Hz, 2H), 7.88 (d, *J* = 2.1 Hz, 1H), 7.67 – 7.63 (m, 2H), 7.61 – 7.55 (m, 2H), 7.45 (s, 1H), 7.36- 7.34 (m, 6H), 7.23 (t, *J* = 7.4 Hz, 1H), 7.10 (d, *J* = 8.1 Hz, 1H), 6.94 (d, *J* =

6.3 Hz, 2H), 6.86 (d, $J = 7.6$ Hz, 1H), 6.72 (d, $J = 5.7$ Hz, 1H), 6.09 (d, $J = 5.7$ Hz, 1H), 6.04 (d, $J = 4.7$ Hz, 1H), 5.86 (d, $J = 4.7$ Hz, 1H).

^{13}C NMR (101 MHz, CD_2Cl_2): δ 147.82, 141.61, 140.70, 136.26, 135.11, 133.30, 132.71, 131.06, 130.93, 130.76, 129.73, 128.90, 128.70, 128.65, 128.22, 127.80, 127.38, 126.82.

ESI-HRMS: m/z calculated for $\text{C}_{46}\text{H}_{26}\text{F}_5\text{N}_3 = 715.2047$ and found = 716.2092[M+1].

UV-Vis (CH_2Cl_2): $\lambda_{\text{max}}/\text{nm}$ ($\epsilon[\text{M}^{-1}\text{cm}^{-1}] \times 10^4$) = 370 (3.90), 620 (1.38).

Quantum yield (Φ_f) = 0.011.

25.2H⁺: ^1H NMR (400 MHz, CD_2Cl_2): δ 10.42 (s, 2H), 9.20 (d, $J = 7.4$ Hz, 1H), 8.96 (s, 1H), 8.39- 8.37 (m, 1H), 7.89- 7.87 (m, 2H), 7.79- 7.76 (m, 2H), 7.70 – 7.67 (m, 4H), 7.46 – 7.40 (m, 4H), 7.33 (d, $J = 7.0$ Hz, 2H), 7.28 (d, $J = 6.8$ Hz, 2H), 7.21 – 7.18 (m, 1H), 6.90 (d, $J = 7.1$ Hz, 1H), 6.32 (d, $J = 5.3$ Hz, 2H), 6.19 (t, $J = 6.5$ Hz, 2H).

UV-Vis (CH_2Cl_2): $\lambda_{\text{max}}/\text{nm}$ ($\epsilon[\text{M}^{-1}\text{cm}^{-1}] \times 10^4$) = 375 (3.27), 720 (2.51).

3.6.5 Synthesis of 26: Solution of **25** (0.025 gm, 0.034 mmol) was dissolved in 30 ml CH_3OH solvent under nitrogen atmosphere and covered with aluminum foil. After that NaBH_4 (0.025 gm, 0.660 mmol) was added gradually to the solution in ice condition and allowed to stir for about 8 hours in room temperature. Then work up was performed, dried by Na_2SO_4 and purified by column chromatography using neutral alumina in 20:80 CH_2Cl_2 : hexane, identified as orange crystalline solid **26** in 50% (12.22 mg, 0.017 mmol) yield.

^1H NMR (400 MHz, CD_2Cl_2): δ 8.78 (s, 2H), 7.34-7.32 (m, 10H), 7.27 (s, 2H), 7.23 (s, 1H), 7.22-7.20 (m, 4H), 5.75 (t, $J = 7.8$ Hz, 2H), 5.66 (s, 2H), 5.60 (t, $J = 7.6$ Hz, 2H), 5.53 (s, 2H), 1.26 (s, 3H).

^{13}C NMR (101 MHz, CD_2Cl_2): δ 148.73, 142.24, 140.40, 138.00, 133.98, 129.59, 128.97, 128.80, 128.35, 127.50, 126.84, 126.73, 107.70, 107.17, 29.53.

ESI-HRMS: m/z calculated for $\text{C}_{46}\text{H}_{30}\text{F}_5\text{N}_3 = 719.2360$ and found = 720.2433[M+1].

UV-Vis (CH_2Cl_2): $\lambda_{\text{max/nm}}$ ($\epsilon[\text{M}^{-1}\text{cm}^{-1}] \times 10^4$) = 469 (5.80).

Quantum yield (Φ_f) = 0.031.

Table 3.2: Crystal data for **26**

Crystal parameters	26
Formula	$\text{C}_{46}\text{H}_{30}\text{F}_5\text{N}_3$
$M/\text{g mol}^{-1}$	719.73
T/K	132
Crystal dimensions/ mm^3	$0.26 \times 0.26 \times 0.25$
Crystal system	triclinic
Space group	$P-1$
$a/\text{\AA}$	12.7546(6)
$b/\text{\AA}$	13.2443(5)
$c/\text{\AA}$	14.8471(7)
$\alpha/^\circ$	68.710(4)
$\beta/^\circ$	67.004(4)
$\gamma/^\circ$	72.432(4)
$V/\text{\AA}^3$	2113.43(19)
Z	2
$\rho_{\text{calcd}}/\text{mg m}^{-3}$	1.131
μ/mm^{-1}	0.678
F(000)	744.0
Reflns. collected	28667
Indep.reflns.[$R(\text{int})$]	7532 [0.0484]
Max/min transmission	0.844, 0.838
Data/restraints/parameters	7532/0/487
GOF on F^2	1.048
Final R indices [$I > 2\sigma(I)$]	$R_1 = 0.0479$, $wR_2 = 0.1377$
R indices (all data)	$R_1 = 0.0507$, $wR_2 = 0.1395$
Largest diff peak and hole [$e \text{\AA}^{-3}$]	0.27 and -0.23

3.7 References

1. Y. Inokuma, J. H. Kwon, T. K. Ahn, M.-C. Yoo, D. Kim, A. Osuka, *Angew. Chem. Int. Ed.* **2006**, *45*, 961-964.

-
2. C. G. Claessens, D. González-Rodríguez, M. S. Rodríguez-Morgade, A. Medina, T. Torres, *Chem. Rev.* **2014**, *114*, 2192-2277.
 3. A. Osuka, E. Tsurumaki, T. Tanaka, *Bull. Chem. Soc. Jpn.* **2011**, *84*, 679-697.
 4. Y. Inokuma, A. Osuka, *Dalton Trans.* **2008**, 2517-2526.
 5. R. Myśliborski, L. Latos-Grażyński, L. Szterenber, T. Lis, *Angew. Chem. Int. Ed.* **2006**, *45*, 3670-3674.
 6. Z.-L. Xue, Z. Shen, J. Mack, D. Kuzuhara, H. Yamada, T. Okujima, N. Ono, X.-Z. You, N. Kobayashi, *J. Am. Chem. Soc.* **2008**, *130*, 16478-16479.
 7. D. Kuzuhara, H. Yamada, Z. Xue, T. Okujima, S. Mori, Z. Shen, H. Uno, *Chem. Commun.* **2011**, *47*, 722-724.
 8. a) K. S. Anju, S. Ramakrishnan, A. Srinivasan, *Org. Lett.* **2011**, *13*, 2498-2501.
b) K. N. Panda, K. G. Thorat, M. Ravikanth, *J. Org. Chem.* **2018**, *83*, 12945-12950.
 9. D. Kuzuhara, Y. Sakakibara, S. Mori, T. Okujima, H. Uno, H. Yamada, *Angew. Chem. Int. Ed.* **2013**, *52*, 3360-3363.
 10. M. Pawlicki, K. Hurej, L. Szterenber, L. Latos-Grażyński, *Angew. Chem. Int. Ed.* **2014**, *53*, 2992-2996.
 11. M. Pawlicki, M. Garbicz, L. Szterenber, L. Latos-Grażyński, *Angew. Chem. Int. Ed.* **2015**, *54*, 1906-1909.
 12. M. Pawlicki, A. Kędzia, L. Szterenber, L. Latos-Grażyński, *Eur. J. Org. Chem.* **2013**, *2013*, 2770-2774.
 13. E. Nojman, A. Berlicka, L. Szterenber, L. Latos-Grażyński, *Inorg. Chem.* **2012**, *51*, 3247-3260.
 14. A. Berlicka, L. Latos-Grażyński, T. Lis, *Angew. Chem. Int. Ed.* **2005**, *44*, 5288-5291.
-

-
15. A. Berlicka, L. Latos-Grażyński, *Inorg. Chem.* **2009**, *48*, 7922-7930.
 16. A. Krivokapic, A. R. Cowley, H. L. Anderson, *J. Org. Chem.* **2003**, *68*, 1089-1096.
 17. M. Pawlicki, L. Latos-Grażyński, L. Szterenberga, *J. Org. Chem.* **2002**, *67*, 5644-5653.
 18. M. Pawlicki, A. Kędzia, D. Bykowski, L. Latos-Grażyński, *Chem. Eur. J.* **2014**, *20*, 17500-17506.
 19. A. Berlicka, N. Sprutta, L. Latos-Grażyński, *Chem. Commun.* **2006**, 3346-3348.
 20. E. Pacholska, L. Latos-Grażyński, Z. Ciunik, *Chem. Eur. J.* **2002**, *8*, 5403-5405.
 21. E. Pacholska-Dudziak, A. Gaworek, L. Latos-Grażyński, *Inorg. Chem.* **2011**, *50*, 10956-10965.
 22. V. Kra'1, J. L. Sessler, R. S. Zimmerman, D. Seidel, V. Lynch, B. Andrioletti, *Angew. Chem. Int. Ed.* **2000**, *39*, 1055-1058.
 23. C. Bucher, D. Seidel, V. Lynch, V. Kra'1, J. L. Sessler, *Org. Lett.* **2000**, *2*, 3103-3106.
 24. P. G. Campbell, A. J. V. Marwitz, S.-Y. Liu, *Angew. Chem. Int. Ed.* **2012**, *51*, 6074-6092.
 25. B. Dolensky', J. Krouli'k, V. Kra'1, J. L. Sessler, H. Dvora'kov', P. Bour', M. Berna'tkova', C. Bucher, V. Lynch, *J. Am. Chem. Soc.* **2004**, *126*, 13714 – 13722.
 26. J. L. Sessler, W. S. Cho, V. Lynch, V. Kra'1, *Chem. Eur. J.* **2002**, *8*, 1134.
 27. T. D. Lash, *Chem. Rev.* **2017**, *117*, 2313-2446.

28. B. Adinarayana, A. P. Thomas, P. Yadav, V. Mukundam, A. Srinivasan, *Chem. Eur. J.* **2017**, *23*, 2993-2997.
29. M. Stępień, L. Latos-Grażyński, L. Szterenberga, J. Panek, Z. Latajka, *J. Am. Chem. Soc.* **2004**, *126*, 4566-4580.
30. B. Adinarayana, A. P. Thomas, C. H. Suresh, A. Srinivasan, *Angew. Chem. Int. Ed.* **2015**, *54*, 10478-10482.
31. B. Adinarayana, A. P. Thomas, P. Yadav, A. Kumar, A. Srinivasan, *Angew. Chem. Int. Ed.* **2016**, *55*, 969-973.
32. P. S. Salini, A. P. Thomas, R. Sabarinathan, S. Ramakrishnan, K. C. Gowri Sreedevi, M. L. P. Reddy, A. Srinivasan, *Chem. Eur. J.* **2011**, *17*, 6598 – 6601.

CHAPTER 4

meso-Aryl [20] π Homoporphyrin: The Simplest Expanded Porphyrin with the Smallest Möbius Topology

4.1	Introduction	85
4.1.1	Homoporphyrin	85
4.1.2	Möbius aromaticity	90
4.2	Objective of our work	91
4.3	Results and discussions	92
4.3.1	Spectral characterisation	93
4.3.1.1	Mass spectrometric analysis	93
4.3.1.2	NMR Analysis	95
4.3.1.3	Single crystal X-ray structure and analysis of 17 & 19	100
4.3.1.4	Electronic spectral analysis	107
4.3.1.5	Theoretical calculation	108
4.4	Conclusion	112
4.5	Experimental Section	112
4.5.1	General Information	112
4.5.2	Synthetic procedure and spectral characterization of 16-19	113
4.6	References	115

4.1 Introduction

4.1.1 Homoporphyrin

Expanded porphyrins are porphyrin analogues, which have more than 18π electrons in their conjugated pathway owing to either an increased number of heterocyclic rings or *meso* carbon bridges. Predominantly, these analogues of porphyrin have been extensively studied due to its potential applications in various fields, such as; i) the large core size that can often accommodate more than one metal ions to stabilize multi-metallic complexes; ii) bind with anionic and neutral substrates; iii) MRI contrasting agents; iv) non-linear optical materials (NLO) and v) photodynamic therapeutic agents (PDT).¹⁻⁴ After the serendipitous discovery of 22π sapphyrins by Woodward and co-workers in 1966,⁵ expanded porphyrins received much attention for the porphyrin chemists and paramount study was carried out in this area up to 96π tetracosapphyrin.⁶ However, among the expanded porphyrins, homoporphyrins remain unanticipated for a long time due to their synthetic difficulties as well as stability factors. Homoporphyrins are tetrapyrrolic macrocycles in which four pyrrole rings are connected through five methene bridges, containing an extra atom between a *meso* and α -pyrrolic carbon than the parent porphyrin.⁷ Due to this special structural arrangement, it captivates 17 atoms in the macrocyclic core. According to Sessler, this is the minimum number of atoms required for the fulfilment of expanded category, hence homoporphyrins are designated as the simplest expanded porphyrin.⁸ Depending on the conjugation pathway, homoporphyrins are classified in four types (Figure 4.1). Among them **A** and **B** are unconjugated systems, containing a sp^3 -hybridized centre that interrupts the π -electron conjugation pathway. Whereas, **C** and **D** are fully conjugated and they are 18π & 20π electronic systems respectively. It is observed that the fully conjugated systems (**C** & **D**) are immensely unstable in nature. While, mostly stable

homoporphyrins reported in the literature are of type **A** and considerably contributed by Callot and co-workers.⁹⁻¹¹

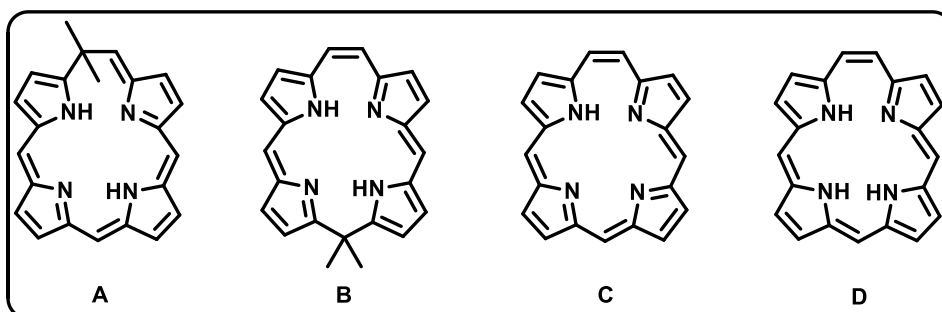
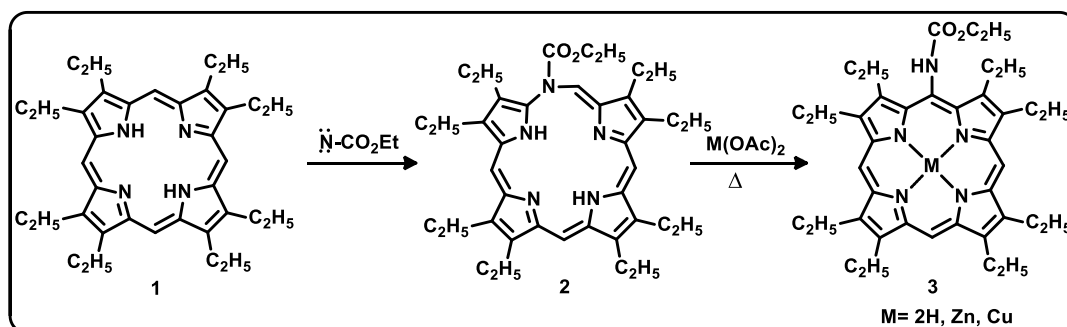
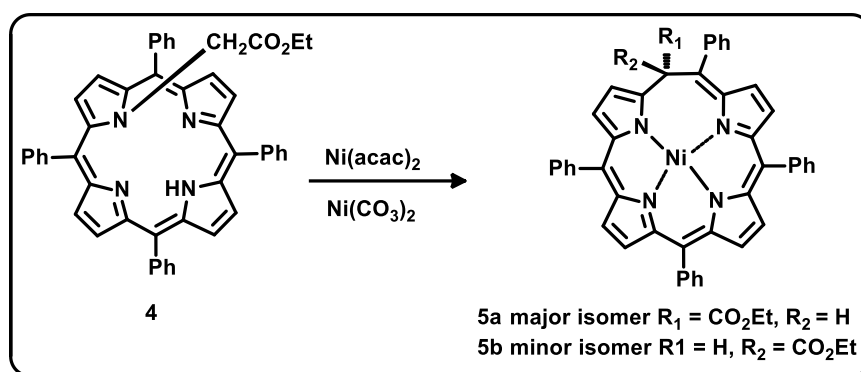


Figure 4.1: Structures of homoporphyrins **A-D**.

The first *N-meso*-azahomoporphyrin **2** was reported by Grigg *et al.* in 1967.¹² The compound **2** was synthesized by reaction between the freebase β -ethyl substituted **1** with nitrene and exhibited the non-aromatic character (Scheme 4.1).¹³ The compound **2** was unstable and decomposed to corresponding metallated porphyrin derivatives **3**, when the reaction was performed with Zn and Cu salts.

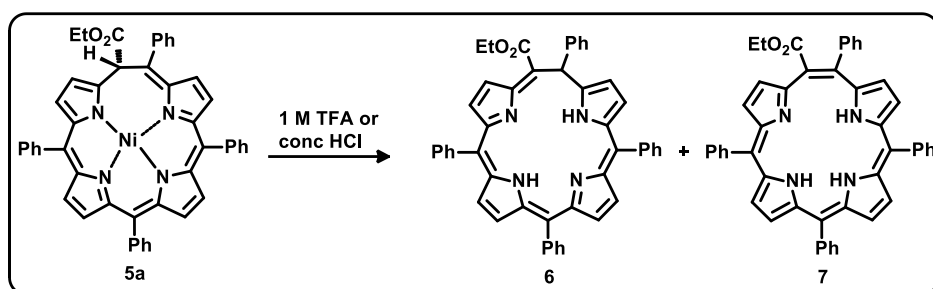


Scheme 4.1: Synthesis of azahomoporphyrin **2** and its decomposition to corresponding metallated porphyrin derivatives.

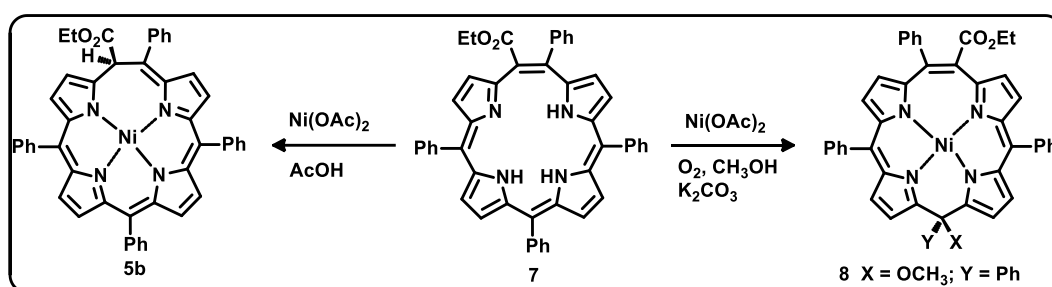


Scheme 4.2: Synthesis of Ni^{II} homoporphyrins.

Subsequently, Callot and co-workers synthesised two isomeric homoporphyrins **5a** and **5b** by the rearrangement of N-substituted tetraarylporphyrin **4** treating with Ni(acac)₂ and Ni(CO₃)₂ in 1,2-dichloroethane solution (Scheme 4.2).⁹⁻¹¹ The reaction afforded a mixture of two epimeric Ni^{II} homoporphyrins **5a** and **5b**, with the major yield of endo epimer **5a**. The electronic absorption spectrum of both epimers **5a** and **5b** have resemblance to the porphyrin type systems. Crystal analyses revealed notable distorted structure of the molecule and such distortion attributed by the insertion of the additional carbon atom into the parent porphyrin ring, hence promotes non-aromatic character.^{14,15} Demetallation experiment of major isomer **5a** was performed at high acid concentration, where two freebase homoporphyrins **6** and **7** were achieved.¹⁶ One of the products **7** was found to be 20π anti-aromatic derivative with three inner N-Hs (Scheme 4.3), however, the compound decomposed even at 0°C. Same group also tried to stabilize **7** by coordinating with Ni(OAc)₂ under different reaction conditions, however the attempts were futile and generated numerous rearranged products (**5b** and **8**) (Scheme 4.4).^{9,16,17, 18}

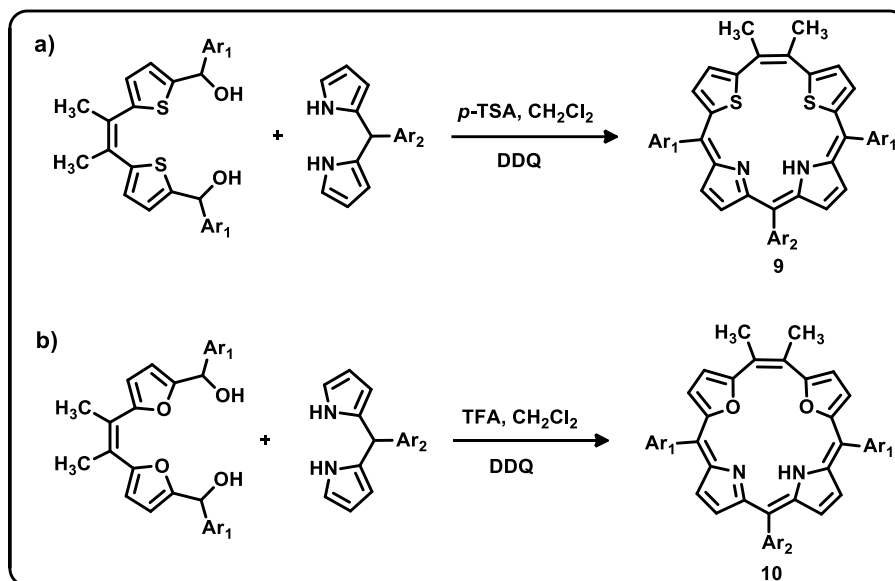


Scheme 4.3: Synthesis of free base homoporphyrins.



Scheme 4.4: Metallation of homoporphyrins.

The first stable core modified nonaromatic homoporphyrins were reported by Ravikanth and co-workers. The corresponding homoporphyrins, [20]dithiahomoporphyrin(2.1.1.1) **9** and [20]dioxahomoporphyrin(2.1.1.1) **10** were synthesized by [2+2] acid-catalyzed condensation of *meso*-aryldipyrromethanes with dithia or dioxa-ethenediol derivatives by *p*-TSA catalyzed condensation followed by oxidation with DDQ (Scheme 4.5). The structural analyzes of **9** and **10** showed significant distortion, thus revealed nonaromatic characteristics.^{19 a,b}



Scheme 4.5: Synthesis of core-modified homoporphyrins.

Recently, the *m-o-m* **11** and *p-o-p* **12** terphenyl embedded homocarbaporphyrinoids and their Rh^{I} complexes are reported from our group (Figure 4.2).²⁰ The distinct bonding modes of terphenyl system in the macrocyclic core produced two structural isomers of carba analogue of homoporphyrin. The spectral and structural analyses revealed that the restricted conjugation in *m-o-m* derivative and non planarity of *p-o-p* macrocycle to provide overall nonaromatic characteristics to the free bases and their metal complexes. Though the stable core-modified homoporphyrinoid and the carba derivatives are known, till date, the respective all aza analogue is hitherto unknown in the literature.

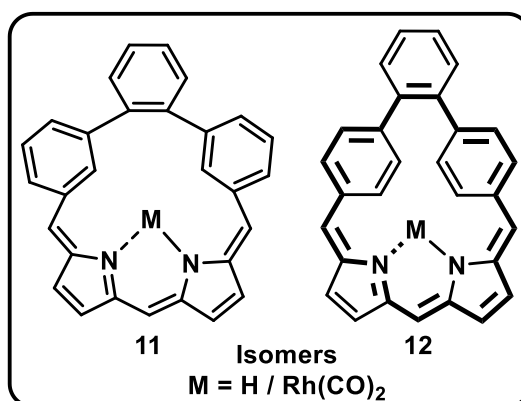


Figure 4.2: Structures of carba-homoporphyrins.

4.1.2 Möbius aromaticity

In 1964, Heilbronner proposed the concept of Möbius aromaticity and predicted the aromatic character of $[4n]\pi$ annulenes lying on a single-sided, non-orientable Möbius strip.²¹ However, after forty year of invention, the first experimental evidence of Möbius aromatic molecule was recognized by Herges and coworkers in 2003.²¹ Thereafter, numerous cyclic annulenes and its derivatives with $[4n]\pi$ Möbius aromaticity were reported.

In 2007, Latos-Grażyński and coworkers reported the first example of expanded porphyrin analogue which exhibit Möbius aromaticity.²² They validated that di-*p*-benzi-[28]Hexaphyrin **13** (Figure 4.3) switches between Hückel and Möbius topologies depending on temperature variation and the solvent polarity. Upon temperature variation, the inner pyrrolic NH and phenylene CH protons were shifted upfield, thus revealed aromaticity switching of Hückel $4n\pi$ anti-aromatic character to Möbius aromaticity. In addition, the broad absorption band in presence of non-polar solvent at room temperature and Soret and weak Q-like band in presence of polar solvents, suggested aromatic switching depends on the solvent polarity. The Möbius topology was further confirmed by crystal analyses.

Subsequently, plethora examples of expanded porphyrins with Möbius aromaticity were reported by Osuka *et al.* and Kim *et al.* They used several external stimuli to generate Möbius aromaticity in various expanded porphyrins such as i) varying temperature,²³ ii) coordination,²⁴ iii) thermal fusion,²⁵ iv) protonation,²⁶ v) oxidation/reduction,²⁷ and vi) changing the solvent.²²

In spite of these widespread reports, N-fused $[24]\pi$ pentaphyrin with a Rh^I salt **6** is the smallest structurally elucidated Möbius aromatic expanded porphyrin to date.²⁸

Osuka *et al.* synthesized **14** (Figure 4.3) by treating its free ligand with Rh^I salt in the presence of sodium acetate. The crystal analysis confirmed the formation of the N-fused tripentacyclic ring and maintained planarity, however, the Rh^I ion coordinated dipyrin unit was tilted from the mean plane to attain the Möbius topology without breaking conjugation in the framework. The results were further supported by spectral analyses and theoretical calculations. The ¹H NMR analysis of **14** displayed the inner β-CH and NH protons were resonated at 0.10 and 0.68 ppm. The NICS(0) value of **14** is -16.1 ppm and bond length alternation (BLA) value is 0.100 Å.

Recently, Harapriya and coworkers reported a core-modified heterocyclic [20]π tripyrrane derivative **15** (Figure 4.3) and claimed that it was a Möbius aromatic system by spectral and theoretical studies.²⁹ Calculated Δδ value of **15** is 6.0 ppm, therefore a weak diatropic ring current persisted in the molecule. Also, NICS(0) value of > -11 ppm supports its aromatic character.

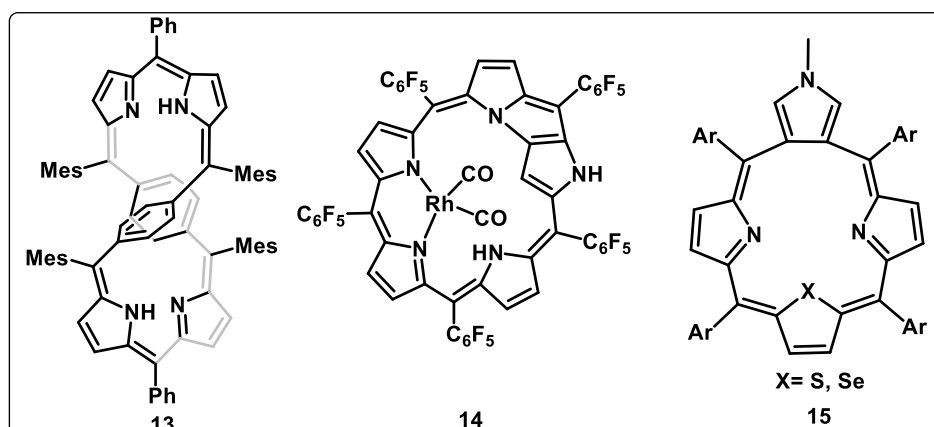


Figure 4.3: Selective examples of Möbius aromatic expanded porphyrins

4.2 Objective of our work

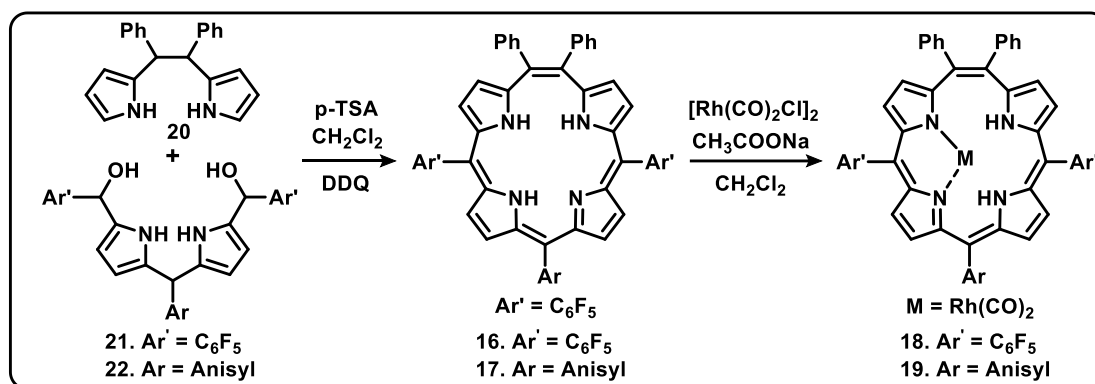
The first Homoporphyrin was reported in 1971, where the macrocycle is found to be unstable and also unable to afford stable metal complexes. Recently reported stable

core-modified and carba derivatives were nonaromatic in nature. However, to the best of our knowledge even after four decades of the discovery of Homoporphyrin, a complete conjugated stable freebase azahomoporphyrin is still elusive. In addition, it remains as a challenge for the tetrapyrrolic skeleton to achieve Möbius topology within itself. Thus, a reliable synthetic route for Homoporphyrin with Möbius topology is highly desirable and remains as a fascinating area in expanded porphyrin chemistry.

In this chapter, we would like to report the synthesis and structural characterization of stable *meso*-aryl [20] π tetraphyrin(2.1.1.1) (**16**, **17**) and its Rh(I) complex (**18**, **19**). The hitherto unknown azahomoporphyrin represents the smallest molecule to show the simplest Möbius topology in three different forms such as; (a) freebase; (b) protonation and (c) metal ion insertion.

4.3 Results and discussions

The target macrocycles were synthesized by a [2+2] MacDonald-type condensation between *meso*-5,6-diphenyldipyrroethane **20**³⁰ and 1,9-bis(pentafluorophenylhydroxymethyl)-5-(aryl)dipyrromethanes **21** and **22** in dry CH₂Cl₂ under the catalysis of *p*-toluenesulphonic acid (*p*-TSA), followed by oxidation with 2,3-dichloro-5,6-dicyano-*p*-benzoquinone (DDQ) (Scheme 4.6).



Scheme 4.6: Synthesis of **16** and **17** and their Rh^I complexes **18** and **19**.

The crude mixture was purified by column chromatography on silica gel with $\text{CH}_2\text{Cl}_2/n$ -hexane as the eluent. The desired products **16** and **17** were obtained as green compounds in 15% yield and were found to be highly stable. The coordination chemistry of **16** and **17** was performed with $[\text{Rh}(\text{CO})_2\text{Cl}_2]$ in the presence of sodium acetate in CH_2Cl_2 under reflux condition resulted the formation of Rh^{I} complex **18** and **19** in quantitative yield (Scheme 4.6).

4.3.1 Spectral characterisation

4.3.1.1 Mass spectrometric analysis

Mass spectrometric analysis of **16** and **17** & **18** and **19** confirmed the exact composition with a molecular-ion signal at m/z 975.1156 ($M+1$) **16** and 915.1786 ($M+1$) **17** & 1132.9846 (M) **18** and 1073.0502 ($M+1$) **19** respectively (Figures 4.4 – 4.7).

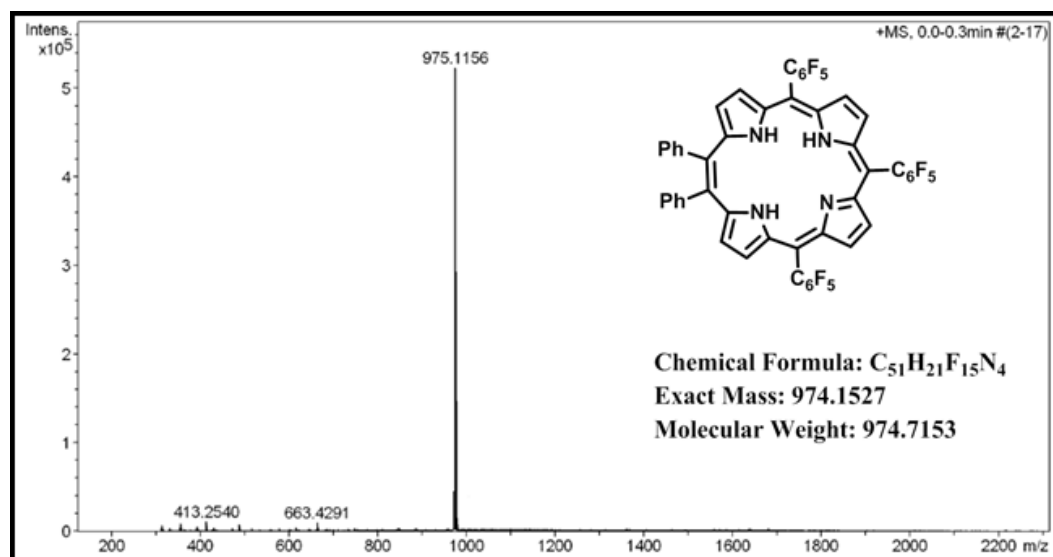


Figure 4.4: ESI-MS spectrum of **16**.

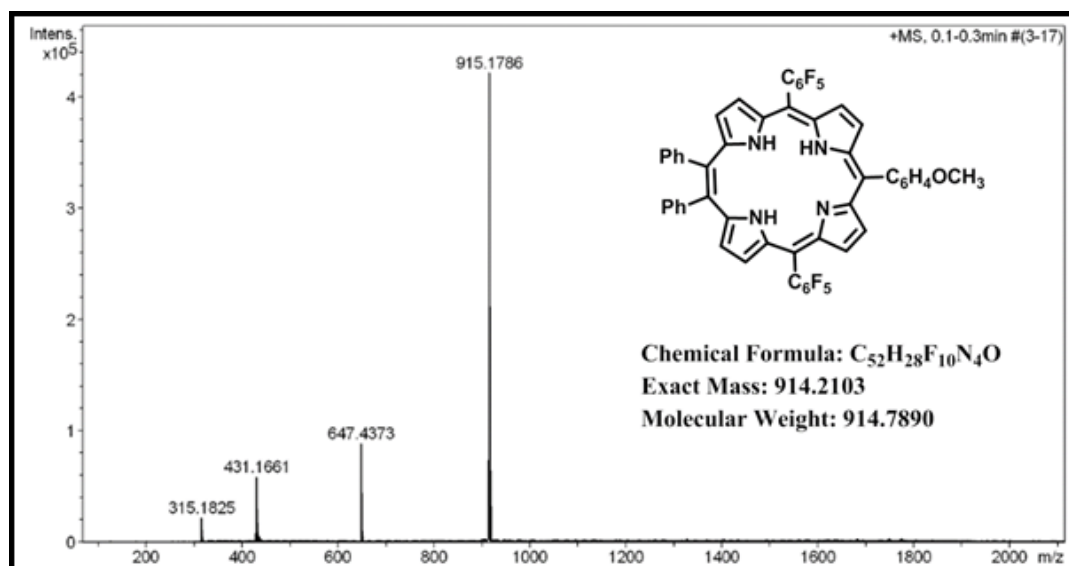


Figure 4.5: ESI-MS spectrum of 17.

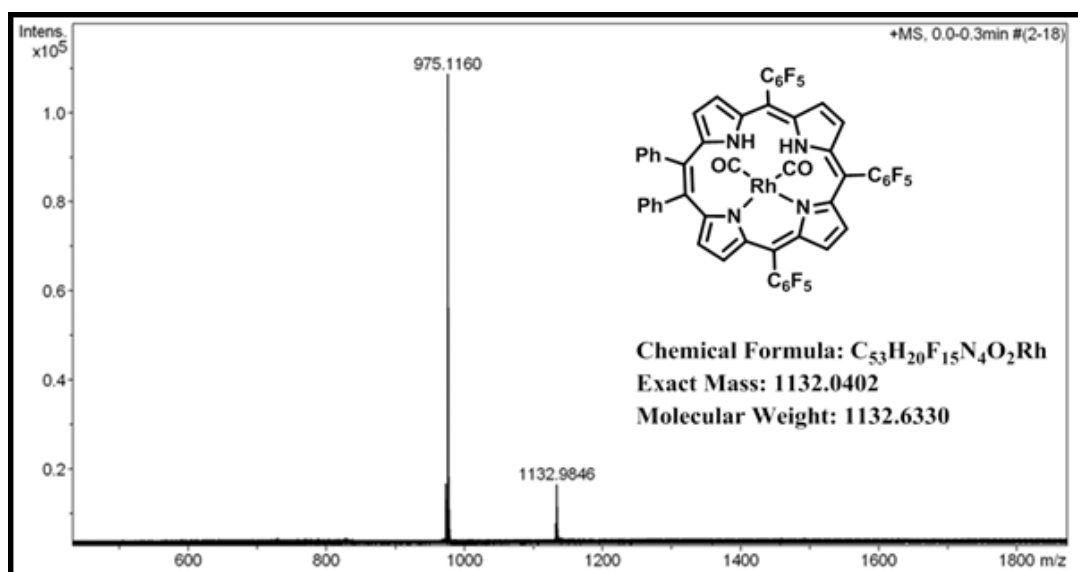


Figure 4.6: ESI-MS spectrum of 18.

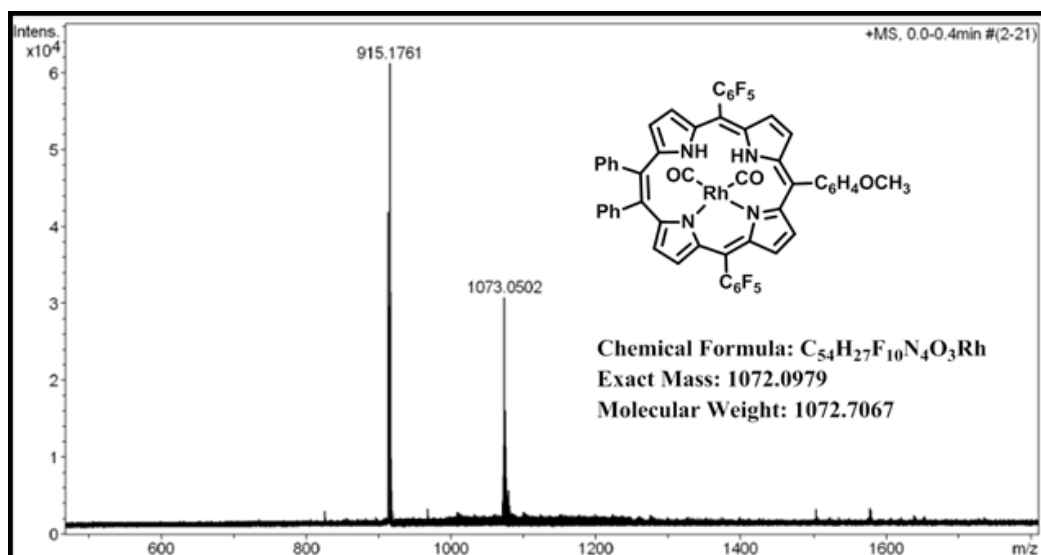


Figure 4.7: ESI-MS spectrum of **19**.

4.3.1.2 NMR Analysis

The ^1H NMR spectrum of **16** in CD_2Cl_2 is shown in Figure 4.8a. At room temperature, the macrocycle **16** exhibits three sets of doublets at 6.43, 6.51, and 6.97 ppm, corresponding to six pyrrolic β -CH hydrogen atoms. The remaining pyrrolic β -CH protons as well as the *meso*-aryl protons resonated between 7.05 and 7.16 ppm. The correlation between the signals at 6.43 and 6.51 ppm revealed that these pyrrole units were linked by a dipyrroethene bridge, and the correlation between the signals at 6.97 and 7.14 ppm revealed that these pyrrole units were linked by dipyrromethene. Owing to rapid tautomerism, one broad signal was observed at 6.25 ppm for the NH hydrogen atoms. To reveal the NH signals, we further performed variable-temperature (VT) ^1H NMR spectroscopy (Figure 4.9). At -20°C , well-resolved NH signals were observed at 6.01 and 6.07 ppm. The pyrrolic β -CH proton signal initially merged with the phenyl proton peaks were separated out and resonated as doublets at 7.16 ppm. The upfield shift of the inner NH signals as compared to those of reported core-modified homoporphyrins^{19,20} clearly suggests that the [20] π homoporphyrin experiences a moderate aromatic character.

After the addition of trifluoroacetic acid (TFA), all the signals for pyrrolic β -CH hydrogen atoms were shifted downfield as compared to the free base and resonated between 6.76 and 7.87 ppm (Figure 4.10). At room temperature, of four NH protons, only two were observed as a broad singlet at 6.45 ppm. The other two NH signals were observed as a sharp singlet at 5.85 ppm. Overall, as observed in the free base, the moderate diatropic ring current was further retained in the protonated state, which suggests the existence of Möbius aromaticity even after protonation.

The insertion of Rh^{I} (**16**) resulted in major changes in the ^1H NMR spectral pattern (Figure 4.8b). Upon coordination, the appearance of two NH signals at 7.43 and 5.34 ppm suggested that the Rh^{I} center coordinated with the ligand in a BODIPY bonding mode, and the β -CH signals of each pyrrole ring resonated as individual peaks between 6.02 and 7.06 ppm, thus reflecting the unsymmetrical nature of the complex. These signals were confirmed by ^1H - ^1H COSY spectral analysis (Figure 4.12). The correlations were found between (i) one of the uncoordinated pyrrolic β -CH protons and the NH proton and the two β -CH protons resonated as triplets at 6.02 and 6.19 ppm, (ii) the pyrrolic β -CH protons correlated with the NH proton and appeared at 6.96 and 7.06 ppm. The Rh^{I} -coordinated pyrrolic β -CH protons were shifted slightly upfield as compared to the free base and appeared between 6.44 and 6.84 ppm. Furthermore, the signal for one of the pyrrolic NH atoms observed at 5.34 ppm at room temperature was shifted upfield upon lowering of the temperature and observed at 4.8 ppm at 193 K (Figure 4.13), thus clearly indicating the Möbius aromatic character of the system even after complexation of the ligand with the Rh^{I} ion.

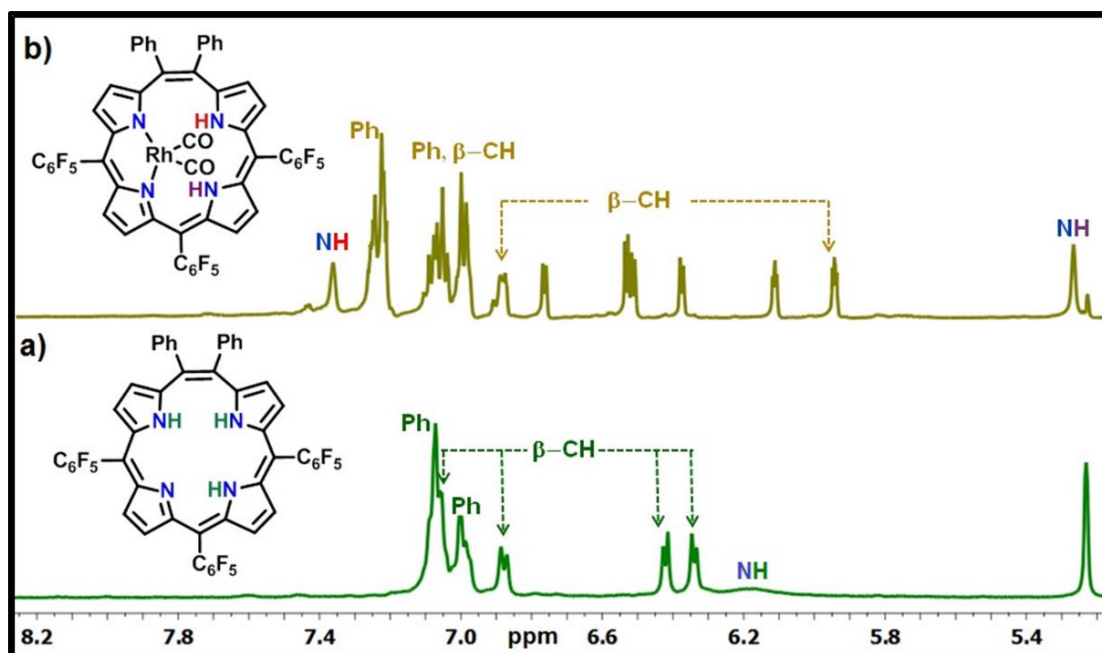


Figure 4.8: ^1H NMR spectra of **16** and **18** in CD_2Cl_2 .

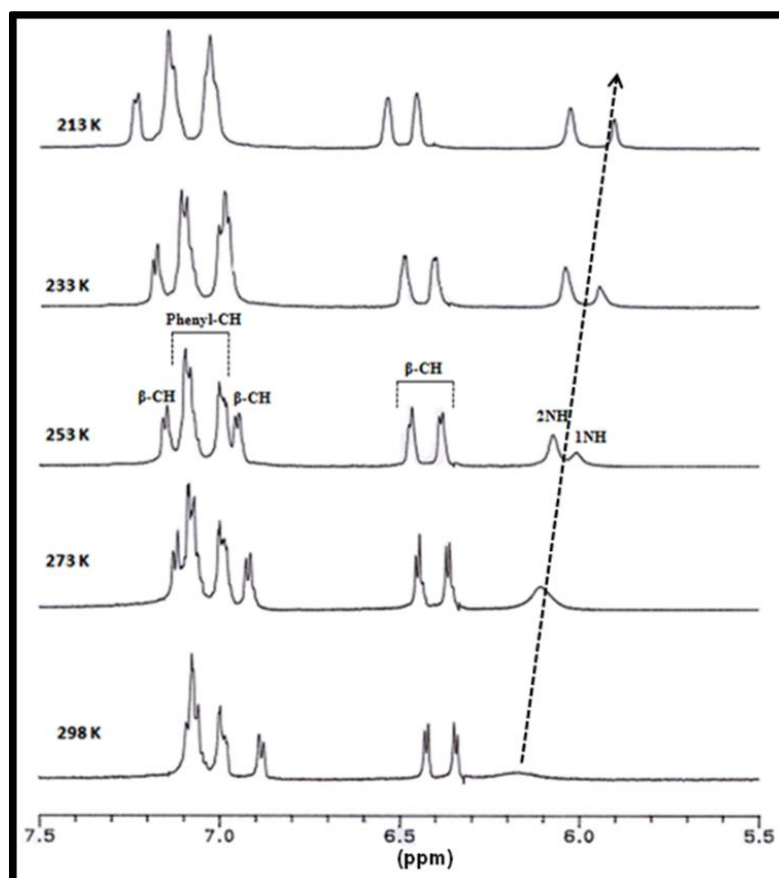


Figure 4.9: Variable temperature ^1H NMR spectrum of **16** in CD_2Cl_2 .

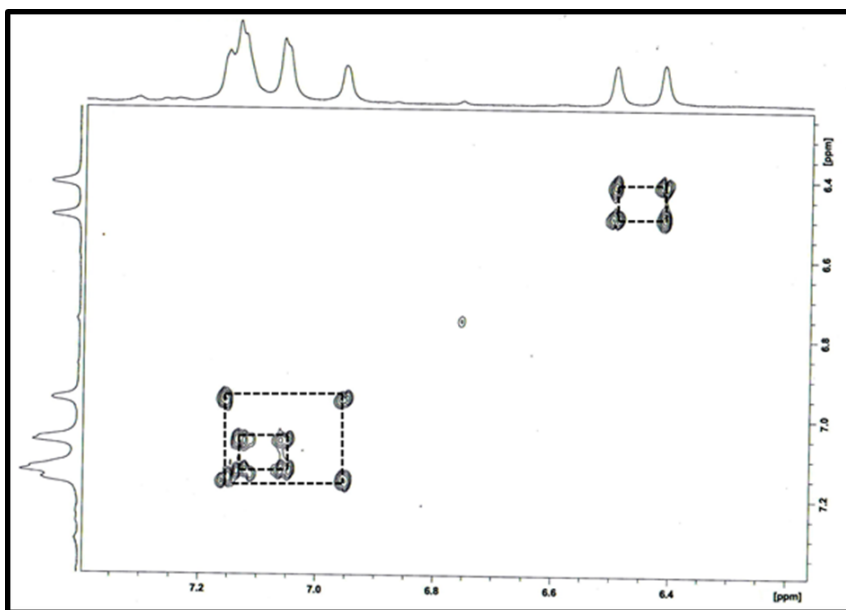


Figure 4.10: $^1\text{H} - ^1\text{H}$ COSY spectrum of **16** in CD_2Cl_2

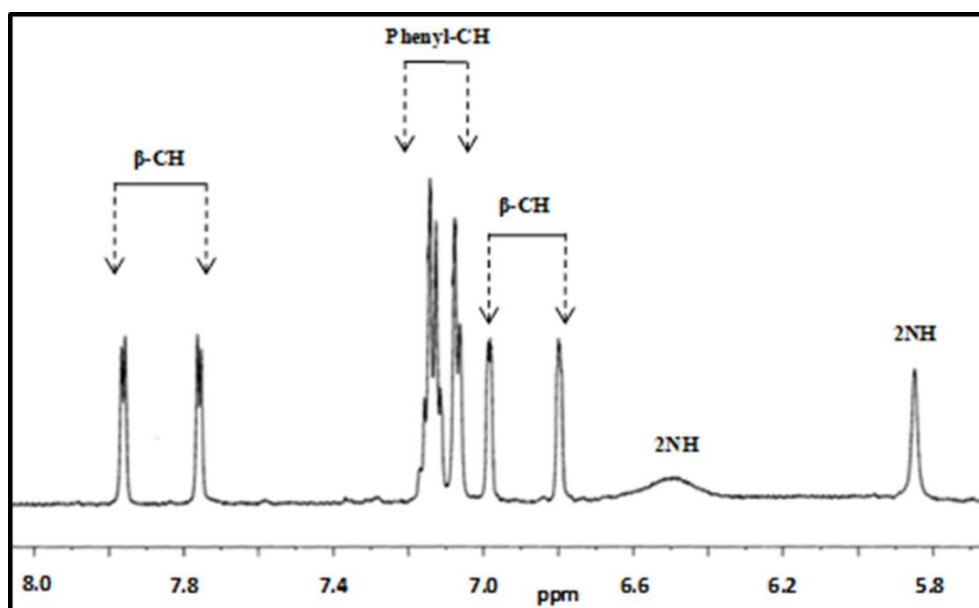


Figure 4.11: ^1H NMR spectrum of **16.H⁺** in CD_2Cl_2 .

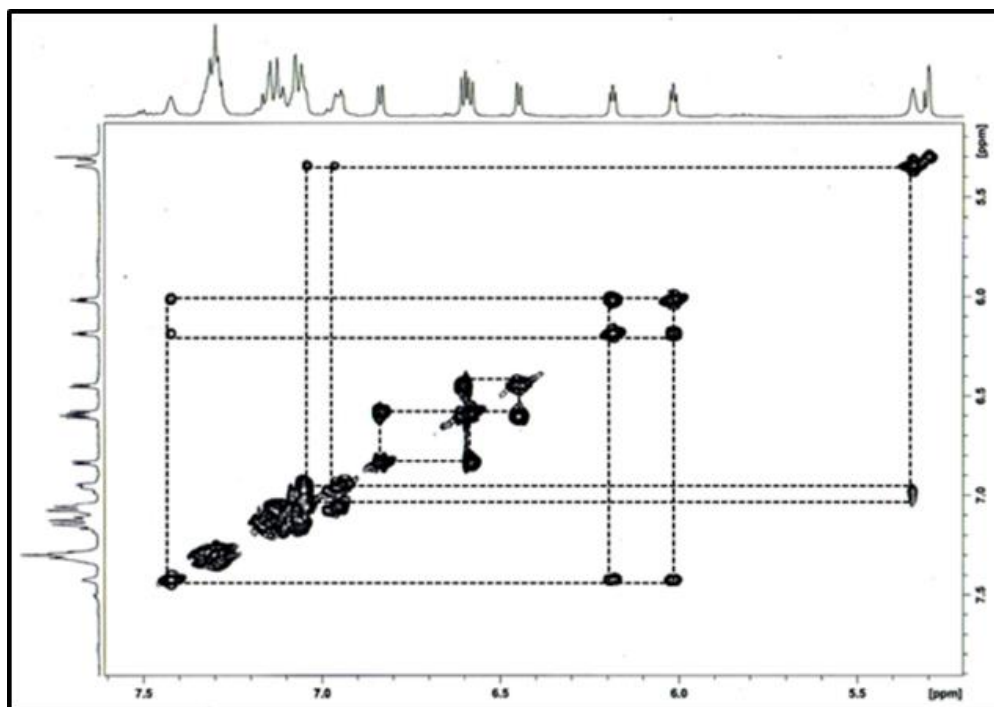


Figure 4.12: $^1\text{H} - ^1\text{H}$ COSY spectra of **18** in CD_2Cl_2 .

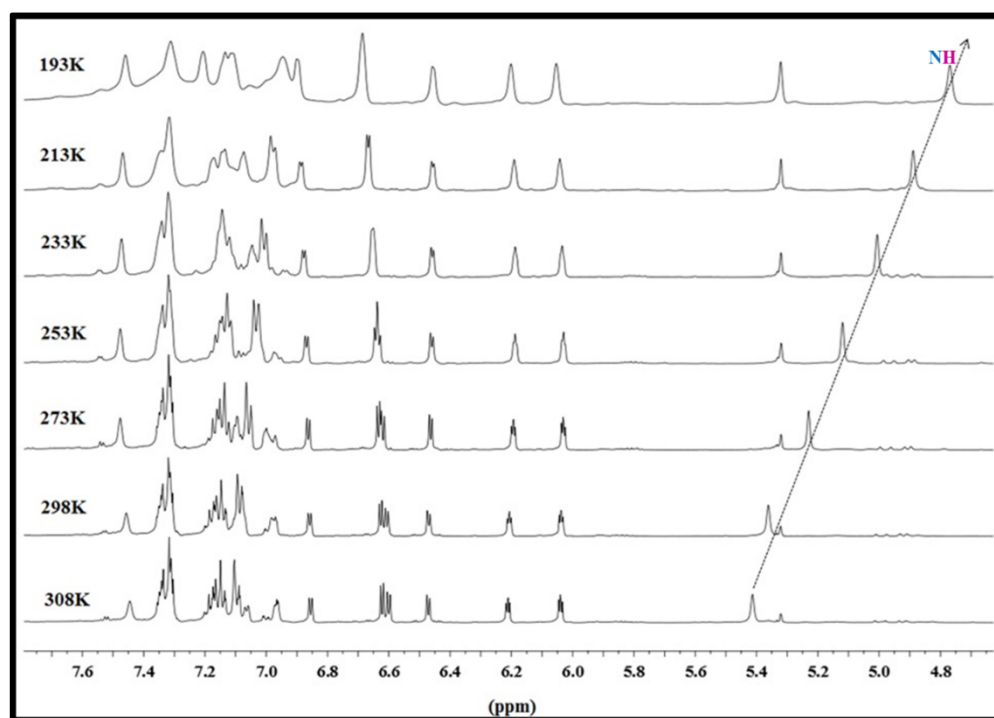


Figure 4.13: Variable temperature ^1H NMR spectroscopy of **18** in CD_2Cl_2 .

4.3.1.3 Single crystal X-ray structure and analysis of **17** & **19**

The explicit structure of homoporphyrin **17** was unambiguously confirmed by single-crystal X-ray diffraction analysis (Figure 4.14a & b and Table 4.2). As observed by NMR analysis, the dipyrroethene and dipyrromethene units are linked by *meso*-aryl bridges, and all pyrrolic nitrogen atoms point inward. Of the four pyrrolic units, three are amino (N1, N3 and N4) and one is imino (N2) in nature. Two amine-like pyrrole units (N1 and N4) are connected through a *meso* phenyl-substituted vinylene and/or ethylene C20-C21 bridge. The structure is substantially distorted from planarity and was found to have a Möbius topology with a 20π electron circuit. The tilt angles of the pyrrole units N1- N4 with respect to the mean plane defined by the 25 inner-core atoms are $42.70(6)^\circ$ [N1], $17.78(5)^\circ$ [N2], $21.12(5)^\circ$ [N3] and $63.69(7)^\circ$ [N4]. The remarkable tilting of the pyrrole rings N1 and N4 is caused by the steric congestion imposed by the *meso*-phenyl-substituted vinylene bridge, which leads to the Möbius conformation with overall π -electron conjugation. Furthermore, the torsion angle at the twisted position (C18-C19-C20-C21) is 72.36° , which is higher than that of Möbius systems reported to date,^{31,32} thus revealing the moderate aromatic behaviour of the $[20]\pi$ system (Table 4.1 and Figure 4.2 a). The single crystal X-ray diffraction analysis also reveals a 1:1 complex of methanol with homoporphyrin **17**. In the solid state, the unprotonated freebase form **17** binds methanol forming an out of plane complex (Figure 4.14 b). There are two intermolecular hydrogen bonding interaction between the amine pyrrole NH (N1) and imine pyrrole N (N2) of **17** with the methanol molecule with the distances and angles for N1-H1A \cdots O2, O2-H2B \cdots N2 are 2.12 \AA , 171.71° and 1.87 \AA , 165.02° respectively. The interactions in **17** involving $N_{\text{pyrrole}}\cdots O_{\text{MeOH}}$ with distance of 2.83 \AA - 2.97 \AA and angle of 165° - 172° .

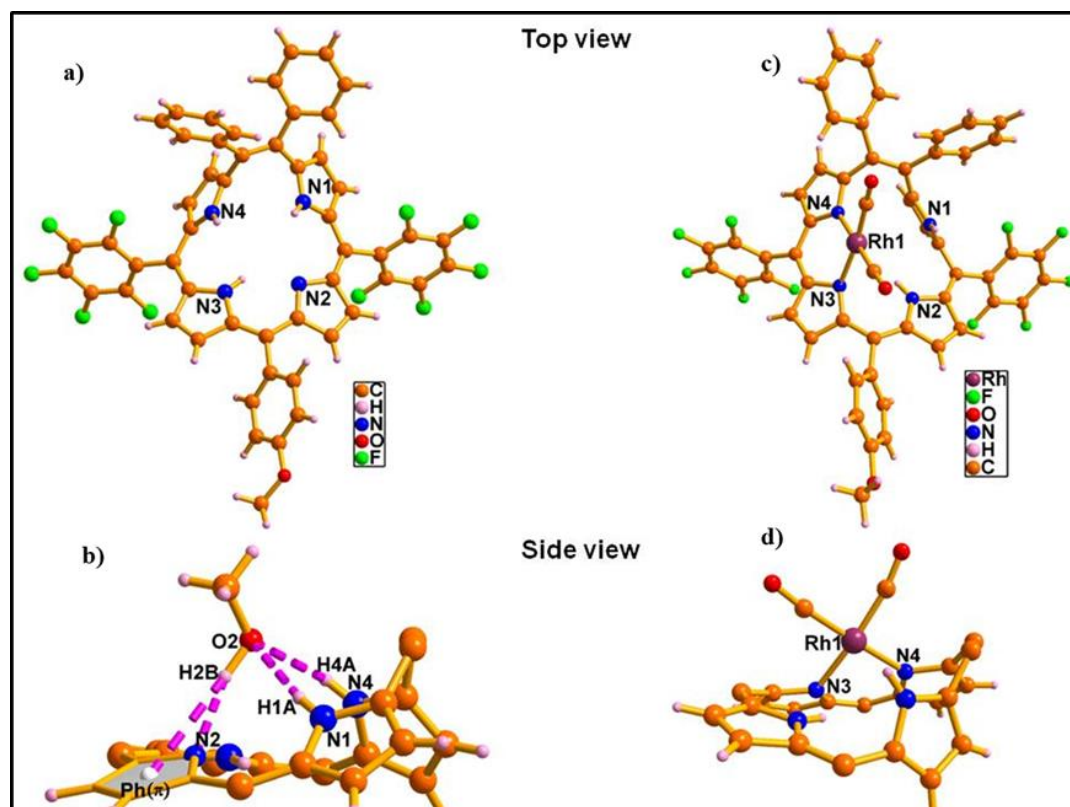


Figure 4.14: Single crystal X-ray structure of **17** and **19**. a) & c) Top view and b) & d) side view. The *meso*-aryl groups in b) and d) and solvent molecule in a) are omitted for clarity.

The insertion of Rh^I (**19**) was confirmed by single-crystal X-ray analysis (Figure 4.14c & d and Table 4.2). The metal ion was coordinated to two of the four pyrrole rings, one from the dipyrroethene unit and another from the dipyrromethene unit. In the twisted Möbius topology of **19** with moderate aromatic character, the pyrrole rings connected to the ethylene bridge (N1 and N4) deviate strongly from the mean plane with tilt angles of 79.48(2)° [N1] and 41.18(2)° [N4] to release the steric strain of the macrocycle, and the torsion angle at C20-C21-C1-C2, found to be 67.6733°, is less than in **17**, thus maintaining the moderate aromatic character of the [20] π system (Table 4.1 and Figure 4.21 b).²³⁻²⁸ Furthermore, the upfield shift of the NMR signal for one of the inner NH atoms was confirmed by the close proximity of the hydrogen atom to the metal center, with a N2-H2 \cdots Rh bond distance and angle of 2.848(1) Å and 128.89(4)°

(Figure 4.22 b). Overall, the variable temperature NMR studies and single crystal analysis proves that both the freebases and the Rh complexes exhibit moderate 20π Möbius aromatic character rather than 20π Hückel antiaromatic character.

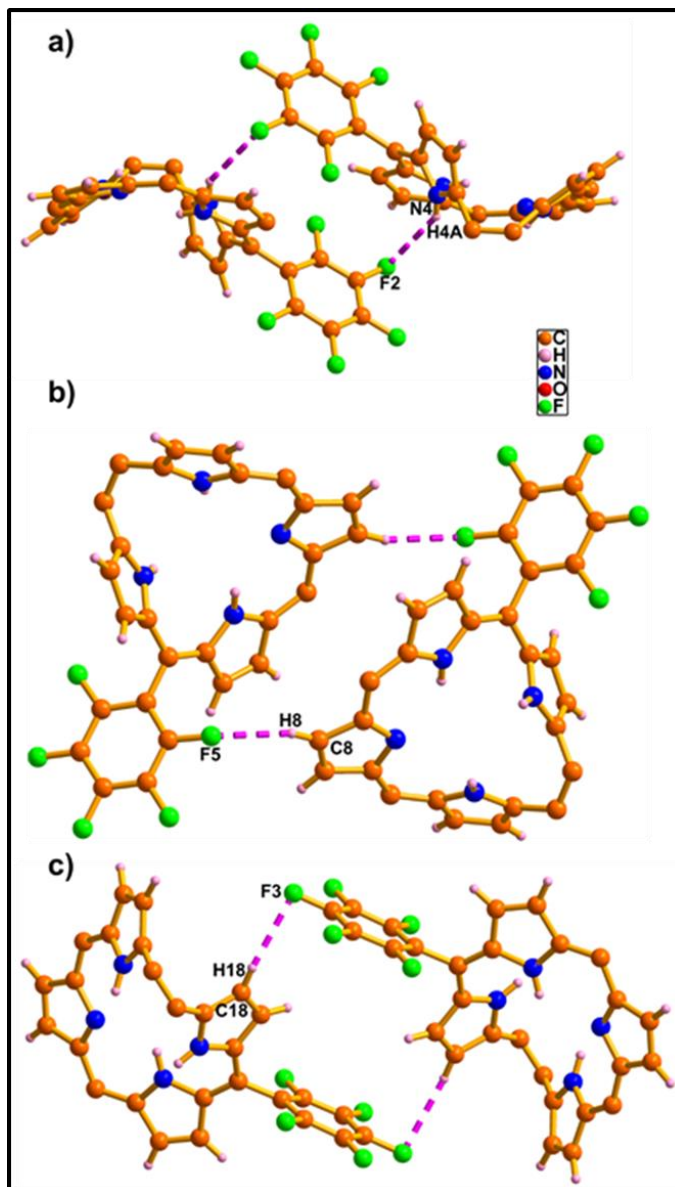


Figure 4.15: Self-assembled dimers of **17**. The bond distances and angles are: a) N4-H4A...F2: 2.878(3) Å & 145.96(3)°; b) C8-H8...F5: 2.469(2) Å & 162.30(1)°; c) C18-H18...F3: 2.641(2) Å & 155.08(2)° respectively.

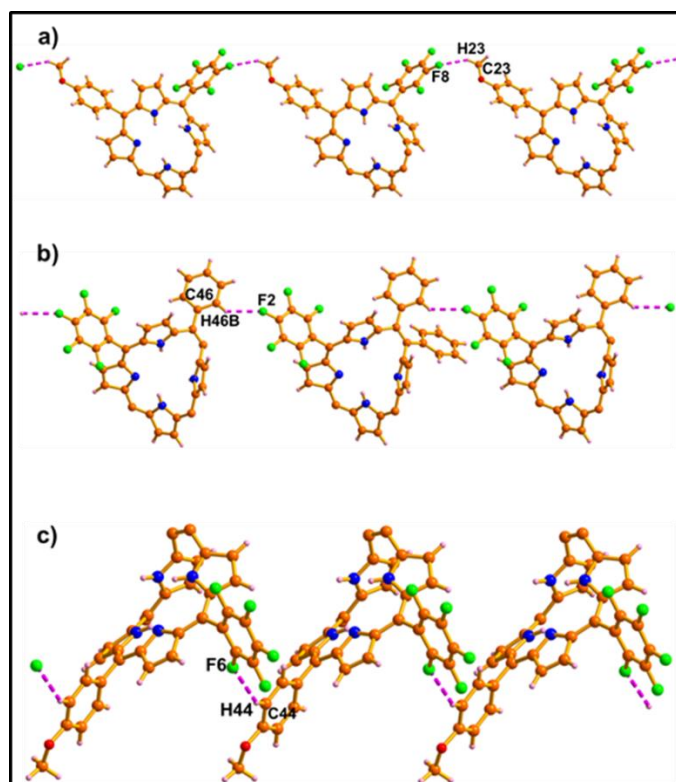


Figure 4.16: 1-D arrays of **17**. The bond distances and angles are: a) C23-H23 \cdots F8: 2.624(2)Å & 139.70(2)°; b) C46-H46B \cdots F2: 2.565(2)Å & 146.19(2)°; c) C44-H44 \cdots F6: 2.634(2)Å & 142.43(1)° respectively.

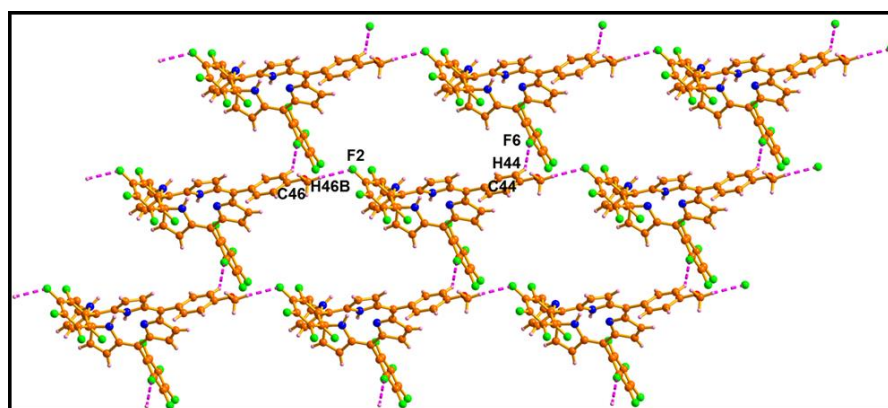


Figure 4.17: 1-D arrays of **17**. The bond distances and angles are: C46-H46B \cdots F2: 2.565(2) Å & 146.19(2)°; c) C44-H44 \cdots F6: 2.634(2) Å & 142.43(1)°.

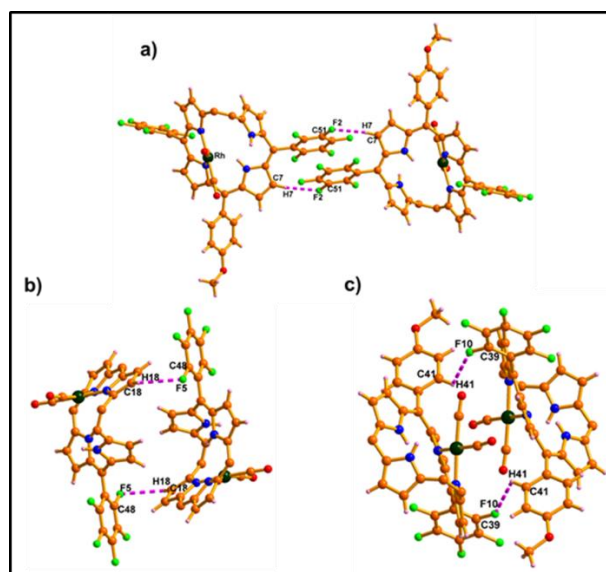


Figure 4.18: self-assembled dimers of **19**. a), b) and c) are self-assembled dimers. The bond distances and angles are: a) C7-H7 \cdots F2: 2.503(5)Å & 166.47(5) $^\circ$; b) C18- H1 \cdots F5 2.806(5)Å & 128.19(4) $^\circ$ and c) C41- H41 \cdots F10: 2.601(4)Å & 107.23(4) $^\circ$ respectively.

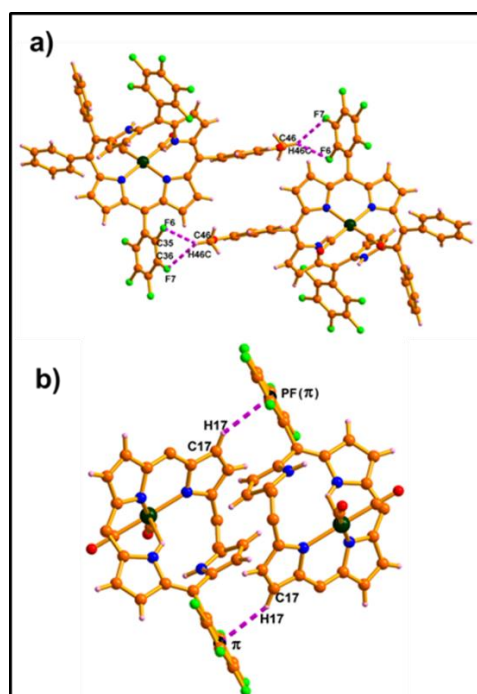


Figure 4.19: Self-assembled dimers of **19**. a) and b) are self-assembled dimers. The bond distances and angles are: a) C46-H46C \cdots F6: 2.741(5)Å & 125.17(6) $^\circ$; C46-

H46C \cdots F7: 2.711(7)Å & 134.02(6)° and b) C17-H17 \cdots PF(π): 2.844(9)Å & 150.66(4)° respectively.

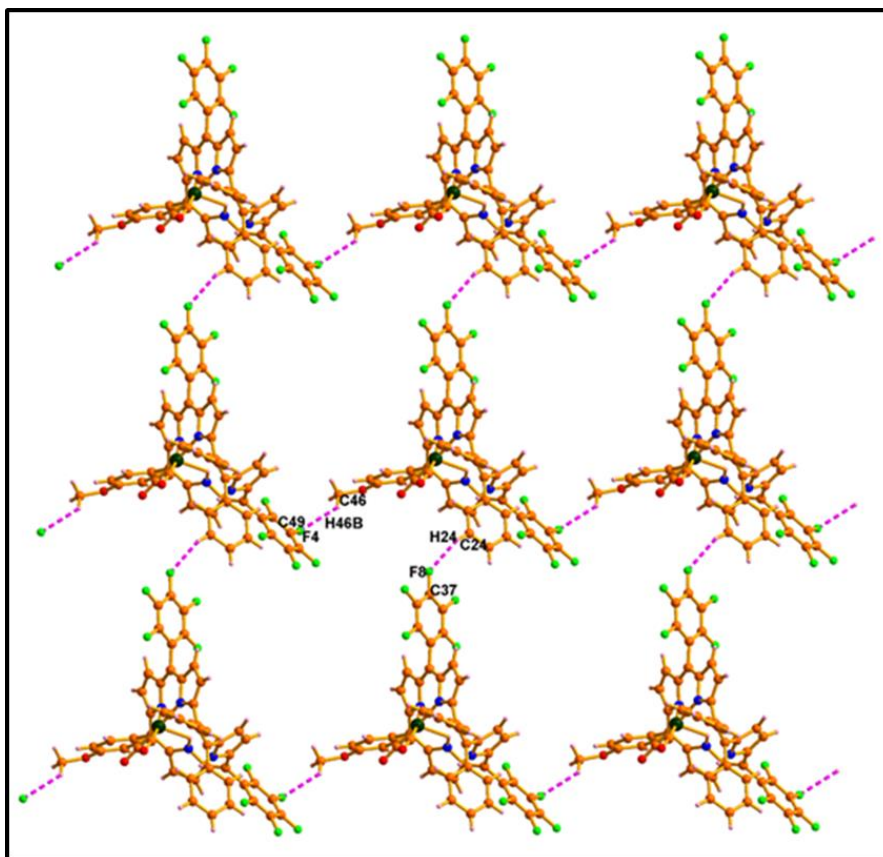


Figure 4.20: 2-D array of **19**. The bond distances and angles are: C46- H46B \cdots F4: 2.696(5)Å & 129.28(6)°; b) C24-H24 \cdots F8: 2.496(6)Å & 154.38(6)°.

Table 4.1: Torsion angles (°) at the twisted position of **17** and **19**:

	17	19
C18-C19-C20-C21	-72.35°	-125.30°
C19-C20-C21-C1	-21.35°	13.96°
C20-C21-C1-C2	136.22°	67.32°

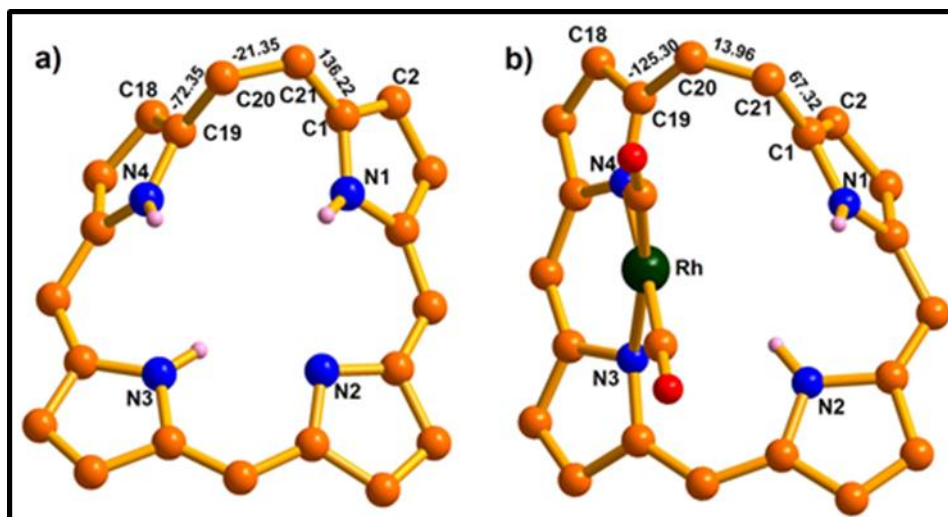


Figure 4.21: Torsion angles at the twisted position (in deg.) in **17** (a) and **19** (b). (*meso* substituents were omitted for clarity).

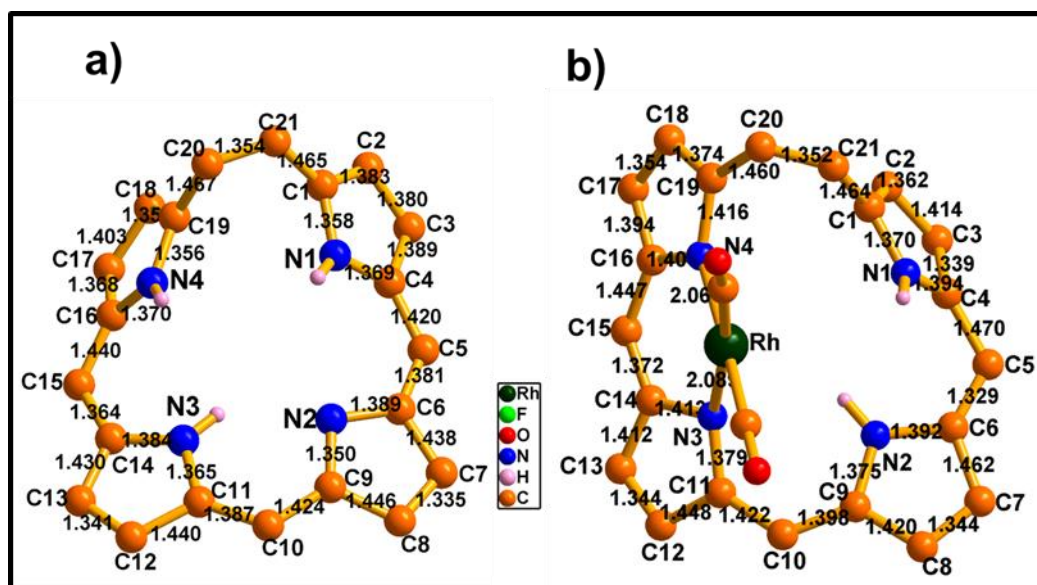


Figure 4.22: Bond lengths in **17** (a) and **19** (b) (Å).

Table 4.2: Crystal data for **17** and **19**

Crystal parameters	17	19
Formula	C ₅₂ H ₂₈ F ₁₀ N ₄ O	C ₅₄ H ₂₇ F ₁₀ N ₄ O ₃ Rh
<i>M</i> /g mol ⁻¹	914.78	1072.70
<i>T</i> /K	293 K	100 K
Crystal dimensions/mm ³	0.3 × 0.25 × 0.2	0.12 × 0.08 × 0.09
Crystal system	triclinic	triclinic
Space group	<i>P</i> -1	<i>P</i> -1
<i>a</i> /Å	9.9591(4)	11.829(2)
<i>b</i> /Å	14.3493(6)	14.780(3)
<i>c</i> /Å	16.3623(7)	15.134(3)
α /°	74.593(2)	88.57(3)
β /°	86.207(2)	75.02(3)
γ /°	85.015(2)	83.42(3)
<i>V</i> /Å ³	2243.46(16)	2539.1(10)
<i>Z</i>	2	2
ρ_{calcd} /mg m ⁻³	1.402	1.403
μ /mm ⁻¹	0.115	0.419
<i>F</i> (000)	968.0	1076.0
Reflns. Collected	49210	29895
Indep.reflns.[<i>R</i> (int)]	10883 [0.0380]	9344 [0.2748]
Max/min transmission	0.977 and 0.926	0.745 and 0.398
Data/restraints/parameters	10883/0/640	9344/0/650
GOF on <i>F</i> ²	1.027	0.917
Final <i>R</i> indices [<i>I</i> > 2 σ (<i>I</i>)]	<i>R</i> 1 = 0.0539, w <i>R</i> 2 = 0.1529	<i>R</i> 1 = 0.0854, w <i>R</i> 2 = 0.1942
<i>R</i> indices (all data)	<i>R</i> 1 = 0.0902, w <i>R</i> 2 = 0.1862	<i>R</i> 1 = 0.1719, w <i>R</i> 2 = 0.2271
Largest diff peak and hole [e Å ⁻³]	0.66 and -0.24	1.32 and -1.29

The crystals have been deposited in the Cambridge Crystallographic Data Centre with reference no. CCDC 1565611, CCDC 1501407. The highly disordered solvent molecules in **17** were removed by the SQUEEZE routine using the PLATON program to proceed to the final refinement of the main structure.³³

4.3.1.4 Electronic spectral analysis

The electronic absorption spectra of **16**, protonated derivative **16.H⁺** and Rh^I complexes **18** were recorded in CH₂Cl₂ (Figures 4.23). For example, the macrocycle **16**

showed broad absorption bands from 366 to 442 nm and a prominent Q-like band at 683 nm. Upon protonation of **16** with TFA, the broad bands were split into two well-defined bands at 407 and 499 nm, whereas the Q-like band was red-shifted by 84 nm and observed at 767 nm. On the other hand, the Rh^I complex **18** displayed a Soret-like band at 416 nm along with a shoulder at 470 nm and the lower-energy band was red-shifted by 59 nm in comparison to **16** and appeared at 742 nm. The molar extinction coefficients of these molecules were found to be in the order of 10⁵, thus suggesting their aromatic behavior and Möbius aromaticity instead of Hückel antiaromatic character.

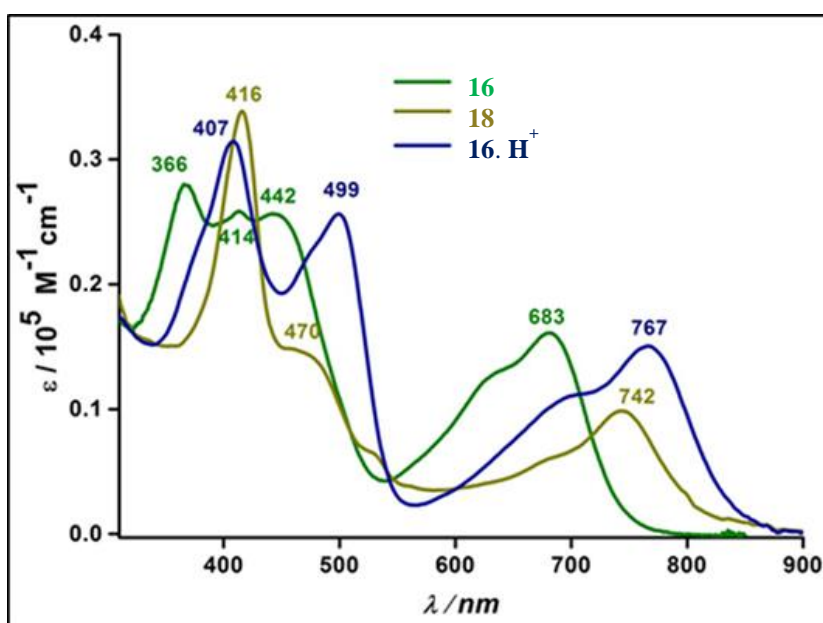


Figure 4.23: Electronic absorption spectra of **16**, **16.H⁺** and **18** in CH₂Cl₂.

4.3.1.5 Theoretical calculation

The molecular systems **16**, **17**, **16.H⁺**, **17.H⁺**, **18** and **19** were optimized at the B3LYP/DGDZVP level of density functional theory.³⁴ For evaluation of the degree of aromaticity, NICS(0), HOMA, and BLA calculations and AICD plots were considered as the best index.³⁵ The NICS(0) and HOMA values of **16** and **18** are shown in Figure

4.24 and the NICS(0), HOMA and BLA values of **16-19** are listed in Table 4.3. The NICS(0) values found are between -6.30 and -9.16 ppm; the HOMA values are 0.53 and 0.68 and the BLA values are between 0.081 and 0.104 Å (Table 4.3 and Figure 4.26). All these values are comparable with those previously reported for antiaromatic molecules with Möbius aromatic character.²³⁻²⁸ The clockwise current density from the AICD plots further supports the diatropic ring current and aromaticity (Figure 4.25). In particular, a higher degree of aromaticity in **16.H⁺** as compared to **16** and **18** was reflected by the moderate increase in diatropic ring current indicated by NMR analysis, the lower torsion angles of the optimized geometry (Table 4.4), and high negative NICS(0) values. Overall, the Möbius aromatic character was further corroborated by the theoretical studies.

Table 4.3. NICS(0) (ppm), HOMA and BLA (Å) values of **16**, **17**, **16.H⁺**, **17.H⁺**, **18** and **19**

Calculation	16	17	16.H⁺	17.H⁺	18	19
NICS(0)	-6.30	-6.80	-9.16	-9.08	-6.53	-6.90
HOMA	0.62	0.63	0.68	0.65	0.58	0.53
BLA	0.102	0.099	0.084	0.081	0.104	0.102

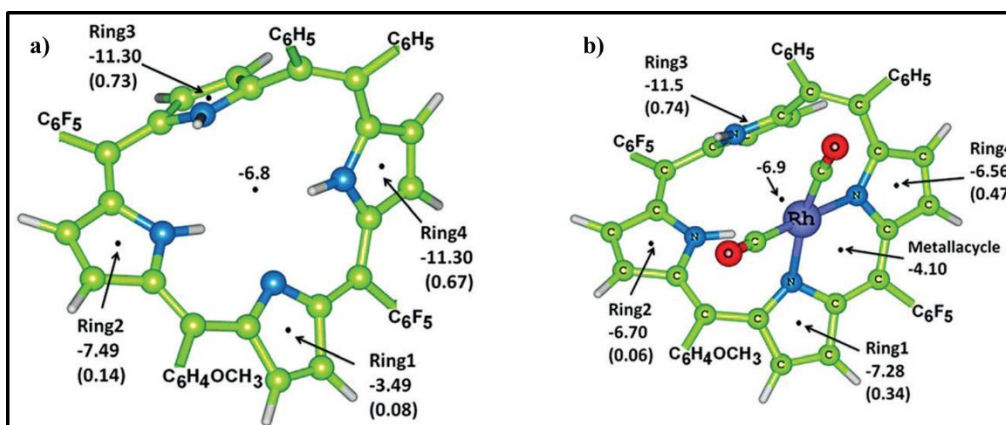


Figure 4.24: Optimized geometry (B3LYP/DGDZVP level) of a) **16** and b) **18** with NICS(0) and HOMA values (in parentheses).

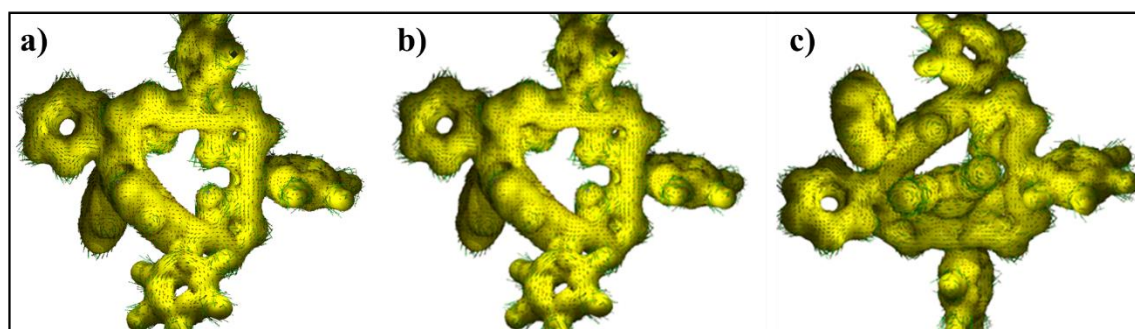


Figure 4.25: a), b) and c) are AICD Plots of **16** (a), **16.H⁺** (b) and **18** (c) at isosurface value 0.015 calculated at B3LYP/DGDZVP level of DFT.

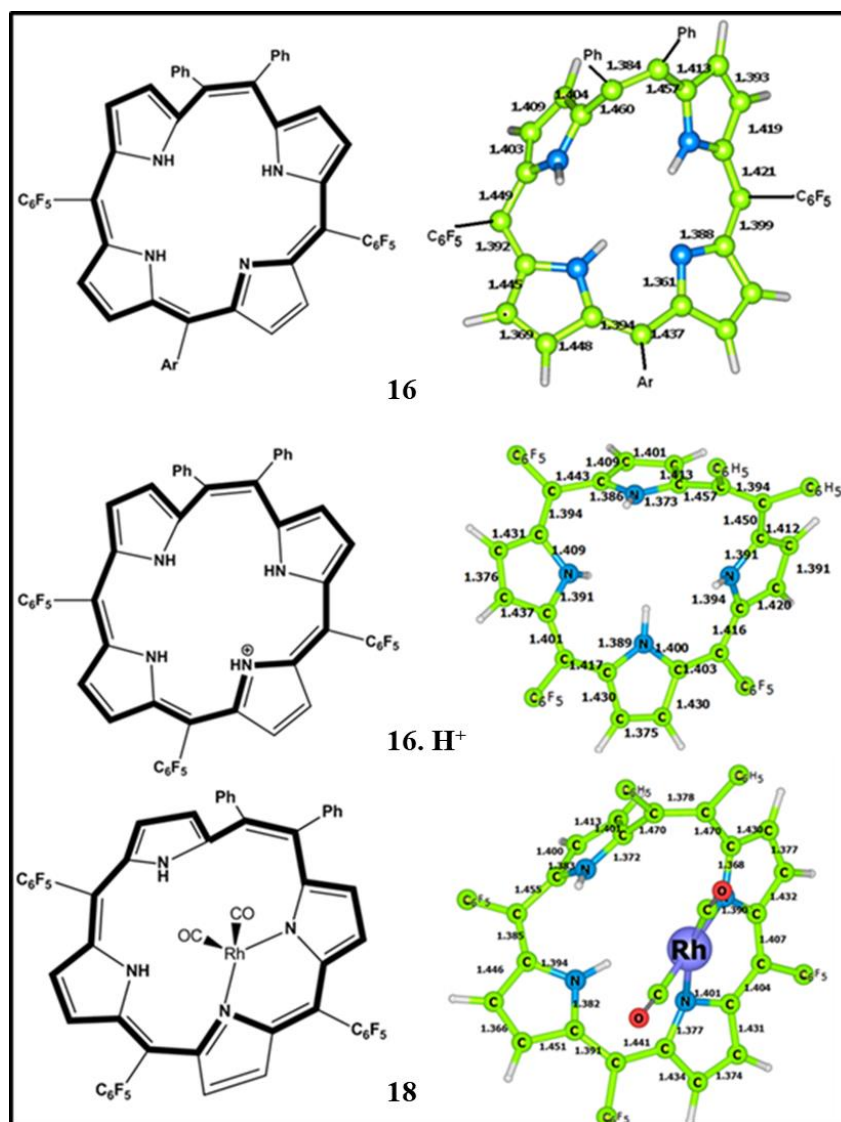


Figure 4.26: Bond length data in Å for **16**, **16.H⁺** and **18** at B3LYP/DGDZVP level.

Table 4.4: Torsion angles at the twisted position of **16-19** obtained from optimized structure:

	16	17	16.H⁺	17.H⁺	18	19
C18-C19-C20-C21	-53.16°	-52.59°	-49.41°	-48.82°	-133.27°	-133.27°
C19-C20-C21-C1	-26.84°	-27.11°	-32.13°	-32.87°	20.72°	21.18°
C20-C21-C1-C2	147.86°	148.41°	145.69°	146.88°	61.27°	60.51°

4.4 Conclusion

In summary, we have successfully isolated a stable *meso*-aryl [20] π tetraphyrin(2.1.1.1): a system reported to be unstable until now. Thus, we have described the simplest expanded porphyrin, a missing link in the rich area of expanded porphyrinoids, for the first time. The present study demonstrated the smallest Möbius aromatic character of [20] π homoporphyrins in three different forms: neutral, protonated, and as Rh^{I} ion complexes. The Möbius aromaticity was unambiguously supported by spectral studies and theoretical calculations and finally confirmed by crystal analysis.

4.5 Experimental Section

4.5.1 General Information

The reagents and materials for the synthesis were used as obtained from Sigma – Aldrich chemical suppliers. All solvents were purified and dried by standard methods prior to use. NMR solvents were used as received. The NMR spectra were recorded with Bruker 400 MHz or 500 MHz with TMS as internal standard. ESI mass spectra were recorded on Bruker, micro-TOF-QII mass spectrometer. Electronic absorption spectra was recorded on Perkin Elmer - Lambda 25 UV-Visible spectrophotometer. X-ray quality crystals for the compounds were grown by the slow diffusion of *n*-hexane over CH_3OH in **17** and *n*-hexane over CH_2Cl_2 in **19**. Single-crystal X-ray diffraction data of **17** and **19** were collected on a Bruker KAPPA APEX-II, four angle rotation system, Mo- $\text{K}\alpha$ radiation (0.71073 Å). Geometry optimization of **16-19** were done at the B3LYP level of density functional theory³⁴ using the DGDZVP basis set (double- ζ valence plus polarization). All structures were verified as energy minima using

frequency calculation. For all the calculations, Gaussian09 suites of programs were used.

4.5.2 Synthetic procedure and spectral characterization

4.5.2.1 Synthesis of 16: To a 250 ml round bottom flask containing *meso*-5,6-diphenyldipyrroethane (**20**) (0.2 g, 0.64 mmol) and 1,9-bis(pentafluorophenylhydroxymethyl)-5-(pentafluorophenyl)-dipyrromethane (**21**) (0.45 g, 0.64 mmol) was added in 150 ml of dry CH₂Cl₂ and stirred for 15 min under N₂ atmosphere with light protection. *p*-Toluenesulfonic acid (*p*-TSA) (0.024 g, 0.128 mmol) was added and the mixture was allowed to stir for 1 h. To the reaction mixture, 2,3-dichloro-5,6-dicyano-*p*-benzoquinone (DDQ) (0.44 g, 1.92 mmol) was added and allowed to stir for further 1 h at room temperature. The entire reaction mixture was filtered through a pad of alumina and eluted with CH₂Cl₂ until the eluent was no longer dark. The resulting crude mixture was concentrated by rotary evaporator to give a dark solid. The crude solid was purified by silica gel column chromatography (100-200 mesh). The green fraction eluted with 15% CH₂Cl₂/*n*-hexane and identified as homoporphyrin **16** in 15% yield.

¹H NMR (400 MHz, CDCl₃, 298 K): δ = 7.16 (s, 5H), 7.14 (m, 2H), 7.11 - 7.05 (m, 5H), 6.97 (d, *J* = 4.9 Hz, 2H), 6.51 (d, *J* = 3.9 Hz, 2H), 6.43 (d, *J* = 3.9 Hz, 2H), 6.28 (brs, 2H).

UV-Vis (CH₂Cl₂): $\lambda_{\max/\text{nm}}$ ($\epsilon/\text{M}^{-1}\text{cm}^{-1}$) = 366 (2.79×10^4), 414 (2.58×10^4), 442 (2.56×10^4), 683 (1.61×10^4).

ESI-MS: *m/z* calculated for C₅₁H₂₁F₁₅N₄ = 974.1527; found = 975.1156 (M+1).

4.5.2.2 Spectral data for 16.H⁺: ¹H NMR (400 MHz, CD₂Cl₂, 298K): $\delta = 7.87$ (d, $J = 4.5$ Hz, 2H), 7.67 (d, $J = 4.5$ Hz, 2H), 7.16 - 7.07 (m, 10H), 6.92 (t, $J = 3$ Hz, 2H), 6.76 (t, $J = 3$ Hz, 2H), 6.45 (brs, 2H).

UV-Vis (CH₂Cl₂): $\lambda_{\max/\text{nm}}$ ($\epsilon/\text{M}^{-1}\text{cm}^{-1}$) = 407 (3.13×10^4), 499 (2.55×10^4), 767 (1.50×10^4).

4.5.2.3 Synthesis of 17: The above procedure was followed by using 5,6-diphenyldipyrroethane (**20**) (0.30 g, 0.96 mmol), 1,9-bis(pentafluorophenylhydroxymethyl)-5-(4-methoxyphenyl)-dipyrromethane (**22**) (0.62 g, 0.96 mmol), *p*-TSA (0.036 g, 0.192 mmol) and DDQ (0.65 g, 2.88 mmol). The green fraction was eluted with 25% CH₂Cl₂/*n*-hexane and identified as **17** in 15% yield.

¹H NMR (400 MHz, CDCl₃, 298 K): $\delta = 7.43$ (d, $J = 8.5$ Hz, 2H), 7.13 - 7.10 (m, 8H), 7.07 - 7.04 (m, 6H), 7.00 (d, $J = 8.7$ Hz, 2H), 6.45 (d, $J = 4.0$ Hz, 2H), 6.37 (d, $J = 4.0$ Hz, 2H), 3.87 (s, 3H).

UV-Vis (CH₂Cl₂): $\lambda_{\max/\text{nm}}$ ($\epsilon/\text{M}^{-1}\text{cm}^{-1}$) = 369 (3.65×10^4), 418 (3.67×10^4), 453 (3.51×10^4), 693 (2.07×10^4).

ESI-MS: m/z calculated for C₅₂H₂₈F₁₀N₄O = 914.2103; found = 915.1786 (M+1).

4.5.2.4 Spectral data for 17.H⁺: ¹H NMR (700 MHz, CD₂Cl₂): $\delta = 7.76$ (d, $J = 4.3$ Hz, 2H), 7.62 (s, 4H), 7.19 (m, 4H), 7.10 (m, 4H), 7.02 (m, 2H), 6.97 (m, 1H), 6.87 (s, 1H), 6.75 (d, $J = 3.6$ Hz, 2H), 6.67 (s, 2H), 3.90 (s, 3H).

UV-Vis (CH₂Cl₂): $\lambda_{\max/\text{nm}}$ ($\epsilon/\text{M}^{-1}\text{cm}^{-1}$) = 384 (3.22×10^4), 414 (3.36×10^4), 495 (2.86×10^4), 782 (2.12×10^4).

4.5.2.5 Synthesis of 18: To a solution of **16** (0.02 g, 0.02 mmol) in 20 ml of CH₂Cl₂, anhydrous sodium acetate (0.017 g, 0.2 mmol) was added followed by [Rh(CO)₂Cl]₂ (0.016 g, 0.04 mmol). The reaction was heated under reflux for 12 h. The resulting crude mixture was concentrated by rotary evaporator to give a dark solid. The crude

solid was purified by silica gel column chromatography (100 - 200 mesh). The green fraction eluted with 10% CH₂Cl₂/*n*-hexane and identified as the rhodium complex **18** in quantitative yield.

¹H NMR (400 MHz, CD₂Cl₂, 298 K): δ = 7.43 (s, 1H), 7.29 (t, *J* = 4.6 Hz, 4H), 7.15 - 7.12 (m, 3H), 7.09 - 7.04 (m, 4H), 6.96 - 6.94 (m, 1H), 6.84 (d, *J* = 4.5 Hz, 1H), 6.59 (dd, *J* = 8.1, 4.5 Hz, 2H), 6.45 (d, *J* = 4.4 Hz, 1H), 6.19 (t, *J* = 3.0 Hz, 1H), 6.02 (t, *J* = 3.0 Hz, 1H), 5.34 (s, 1H).

ESI-MS: *m/z* calculated for C₅₃H₂₀F₁₅N₄O₂Rh = 1132.0402; found = 1132.9846 (M).

UV-Vis (CH₂Cl₂): λ_{max}(nm) (ε[M⁻¹cm⁻¹]) = 416 (3.38 × 10⁴), 470 (1.45 × 10⁴), 742 (0.99 × 10⁴).

4.5.2.6 Synthesis of 19: The above procedure was followed by using **19** (0.02 g, 0.022 mmol), [Rh(CO)₂Cl]₂ (0.017 g, 0.044 mmol) and anhydrous sodium acetate (0.018 g, 0.22 mmol). The green fraction eluted with 20% CH₂Cl₂/*n*-hexane and identified as **19** in 50% yield.

¹H NMR (500 MHz, CD₂Cl₂, 298 K): δ = 7.51 (d, *J* = 8.5 Hz, 2H), 7.36 - 7.28 (m, 7H), 7.16 - 7.04 (m, 5H), 7.02 - 7.00 (m, 3H), 6.78 (d, *J* = 4.5 Hz, 1H), 6.63 - 6.61 (m, 2H), 6.43 (d, *J* = 4.5 Hz, 1H), 6.16 (t, *J* = 3 Hz, 1H), 5.99 (t, *J* = 3 Hz, 1H), 5.09 (brs, 1H), 3.88 (s, 3H).

ESI-MS: *m/z* calculated for C₅₄H₂₇F₁₀N₄O₃Rh = 1072.0979; found = 1073.0502 (M+1).

UV-Vis (CH₂Cl₂): λ_{max}(nm) (ε[M⁻¹cm⁻¹]) = 423 (2.85 × 10⁴), 477 (2.17 × 10⁴), 774 (1.7 × 10⁴).

4.6 References

1. T. Tanaka, A. Osuka, *Chem. Rev.* **2017**, *117*, 2584-2640.

-
2. Y. M. Sung, J. Oh, W.-Y. Cha, W. Kim, J. M. Lim, M.-C. Yoon, D. Kim, *Chem. Rev.* **2017**, *117*, 2257-2312.
 3. Y. Ding, W.-H. Zhu, Y. Xie, *Chem. Rev.* **2017**, *117*, 2203-2256.
 4. S. Saito, A. Osuka, *Angew. Chem. Int. Ed.* **2011**, *50*, 4342-4373.
 5. R. B. Woodward, Aromaticity Conference, Sheffield, UK, 1966.
 6. J.-I. Setsune, S. Maeda, *J. Am. Chem. Soc.* **2000**, *122*, 12405-12408.
 7. A. Jasat, D. Dolphin, *Chem. Rev.* **1997**, *97*, 2267-2287.
 8. J. L. Sessler, D. Seidel, *Angew. Chem. Int. Ed.* **2003**, *42*, 5134-5175.
 9. H. J. Callot, E. Schaeffer, *J. Org. Chem.* **1977**, *42*, 1567-1570.
 10. H. J. Callot, T. Tschamber, *Tetrahedron Lett.* **1974**, *15*, 3155-3158.
 11. H. J. Callot, T. Tschamber, *J. Am. Chem. Soc.* **1975**, *97*, 6175-6178.
 12. R. Grigg, *J. Chem. Commun.* **1967**, 1238-1239.
 13. R. Grigg, *J. Chem. Soc. C* **1971**, 3664-3668.
 14. B. Chevrier, R. Weiss, *J. Chem. Soc., Chem. Commun.* **1974**, 884-885.
 15. B. Chevrier, R. Weiss, *J. Am. Chem. Soc.* **1975**, *97*, 1416-1421.
 16. H. J. Callot, T. Tschamber, E. Schaeffer, *Tetrahedron Lett.* **1975**, *16*, 2919-2922.
 17. H. J. Callot, *Dalton Trans.* **2008**, 6346-6357.
 18. B. Chevrier, R. Weiss, *Inorg. Chem.* **1976**, *15*, 770-774.
 19. a) E. Ganapathi, W.-Z. Lee, M. Ravikanth, *J. Org. Chem.* **2014**, *79*, 9603-9612.
b) E. Ganapathi, S. Kuilya, T. Chatterjee, M. Ravikanth, *Eur. J. Org. Chem.* **2016**, 282-290.
 20. B. Adinarayana, M. Das, C. H. Suresh, A. Srinivasan, *Chem. Eur. J.* **2019**, *25*, 4683-4687.
 21. E. Heilbronner, *Tetrahedron Lett.* **1964**, *29*, 1923-1928.
-

-
22. M. Stępień, L. Latos-Grażyński, N. Sprutta, P. Chwalisz, L. Szterenberga, *Angew. Chem. Int. Ed.* **2007**, *46*, 7869-7873.
 23. J. Sankar, S. Mori, S. Saito, H. Rath, M. Suzuki, Y. Inokuma, H. Shinokubo, K. S. Kim, Z. S. Yoon, J.-Y. Shin, J. M. Lim, Y. Matsuzaki, O. Matsushita, A. Muranaka, N. Kobayashi, D. Kim, A. Osuka, *J. Am. Chem. Soc.* **2008**, *130*, 13568-13570.
 24. T. Higashino, B. S. Lee, J. M. Lim, D. Kim, A. Osuka, *Angew. Chem. Int. Ed.* **2012**, *51*, 13105-13109.
 25. T. Higashino, T. Soya, W. Kim, D. Kim, A. Osuka, *Angew. Chem. Int. Ed.* **2015**, *54*, 5456-5460.
 26. J. M. Lim, J.-Y. Shin, Y. Tanaka, S. Saito, A. Osuka, D. Kim, *J. Am. Chem. Soc.* **2010**, *132*, 3105-3108.
 27. M. Inoue, A. Osuka, *Angew. Chem. Int. Ed.* **2010**, *49*, 9488-9491.
 28. J. K. Park, Z. S. Yoon, M.-C. Yoon, K. S. Kim, S. Mori, J.-Y. Shin, A. Osuka, D. Kim, *J. Am. Chem. Soc.* **2008**, *130*, 1824-1827.
 29. A. Mallick, H. Rath, *Chem. Asian J.* **2016**, *11*, 986-991.
 30. K. S. Anju, S. Ramakrishnan, A. P. Thomas, E. Suresh, A. Srinivasan, *Org. Lett.* **2008**, *10*, 5545-5549.
 31. M. Stępień, N. Sprutta, L. Latos-Grażyński, *Angew. Chem. Int. Ed.* **2011**, *50*, 4288-4292.
 32. A. Osuka, S. Saito, *Chem. Commun.* **2011**, *47*, 4330-4332.
 33. A. Spek, *Acta Crystallogr.* **2015**, *C71*, 9-18.
 34. C. Lee, W. Yang, R. G. Parr, *Phys. Rev. B* **1988**, *37*, 785-795.
 35. P. von R. Schleyer, C. Maerker, A. Dransfeld, H. Jiao, N. J. R. van Eikema Hommes, *J. Am. Chem. Soc.* **1996**, *118*, 6317-6320.

CHAPTER 5

Isosmaragdyrin(1.1.1.0.0) with a N_3C_2 Core: A Bimodular Ligand Stabilizing Rh^I and Organo- Pt^{II} Complexes

5.1	Introduction	120	
5.2	Objective of our work	127	
5.3	Results and discussions	128	
	5.3.1	Synthesis	128
	5.3.2	Spectral characterisation	129
	5.3.2.1	Mass spectrometric analysis	129
	5.3.2.2	NMR Analysis	130
	5.3.2.3	Single crystal X-ray analysis 38, 39 and 40	133
	5.3.2.4	Electronic absorption and Emission analyses	143
	5.3.2.5	Electrochemical properties	146
5.4	Conclusion	147	
5.5	Experimental Section	148	
	5.5.1	General Information	148
	5.5.2	Synthetic procedure and spectral characterization of 38-41	148
5.6	References	152	

5.1 Introduction

In the previous chapter, we have already discussed about the expanded porphyrin and its applications. The present chapter mainly focuses on expanded porphyrins with five pyrrole / heterocyclic rings in the macrocyclic core. In this series, sapphyrins, pentaphyrins, smaragdyrins, isosmaragdyrin, orangarin and ozaphyrin are known in the literature. In the introduction part, we highlight mainly pentaphyrin (**1**), sapphyrin (**2**) and smaragdyrin (**3**) (Figure 5.1). Depending on the number of *meso*-carbons between the five pyrrole / heterocyclic units, these analogues are classified as follows. In the case of pentaphyrins, the pyrrole rings are connected with five *meso*-carbon atoms,² whereas, the number of *meso* carbon atoms are reduced to four in sapphyrin and three in smaragdyrin along with one and two direct bonds between α -carbon atoms of pyrrole / heterocyclic rings respectively.³

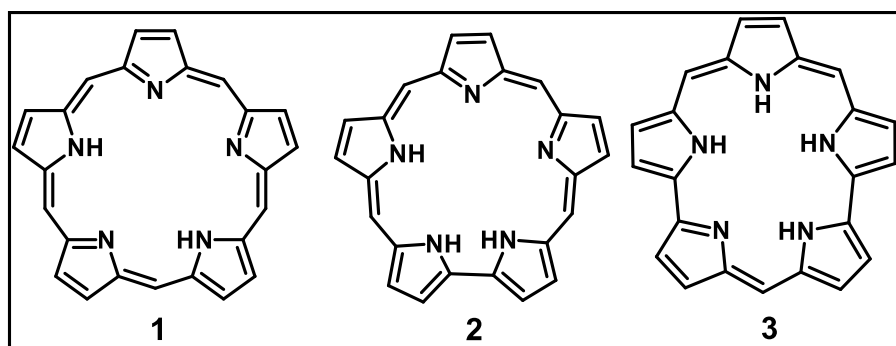
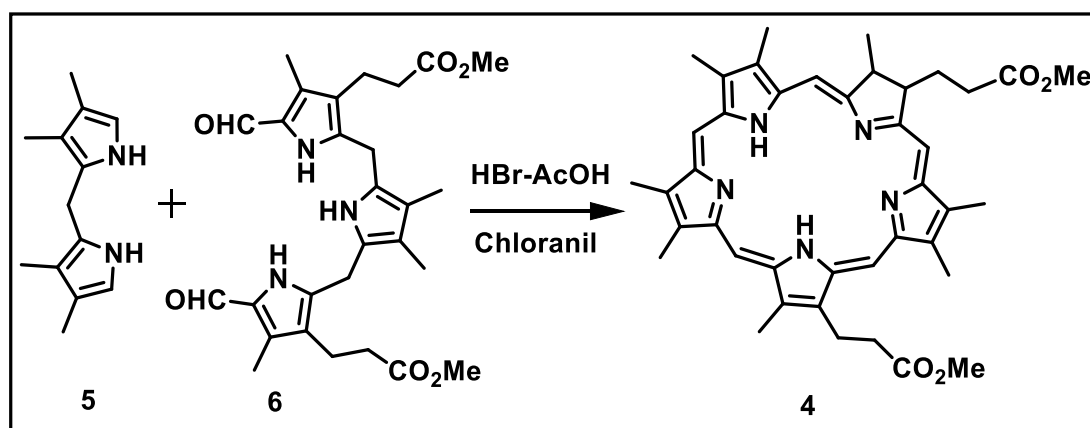


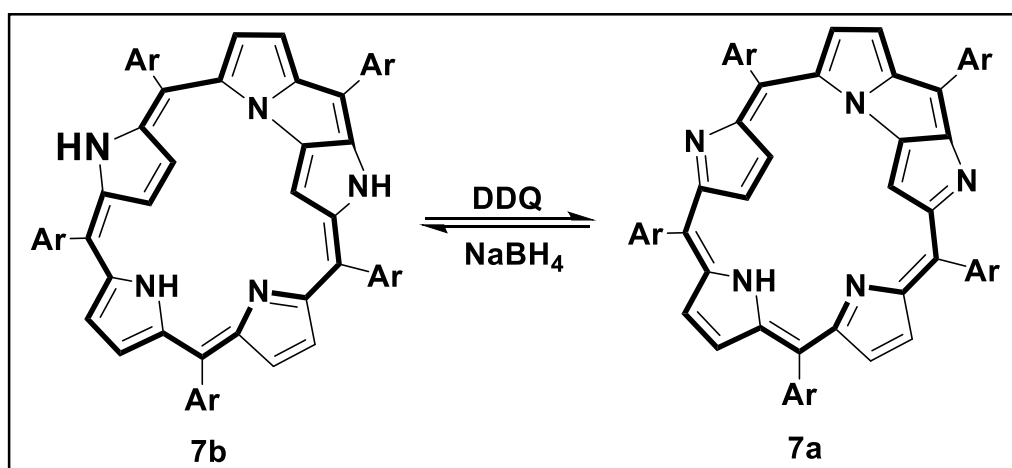
Figure 5.1: Chemical structures of **1**) pentaphyrin, **2**) sapphyrin and **3**) smaragdyrin.

The first stable pentaphyrin, β -Decaalkyl-substituted [22]pentaphyrin(1.1.1.1.1) **4** was synthesized by Gossauer et al.² The compound **4** was synthesized by condensation of the known dipyrromethane **5** with the dialdehyde **6** in the presence of 33% hydrobromic acid in acetic acid followed by oxidation with chloranil and afforded in 31% overall yield (Scheme 5.1).



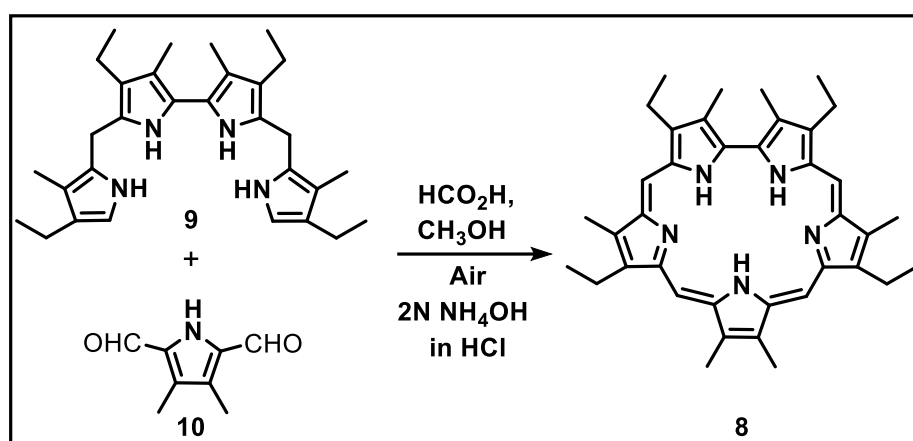
Scheme 5.1: Synthesis of **4**.

On the other hand, the *meso*-aryl pentaphyrins are known to undergo spontaneous N-fusion reaction. The first example of a *meso*-aryl fused expanded porphyrin, i.e. N-fused penta-pyrin (NFP₅) (**7**) was reported by Osuka and coworkers.⁴ **7** was synthesized by Rothmund-type acid-catalyzed condensation of pentafluorobenzaldehyde with pyrrole and followed by oxidation with 2,3-dichloro-5,6-dicyano-1,4-benzoquinone (DDQ). Two major products **7a** and **7b** were obtained whose parent mass peaks reflected to the pentapyrrolic macrocycle with overall isolated yield of **7** was 15%. The ratio of product (**7a** and **7b**) formation changed impressively depending on the oxidant used and converged to **7a** when DDQ was used in excess (2.5 equiv) (Scheme 5.2). The crystal analysis of **7b** revealed the formation of fused tri-pentacyclic ring in the core. The ¹H NMR spectral studies suggested the 24π antiaromatic characteristics of **7b** based on the presence of NH proton at 13.73 ppm and the β-CH protons at 8.2 to 5.5 ppm.



Scheme 5.2: Redox reaction between **7b** and **7a**.

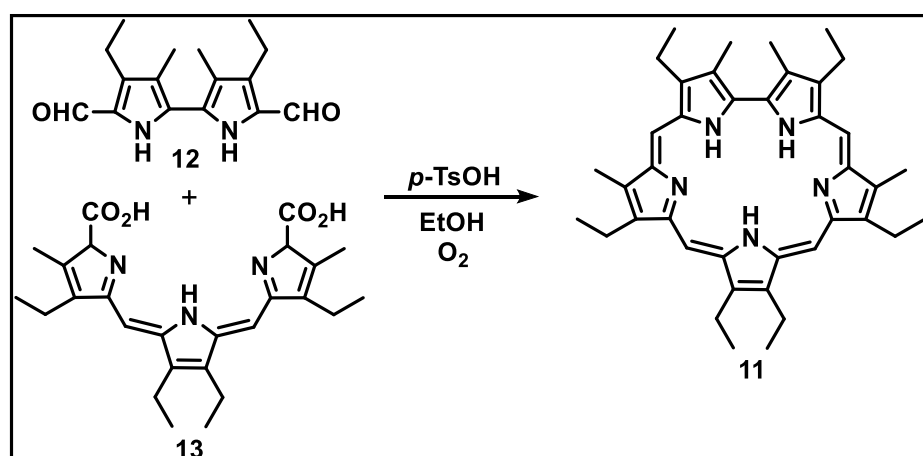
In 1966, another pentapyrrolic analogue sapphyrin was first synthesized by Woodward during their efforts to synthesize vitamin B₁₂.¹ These pentapyrrolic compounds were termed as “sapphyrins” due to their intense blue-colored crystalline form. Initially, sapphyrin (**8**) was obtained in 1% yield by [4 + 1] acid catalyzed condensation between the linear tetrapyrrolic precursors (**9**) and 2,5-diformyl-3,4-dimethylpyrrole (**10**) under aerial oxidation (Scheme 5.3).



Scheme 5.3: Synthesis of **8**.

Later, [22]sapphyrins have been widely exploited specifically as anionic sensors by Sessler et al.⁵ The modified synthetic methodologies were reported for the synthesis of sapphyrin (**11**) and shown in scheme 5.4.⁶ The [3 + 2] MacDonalld type condensation of directly pyrrole-pyrrole linked

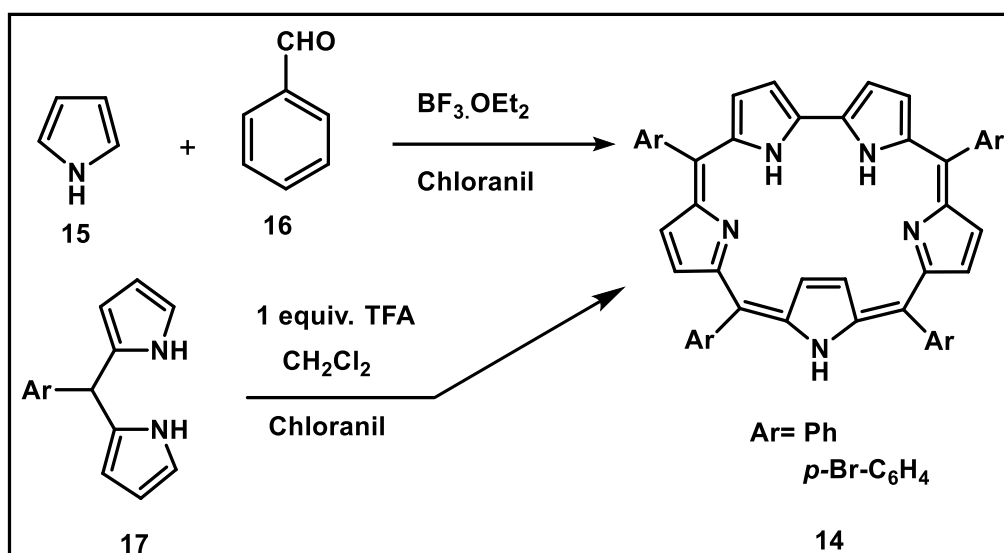
precursor **12** with tripyrromethene dicarboxylic acid (**13**) afforded **11** in ~40% yield.



Scheme 5.4: Synthesis of **11**.

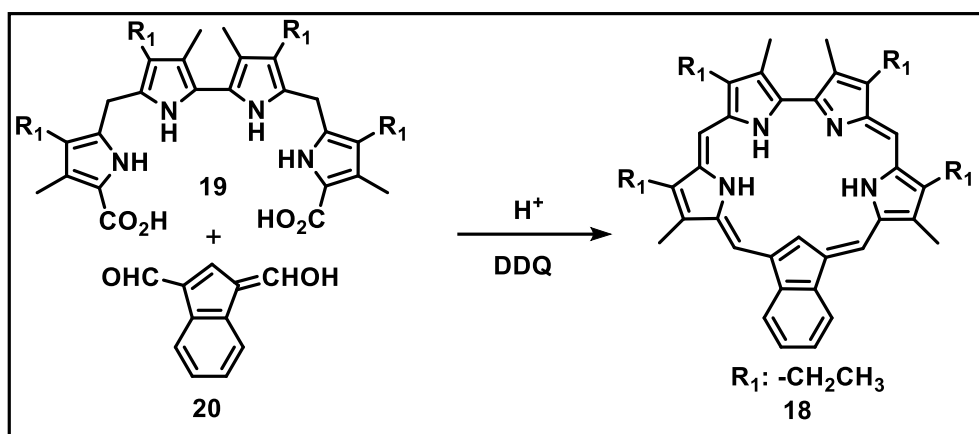
The first *meso*-aryl sapphyrin (**14**) was reported by Latos-Grażyński and co-workers.⁷ **14** was obtained by Rothmund type of reaction between pyrrole (**15**) and benzaldehyde (**16**), using $\text{BF}_3 \cdot \text{OEt}_2$ as acid catalyst (Scheme 5.5) in 1% yield. The ^1H NMR spectral analysis revealed that the pyrrole unit opposite to the bipyrrole ring was inverted and both $\beta\text{-CH}$ protons were in aromatic ring current. Upon protonation by trifluoroacetic acid (TFA), the respective pyrrole ring was 180° rotated to obtain a normal structure as observed in **8** and **11**.

The modified synthetic methodologies with better yield was reported by Chandrashekar and co-workers. The 5-phenyl dipyrromethane (**17**) was treated with 1 equiv. of TFA followed by chloranil oxidation gave the sapphyrin (**14**) in 11% yield (Scheme 5.5).⁸



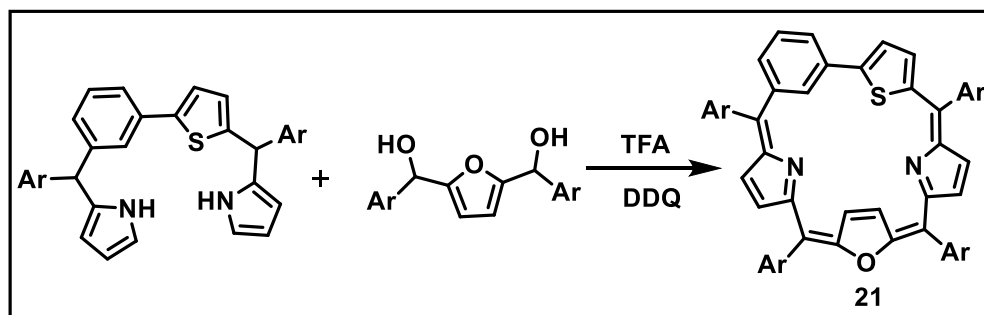
Scheme 5.5: Synthesis of **14**.

The first carbasapphyrin **18** was reported by Lash and coworkers. The [4 + 1] MacDonald condensation between tetrapyrrole dicarboxylic acid (**19**) and 1,3-diformyl indene (**20**) (Scheme 5.6) followed by oxidation with DDQ to afford **18** in 38% yield.⁹



Scheme 5.6: Synthesis of Carbasapphyrin **18**.

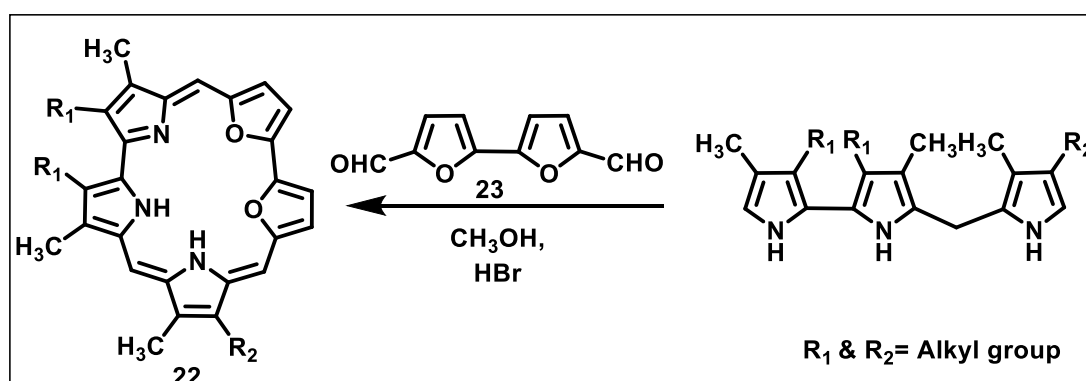
Very recently unsymmetrical heterobenzisapphyrin **21** was reported by Ravikanth and co-workers by adopting [4 + 1] acid-catalyzed condensation reaction to obtain **21** in ~9% yield (Scheme 5.7).¹¹ The spectral and structural analyses revealed that **21** is a planar molecule with an inverted furan ring and overall adopt nonaromatic characteristic (Scheme 5.7).



Scheme 5.7: Synthesis of Carbasapphyrin **21**.

The chemistry of sapphyrins has been well-established due to proficient synthetic approaches. On the other hand, smaragdyrins are not explored considerably as the molecules are unstable, however, recently several attempts have been made to synthesize smaragdyrins.

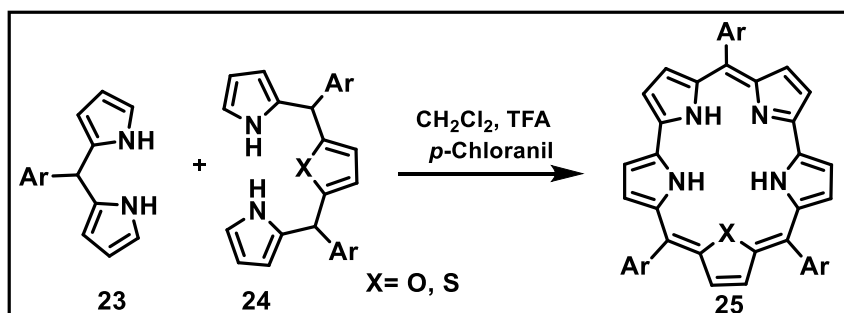
Woodward and co-workers first recognized the existence of smaragdyrin.¹ The term “smaragdyrin” originated as the colour of the macrocycle resembles with emerald stone. In 1972, while synthesizing sapphyrins, Broadhurst, Grigg, and Johnson obtained smaragdyrin (**22**) and coined the name as norsapphyrins (scheme 5.8).¹¹ Interestingly, they called the molecule norsapphyrins but the spectral confirmation suggested norsapphyrins and smaragdyrin[1.1. 0.1.0] are identical.



Scheme 5.8: Synthesis of **22**.

Finally, Chandrashekar and co-workers succeeded through rational synthetic approach to make stable *meso*-aryl core-modified smaragdyrins **25**.¹² In the

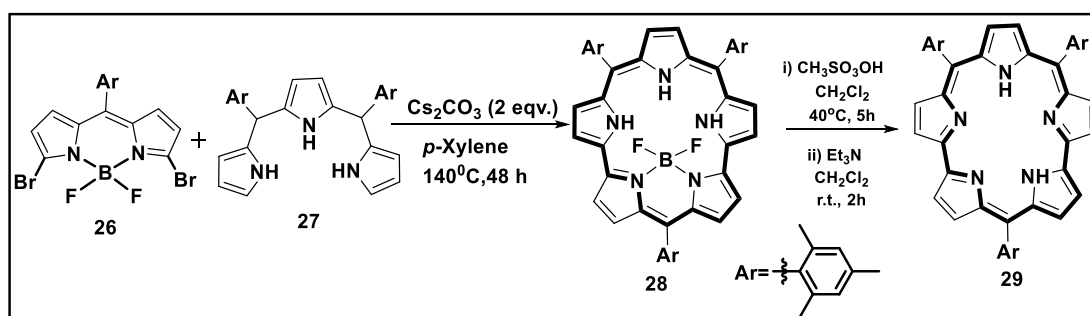
presence of TFA acid-catalyst, they adopted [3 + 2] oxidative coupling reaction between *meso*-aryl dipyrromethane **23** and oxatripyrrane / thiatripyrrane **24** followed by chloranil oxidation to obtain **25** in ~50% yield (scheme 5.9).



Scheme 5.9: Synthesis of **25**.

Thereafter, several core-modified smaragdyrin molecules were reported by Ravikanth and co-workers and exploited its coordination chemistry as well as sensing properties.

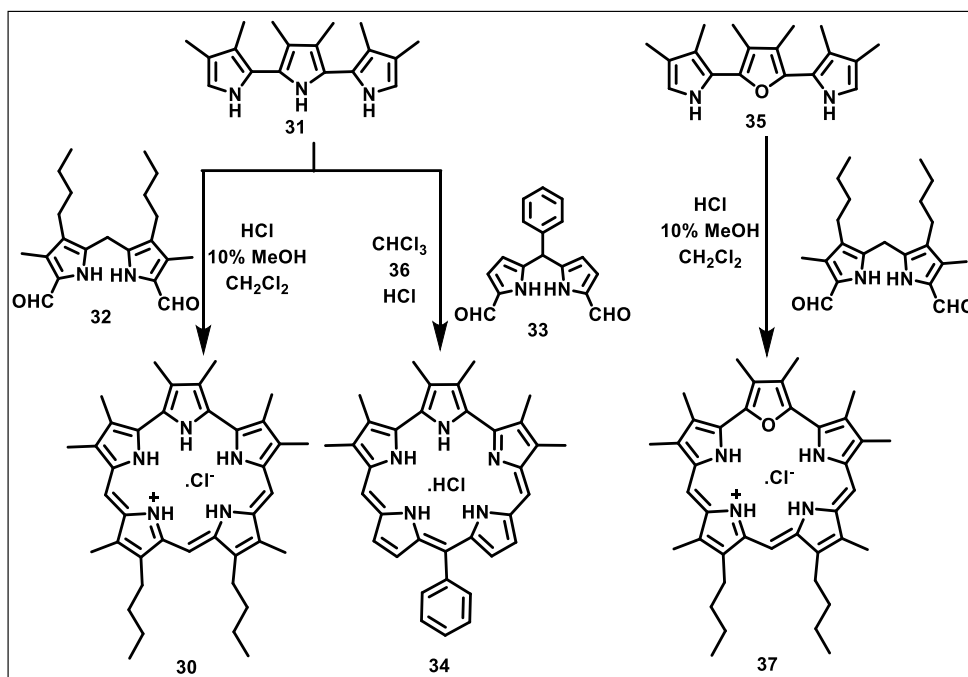
Recently, Song and co-workers demonstrated the synthesis of BF_2 complex of **28**, which was obtained in 13% yield by Substitution Aromatic Nucleophilic ($\text{S}_{\text{N}}\text{Ar}$) reaction with BF_2 complex of 1,9-dibromo-5-mesityldipyrromethane (**26**) with 5,10-dimesityltripyrrromethane (**27**). The BF_2 unit was removed by *p*-toluenesulphonic acid (*p*-TSA) condition to afford freebase **29** in 90% yield with antiaromatic characteristics (scheme 5.10).¹³



Scheme 5.10: Synthesis of **28** and **29**.

The structural isomer of smaragdyrin known as isosmaragdyrin (1.1.1.0.0) was first reported by Sessler and co-workers. The HCl acid-catalyzed condensation of α -free tripyrrole (**31**) with diformyl dipyrromethane (**32**) to obtain **30** in 38% yield,

whereas, **34** was in 38% yield by using **33**, instead of **32**, under similar reactions conditions. Similarly, the respective core-modified analogue **37** was obtained in 38% yield. The macrocycles **30**, **34** and **37** are aromatic and found stable in protonated form as shown in Scheme 5.10 (Scheme 5.11).^{14,15}



Scheme 5.11: Synthesis of **30**, **34** and **37**.

5.2 Objective of our work

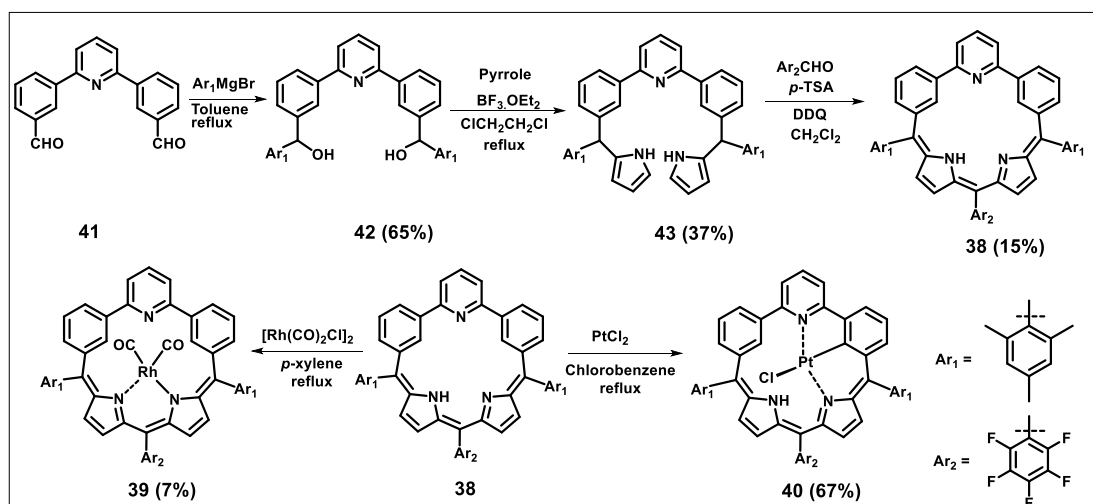
As per the literature survey, the syntheses of smaragdyrin [1.1.0.1.0] and its core-modified analogues are well known in the literature, however, only one report on respective structural isomer, isosmaragdyrin [1.1.1.0.0] and its core-modified derivative is known till date. Both the analogues are stable in the anion bound form and their coordination chemistry is hitherto unknown in the literature. Hence, the main objective of this chapter is to isolate the stable isosmaragdyrin in its freebase form and also to explore its coordination chemistry.

In this chapter, we wish to report the synthesis, spectral and structural characterization of isosmaragdyrin [1.1.1.0.0] with a N_3C_2 core. Tripyrrole in the

macrocyclic core is replaced by 2,6-diphenylpyridyl unit, where the arene and pyridyl units are incorporated in the macrocyclic core for the first time. The core is utilized to stabilize the trifluoroacetate anion, Rh and Pt ion in +1 and +3 oxidation state to form Rh(I) and organo-Pt(III) complex. The local aromaticity of the *m*-arene unit (*m1* and *m2*) and pyridyl unit (*Py*) in the core leads to overall nonaromatic characteristics in (i) freebase; (ii) protonated and (iii) metal ion inserted form.

5.3 Results and discussions

5.3.1 Synthesis



Scheme 5.12: Synthesis of **38**, **39** and **40**.

The requisite key precursors for the synthesis of target molecule are obtained as follows: The Suzuki-Miyaura cross coupling reaction of formylphenylboronic acid in 1:3 mixture of H_2O and tetrahydrofuran gave 3,3'-(pyridine-2,6-diyl)dibenzaldehyde **41** in 85% yield. The Grignard reaction of **41** with freshly prepared mesitylmagnesium bromide in dry toluene under reflux conditions afforded (pyridine-2,6-diylbis(3,1-phenylene))bis(mesityl-methanol) **42** in 65% yield. 2,6-bis(3-(mesityl(1H-pyrrol-2-yl)methyl)phenyl)pyridine **43** was synthesized by refluxing a 1,2-dichloroethane solution of **42** with excess pyrrole in the presence of $\text{BF}_3\cdot\text{OEt}_2$. The *p*-toluenesulfonic acid catalyzed

condensation of **43** with 2,3,4,5,6-pentafluorobenzaldehyde followed by oxidation with 2,3-dichloro-5,6-dicyano-1,4-benzoquinone (DDQ) gave the target molecule **38** in 15% yield. The coordination chemistry of **38** was performed under N₂ atmosphere; (i) by refluxing a *p*-xylene solution of **38** in the presence of [Rh(CO)₂Cl]₂ to afford **39** in 7% yield and (ii) by refluxing chlorobenzene solution of **38** with PtCl₂ to form **40** in 67% yield.

5.3.2 Spectral Characterization

5.3.2.1 Mass spectrometric analysis

The high resolution-electron spray ionization (HR-ESI) mass spectrometric analyses of **38**, **39** and **40** were shown in Figure 5.2 – 5.4. The exact composition of **38** was confirmed by observing a mass peak at $m/z = 800.3090$. The molecular ion signal of Rh(I) complex **39** was exhibited at $m/z = 958.1914$ (M+1) (Figure 5.3). Whereas the molecular ion peak of complex **40** was observed with an extrusion of a chlorine atom at $m/z = 993.2521$ (M-Cl) (Figure 5.4).

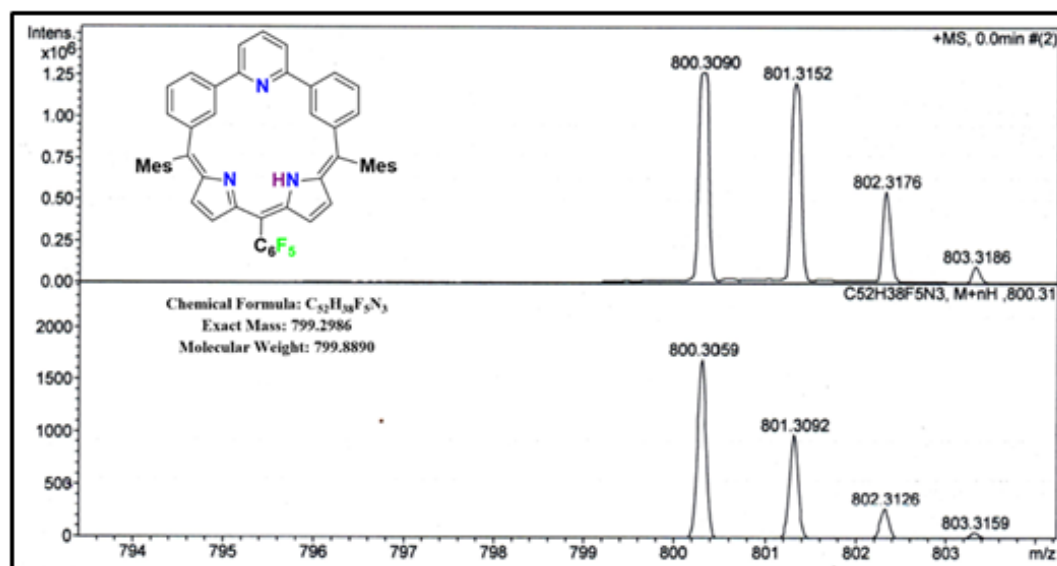


Figure 5.2: ESI-MS spectrum of **38**.

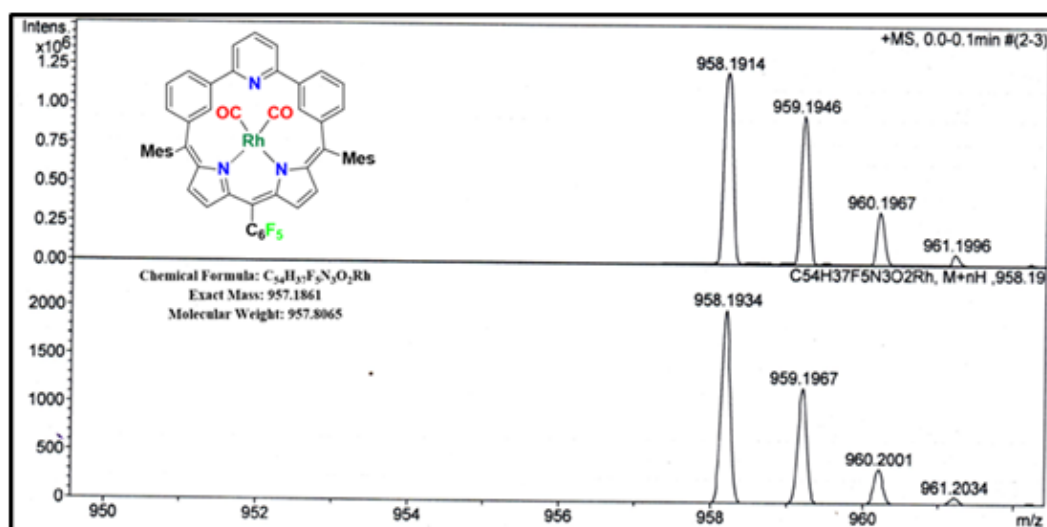


Figure 5.3: ESI-MS spectrum of **39**.

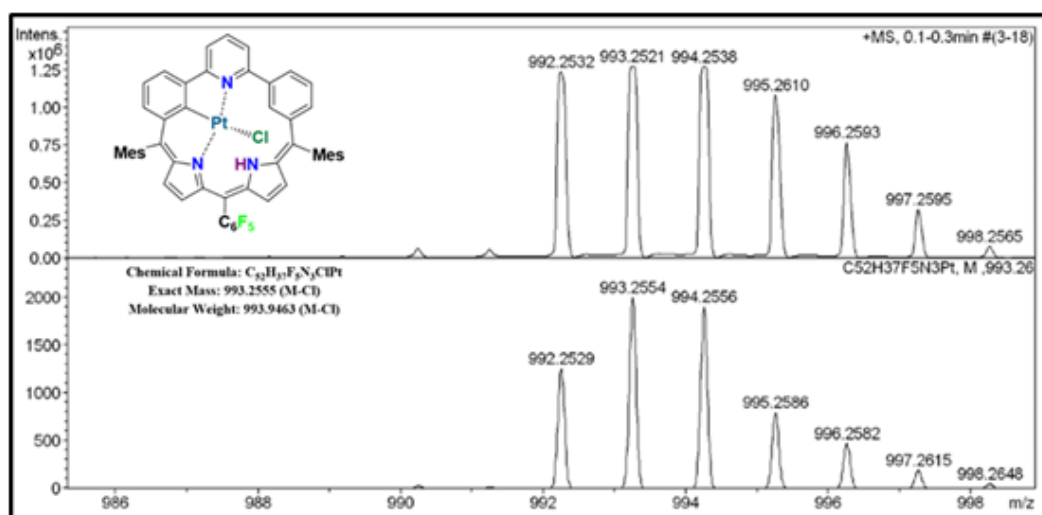


Figure 5.4: ESI-MS spectrum of **40**.

5.3.2.2 NMR Analysis

The 1H NMR spectral analysis of **38** – **40** in CD_2Cl_2 at room temperature are shown in Figure 5.5. The compound **38** with C_2 symmetry / centro symmetry (fix the right symmetry) exhibits the signals exactly for half of the molecule (Figure 5.5a). The pyrrolic β -CHs [H(9, 13)] and [H(8, 14)] observes as a set of doublets at 6.08 and 6.47 ppm. The peripheral *m*-phenylene protons [H(4, 18)] appears as broad signal at 6.90

ppm, whereas [H(2, 20)] and [H(3, 19)] are as a set of doublet and as a triplet at 7.78 and 7.35 ppm and the core protons [H(27, 28)] are as singlet at 9.01 ppm respectively. The signals of a pyridine moiety observe as doublet at 7.74 [H(23, 25)] and a triplet at 7.91 ppm [H(24)]. The mesityl-CH and -CH₃ protons exhibit as singlets at 6.92 ppm and 2.32 & 2.03 ppm. The resonance of inner NH proton evolves as a broad signal at 8.65 ppm at 213 K in variable temperature NMR experiment (Figure 5.6). The diprotonated ligand **38.2H⁺** was accomplished by gradual addition of trifluoroacetic acid (TFA) into CD₂Cl₂ solution of **38** (Figure 5.7). After 38 equiv. the resonance of amine and protonated imine protons appeared as singlet at 12.01 ppm and the pyridinium NH at 14.36 ppm. The overall spectral pattern in **38** and **38.2H⁺** simulate typical nonaromatic characteristics as observed in *m*-benzporphyrinoids, pyriporphyrinoids and its expanded analogues.¹⁰

The ¹H NMR spectral pattern of **39** is reminiscent to that of **38** with moderate changes in chemical shift values and shown in Figure 5.5b. The absence of inner core pyrrolic NH [H(2)] and the presence of two *m*-phenylene CH protons [H(27,28)] at 9.76 ppm reveals that the coordination occurs only in the dipyrromethene moiety. The pyrrolic β-CHs are resonated as a set of doublets at 5.97 and 6.42 ppm. The peripheral *m*-phenylene protons are appeared at 6.78 [H(4,18)], 7.40 [H(2,20)] and 7.21 [H(3,19)] ppm. The pyridine protons are resonated as a doublet at 7.65 [H(23,25)] and a triplet at 7.92 [H(24)] ppm. The aromatic mesityl-CH protons are observed at 6.87 and 6.99 ppm and the methyl protons are at 2.34, 2.33 and 1.72 ppm. Overall, the ¹H NMR analysis of **39** retains its nonaromatic character as observed in **38**.

The ¹H NMR spectrum of **40** shows the unsymmetrical nature as compared to **38** and shown in Figure 5.5c. signals. The disappearance of one of the *m*-phenylene

(*m*2) inner core CH protons [H(27)] and appearance of other *m*-phenylene (*m*1) CH proton [H(28)] at 8.53 ppm and pyrrolic NH [H(2)] at 11.96 ppm reveal the formation of organo-Pt(II) complex and suggests the different mode binding as compared to **39**. The deshielded NH proton suggests strong intramolecular hydrogen bonding interaction. The pyrrolic β -CH protons are resonated between 5.95 and 6.69 ppm. The peripheral-CH protons [H(2,3,4)] of cyclometallated phenyl rings are appeared between 7.07 and 7.54 ppm, whereas the -CH protons [H(18,19,20)] of non-cyclometallated phenyl rings are observed between 6.82 and 7.65 ppm. The meso-mesityl -CH and methyl protons are resonated as singlets in the range of 6.88-7.03 and 1.88-2.35 ppm, respectively.

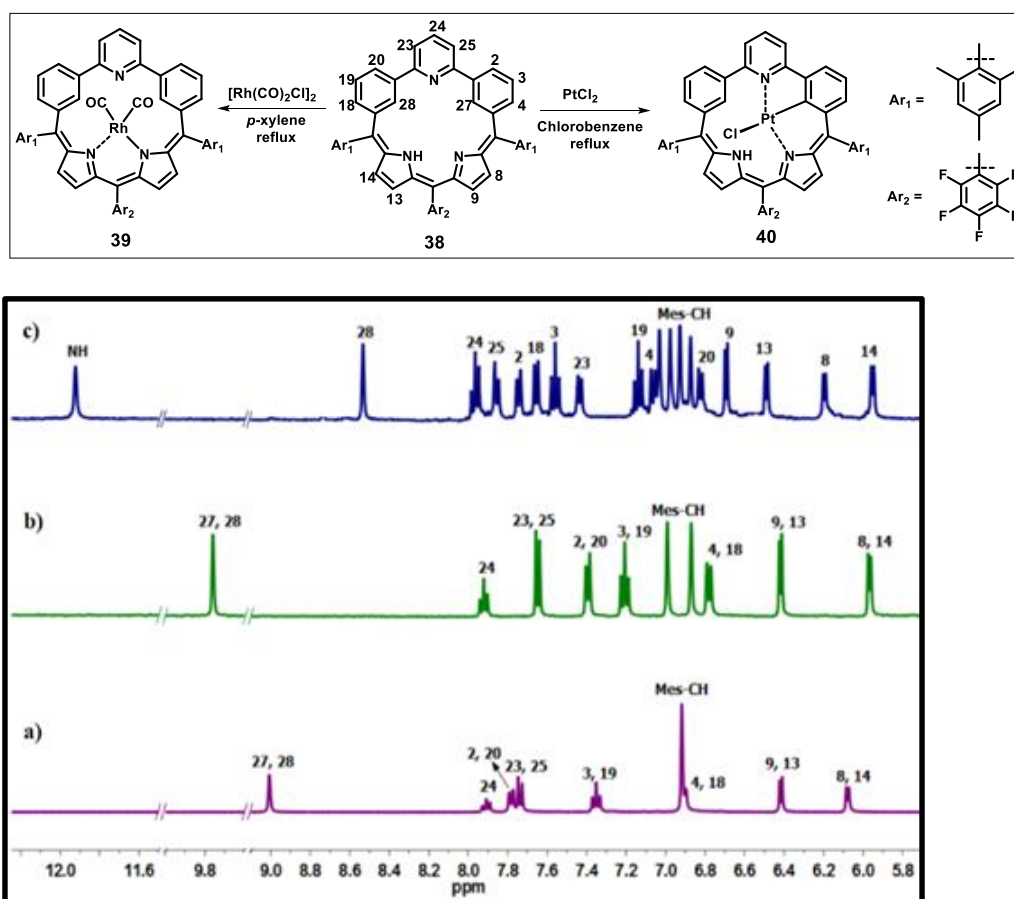


Figure 5.5: $^1\text{H-NMR}$ spectra of **38**, **39** and **40** in CD_2Cl_2 .

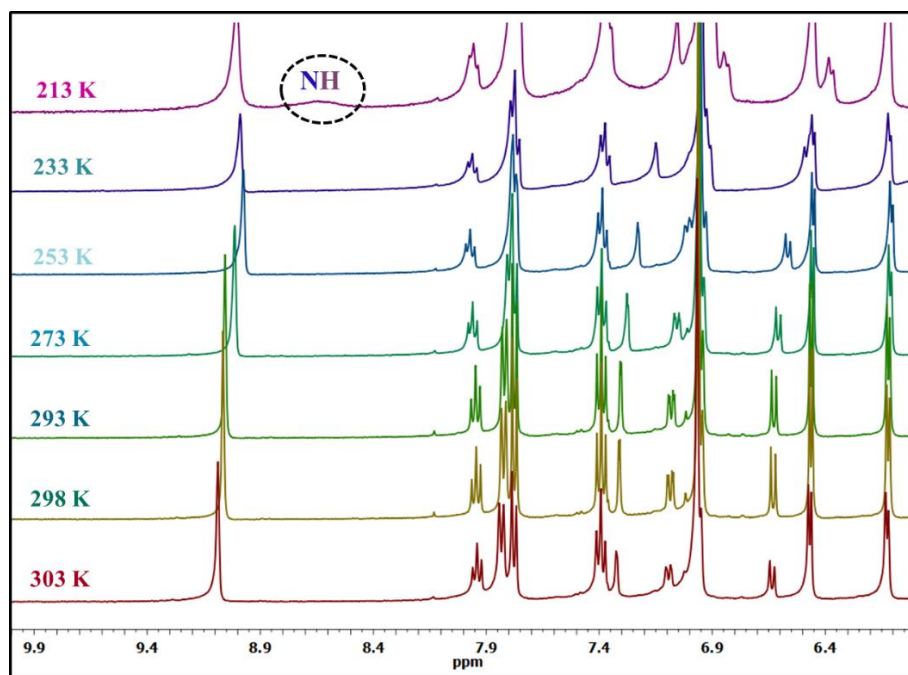


Figure 5.6: Variable temperature ¹H-NMR spectrum of **38** CD₂Cl₂.

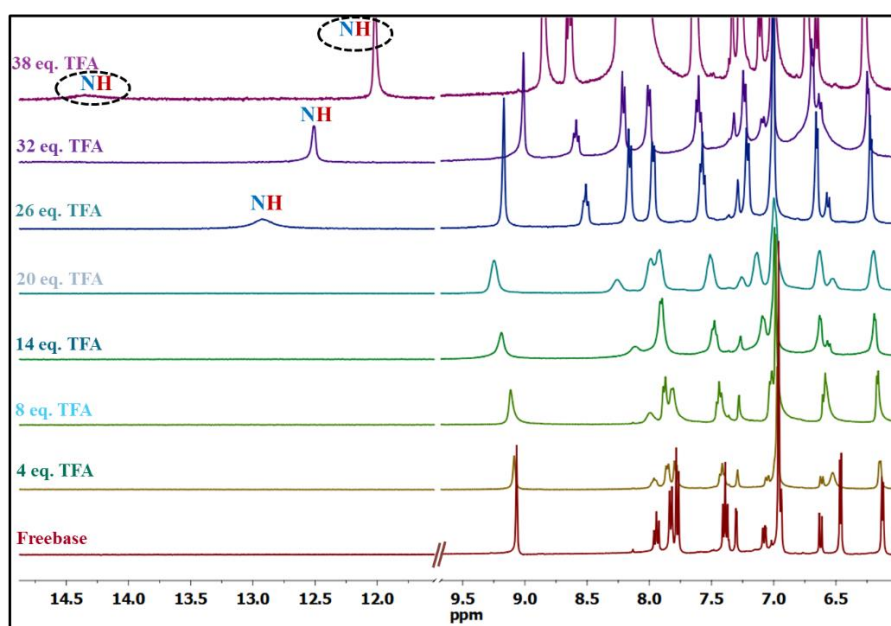


Figure 5.7: ¹H NMR of **38** with various equiv. of TFA in CD₂Cl₂.

5.3.2.3 Single crystal X-ray structure and analysis of **38**, **39** and **40**

The molecular structures of **38**, **38.2H⁺**, **39** and **40** were unambiguously confirmed by single crystal X-ray analyses and shown in Figure 5.8 & 5.9 and the crystal data are in Table 5.1. All the crystals were grown in CH₂Cl₂/*n*-pentane solvent

mixture. The anticipated nonaromatic character of **38** from ^1H NMR spectral analysis is further reflected from the crystal analyses. The carbon-carbon bond lengths in the dipyrromethene moiety exhibit an alternative single and double bond characters, proves the effective π -delocalization (Figure 5.17). However, the bond lengths within the *m*-phenylene rings and pyridine units are between 1.333(5) Å and 1.417(5) Å, which resembles with $\text{sp}^2\text{-sp}^2$ double-bond character. The *m*-phenylene units are connected with pyridine as well as dipyrromethene unit by $\text{sp}^2\text{-sp}^2$ single bond [1.472(6) Å & 1.482(5) Å] lengths. The 2,6-diphenylpyridyl unit in the core maintains individual aromatic character, thus the effective π -electron delocalization in the dipyrromethene units are restricted by *m*-phenylene (*m1* & *m2*) and pyridyl (*Py*) units and adopts nonaromatic characteristic. Further, the crystal analyses revealed that the *m*-phenylene units are highly deviated from the mean plane containing 18 inner core atoms with the dihedral angle of $41.88(1)^\circ$ (*m1*) and $36.04(1)^\circ$ (*m2*), where the pyridine units is deviated from the plane with the tilt angle of $21.94(9)^\circ$ (*Py*).

The molecular structure of **38.2H⁺** exists in crystallographic two-fold axis (Figure 5.18), thus, more symmetric as compared to **38**. All the imine nitrogens are protonated and are in intermolecular hydrogen bonding with one trifluoroacetate anion and located above the mean macrocyclic plane. The bond distance and angle of N2-H2...F6 and N3-H3...O1 are 2.85 (3) Å & $102.37(7)^\circ$ and 2.34 (2) Å & $139.90(7)^\circ$. The bond lengths within *m*-phenylene rings (*m1* & *m2*) and the pyridine ring (*Py*) are similar as observed in **38**, thus maintains the individual aromatic character and overall retain the nonaromatic character.

As observed from the ^1H NMR studies, the crystal structure of **39** (Figure 5.8c & d) reveals that the dipyrromethene unit is coordinated with $\text{Rh}(\text{CO})_2$ unit and the Rh ion is in +1 oxidation state and is located at 2.05 Å below the mean plane containing

18 inner core atoms. The bond lengths between N1-Rh & N2-Rh are 2.120(7) Å and 2.149(7) Å respectively. The bond angles around Rh(I) metal ion are N1-Rh...N2: 90.41(2)°, N2-Rh...C53: 90.11(4)°, C53-Rh...C54: 86.25(5)° and C54-Rh...N1: 92.71(4)°, thus, the geometry around the metal center is square planar. In addition, there is no major deviation in the bond lengths in *m*-phenylene (*m1* & *m2*), pyridine (*Py*) and dipyrromethene units (Figure 5.19), thus maintains the nonaromatic character as observed in **38**.

In the molecular structure of **40**, the pyrrole (N2), *m*-phenylene (*m2*) and pyridine (*Py*) are coordinated with Pt ion and the additional coordination site is occupied by the chloride ligand to generate the organo-Pt(II) complex. The bond lengths around the metal center are Pt-N3, Pt-C27, Pt-N2 and Pt-Cl are 2.087(9) Å, 1.964(1) Å, 2.044(8) Å and 2.414(3) Å (Figure 5.20) and the bond angles of N3-Pt-C27, N2-Pt-C27, N3-Pt-Cl and N2-Pt-Cl are 80.21 (4)°, 92.82 (4)°, 99.43 (2)° and 88.31 (2)° respectively, thus the geometry around the metal center is square planar. It is pertinent to point out that the particular arrangement of Pt(II) complex in the core reveals the typical unsymmetrical pincer complex inside the macrocyclic core by forming one five membered ring (Pt-N3-C26-C1-C27) and a six membered ring (Pt-N2-C7-C6-C5-C27). The observed deshielded NH signal in the ¹H NMR studies is further supported by the crystal analyses with strong intermolecular hydrogen bonding between the axial chloride ligand (Cl) and pyrrole (N1-H1) with bond length and angle of N1-H1...Cl 2.32(3) Å and 155.00(6)°. Notably, due to the incorporation of metal-chloride bond into the macrocyclic core, N3-Pt-N2 fragment is distorted from linearity [172.15(3)°] and also C27-Pt-Cl is bent at an angle of 161.98(4)°. As a consequence; (i) the distance between C1 of *m2* ring and Pt(II) ion is 2.85(1) Å, which is in between the van der Waals and covalent diameter, thus forms η¹ coordination. (ii) In addition to N1-H1...Cl,

the intermolecular interaction is further observed between N1-H1 and Pt(II) and the bond length and angle of N1-H1...Pt is 2.79 (7) Å and 136.52(5)°. Finally, the nonaromatic characteristic as reflected in **38** and **39** are further observed in the crystal analysis of **40**, thus retained as such.

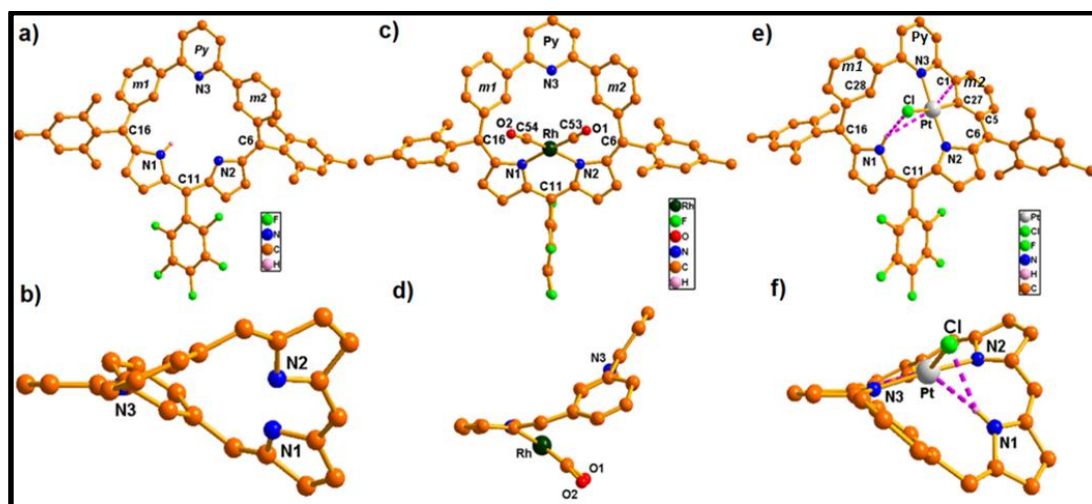


Figure 5.8: The solid state structures of **38**, **39** and **40**. a), c) and e) top views and b), d) and e) side views. The hydrogen atoms and *meso*-aryl substituents are omitted clarity.

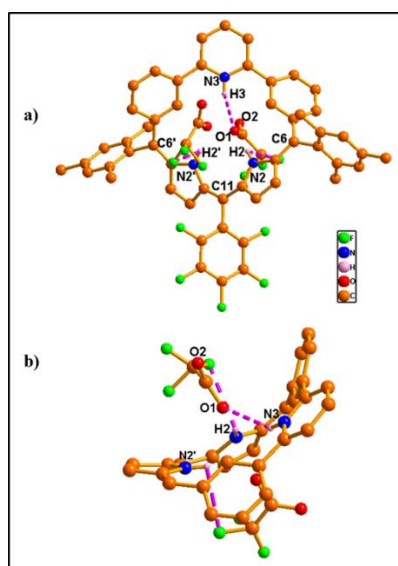


Figure 5.9: Single crystal X-ray structure of **38.2H⁺** with trifluoroacetate anion. a) Top view and b) side view. The hydrogen atoms and *meso*-aryl groups are omitted for clarity.

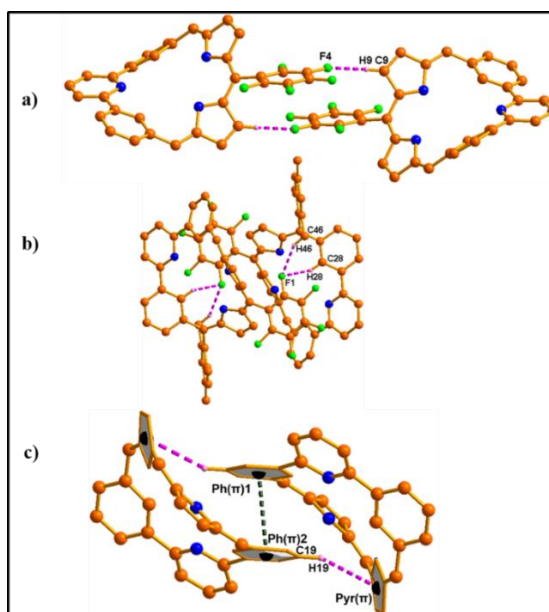


Figure 5.10: a), b), c) are Self-assembled dimers **38**. The bond distances and angles are: a) C9-H9...F4: 2.628(3) Å & 144.42(3)°; b) C28-H28...F1: 2.527(2) Å & 127.72(3)° and C46-H46...F1: 2.546(2) Å & 151.91(2)°; c) C19-H19...Py(π): 3.010(1) Å and 152.24(3)°; Ph(π)1- Ph(π)2: 3.634(3) respectively (hydrogens and the *meso*-aryl groups are omitted for clarity).

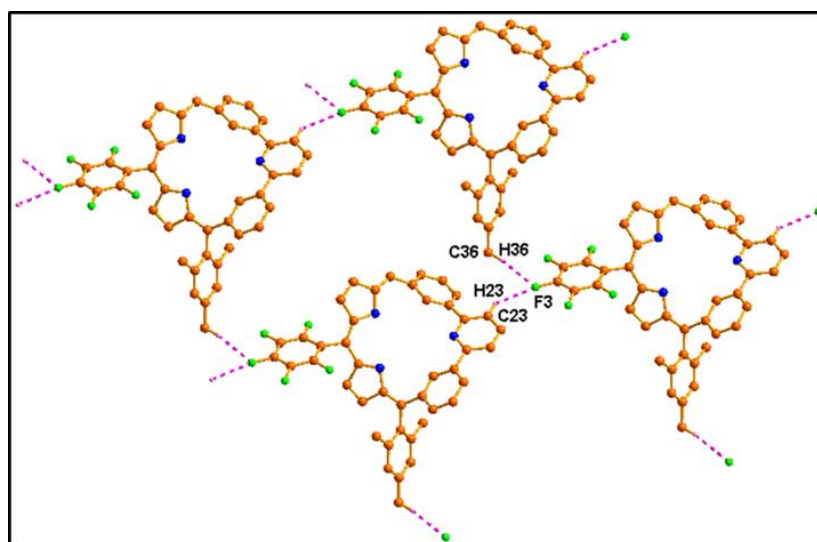


Figure 5.11: 2-D array of **38**. The bond distances and angles are C23-H23...F3: 2.548(2)Å and 133.91(3)°; C36-H36...F3: 2.541(3)Å and 150.59(3)° respectively (hydrogens and the *meso*-aryl groups are omitted for clarity).

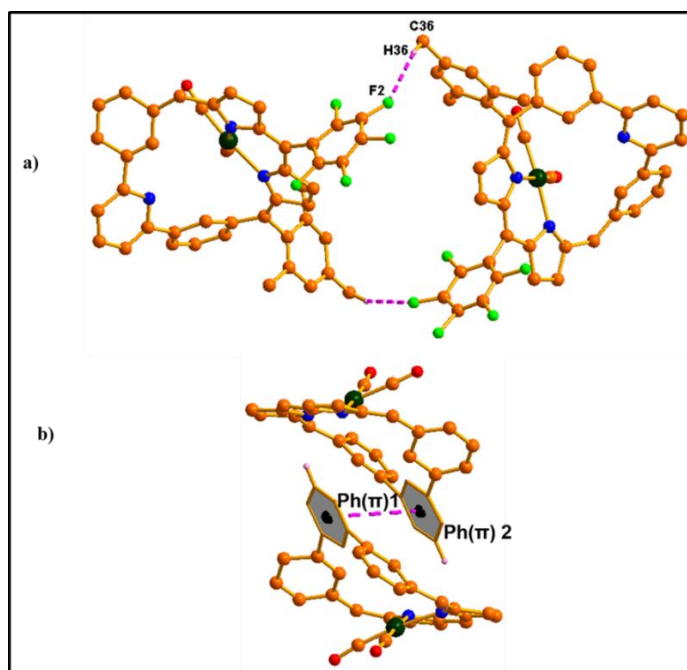


Figure 5.12: a), b) are Self-assembled dimers **39**. The bond distances and angles are: a) C36-H36...F2: 2.774(1) Å & 157.66(1)°; b) Ph(π)1-Ph(π) 2: 4.390(1) Å respectively (hydrogens and the *meso*-aryl groups are omitted for clarity).

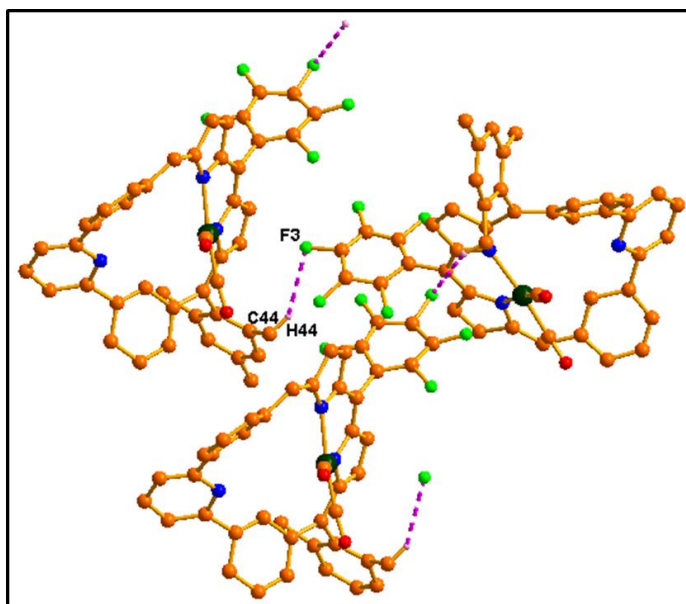


Figure 5.13: 1-D array of **39**. The bond distances and angles are C44-H44...F3: 2.877(1)Å and 142.23(1)°; respectively (hydrogens and the *meso*-aryl groups are omitted for clarity).

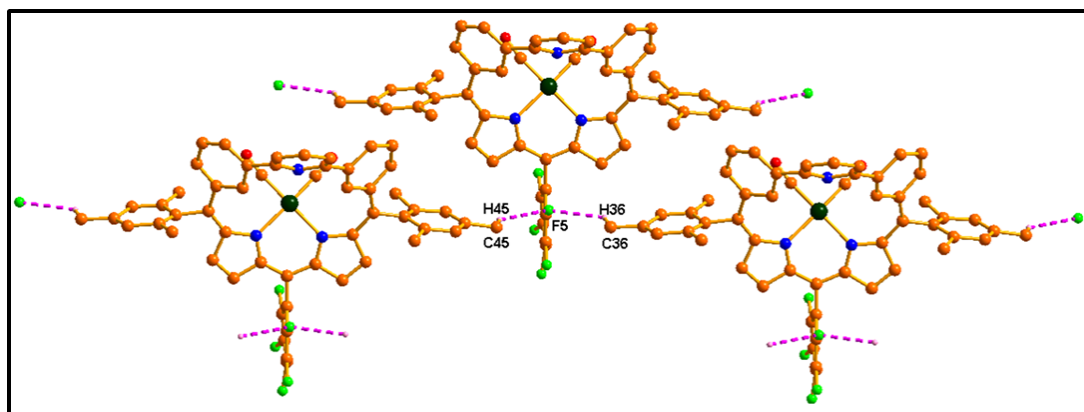


Figure 5.14: 2-D array of **39**. The bond distances and angles are C45-H45...F5: 2.759(1) Å and 133.87(1)°; C36-H36...F5: 2.702(1) Å and 127.16(9)° respectively (hydrogens and the *meso*-aryl groups are omitted for clarity).

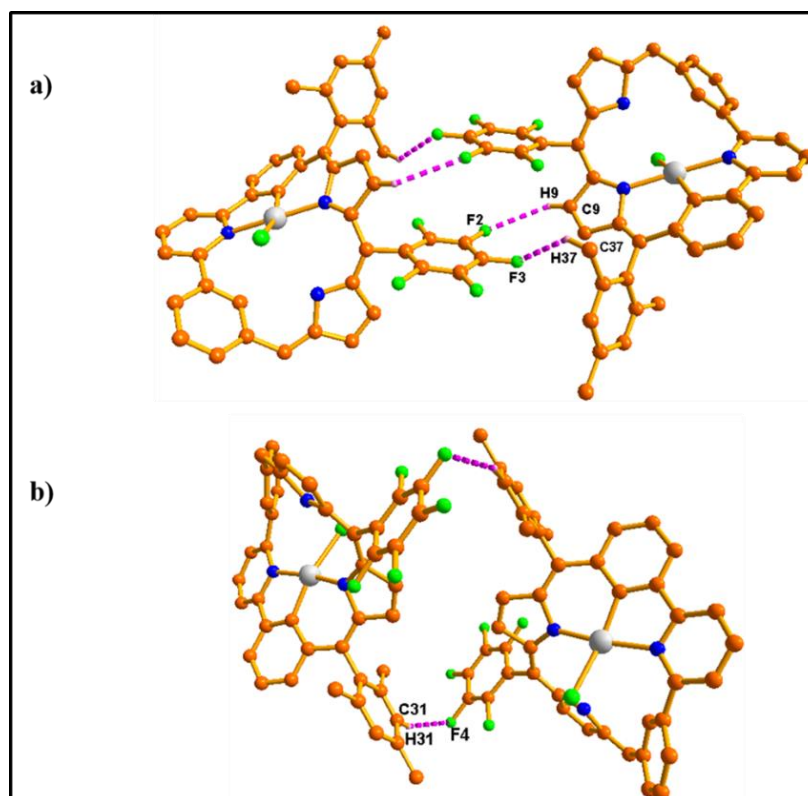


Figure 5.15: a), b) are Self-assembled dimers **40**. The bond distances and angles are: a) C9-H9...F2: 2.821(8) Å & 133.99(7)° and C37-H37...F3: 2.477(9) Å & 135.89(9)°; b) C31-H31...F4: 2.604(8) Å & 155.95(8)° respectively (hydrogens and the *meso*-aryl groups are omitted for clarity).

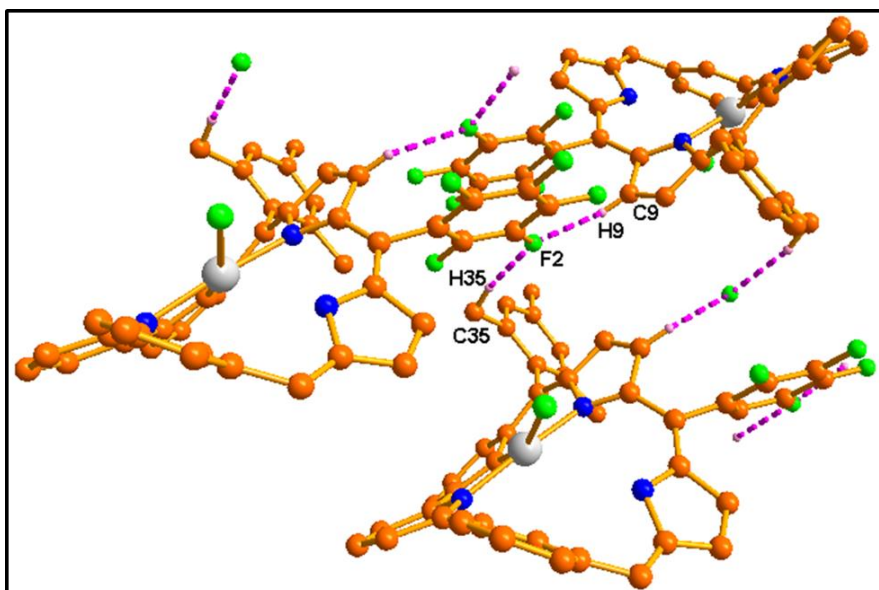


Figure 5.16: 2-D array of **40**. The bond distances and angles are C35-H35...F2: 2.579(9)Å and 159.43(7)°; C9-H9...F2: 2.821(8)Å and 133.99(7)° respectively (hydrogens and the *meso*-aryl groups are omitted for clarity).

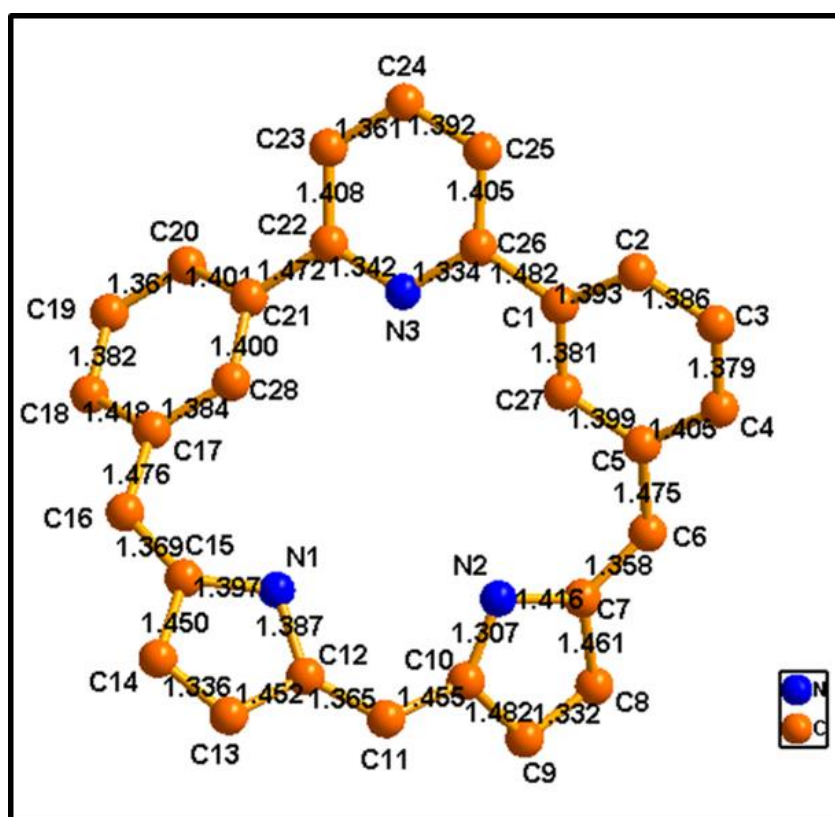


Figure 5.17: Bond lengths of **38** in (Å).

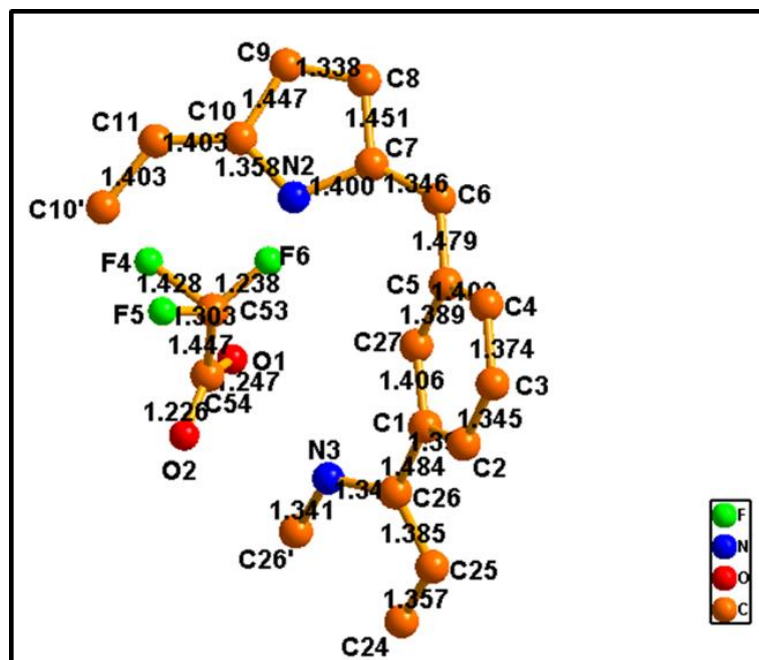


Figure 5.18: Bond lengths of 38.2H⁺ in (Å).

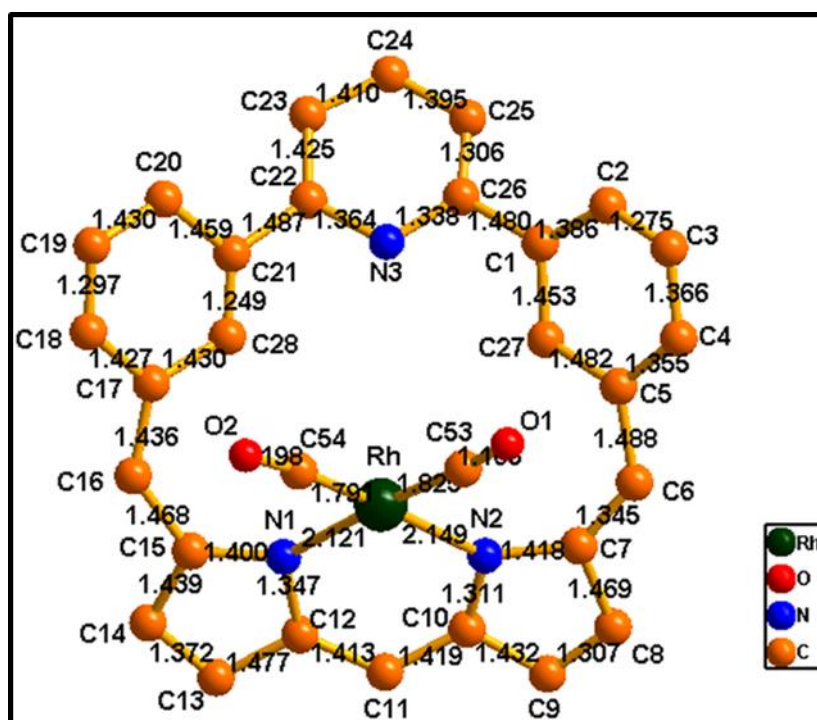


Figure 5.19: Bond lengths of 39 in (Å).

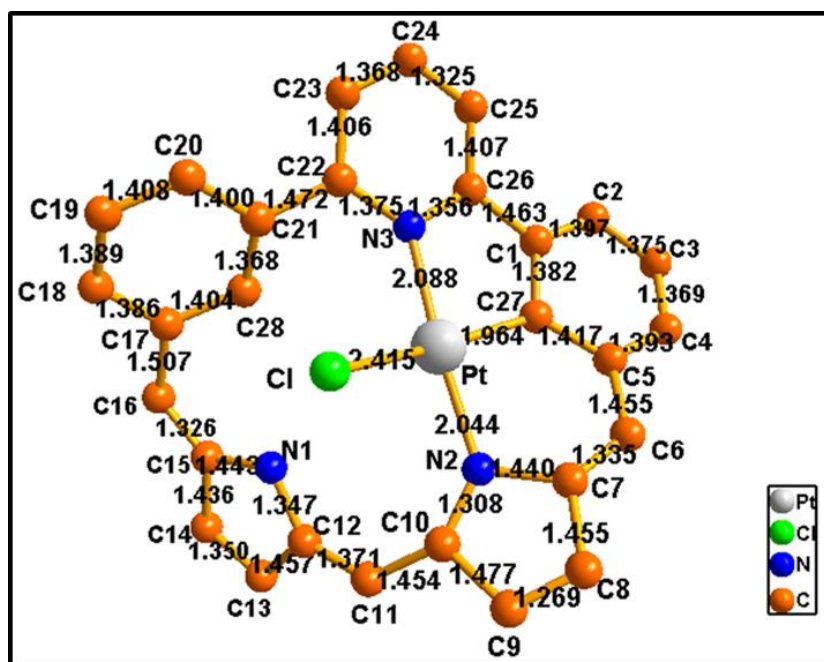


Figure 5.20: Bond lengths of 40 in (Å).

Table 5.1: Crystal data for **38**, **38.2H⁺**, **39** and **40**

Crystal parameters	38	38.2H⁺	39	40
Formula	C ₅₂ H ₃₈ F ₅ N ₃	C ₅₆ H ₄₀ F ₁₁ N ₃ O ₄	C ₅₄ H ₃₇ F ₅ N ₃ O ₂ Rh	C ₅₂ H ₃₇ F ₅ N ₃ ClPt
<i>M</i> /g mol ⁻¹	799.85	1027.91	957.79	1029.39
<i>T</i> /K	100	268(40)	296.87(10)	299.2(4)
Crystal dimensions/mm ³	0.729 × 0.452 × 0.192	0.18 × 0.16 × 0.1	0.22 × 0.15 × 0.12	0.362 × 0.25 × 0.212
Crystal system	triclinic	monoclinic	orthorhombic	monoclinic
Space group	<i>P</i> -1	<i>C</i> 2/ <i>c</i>	<i>C</i> 222 ₁	<i>C</i> 2/ <i>c</i>
<i>a</i> /Å	12.1765(4)	17.3774(4)	12.7471(2)	31.6392(15)
<i>b</i> /Å	13.0482(6)	19.4464(3)	24.2024(4)	8.7956(4)
<i>c</i> /Å	15.2310(5)	20.1641(4)	35.7587(13)	37.084(2)
α/°	111.513(4)	90	90	90
β/°	112.548(4)	97.8318(19)	90	93.548(5)
γ/°	93.946(3)	90	90	90
<i>V</i> /Å ³	2016.53(15)	6750.4(2)	11031.9(5)	10300.1(9)
<i>Z</i>	2	4	8	1
ρ _{calcd} /mg m ⁻³	1.317	1.011	1.156	1.489
μ/mm ⁻¹	0.765	0.727	2.958	5.819
<i>F</i> (000)	832.0	2112.0	3920.0	4593.0
Reflns. collected	28909	47161	22736	39416
Indep.reflns.[<i>R</i> (int)]	7384 [0.2074]	5960 [0.0793]	11555 [0.0730]	9420 [0.1227]
Max/min transmission	0.863, 0.693	0.930, 0.877	0.701, 0.617	0.291, 0.218
Data/restraints/parameters	7384/0/535	5960/90/404	11555/582/592	9420/0/565
GOF on <i>F</i> ²	0.952	1.103	1.120	0.994
Final <i>R</i> indices [<i>I</i> > 2σ(<i>I</i>)]	<i>R</i> ₁ = 0.0804, w <i>R</i> ₂ = 0.2193	<i>R</i> ₁ = 0.1135, w <i>R</i> ₂ = 0.4346	<i>R</i> ₁ = 0.1014, w <i>R</i> ₂ = 0.2736	<i>R</i> ₁ = 0.0907, w <i>R</i> ₂ = 0.2424
<i>R</i> indices (all data)	<i>R</i> ₁ = 0.1331, w <i>R</i> ₂ = 0.2602	<i>R</i> ₁ = 0.1184, w <i>R</i> ₂ = 0.4527	<i>R</i> ₁ = 0.1123, w <i>R</i> ₂ = 0.2901	<i>R</i> ₁ = 0.1237, w <i>R</i> ₂ = 0.2739
Largest diff peak and hole [e Å ⁻³]	0.41 and -0.41	0.52 and -0.31	1.89 and -2.49	4.56 and -1.81

5.3.2.4 Electronic absorption and Emission analyses

The steady state electronic absorption spectra of **38**, **38.2H⁺**, **39** and **40** were recorded in CH₂Cl₂ and shown in Figure 5.21 and their molar extinction coefficients were listed in table 5.2. The spectral pattern and the molar extinction coefficient values are in the order of 10⁴ reflects further the nonaromatic characteristic as observed in

contracted, normal and expanded *m*-benzporphyrinoids.¹¹ Compound **38** exhibits relatively two sharp absorption bands at 299 and 359 nm and a broad absorption band at 552 nm. In contrast, **38.2H⁺** shows two prominent absorption bands with almost an equal intensity at 347 and 664 nm, where the higher energy band is 112 nm bathochromically shifted with respect to **38** along with higher molar extinction coefficient. In **39**, two intense bands at 366 nm and 700 nm along with shoulder band at 656 nm are observed. The intense bands are bathochromically shifted and their molar extinction coefficient values are the highest as compared to **38**, **38.2H⁺** and **40**. In addition to these bands, a shoulder appeared at 656 nm. However, the compound **40** exhibited three broad bands at 309, 389 and 700 nm and a shoulder band at 495 nm.

The emission spectra of **38**, **39** and **40** were investigated in CH₂Cl₂ and shown in Figure 5.22. The ligand **38** and the complex **40** are weakly emissive, however, complex **39** is non-emissive. The compound **38** shows an emission maximum at 398 nm whereas **40** exhibits emission maxima at 370 and 414 nm. The fluorescence quantum yield (Φ_F) of **38** and **40** were found to be 0.003 and 0.001 respectively.

Table 5.2. Electronic absorption spectral data of **38**, **38.2H⁺**, **39** and **40** & emission spectral data of **38** and **40**

Compd. ^[a]	λ_{\max}/nm ($\epsilon/\text{M}^{-1}\text{cm}^{-1}$)	$\lambda_{\text{em}}/\text{nm}$	$\phi_f/\%$ ^[b]
38	299 (2.83), 359 (2.95), 552 (1.93)	398	0.3
38.2H⁺	347 (4.56), 664 (4.43)	---	---
39	366 (7.02), 656 (4.49), 710 (7.45)	---	---
40	309 (1.89), 389 (1.57), 495 (0.51), 700 (1.34)	370, 414	0.1

[a]Concentration $\approx 10^{-6}$ M; [b] quantum yield calculated with respect to 5,10,15-

tetraphenylporphyrin.

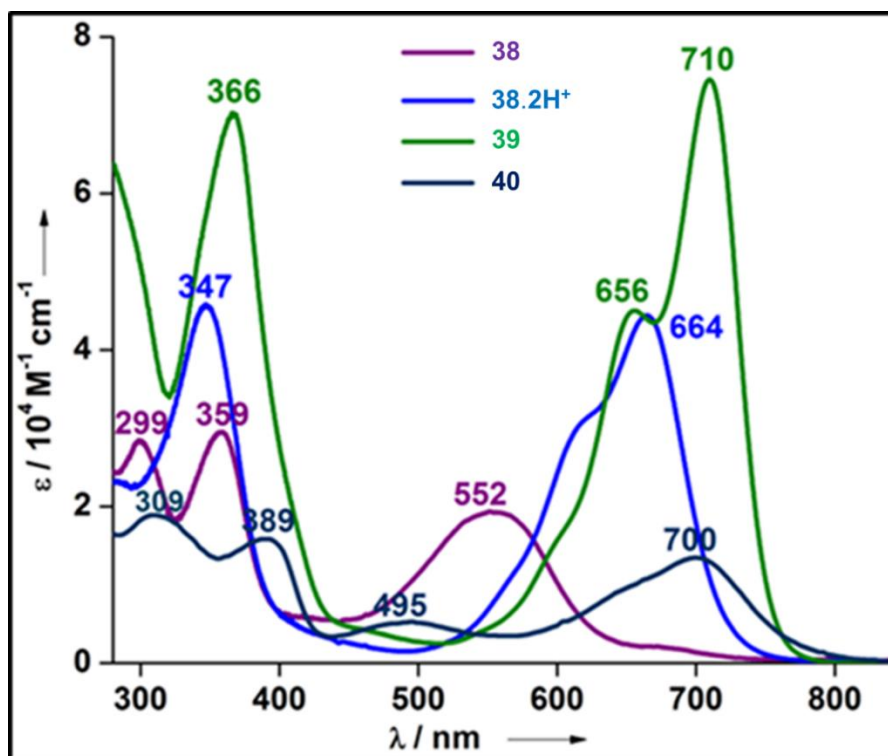


Figure 5.21: The electronic absorption spectra of **38**, **38.2H⁺**, **39** and **40** in CH₂Cl₂.

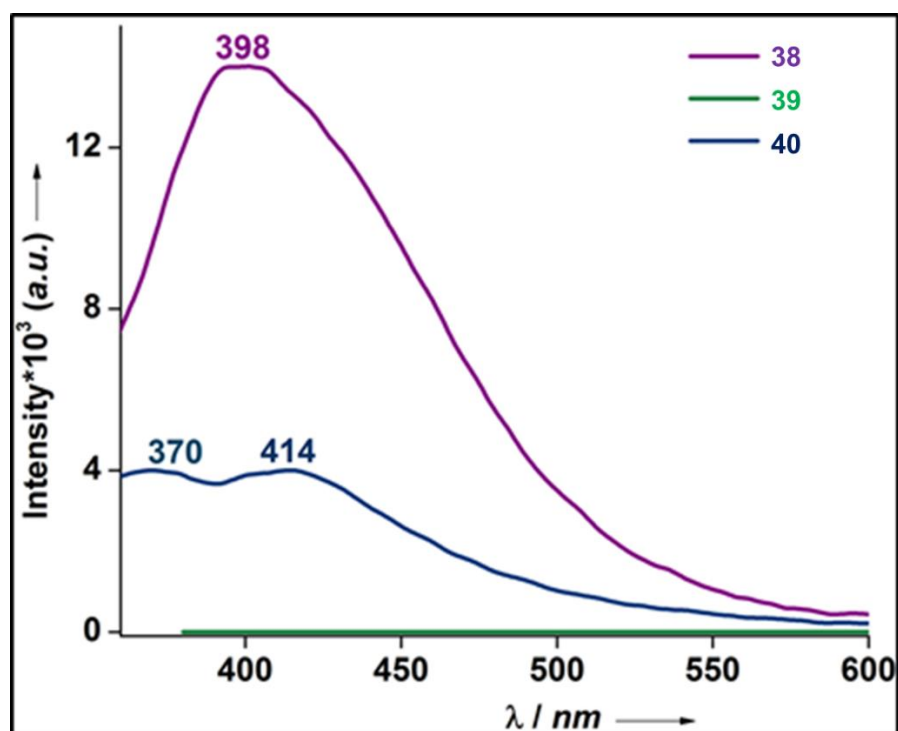


Figure 5.22: The emission spectra of **38** and **40** in CH₂Cl₂.

5.3.2.5 Electrochemical properties

The electrochemical properties of **38** – **40** were investigated by cyclic voltammetry (CV) and differential pulse voltammetry (DPV) in a CH₂Cl₂ solution containing 0.1 M tetrabutylammonium hexafluorophosphate (TBAPF₆) (Figure 5.25) and their electrochemical potentials were listed in table 5.3. Four irreversible oxidation waves at 0.14, 0.27, 0.58 and 0.70 V and a quasi-reversible reduction wave at -1.68 V were observed for **38**. On the other hand, complex **39** exhibited three quasi-reversible oxidation waves at 0.05, 0.28 and 0.23 V and an irreversible and a quasi-reversible reduction waves at -1.68 and -1.75 V respectively. To our surprise, the first reduction potential in **39** was same as observed in **38** and its oxidation potential was positively shifted only by 0.01 V suggested that the redox process in **39** is ligand centered rather than metal centered. As compared to **38** and **39**, the electrochemical potential values were different for **40**. The first reduction and the second oxidation waves were reversible and appeared at -1.60 and 0.10 V respectively. Whereas the second reduction appeared as a quasi-reversible wave at -1.75 V which is consistent with the reduction of heteroaromatic ring of cyclometalated-Pt^{II} complexes. All other oxidation processes were irreversible and appeared at -0.18, 0.42 and 0.68 V. Eventually, the electrochemical HOMO-LUMO gap (ΔE_{H-L}) of **38**, **39** and **40** were found to be 1.82, 1.73 and 1.41 V. The abrupt change in ΔE_{H-L} of **40** might be accounted for the sigma donation from carbon atom of the cyclometalated ligand to Pt^{II} which uplifts the energy level of HOMO.

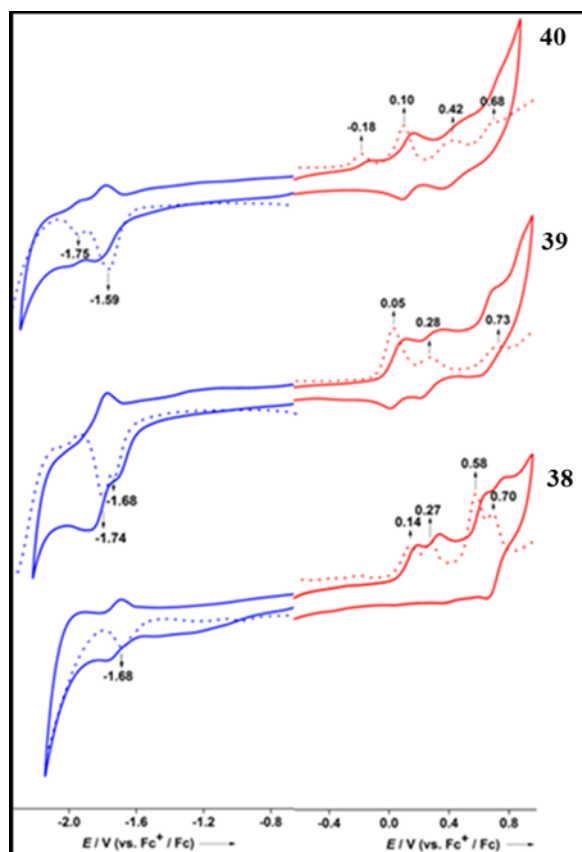


Figure 5.23: Cyclic (—) and differential pulse (....) voltammograms of **38**, **39** and **40**.

Table 5.3. Electrochemical data of **38**, **39** and **40**

Compound	E_{ox4}	E_{ox3}	E_{ox2}	E_{ox1}	E_{red1}	E_{red2}	$\Delta E_{HL}(eV)$
38	0.68	0.42	0.10	-0.18	-1.56	-1.75	1.41
39	...	0.73	0.28	0.05	-1.68	-1.74	1.73
40	0.70	0.58	0.27	0.14	-1.68	...	1.82

5.4 Conclusion

In summary, we have successfully demonstrated the synthesis, spectral and structural characterization of arene and pyridyl unit incorporated isosmaragdyrin [1.1.1.0.0]. To the best of our knowledge, this is the first stable isosmaragdyrin in the freebase form. The bimodular N_3C_2 core was further explored for coordination chemistry, where the trifluoroacetate anion is stabilized upon protonation and Rh(I) and organo-Pt(II) complexes are inserted upon metalation. The spectral analyses revealed the nonaromatic characteristic in all the compounds and further confirmed by crystal

analyses. Finally, the electrochemical studies revealed that the redox process was of ligand centered rather than metal upon Rh(I) ion insertion, whereas the influence of M-C bond was observed from Pt(II) complex.

5.5 Experimental Section

5.5.1 General Information

The reagents and materials for the synthesis were used as obtained from Sigma Aldrich chemical suppliers. All solvents were purified and dried by standard methods prior to use. The NMR solvents were used as received and the spectra were recorded in Bruker 400 MHz and 700 MHz spectrometer with TMS as an internal standard. The ESI mass spectra were recorded in Bruker, micro-TOF-QII mass spectrometer. The Electronic absorption spectra were recorded in Jasco V-730 UV-Visible spectrophotometer. The X-ray quality crystals for the compounds were grown by slow diffusion of *n*-pentane over CH₂Cl₂ solution. Single-crystal X-ray diffraction data of **38**, **38.2H⁺**, **39** and **40** were collected in a Rigaku Oxford diffractometer. Fluorescence quantum yields were determined by using *meso*-tetraphenylporphyrin (TPPH₂) ($\Phi_f = 0.11$) as a reference.

5.5.2 Synthesis and spectral characterization

5.5.2.1 Synthesis of 41: 2,6 dibromo pyridine (3 gm, 12.6 mmol) and 3 formyl phenyl boronic acid (4.7 gm, 31.6 mmol) was dissolved in 3:1 (V/V) THF and water solvents mixture under nitrogen atmosphere. K₂CO₃ (8.7 gm, 63 mmol) was immediately added to the reaction mixture and purged with for about 15 minutes. Pd(Ph₃P)₄ (1.16 gm, 1 mmol) was added under nitrogen atmosphere. The reaction was kept for 8 hours then work up was performed. The compound was purified by column chromatography using

silica gel (100-200 mesh) in Hexane / EtOAc (70:30) mixture to afford white crystalline solid **41** in 85% Yield.

¹H NMR (700 MHz, CDCl₃, 298K): δ = 10.15 (s, 2H), 8.62 (s, 2H), 8.48 (d, J = 7.7 Hz, 2H), 7.97 (d, J = 7.5 Hz, 2H), 7.92 (t, J = 7.8 Hz, 1H), 7.83 (d, J = 7.8 Hz, 2H), 7.70 (t, J = 7.6 Hz, 2H).

¹³C NMR (176 MHz, CDCl₃): δ = 192.43, 155.80, 140.24, 138.22, 137.01, 133.06, 130.43, 129.69, 128.24, 119.60.

ESI-MS: m/z calculated for C₁₉H₁₃NO₂ = 287.0946; found = 288.1048 (M+1).

5.5.2.2 Synthesis of 42: The compound **41** (1.5 gm, 5.2 mmol) was dissolved in toluene under nitrogen atmosphere. Freshly prepared solution of mesityl magnesium bromide was added dropwise in ice bath condition. Then the reaction was refluxed overnight. The reaction mixture was quenched with 2N HCl and work up was performed, dried by sodium sulphate and purified by column chromatography using silica gel (100-200 mesh) in Hexane / EtOAc (70:30) to afford **42** in 65% yield.

¹H NMR (700 MHz, CDCl₃, 298K): δ = 8.13 (s, 2H), 8.02 (d, J = 7.6 Hz, 2H), 7.76 (t, J = 7.7 Hz, 1H), 7.64 (d, J = 7.8 Hz, 2H), 7.40 (t, J = 7.7 Hz, 2H), 7.23 (t, J = 6.5 Hz, 2H), 6.88 (s, 4H), 6.41 (s, 2H), 2.38 (s, 2H), 2.29 (s, 18H).

¹³C NMR (176 MHz, CDCl₃): δ = 156.84, 143.63, 139.40, 137.42, 137.36, 137.10, 136.43, 130.10, 128.57, 126.93, 126.19, 125.39, 124.15, 118.77, 71.13, 20.92, 20.71.

ESI-MS: m/z calculated for C₃₇H₃₇NO₂ = 527.2824; found = 528.2903 (M+1).

5.5.2.3 Synthesis of 43: The compound **42** (0.500gm, 0.90 mmol) was dissolved in DCE under nitrogen atmosphere. Pyrrole (6.2 ml, 90 mmol) was added to the solution and allowed to stir for 10 minutes. Then BF₃.OEt₂ (0.702ml, 5.68 mmol) was slowly added and reaction mixture was allowed to reflux for 8 hours. Further workup was performed using CH₂Cl₂ and water, dried by sodium sulphate and purified by column

chromatography using silica gel (100-200 mesh) in Hexane / EtOAc (90:10) to afford **43** in 37% yield.

¹H NMR (700 MHz, CDCl₃, 298K): δ = 8.01 (d, J = 7.7 Hz, 2H), 7.98 (s, 2H), 7.86 (s, 2H), 7.73 (t, J = 7.8 Hz, 1H), 7.57 (d, J = 7.8 Hz, 2H), 7.40 (t, J = 7.7 Hz, 2H), 7.23 (d, J = 7.6 Hz, 2H), 6.89 (s, 4H), 6.69 (s, 2H), 6.17 (d, J = 4.6 Hz, 2H), 6.02 (s, 2H), 5.90 (s, 2H), 2.30 (s, 6H), 2.09 (s, 12H).

¹³C NMR (176 MHz, CDCl₃): δ = 156.78, 141.67, 139.55, 137.79, 136.41, 135.76, 132.98, 130.39, 129.39, 128.83, 127.44, 125.27, 118.71, 116.46, 108.49, 107.51, 44.88, 21.26, 20.92.

ESI-MS: m/z calculated for C₄₅H₄₃N₃ = 625.3457; found = 626.3521 (M+1).

5.5.2.4 Synthesis of 38: The compound **43** (0.150gm, 0.24 mmol) was mixed in 120 ml CH₂Cl₂ under nitrogen atmosphere covered with aluminum foil. Pentafluorobenzaldehyde (0.061gm, 0.311 mmol) was added in the reaction mixture and allowed to stir. After 10 minutes *p*-TSA (0.020 gm, 0.119 mmol) was added under same condition and allowed to stir for about 6 hours. Then DDQ (0.163 gm, 0.718 mmol) was added and reaction was continued for another 2 hour in absence of nitrogen atmosphere. The crude product was passed through basic alumina and purified by using silica gel column (100-200 mesh). The purple color band was eluted with CH₂Cl₂ / Hexane (60:40) and identified as **38** in 15% yield.

¹H NMR (400 MHz, CD₂Cl₂, 298K): δ = 9.01 (s, 2H), 7.91 (t, J = 7.8 Hz, 1H), 7.78 (d, J = 7.7 Hz, 2H), 7.74 (d, J = 7.8 Hz, 2H), 7.35 (t, J = 7.8 Hz, 2H), 6.92 (s, 4H), 6.90 (s, 2H), 6.47 (d, J = 5.2 Hz, 2H), 6.08 (d, J = 5.1 Hz, 2H), 2.32 (s, 6H), 2.03 (s, 12H).

¹³C NMR (100 MHz, CD₂Cl₂): δ = 160.64, 157.34, 152.04, 149.93, 142.69, 139.62, 138.84, 138.13, 137.57, 137.45, 137.24, 135.12, 130.12, 129.06, 128.75, 128.37, 128.16, 125.66, 123.88, 123.47, 119.39, 115.79, 31.33, 29.69, 29.66, 29.37, 29.34.

ESI-MS: m/z calculated for $C_{52}H_{38}F_5N_3 = 799.2986$; found = 800.3090 [M+1].

UV-Vis (CH₂Cl₂): $\lambda_{\max}(\text{nm})$ ($\epsilon[M^{-1}\text{cm}^{-1}]$) = 299 (2.83×10^4), 359 (2.95×10^4), 552 (1.93×10^4).

5.5.2.5 38.2H⁺: ¹H NMR (400 MHz, CD₂Cl₂, 298K): $\delta = 14.58$ (s, 1H), 12.47 (s, 2H), 8.97 (s, 2H), 8.55 (t, $J = 7.9$ Hz, 1H), 8.17 (d, $J = 7.9$ Hz, 1H), 7.98 (s, 1H), 7.57 (t, $J = 7.6$ Hz, 2H), 7.28 (s, 1H), 7.20 (d, $J = 7.7$ Hz, 2H), 7.05 (d, $J = 7.8$ Hz, 1H), 6.97 (s, 2H), 6.65 (d, $J = 5.0$ Hz, 2H), 6.60 (s, 2H), 6.21 (d, $J = 5.0$ Hz, 2H), 2.33 (s, 6H), 2.01 (s, 6H), 1.39 (s, 6H).

UV-Vis (CH₂Cl₂): $\lambda_{\max}(\text{nm})$ ($\epsilon[M^{-1}\text{cm}^{-1}]$) = 347 (4.56×10^4), 664 (4.43×10^4).

5.5.2.6 Synthesis of 39: The compound **38** (0.010 gm, 0.001 mmol) was dissolved in 20 ml *p*-xylene under nitrogen atmosphere. The solution was purged with nitrogen for 10 minutes. [Rh(CO)₂Cl]₂ (20 mg, 0.028 mmol) was added to it. The reaction was continued to reflux for overnight. The crude product was purified using neutral alumina column in CH₂Cl₂ / CH₃OH (90:10) to obtain green fraction. The green crystals were identified as **39** in 7% yield.

¹H NMR (400 MHz, CD₂Cl₂, 298K): $\delta = 9.76$ (s, 2H), 7.92 (t, $J = 7.7$ Hz, 1H), 7.65 (d, $J = 7.7$ Hz, 2H), 7.40 (d, $J = 7.6$ Hz, 2H), 7.21 (t, $J = 7.7$ Hz, 2H), 6.99 (s, 2H), 6.87 (s, 2H), 6.78 (d, $J = 8.0$ Hz, 2H), 6.42 (d, $J = 5.3$ Hz, 2H), 5.97 (d, $J = 5.3$ Hz, 2H), 2.34 (s, 6H), 2.33 (s, 6H), 1.72 (s, 6H).

¹³C NMR (100 MHz, CD₂Cl₂): $\delta = 141.30$, 141.25, 140.22, 138.69, 137.65, 137.48, 137.25, 136.88, 131.45, 129.87, 128.63, 128.21, 128.09, 127.43, 118.27, 20.79, 20.37, 19.56.

ESI-MS: m/z calculated for $C_{54}H_{37}F_5N_3O_2Rh = 957.1861$; found = 958.1914 [M+1].

UV-Vis (CH₂Cl₂): $\lambda_{\max}(\text{nm})$ ($\epsilon[M^{-1}\text{cm}^{-1}]$) = 366 (7.02×10^4), 656 (4.49×10^4), 710 (7.45×10^4).

5.5.2.7 Synthesis of 40: The compound **38** (0.010 gm, 0.0126 mmol) was dissolved in 15 ml of dry chlorobenzene in nitrogen atmosphere. PtCl₂ (0.017 gm, 0.063 mmol) was added into the reaction mixture and refluxed for 24 hours under nitrogen atmosphere. The crude reaction mixture was rotary evaporated and subjected to neutral alumina column chromatography. The blue fraction was eluted with CH₂Cl₂/ hexane (1:9) and recrystallized from CH₂Cl₂/ hexane to obtain **40** in 67% yield.

¹H NMR (400 MHz, CD₂Cl₂, 298K): δ = 11.96 (s, 1H), 8.53 (s, 1H), 7.97 (t, J = 7.7 Hz, 1H), 7.86 (d, J = 7.0 Hz, 1H), 7.74 (d, J = 8.0 Hz, 1H), 7.65 (d, J = 7.1 Hz, 1H), 7.54 (d, J = 7.7 Hz, 1H), 7.44 (d, J = 6.2 Hz, 1H), 7.14 (d, J = 7.7 Hz, 1H), 7.07 (d, J = 7.6 Hz, 1H), 7.03 (s, 1H), 6.98 (s, 1H), 6.93 (s, 1H), 6.88 (s, 1H), 6.82 (d, J = 7.8 Hz, 1H), 6.69 (d, J = 5.3 Hz, 1H), 6.49 (d, J = 4.0 Hz, 1H), 6.19 (d, J = 5.2 Hz, 1H), 5.95 (d, J = 5.1 Hz, 1H), 2.35 (s, 3H), 2.32 (s, 3H), 2.26 (s, 3H), 2.03 (s, 3H), 2.00 (s, 3H), 1.88 (s, 3H).

¹³C NMR (100 MHz, CD₂Cl₂): δ = 167.03, 141.66, 141.24, 138.58, 138.27, 137.95, 137.71, 136.46, 135.22, 134.98, 134.15, 132.70, 130.42, 129.98, 129.81, 129.00, 128.46, 128.41, 128.16, 128.01, 127.81, 127.35, 125.34, 124.43, 123.79, 117.92, 20.84, 20.50, 20.40, 19.51, 19.36.

ESI-MS: m/z calculated for C₅₄H₃₇F₅N₃ClPt = 993.2555 (M-Cl); found = 992.2532 [M-Cl].

UV-Vis (CH₂Cl₂): λ_{\max} (nm) (ϵ [M⁻¹cm⁻¹]) = 309 (1.89 × 10⁴), 389 (1.57 × 10⁴), 495 (0.51 × 10⁴), 700 (1.34 × 10⁴).

5.6 Reference

1. R. B. Woodward, Aromaticity Conference, Sheffield, UK, **1966**.
2. H. Rexhausen, A. Gossauer, *J. Chem. Soc., Chem. Commun.* **1983**, 275.
3. T. Chatterjee, A. Srinivasan, M. Ravikanth, T. K. Chandrashekar. *Chem. Rev.*

-
- 2017, *117*, 3329–3376.
4. J.-Y. Shin, H. Furuta, A. Osuka, *Angew. Chem. Int. Ed.* **2001**, *40*, 619-621.
 5. J. L. Sessler, J. M. Davis, *Acc. Chem. Res.* **2001**, *34*, 989–997.
 6. J. L. Sessler, M. J. Cyr, V. Lynch, *J. Am. Chem. Soc.* **1990**, *112*, 2810.
 7. P. J. Chmielewski, L. L.-Grażynski, K. Rachlewicz, *Chem. - Eur. J.* **1995**, *1*, 68–73.
 8. S. J. Narayanan, B. Sridevi, A. Srinivasan, T. K. Chandrashekar, R. Roy, *Tetrahedron Lett.* **1998**, *39*, 7389–7392.
 9. D. T. Richter, T. D. Lash, *J. Org. Chem.* **2004**, *69*, 8842–8850.
 10. S. Kumar, K. G. Thorat, M. Ravikanth, *J. Org. Chem.* **2019**, *84*, 417–422.
 11. M. J. Broadhurst, R. Grigg, A. W. Johnson, *J. Chem. Soc., Perkin I*, **1972**, *1*, 2111–2116.
 12. S. J. Narayanan, B. Sridevi, T. K. Chandrashekar, U. Englisch, K. R. -Senge, *Org. Lett.* **1999**, *1*, 587–590.
 13. D. Xie, Y. Liu, Y. Rao, G. Kim, M. Zhou, D. Yu, L. Xu, B. Yin, S. Liu, T. Tanaka, N. Aratani, A. Osuka, Q. Liu, D. Kim, J. Song, *J. Am. Chem. Soc.* **2018**, *140*, 16553–16559.
 14. J. L. Sessler, D. Seidel, C. Bucher, V. N. Lynch, *Tetrahedron*, **2001**, *57*, 3743–3752.
 15. J. L. Sessler, J. M. Davis, V. Lynch, *J. Org. Chem.* **1998**, *63*, 7062–7065.
 16. R. Sengupta, K. G. Thorat, M. Ravikanth, *J. Org. Chem.* **2018**, *83*, 11794–11803.
-

CHAPTER 6

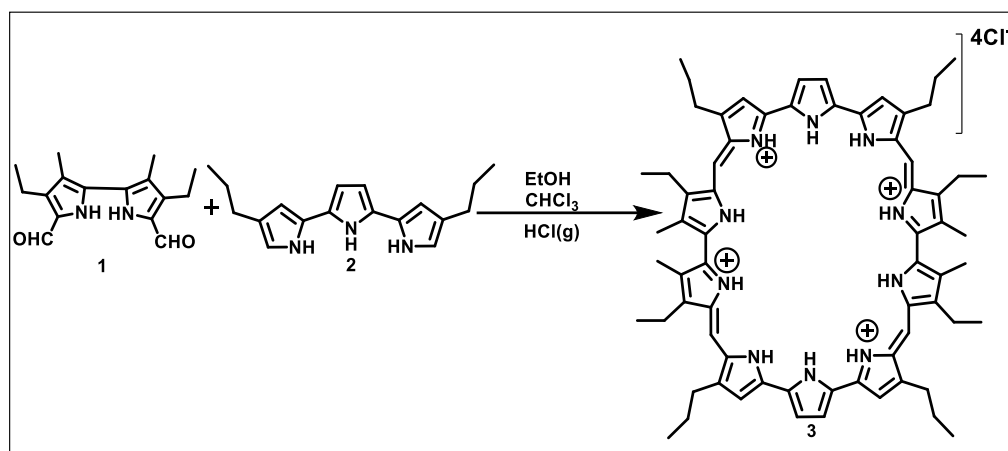
Di-(*m-m-m*)terphenyl-Embedded Decaphyrin and Its Bis-Rh(I) Complex

6.1	Introduction	156
6.2	Objective of our work	159
6.3	Results and discussions	159
6.3.1	Synthesis	159
6.3.2	Spectral characterisation	160
6.3.2.1	Mass spectrometric analyses	160
6.3.2.2	NMR Analysis	161
6.3.2.3	Single crystal X-ray structure and analyses of 14 and 15	163
6.3.2.4	Electronic absorption spectral analysis	171
6.4	Conclusion	171
6.5	Experimental Section	172
6.5.1	General Information	172
6.6	Synthetic procedure and spectral characterization of 14-16	172
6.7	Reference	175

6.1 Introduction

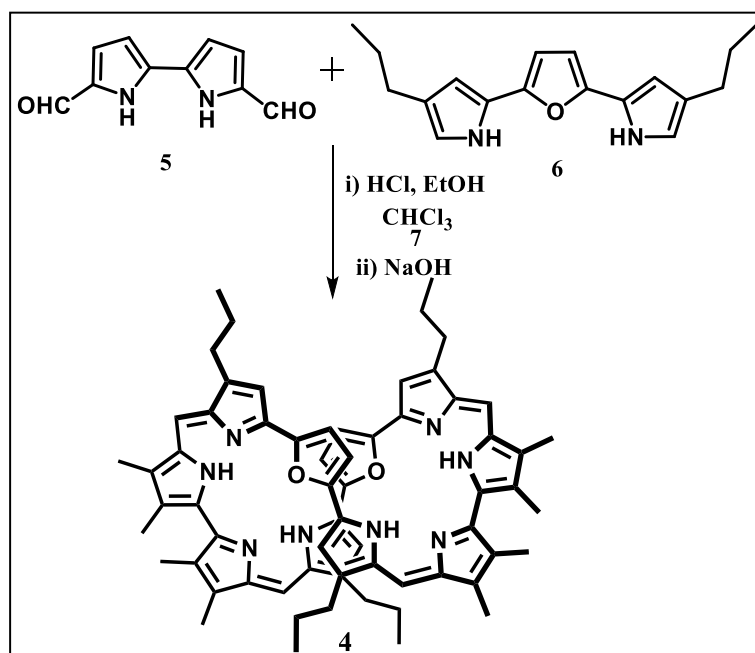
Decaphyrin is an expanded porphyrin analogue in which ten hetero-/carbocyclic rings are connected with or without *meso* carbon bridges. Expanded porphyrins with eight pyrrole / heterocyclic rings are well documented in literature, however, the higher analogues are hardly reported due to synthetic difficulties, conformation flexibilities and stability.

The first decaphyrin, turcasarin, a [40]decaphyrin[1.0.1.0.0.1.0.1.0.0] (**3**) was reported by Sessler and co-workers.¹ The compound **3** was synthesized by acid-catalyzed condensation of 4,4-diethyl-5.5'-diformyl-3,3'-dimethyl-2,2'-bipyrrole (**1**) with 2,5-bis(4-propyl-2-pyrrolyl)pyrrole (**2**) in the presence of HCl (Scheme 6.1). ¹H NMR analysis of **3** revealed nonaromatic character of the crystal analysis confirmed that **3** owned twisted "figure-eight" conformation with C₂-symmetry.



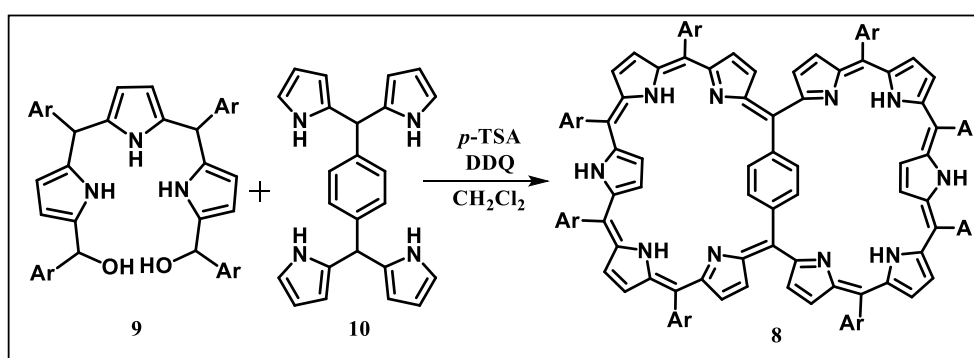
Scheme 6.1: Synthesis of turcasarin (**3**).

The same group also demonstrated the synthesis of respective core-modified analogue. The synthesis of di-oxa derivative of turcasarin (**4**) was shown in Scheme 6.2. The compound **4** was achieved by HCl acid-catalyzed condensation of 5.5'-diformyl-2,2'-bipyrrole (**5**) with 2,5-bis(4-propyl-2-furanyl)pyrrole (**6**). As observed in **3**, the macrocycle (**4**) also adopted figure-eight conformation in the solid state.²



Scheme 6.2: Synthesis of dioxo-turcasarin (4).

Afterwards the synthetic endeavor was diverted to achieve planar decaphyrin in lieu of figure-eight conformation. The first planar octaphyrin (8) was reported by Osuka and coworkers by introducing a bridging moiety inside the macrocyclic core. The planar molecule was synthesized by acid-catalyzed condensation followed by oxidation between tripyrro-methane diol (9) and two equivalents of 1,4-phenyldipyrrromethane (10) (Scheme 6.3).³

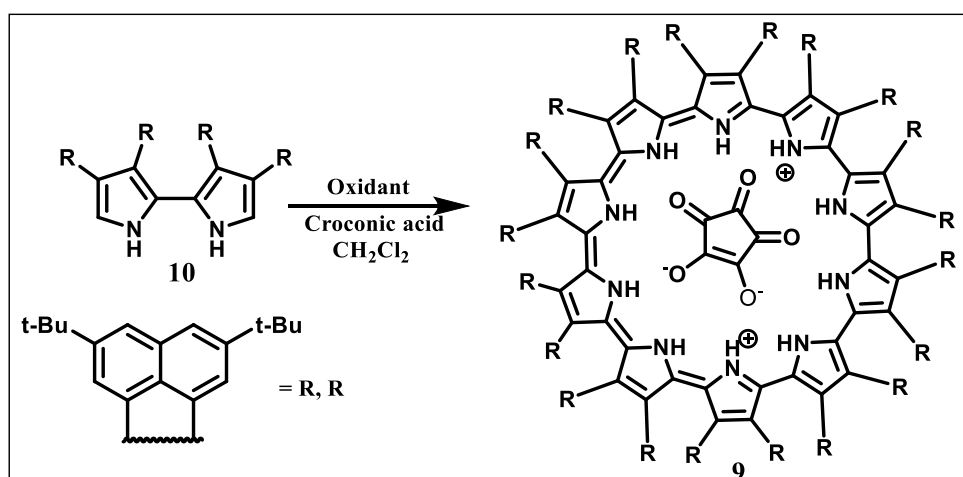


Scheme 6.3: Synthesis of planar decaphyrin (8).

The crystal analysis of 8 revealed that the macrocycle adopted C₂-symmetric nonplanar structure, instead of regular figure-eight conformation. The introduction of phenylene

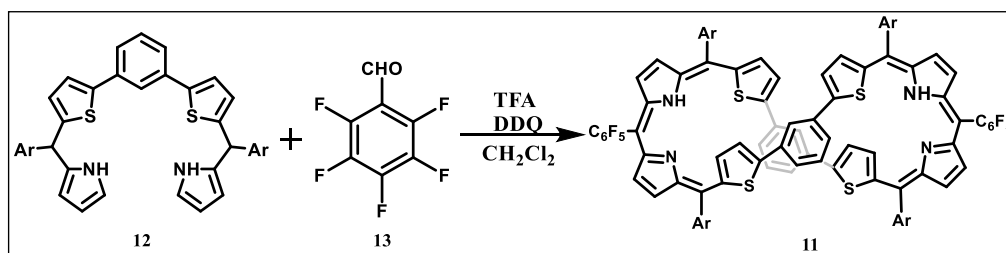
bridge inside the core led to substantially influence the structural as well as electronic properties.

In porphyrinoids, the pyrrole units are mainly connected with *meso*-carbon bridges. In expanded porphyrin, pyrrole units in the core was not connected with *meso*-carbon units. The first *meso*-free decaphyrin (**9**) was synthesized by T. Okujima and coworkers.⁴ The cyclo[10]pyrrole (**9**) was achieved by croconic acid-catalyzed oxidative coupling of acenaphthylene ring appended bipyrrole unit, where the croconate dianion played as template (Scheme 6.4). The crystal analysis proved the binding of croconate dianion. In addition, the absence of *meso*-atoms resulted the saddle type conformation in the solid state.



Scheme 6.4: Template Synthesis of decaphyrin (**9**).

The arene ring incorporated core-modified decaphyrin, dibenzidecacphyrin (1.1.1.0.0.1.1.1.0.0.0) (**11**) and its Bis-BF₂ complexes was reported by Ravikanth and coworkers (Scheme 6.5).⁵ The compound **11** was synthesized by TFA acid-catalyzed condensation followed by oxidation of *m*-phenylene based pentapyrrane (**12**) with pentafluorobenzaldehyde (**13**). The figure-eight conformation was reflected from the single crystal X-ray analysis of **11**.



Scheme 6.5: Synthesis of decaphyrin (**11**).

6.2 Objective of our work

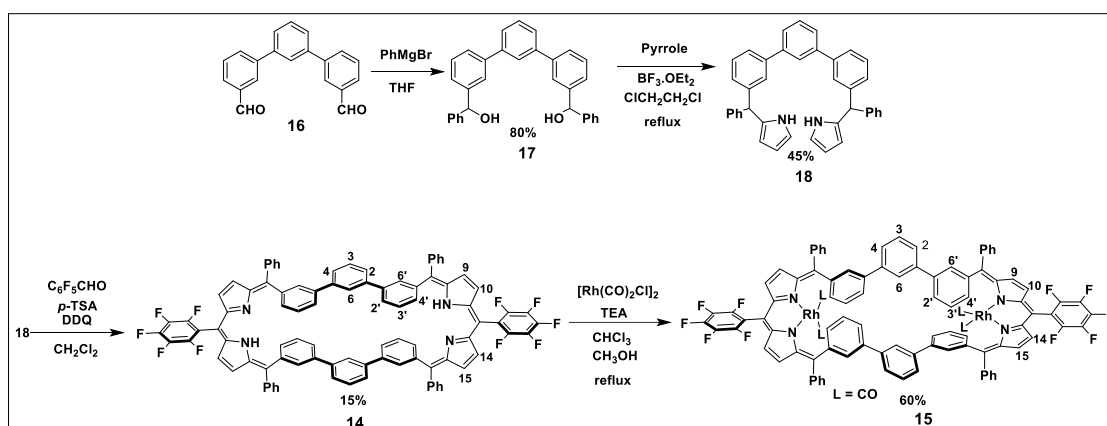
From the literature reports, the decaphyrin mainly adopts figure-eight conformation. In order to avoid such flexible conformation, the researchers introduced (a) insertion of bridging unit between the *meso*-carbon atoms and (ii) reduction of number of *meso*-carbon units in the macrocyclic framework. Further, the coordination chemistry of these macrocycles is scarcely reported. To explore such chemistry in open framework decaphyrin is hitherto unknown in the literature. In addition, though variety of expanded carba porphyrinoids are known, however, only two reports on decacarbaporphyrinoids are reported in the literature. Hence, the main objective of this chapter is to (i) introduce higher arene units in order to achieve an open framework in the decaphyrin macrocycle (**14**) and (ii) also explore its coordination chemistry (**15**).⁶

6.3 Results and discussions

6.3.1 Synthesis

The starting material terphenyl dicarbaldehyde **16** was synthesized as per the reported procedure.⁷ By using freshly prepared phenylmagnesium bromide in dry THF, compound **16** is converted into respective diol **17** in 80% yield. The final precursor, terphenyl dipyrromethane **18**, is synthesized in 45% yield by Lewis acid catalyzed condensation of diol **17** with pyrrole in dichloroethane under reflux condition. The final target macrocycle **14** was achieved by [5 + 5] acid-catalyzed condensation of **18** with

2,3,4,5,6-pentafluoro benzaldehyde in the presence of *p*-toluenesulfonic acid (*p*-TSA) followed by oxidation with 2,3-dichloro-5,6-dicyano-1,4-benzoquinone (DDQ). The crude reaction mixture was purified by silica gel (100–200 mesh) column chromatography using CH₂Cl₂/*n*-hexane (1:4) as eluent and afforded **14** as blue crystalline solid in 15% yield. The coordination chemistry was performed by treating CHCl₃ solution of **14** with [Rh(CO)₂Cl]₂ salt in presence of triethylamine in CH₃OH, where the Rh(I) complex **15** was obtained in 60% yield (Scheme 6.6).



Scheme 6.6: Synthesis of **14** and **15**.

6.3.2 Spectral Characterization

6.3.2.1 Mass spectral analyses

The exact composition of **14** and **15** were confirmed by mass spectrometric analysis and exhibited a molecular ion signal at m/z : 1429.4235 [M+1] (**14**) (Figure 6.1) and 1744.1966 [M] (**15**) (Figure 6.2).

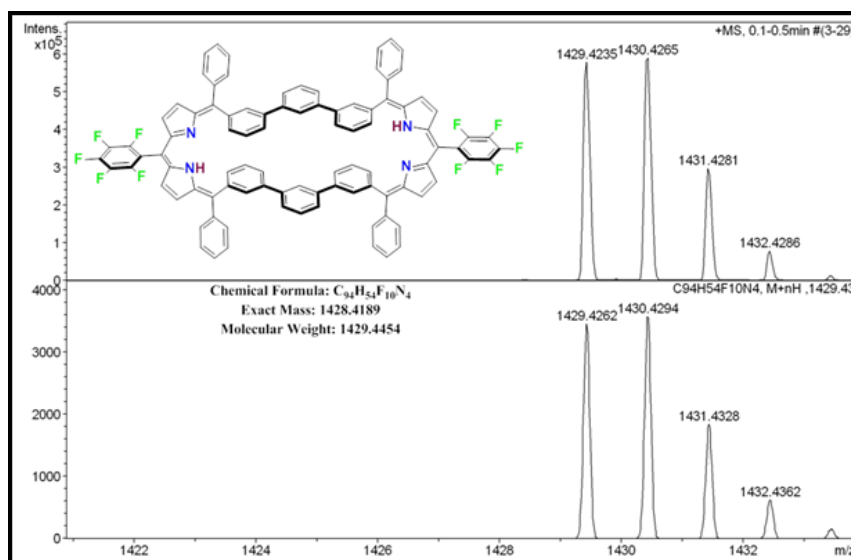


Figure 6.1: HR-MS spectrum of **14**.

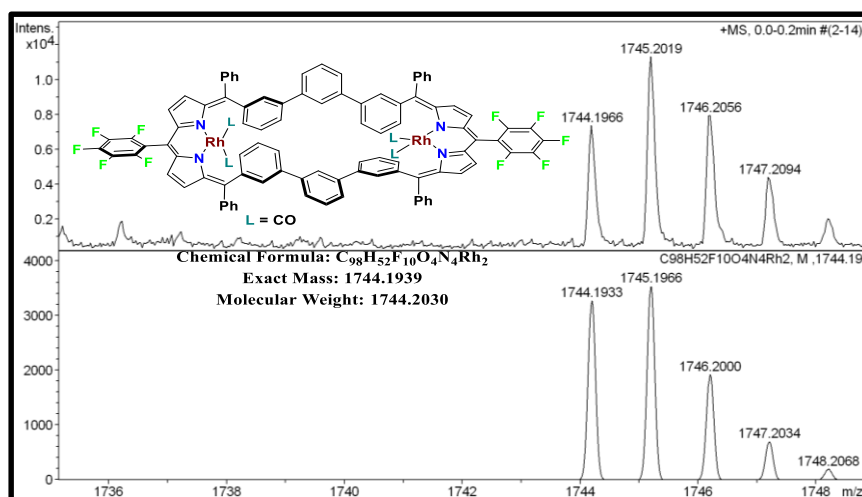


Figure 6.2: HR-MS spectrum of **15**.

6.3.2.2 NMR Analyses

The ^1H NMR spectrum of **14** is shown in Figure 6.3a. The macrocycle has C_{2h} symmetry and exhibits only half of the signals. The pyrrolic β -CH protons were resonated as a set of doublet at 6.23 ppm [H(9,15)] and 6.71 ppm [H(10,14)], whereas the NH was observed as a broad signal at 13.75 ppm and further confirmed by D_2O exchange experiment. The large deshielded NH signal suggests an intramolecular hydrogen bonding with the imine nitrogens. The terminal *m*-phenylene protons were

appeared as two well-separated doublets at 6.76 ppm [H(2')] & 8.01 ppm [H(4')] and a triplet, multiplet at 7.07 ppm [H(3')] and 7.31 ppm [H(6')], respectively. Whereas the middle *m*-phenylene protons were observed at 7.04 ppm [H(6)] as singlet, 7.52 ppm [H(4)] & 7.51 ppm [H(2)] as doublet and 7.48 ppm [H(3)] as triplet. Overall, the spectral pattern in **14** resembles typical nonaromatic characteristics as observed in *m*-benziporphyrinoids⁸ and its expanded analogues.^{5,9-11}

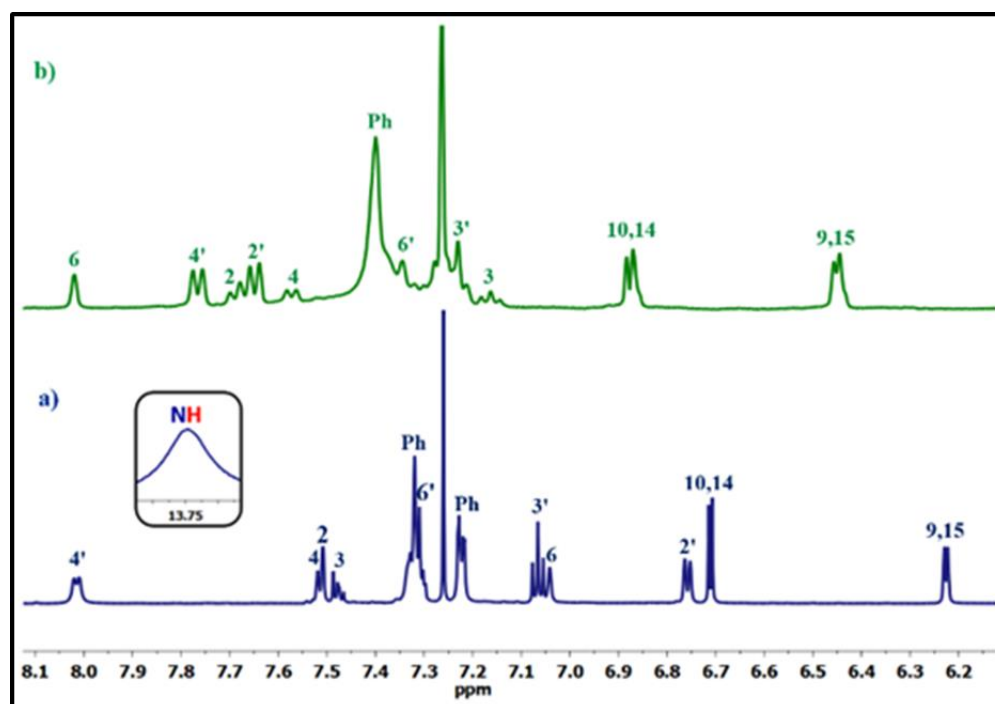


Figure 6.3: ^1H NMR spectra of **14** (a) and **15** (b) in CDCl_3 .

The absence of NH signal in the ^1H NMR spectral analysis proves the metal ion insertion in the dipyrromethene units of the macrocyclic framework (Figure 6.3b). Upon metal ion insertion, the pyrrolic β -CH protons [H(9,15) and H(10,14)], terminal [H(6',3',2')] and half of the middle *m*-phenylene CH [H(2,4)] protons are slightly deshielded, whereas the remaining half are moderately upfield shifted. The pyrrolic β -CH protons are resonated at 6.45 [H(9,15)] and 6.87 ppm [H(10,14)]. The terminal *m*-phenylene CH protons are observed at 7.65 [H(2')], 7.34 [H(6')], 7.76 [H(4')] and 7.22

ppm [H(3')], respectively. The middle *m*-phenylene CH protons are resonated at 7.57 [H(4)], 7.69 [H(2)], 8.02 [H(6)] and 7.16 ppm [H(3)]. Overall, the ^1H NMR spectral pattern of **15** maintains the nonaromatic characteristic even after metal ion insertion.

6.3.2.3 Single crystal X-ray analyses of **14** and **15**

The structure of **14** was determined through single crystal X-ray diffraction analysis (Figure 6.4a & c and Table 6.1). The compound crystallizes in monoclinic crystal lattice with $P2_1/n$ space group. The structure reveals that a set of *meso*-pentafluorodipyrromethene and terphenylene units are connected by *meso*-phenyl moieties and exhibited rectangular shape. The deshielded NH signal from spectral studies is reflected from crystal analysis with a strong intramolecular hydrogen bonding interaction between the pyrrolic amine NH (N1-H1/ N1'-H1') and imine nitrogen (N2/ N2') with bond distance and angle of 2.179(3) Å and 122.39 (1)° (N1-H1...N2/ N1'-H1'...N2'). The bond lengths within the *m*-phenylene ring of the terphenylene units are between 1.363(5) Å and 1.404(5) Å and are individually connected by $\text{sp}^2\text{-sp}^2$ single bond [1.494(4) Å & 1.491(5) Å] and rest of the macrocyclic framework [1.468(4) Å & 1.475(5) Å], thus maintains the individual aromatic character. Whereas, the effective π -delocalization is observed in the dipyrromethene unit with alternate $\text{sp}^2\text{-sp}^2$ single 1.458(5) Å and double 1.317(6) Å bond character (Figure 6.9). Overall, two individual aromatic characters combine together to generate nonaromatic character in the macrocyclic framework. The crystal analysis reveals that the terphenylene units are parallel to each other and separated with the distance of 5.167(2) Å (A...A') and 3.956(2) Å (B...B'). The pyrrole units are hardly deviated from the mean plane containing *meso*-carbon atoms (C7-C12-C17-C7'-C12'-C17') with a maximum deviation of 3.39(3)° (N2), whereas ring in the terphenylene units are deviated by

77.59(1)° (A & A') and 56.58(1)° (B & B'). Further, the macrocycle also generates series of arrays through C-H...F intermolecular interactions in the solid state (Figure 6.5-6.6).

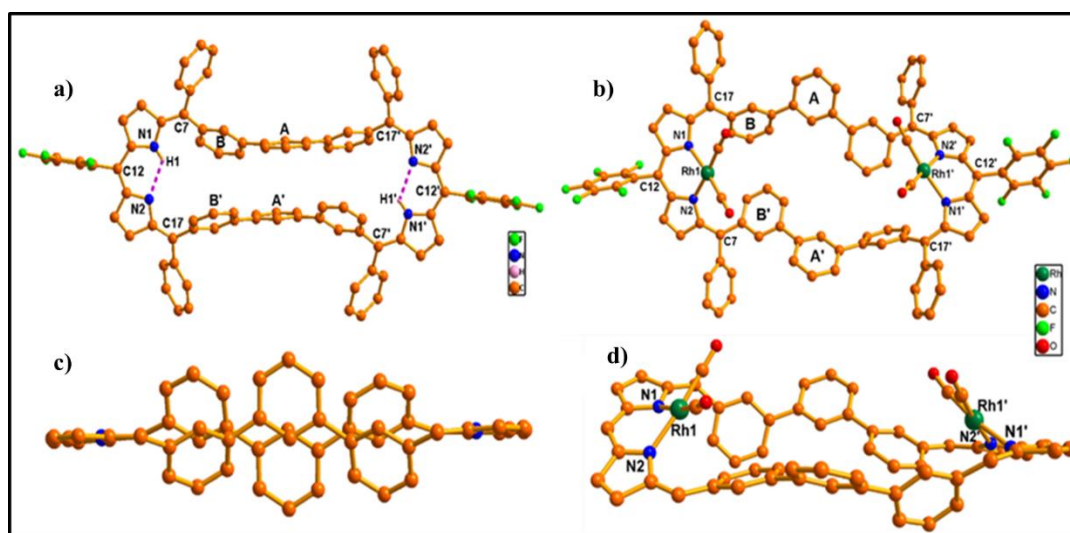


Figure 6.4: Single crystal X-ray structures of **14** and **15**. a) & b) Top views and c) & d) side views. Peripheral hydrogen atoms in a) & d) and *meso*-aryl groups in c) & d) are omitted for clarity.

The final proof for the proposed metal complex **15** has come from the single crystal X-ray structure as shown in (Figure 6.4b & d and Table 6.1). The complex crystallizes in triclinic crystal lattice with $C2/c$ space group. The geometry around the metal center is square planar where other two coordination sites are occupied by carbonyl ligands. As reflected from the spectral studies, two Rh^I ions are coordinated only with the dipyrromethene moieties. The bond lengths of Rh1-N1 / Rh2-N1' and Rh1-N2 / Rh2-N2' are 2.082(2) Å, 2.082(3) Å, which are longer than Rh(I) complex of tris-*p*-benzi nonaphyrin.¹² Both the Rh^I ion is 1.10 Å above the mean macrocyclic plane (C7-C12-C17-C7'-C12'-C17'). In order to accommodate the Rh(I) ion in the core, one of the terminal *m*-phenylenes (68.94°) [B] and the pyrrole units [17.81°(N1)] and [29.14°(N2)] are tilted away from the plane; whereas the middle *m*-phenylene [34.36° (A & A')] and remaining terminal *m*-phenylene units [16.75° (B')] are moved towards

the plane. In addition, the distance between the terphenylene units are higher [8.535(3) Å (A...A') and 5.012(2) Å (B...B')] as compared to **14**. As observed in **14**, there are only marginal difference in sp^2 - sp^2 double bond lengths in the terphenylene unit and sp^2 - sp^2 single and double bond character in the dipyrromethene unit (Figure 6.10), thus retains the nonaromatic character as such.

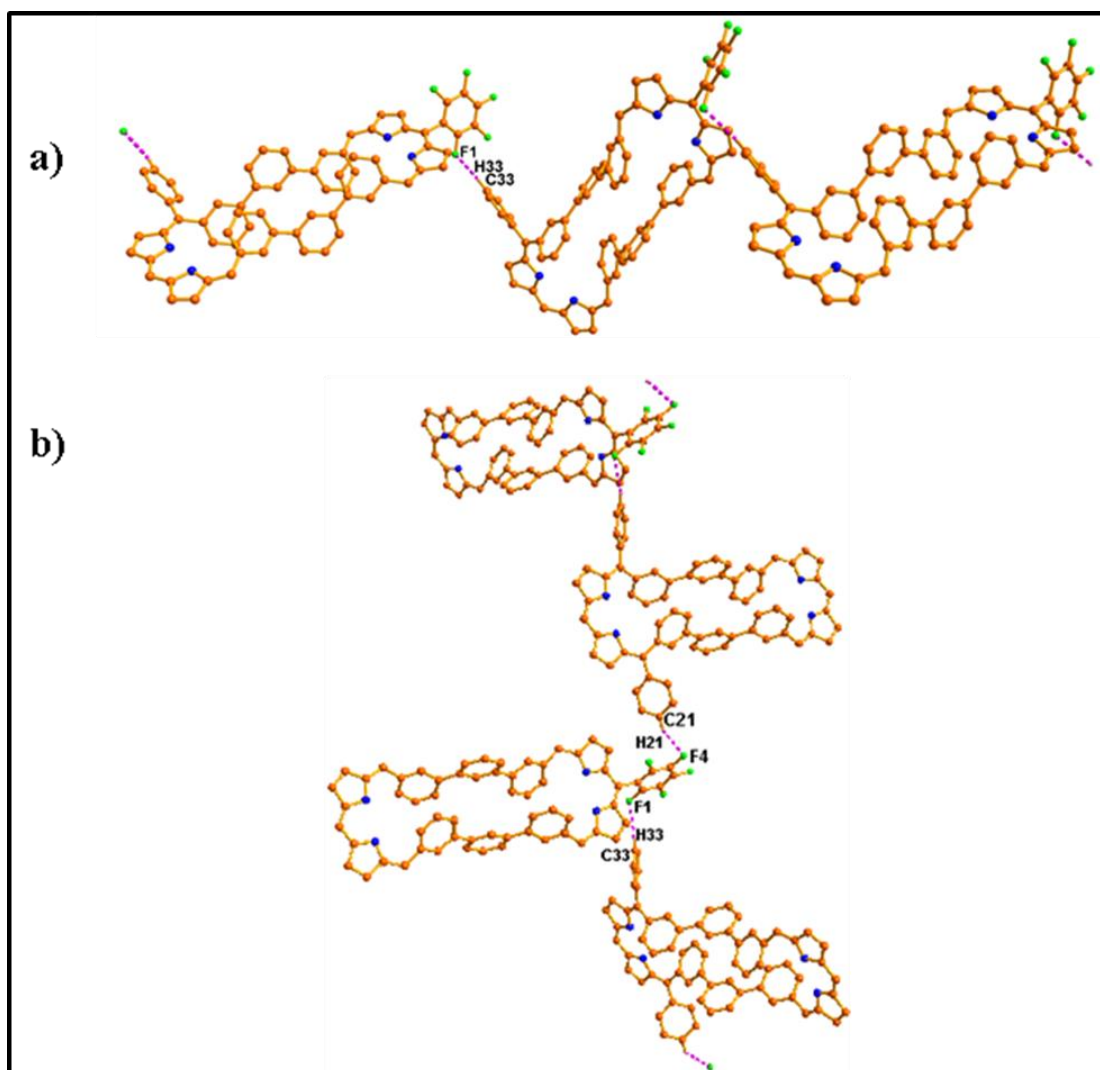


Figure 6.5: 1-D arrays of **14**. The bond distances and angles are: a) C33-H33...F1: 2.598(2) Å and 160.30(3)°; b) C21-H21...F4 2.632(3) Å and 135.35(3)° respectively. The hydrogen atoms and *meso*-aryl groups which are not in hydrogen bonding interactions are omitted for clarity.

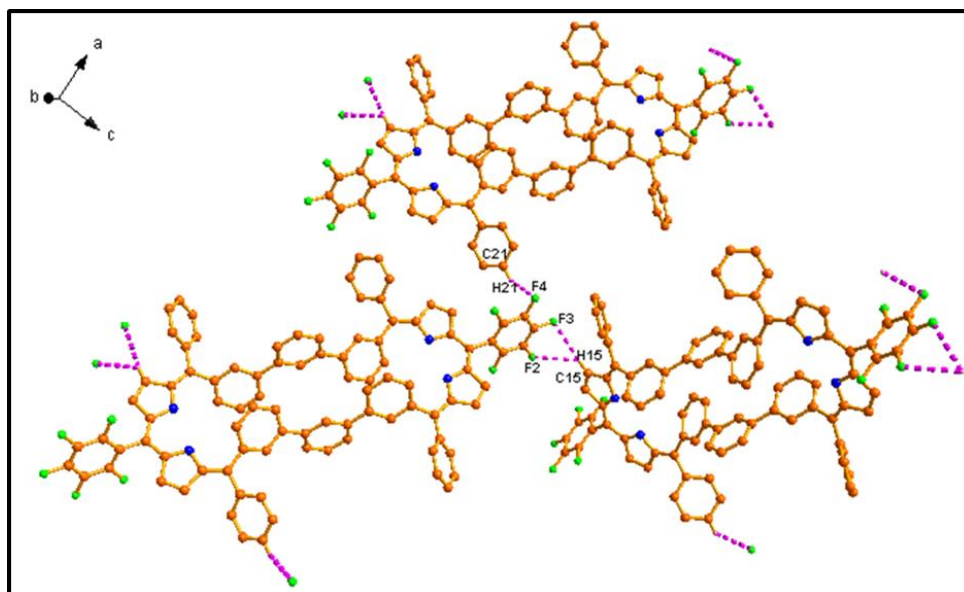


Figure 6.6: 3-D arrays of **14**. The bond distances and angles are C15-H15...F2: 2.865(3) Å and 128.23(2)°; C15-H15...F3 2.862(3) Å and 170.25(2)° ; C21-H21...F4 2.632(3) Å and 135.35(3)° respectively. The hydrogen atoms and *meso*-aryl groups which are not in hydrogen bonding interactions are omitted for clarity.

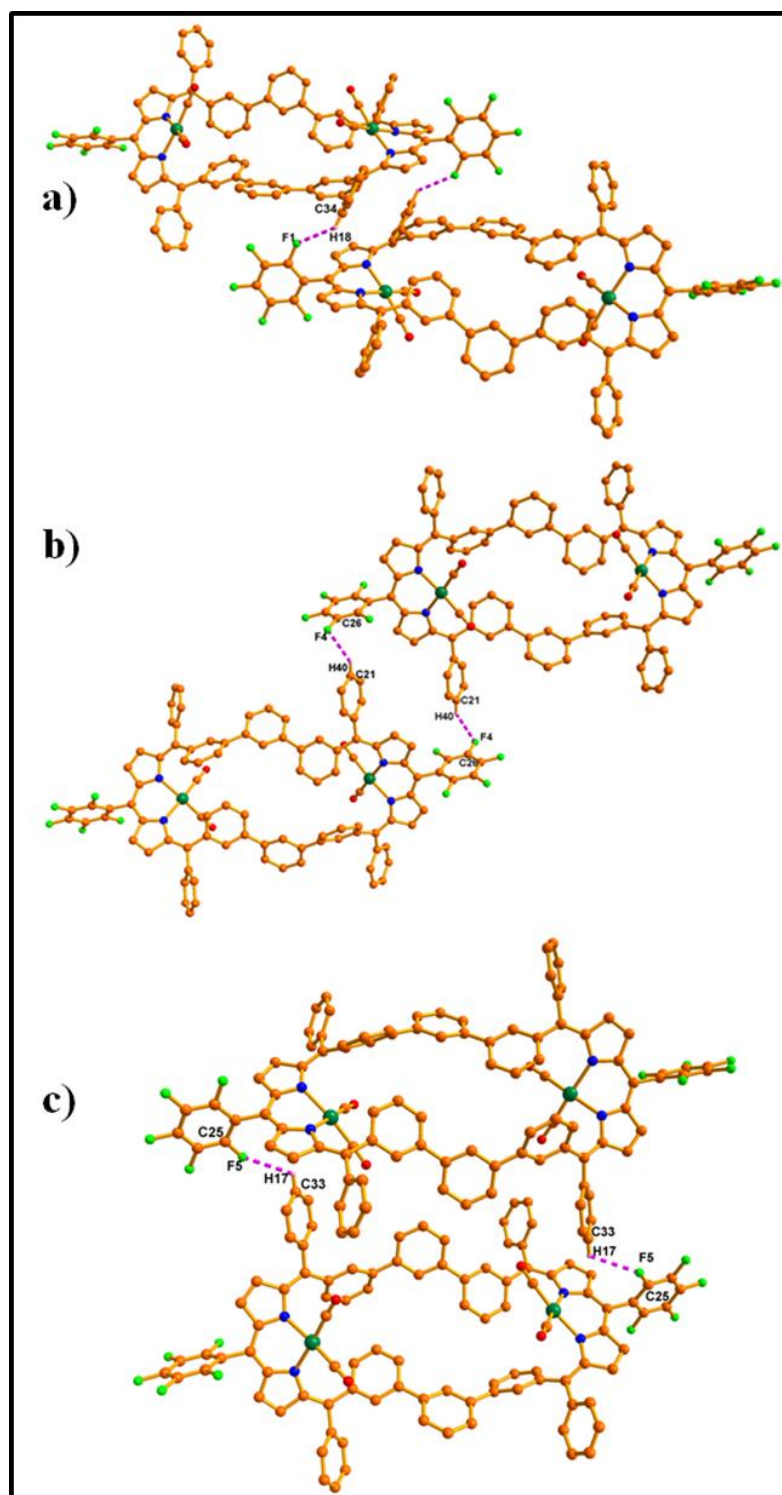


Figure 6.7: Self-assembled dimers of **15**. The bond distances and angles are: a) C34-H18...F1: 2.579(4) Å and 130.53(3)°; b) C21-H40...F4 2.792(4) Å and 145.89(5)°; c) C33-H17...F5: 2.738(3) Å and 113.81(3)° respectively. Peripheral hydrogen atoms are omitted for clarity.

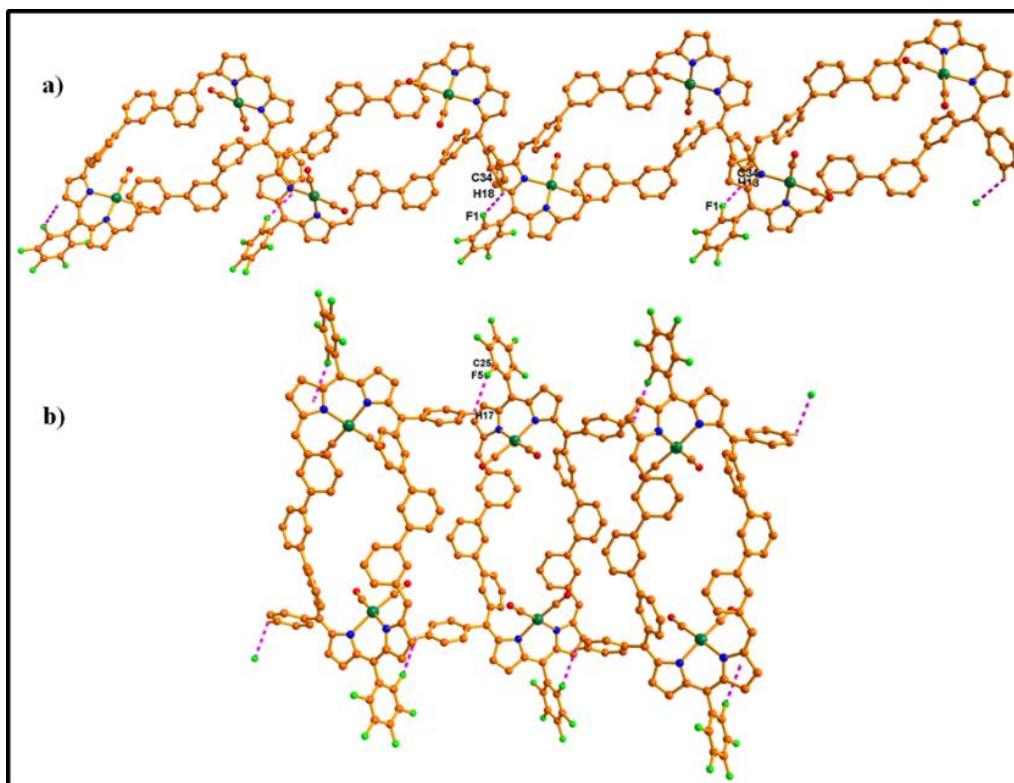


Figure 6.8: 1-D arrays of **15**. The bond distances and angles are: a) C34-H18...F1: 2.579(4) Å and 130.53(3)°; b) C25-H17...F5 2.738(3) Å and 126.96(3)° respectively. The hydrogen atoms and *meso*-aryl groups which are not in hydrogen bonding interactions are omitted for clarity.

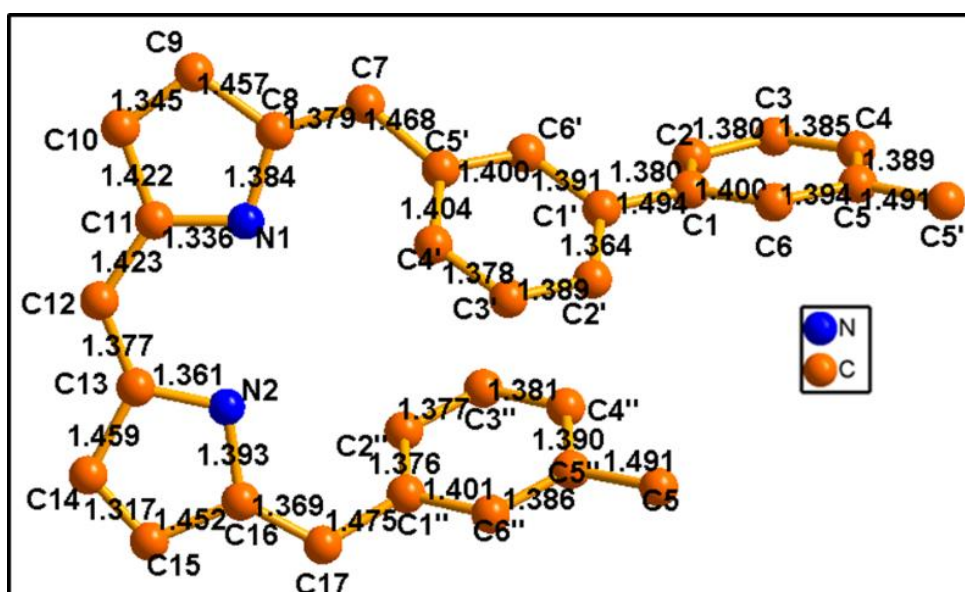


Figure 6.9: Bond lengths in (Å) **14** as present in the unit cell.

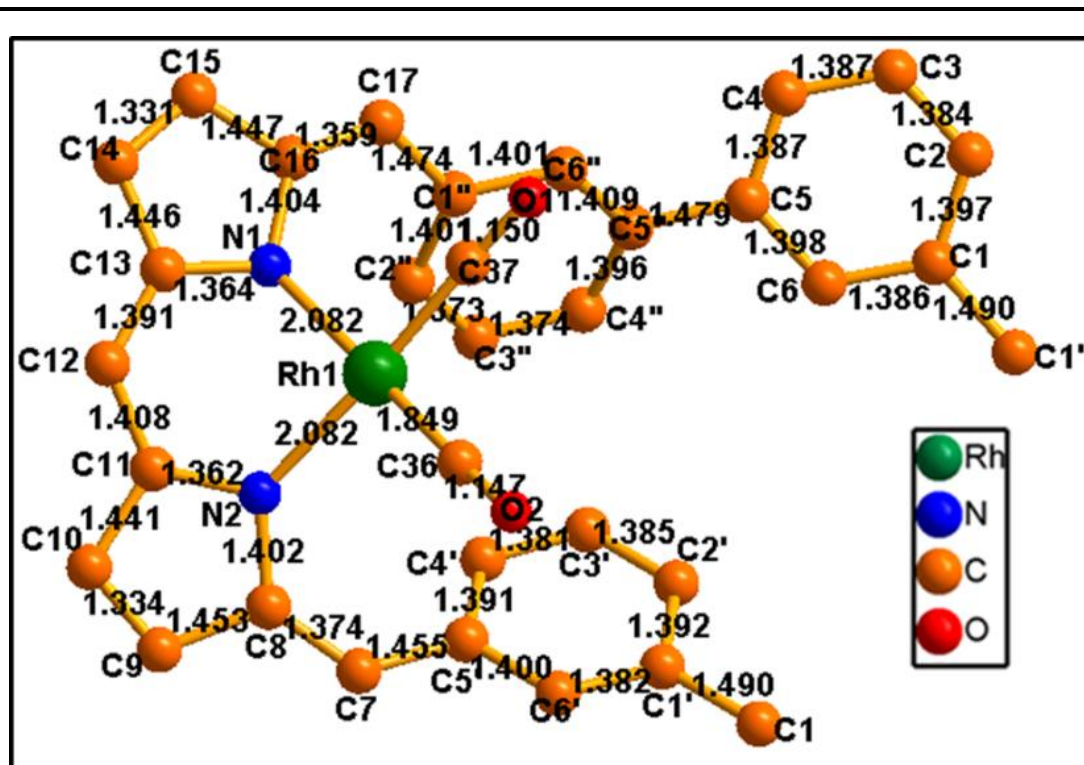


Figure 6.10: Bond lengths in (Å) **15** as present in the unit cell.

Table 6.1: Crystal data for **14** and **15**

Crystal parameters	14	15
Formula	C ₉₄ H ₅₄ F ₁₀ N ₄	C ₉₈ H ₅₂ F ₁₀ N ₄ O ₄ Rh ₂
<i>M</i> /g mol ⁻¹	1428.4189	1744.1939
<i>T</i> /K	100(2) K	293(2) K
Crystal dimensions/mm ³	0.25 × 0.22 × 0.2	0.2 × 0.15 × 0.12
Crystal system	monoclinic	monoclinic
Space group	<i>P</i> 21/ <i>n</i>	<i>C</i> 2/ <i>c</i>
<i>a</i> /Å	9.1781(4)	32.7594(13)
<i>b</i> /Å	11.6698(6)	13.8658(7)
<i>c</i> /Å	36.956(2)	21.7462(8)
α /°	90	90
β /°	93.560(4)	105.234(4)
γ /°	90	90
<i>V</i> /Å ³	3950.6(3)	9530.8(7)
<i>Z</i>	4	8
ρ calcd/mg m ⁻³	1.202	1.216
μ /mm ⁻¹	0.086	3.371
F(000)	1472.0	3520.0
Reflns. collected	40798	47279
Indep.reflns.[<i>R</i> (int)]	7268 [0.0946]	9913 [0.1438]
Max/min transmission	0.745 and 0.654	1.000 and 0.164
Data/restraints/parameters	7268/0/487	9913/0/502
GOF on <i>F</i> ²	1.033	1.060
Final <i>R</i> indices [<i>I</i> > 2σ(<i>I</i>)]	<i>R</i> 1 = 0.0796, w <i>R</i> 2 = 0.2166	<i>R</i> 1 = 0.0616, w <i>R</i> 2 = 0.1691
<i>R</i> indices (all data)	<i>R</i> 1 = 0.1414, w <i>R</i> 2 = 0.2379	<i>R</i> 1 = 0.0915, w <i>R</i> 2 = 0.1861
Largest diff peak and hole [e Å ⁻³]	0.45 and -0.43	1.10 and -1.14

The crystals have been deposited in the Cambridge Crystallographic Data Centre with reference no. CCDC 1895632 (**14**), CCDC 1895633 (**15**). These data can be obtained free of charge from the Cambridge Crystallographic Data Centre via www.ccdc.cam.ac.uk/data_request/cif.

6.3.2.4 Electronic absorption spectral analysis

The electronic absorption spectra of **14** and **15** were recorded in CH₂Cl₂ and shown in Figure 6.11. The compound **14** shows an intense band at 372 nm and a broad band at 634 nm with molar absorption coefficient values in the order of 10⁴. Upon Rh^I ion insertion, the color of the solution changes from blue to green. The bands in **15** are red shifted by 6 nm and 82 nm and appeared at 378 nm and 716 nm with marginal decrease and increase in the molar extinction coefficient values of respective lower and higher wavelength bands. Overall, the spectral pattern resembles typical nonaromatic characteristics as observed in *m*-benzporphyrinoids⁸ and its expanded analogues.^{5, 9-11}

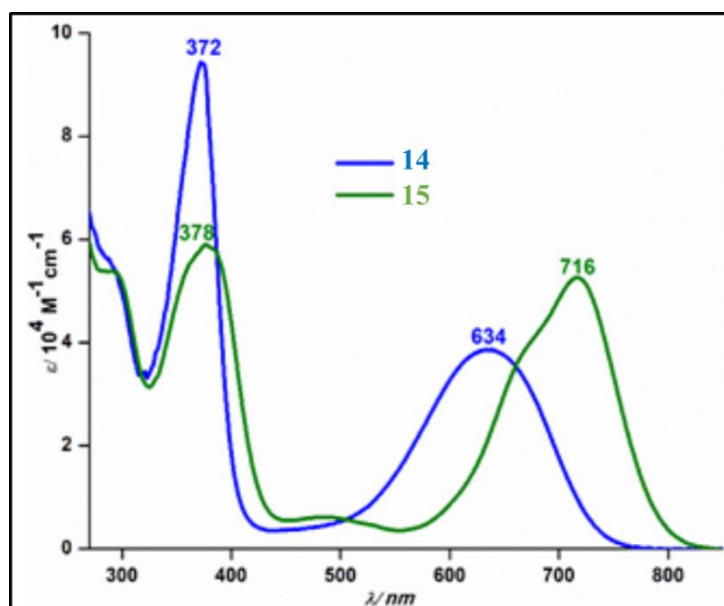


Figure 6.11: The electronic absorption spectra of **14** and **15** in CH₂Cl₂.

6.4 Conclusion

In conclusion, we have successfully synthesized terphenylene unit (*m-m-m*) incorporated decaphyrin with nonaromatic characteristics. For metal ion insertion, the open framework is effectively adjusted to stabilize the Rh^I ion in square planar geometry and retain the nonaromatic characteristics as such. These results are supported

by spectral studies and further confirmed by crystal analyses, where the conjugation is restricted at the terphenylene units.

6.5 Experimental Section

6.5.1 General Information

The reagents and materials for the synthesis were used as obtained from Sigma Aldrich chemical suppliers. All solvents were purified and dried by standard methods prior to use. The NMR solvents were used as received and the spectra were recorded in Bruker 400 and 700 MHz spectrometer with TMS as internal standard. The ESI (HR-MS) mass spectra were recorded in Bruker, micro-TOF-QII mass spectrometer. The Electronic absorption spectra were recorded in Perkin Elmer–Lambda 750 UV-Visible spectrophotometer. The X-ray quality crystals for **14** and **15** were grown by slow diffusion of *n*-hexane over CH₂Cl₂ solution. Single-crystal X-ray diffraction data of **14** and **15** were collected in a Bruker KAPPA APEX-II and Rigaku Oxford diffractometer respectively.

6.6 Synthetic procedure and spectral characterization

6.6.1 Synthesis of 16: The compound **16** was synthesized by using reported procedure.⁷

¹H NMR (400 MHz, CDCl₃, 298K): δ = 10.10 (s, 2H), 8.15 (s, 2H), 7.90 (t, *J*=9.0, 5H), 7.85 (s, 1H), 7.66 (d, *J*=8.5, 2H), 7.62 (s, 1H), 7.59 – 7.55 (m, 1H).

¹³C NMR (100 MHz, CDCl₃, 298K): δ = 192.24, 141.77, 141.72, 140.55, 140.51, 136.99, 133.15, 133.13, 129.72, 129.64, 128.11, 128.08, 126.79, 126.02, 125.97.

HR-MS (ESI-MS): *m/z* calculated for C₂₀H₁₄O₂ = 286.0994; found = 309.0898 (M+Na).

6.6.2 Synthesis of 17: Freshly prepared phenylmagnesiumbromide (9.05 g, 50 mmol) solution in THF (50 ml) was added under N₂ atmosphere at 0 °C into the solution of **16** (2.9 g, 10 mmol) in 100 ml THF and then allowed to stir at RT for 4 h. The completion

of the reaction was monitored by TLC and the reaction was quenched with 2N HCl. The crude mixture was extracted with EtOAc, dried over Na₂SO₄ and concentrated by rotary evaporator. Compound was purified by column chromatography using silica gel (100-200 mesh) in 15% EtOAc/*n*-hexane to afford **17** in 80% yield.

¹H NMR (400 MHz, CDCl₃, 298K): δ = 7.79 (s, 1H), 7.69 (s, 2H), 7.56 (d, *J* = 6.0 Hz, 5H), 7.45-7.41 (m, 6H), 7.39 – 7.33 (m, 6H), 7.29 (t, *J* = 7.2 Hz, 2H), 5.89 (s, 2H), 2.44 (s, 2H).

¹³C NMR (100 MHz, CDCl₃, 298K): δ = 144.52, 143.85, 141.78, 141.54, 129.30, 129.13, 128.72, 127.82, 126.72, 126.68, 126.45, 126.35, 125.76, 125.58, 76.47.

HR-MS (ESI-MS): *m/z* calculated for C₃₂H₂₆O₂ = 442.1933; found = 465.1840 (M+Na).

6.6.3 Synthesis of 18: The pyrrole (10 mL) was added into the solution of **17** (2 g, 4.5 mmol) in 1,2-dichloroethane (50 mL) which was kept in an inert atmosphere. After 10 min 1.4 mL of BF₃·OEt₂ solution was added and the resulting mixture was stirred under reflux for 3 hours. The solution was cooled to room temperature. The compound was extracted with EtOAc, dried over Na₂SO₄ and concentrated by rotary evaporator. The crude mixture was purified by column chromatography using silica gel (100-200 mesh) in 7% EtOAc/*n*-hexane to afford **18** in 45% yield.

¹H NMR (400 MHz, CDCl₃, 298K): δ = 7.86 (s, 2H), 7.68 (s, 1H), 7.52 – 7.42 (m, 8H), 7.39 (t, *J* = 7.6 Hz, 2H), 7.34 – 7.30 (m, 4H), 7.25 – 7.23 (m, 5H), 7.18 (d, *J* = 7.7 Hz, 2H), 6.72 (d, *J* = 4.9 Hz, 2H), 6.18 (d, *J* = 4.8 Hz, 2H), 5.86 (s, 2H), 5.54 (s, 2H).

¹³C NMR (100 MHz, CDCl₃, 298K): δ = 143.67, 142.94, 141.60, 141.35, 128.98, 128.90, 128.58, 127.89, 126.79, 125.68, 117.25, 108.35, 108.09, 50.73.

HR-MS (ESI-MS): *m/z* calculated for C₄₀H₃₂N₂ = 540.2565; found = 563.2445 (M+Na).

6.6.4 Synthesis of 14: Compound **18** (200 mg, 0.37 mmol) and pentafluorobenzaldehyde (86 mg, 0.44 mmol) was dissolved in 200 ml CH₂Cl₂ solution and stirred under N₂ atmosphere covered with aluminium foil. After 10 min *p*-TSA (31 mg, 18 mmol) was added and allowed to stir under same condition for 3 h. Then 2,3-Dichloro-5,6-dicyano-1,4-benzoquinone (251 mg, 1.11 mmol) was added to the reaction mixture and opened to air. The reaction was further continued for 1 h and the formation of product was monitored by TLC. The crude product was passed through basic alumina column followed by silica gel (100-200 mesh) column. The blue band was eluted with 20% CH₂Cl₂/*n*-hexane and identified as **14**. The compound was further recrystallized from CH₂Cl₂/*n*-hexane to afford blue crystalline solid **14** in 15% yield.

¹H NMR (700 MHz, CDCl₃, 298K): δ = 13.75 (s, 2H), 8.01 (d, *J* = 7.3 Hz, 4H), 7.52 (d, *J* = 7.8 Hz, 2H), 7.51 (d, *J* = 7.8 Hz, 2H), 7.48 (t, *J* = 7.8 Hz, 2H), 7.35-7.33 (m, 12H), 7.32-7.30 (m, 4H), 7.23-7.22 (m, 8H), 7.07 (t, *J* = 7.7 Hz, 4H), 7.04 (s, 2H), 6.76 (d, *J* = 7.7 Hz, 4H), 6.71 (d, *J* = 5.1 Hz, 4H), 6.23 (d, *J* = 5.1 Hz, 4H).

¹³C NMR (176 MHz, CDCl₃, 298K): δ = 160.18, 148.45, 140.40, 139.66, 138.65, 133.92, 130.98, 128.13, 127.69, 127.47, 127.45, 127.09, 126.12, 125.04.

HR-MS (ESI-MS): *m/z* calculated for C₉₄H₅₄F₁₀N₄ = 1428.4189; found = 1429.4235 (M+H).

UV-Vis (CH₂Cl₂): λ_{\max} (nm) [ϵ (M⁻¹cm⁻¹)x10⁴] = 372 (9.43), 634 (3.86).

6.6.5 Synthesis of 15: A solution of [Rh(CO)₂Cl]₂ (64 mg, 0.16 mmol) in 5 ml CH₃OH was added into the solution of **14** (20 mg, 0.028 mmol) and 32 μ L of Triethylamine in CHCl₃ (20 ml) under N₂ atmosphere. The reaction was allowed to stir for 4 h and the formation of product was monitored by TLC. The solvent was evaporated by rotary evaporator. The crude complex was purified by neutral alumina column. The green

band was eluted with 30% CH₂Cl₂/*n*-hexane and identified as **15**. The compound was further recrystallized from CH₂Cl₂/*n*-hexane to afford blue crystalline **15** in 60% yield.

¹H NMR (400 MHz, CDCl₃, 298K): δ = 8.02 (s, 2H), 7.76 (d, *J* = 7.6 Hz, 4H), 7.69 (d, *J* = 8.1 Hz, 2H), 7.65 (d, *J* = 7.6 Hz, 4H), 7.57 (d, *J* = 8.0 Hz, 2H), 7.40 (s, 20H), 7.34 (s, 4H), 7.23-7.21 (m, 4H), 7.16 (t, *J* = 7.8 Hz, 2H), 6.87 (d, *J* = 5.3 Hz, 4H), 6.45 (d, *J* = 4.7 Hz, 4H).

¹³C NMR (100 MHz, CDCl₃, 298K): δ = 162.21, 159.56, 142.63, 142.10, 141.68, 141.54, 141.12, 139.13, 138.36, 132.84, 131.42, 129.28, 128.85, 128.10, 127.72, 126.55, 126.08.

HR-MS (ESI-MS): *m/z* calculated for C₉₈H₅₂F₁₀N₄O₄ = 1744.1939; found = 1744.1966 (M).

UV-Vis (CH₂Cl₂): λ_{max}(nm) [ε(M⁻¹cm⁻¹)x10⁴] = 378 (5.85), 716 (5.26).

6.7 Reference

1. J. L. Sessler, S. J. Weghorn, V. Lynch, M. R. Johnson, *Angew. Chem., Int. Ed. Engl.* **1994**, *33*, 1509-1512.
2. J. L. Sessler, D. Seidel, A. Gebauer, V. Lynch, K. A. Abboud, *J. Heterocycl. Chem.* **2001**, *38*, 1419-1424.
3. V. G. Anand, S. Saito, S. Shimizu, A. Osuka, *Angew. Chem. Int. Ed.* **2005**, *44*, 7244-7248.
4. T. Okujima, C. Ando, S. Agrawal, H. Matsumoto, S. Mori, K. Ohara, I. Hisaki, T. Nakae, M. Takase, H. Uno, N. Kobayashi, *J. Am. Chem. Soc.* **2016**, *138*, 7540-7543.
5. S. Kumar, K. G. Thorat, M. Ravikanth, *J. Org. Chem.* **2018**, *83*, 14277-14285.
6. M. Das, B. Adinarayana, M. Murugavel, S. Nayak, A. Srinivasan, *Org. Lett.* **2019**, *21*, 2867-2871.

-
7. G. Bounos, S. Ghosh, A. K. Lee, K. N. Plunkett, K. H. DuBay, J. C. Bolinger, R. Zhang, R. A. Friesner, C. Nuckolls, D. R. Reichman, P. F. Barbara, *J. Am. Chem. Soc.* **2011**, *133*, 10155-10160.
 8. K. Berlin, E. Breitmaier, *Angew. Chem., Int. Ed. Engl.* **1994**, *33*, 1246-1248.
 9. M. Stępień, B. Szyszko, L. Latos-Grażyński, *Org. Lett.* **2009**, *11*, 3930-3933.
 10. J. S. Reddy, V. G. Anand, *Chem. Commun.* **2008**, 1326-1330.
 11. R. J. P. Corriu, B. Geng, J. J. E. Moreau, C. Vernhet, *J. Chem. Soc. Chem. Commun.* **1991**, 211-214.
 12. J.-i. Setsune, M. Toda, T. Yoshida, K. Imamura, K. Watanabe, *Chem. Eur. J.* **2015**, *21*, 12715-12727.